From Scavenger to Metabolic Coordinator:

Novel Roles of LRP1 in CNS Myelin Development and Repair

by

Jing-Ping Lin

A dissertation submitted in partial fulfillment
of the requirements for the degree of
Doctor of Philosophy
(Cell and Developmental Biology)
in the University of Michigan
2018

Doctoral Committee:

Associate Professor Bing Ye, Chair
Associate Professor Ben L. Allen
Professor Roman J. Giger
Professor Lori L. Isom
Associate Professor Brian A. Pierchala

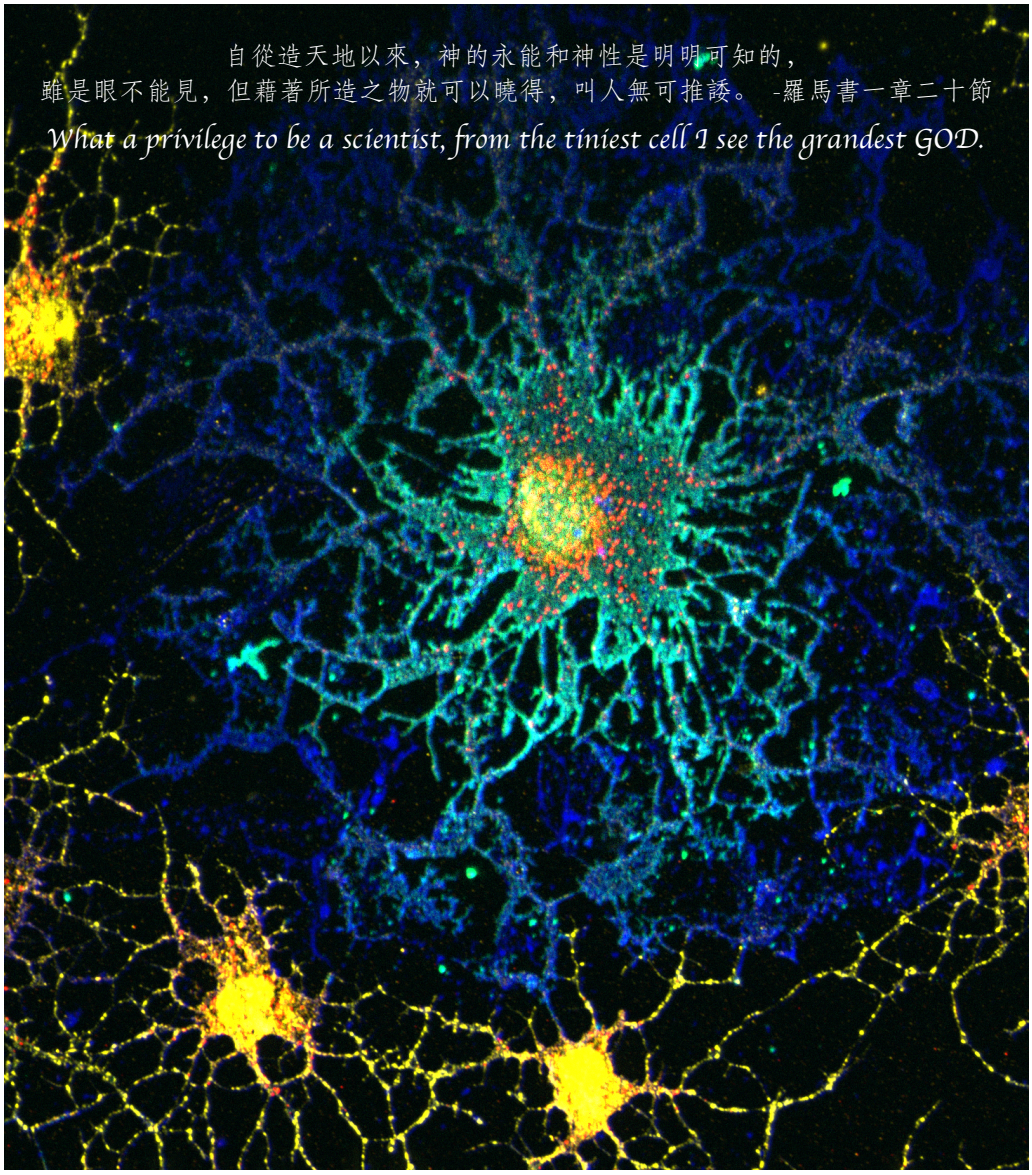
自從造天地以來，神的永能和神性是明明可知的，
雖是眼不能見，但藉著所造之物就可以曉得，叫人無可推諉。 -羅馬書一章二十節
What a privilege to be a scientist, from the tiniest cell I see the grandest GOD.

Jing-Ping Lin

annalin@umich.edu

ORCID iD: 0000-0003-0686-0215

© Jing-Ping Lin 2018

DEDICATION

To my future mentee:
Even without witness, for you I should keep committing to be a better scholar.

ACKNOWLEDGMENTS

I have been fortunate to have so many incredible individuals in my life who have helped me reach this point. I am thankful for all the guidance, encouragement, and even tough love that I have received, every step of the way in the past years all made me who I am today. I could only name a few, in case I doubled the volume of this dissertation; however, this work is only possible because of all of you.

First I would like to thank my advisor, Dr. Roman Giger, for your endless passion for science that is truly inspirational. You are probably the only titled professor that I know of still working on the bench and demonstrating fundamental experiments on a regular basis. You have influenced us to think critically, read broadly, and not be afraid to embark new scientific directions. Thank you for your patience and putting up with my stubbornness in the past years. You always find a way to encourage me to surpass my old self; with this valuable mentorship, it is unlikely for me to fail.

Thank my dissertation committee members: Lori Isom, Brian Pierchala, Bing Ye, and Ben Allen. I learned a lot from you over the past six meetings that I am fortunate to have. With your attention, inputs, and patience, my work can only be better. I cherish these professional relationships, since it will be very hard for me to get such exclusive scholarly consulting from here on. Thank my cooperator, Peter Shrager, for being my steadiest support during manuscript preparation and postdoc searching. For years, as if it is the first day, your persistence and precision toward science urged me to follow your example. Thank Jeff Lee, Chen P, and teacher Liu, for taking a chance on me and helping me to pursue my PhD. Thank Lei Lei, Dawen, and Pierre, for your warm encouragement and sharing your career path during my search for a postdoctoral position. Because of you, I can believe in myself and be more confident.

I would like to pay my appreciation to the staff in the University of Michigan, the Cell & Developmental Biology Department administration, Unit for Laboratory

Animal Medicine, Microscopy & Image Analysis Laboratory, and DNA sequencing core. Thank you for your excellent training and service. None of my research can be done without your support. Many alumni have told us that we have been spoiled with your high-quality work, which is difficult to find elsewhere.

Thank members of the AA Bio-group, thank you for sitting through almost 100 practice talks, seminars, and journal clubs with me for the past four years. Thank you for your participation, feedback, and sharing of your profession selflessly. I much enjoyed our inter-disciplinary discussion; I get the most exciting ideas for my own research when we brainstorm together. I will miss our AA Big meetings on Thursday, 8 pm, when I leave; I might skype in from time to time.

Thank Giger lab member: Choya, thank you for being so gentle yet so strong, I admire your perseverance when you are doing science, and nothing is more powerful. Xiaofeng, thank you for inspiring people in the lab to read more, to be strategic, and to go green (GO BLUE!). Ashley, thank you for bringing in awareness for being a better lab citizen and for supporting each other's success as a group. Rafi, oh Rafi, you are indeed one of your own kind of Turkish delight. Thank you for stretching my flexibility, increasing my social tolerance, and I kind of see that I might feel devoid without you when I leave. Ryan, your sense of humor from "up north" is my best material for pondering. Lucas, you are my proudest protégé. I enjoyed our philosophical chat about grad school, dreams, and life. Please remind me of this version of myself with the will to be a decent mentor if I ever drift otherwise.

Thank previous lab member: Yuntao, though we didn't overlap long, thank you for your advice on long-distance relationship and showing me the stereotaxic injection, which had become the central part of my dissertation. Travis, I miss your voice and your big heart in the lab, you always make me feel included. It is my honor that you called me a friend. Katie, thank you for being my interpreter when I just started, when English was far more foreign to me than now. You were always willing to stop a conversation and explain each word and cultural reference for me—for that I am ever grateful. Yev, I miss our days locked down in the TC and troubleshooting water for our OPC primary culture. I much enjoyed our

conversation; your clever and witty comments made grad school “so much fun.” Thank you for connecting me with your friends, I am so lucky to have you hub me to the glia world.

Thank our lab manager, Sarah and Dao. Sarah, thank you for bringing in order and system into our lab. Your proactive attitude and leadership helped me when I needed the most in my senior years. I have no doubt that you will do great in the grad school. Dao, thank you for bringing in fun and creativity to our lab, your sense of humor lightened our life and your great cooking made our bellies heavy. You always find a way to cheer me up in my stressed moments. I see you as my sister in the lab. I would like to thank our undergrads: Sandy, Sophia, Dava, Riley, Lily, Kevin, Kim, Olivia, and Inwoo. Thank you for your great work, so the lab is running smoothly and we too have assurance to focus on research. Thank Allen lab, for putting up with the Giger lab, especially when we had loud previous lab members. Though I am not particularly disturbing when I am working, I am guilty for frequently “borrowing” your reagents, equipment, Justine, and Martha.

Justine, thank you for being my first friend and best friend in Ann Arbor. You imprinted on me. Thank you for always be there for me; my grad school won’t be the same without you. I am still holding on the idea that we open our lab together. I am the bad cop, and you are the nice one. I am sure we will be a great team. And thank you for introducing me another beautiful soul, Blu. It is my honor to know both of you. Martha, thank you for staying chic and your positive energy. Ting HA, how lucky am I to have you from the beginning to the end to this journey. Cynthia, thank you for being my personal editor for years, from my wedding invitation, all kinds of application materials, to this dissertation. Thank you for witness all my milestones in life. In memory of my friend Ming-Cheng, a brilliant mind, his life was tragically cut short during the writing of this dissertation. Ming-Cheng, I will continue the dream that you started in the path of science on your behalf. Thank you Ann Arbor, you’ve treated me well for the past 5.5 years. This is my first ever city in the State that I lived in, I think I will call AA my home from now on when I am not here. Thank AA sister group: Jorli, Bin, Chih, Jane, Jean, and Sumac Wolverines, thank you for feeding me, clothing me, and housing me when I am too busy to care about living.

Without you I would not be able to survive, literally. You are my family and the reason I call here home.

To my family and in-laws back in Taiwan, thank you for being my biggest fans and always cheering for me; I miss all of you. Dad, you enlightened me with science when I was little. Your broad knowledge of plant taxonomy when we were outdoors still impresses me. Mom, thank you for always putting my welfare before my accomplishments, so I know that I have a safety net to fall back to.

Special shout out for my endearing husband, Chang-Ting, you are my champion, my hero. I think you deserve two PhDs. You were there every late night, discussed my experiments, found technique supports, went through my presentation, and read my journal club papers. How lucky I am to have such a good friend, an intellectual equal, and the most reliable collaborator in my career. Thank you for being the husband that I always wanted. You were dedicated to being creative in making me feel better about myself, and you always succeeded. Though we are apart all these years to pursue our degrees, we are closer than ever because of you. Thank you for taking most of the hit in the long-distance relationship concerning travel. Hang in there, I will be by your side soon.

Lastly, to myself and to my high school teacher Hong-heng Yang, she made me brave with this poem, which I would like to share with whoever is reading.

我不去想是否能夠成功
I think not if I can succeed
既然選擇了遠方
Since I have chosen to go far
便只顧風雨兼程
I shall keep marching no matter what

我不去想能否贏得愛情
I think not if I can win affection
既然鍾情於玫瑰
Since I am in love with roses
就勇敢地吐露真誠
I shall get off the high horses

我不去想身後會不會襲來寒風冷
I think not if the hardship will hit me
既然目標是地平線
Since my aim is the horizon
留給世界的只能是背影
I left this world behind for the reason

我不去想未來是平坦還是泥濘
I think not if my future is leveled or rough
只要熱愛生命
If I just love life
一切，都在意料之中
All, are expected

--熱愛生命 汪國真
Loving life –Guozhen Wang (1956-2015)

TABLE OF CONTENTS

DEDICATION ii

ACKNOWLEDGMENTS iii

LIST OF FIGURES xii

LIST OF TABLES xv

LIST OF ABBREVIATIONS xvi

ABSTRACT xxi

CHAPTER I 1

Introduction: Myelin, A Matter of Fat 1

1.1 Abstract 1

1.2 Introduction: A Necessary Evil? Myelin—An Energy Expensive Structure 1

1.2.1 Necessity—Myelin supports biological complexity and protects neurons 1

1.2.2 Evil—Myelin burdens the CNS in disease and in health 2

— Myelin debris impede neuron and myelin regeneration 3

— Myelin clearance triggers excessive inflammatory responses 4

— Metabolic vulnerability–an energy price paid to myelinate 5

1.2.3 Standing Questions: The Focus of This Chapter 6

1.3 Build the White Matter—Myelin Structure, Composition, and Biology 6

1.3.1 Myelin Morphology 6

— Compact myelin 7

— Node of Ranvier, paranodal junction, and juxtaparanode 10

— Non-Compact Myelin 12

1.3.2 Myelin Building blocks 13

1.3.2.1 Myelin Lipids 13

— Cerebroside 14

— Plasmanogen/Sphingomyelin 15

— Cholesterol 16

1.3.2.2 Myelin Proteins 17

— PLP/DM20: Proteolipid Protein 17
— MBP: Myelin Basic Protein 18
— CNP: 2'3'-cyclic nucleotide 3'-phosphodiesterase 19
— MAG: Myelin-associated Glycoprotein 19
— MOG: Myelin Oligodendrocyte Glycoprotein 20
— Other myelin proteins 20
1.3.3 Myelin Cell Biology—Oligodendrocyte 21
1.3.3.1 Myelination: *De Novo* Synthesis 22
— OL-lineage fate commitment 22
— OPC pool origins 22
— OPC proliferation / apoptosis 23
— OPC migration 24
— OPC differentiation/maturation 25
1.3.3.2 Remyelination: Re-program development 26
— Systems for Studying Remyelination 26
— Identifying Remyelination 27
— Removing Myelin Debris 28
— Recruiting and Differentiating Adult OPCs 29
— Failing at Remyelination 30
1.3.3.3 Myelin Turnover: Dynamic Myelination 30
1.4 The More the Merrier? Precise Myelination Matters 32
1.4.1 To Myelinate or Not, That is the Question 32
1.4.2 Lateral Transfer of Metabolites 33
— Energy Cooperation 33
— Cholesterol homeostasis 35
1.4.3 Signaling Coordinator-LRP1 36
1.5 Bibliography 41
CHAPTER II 60
LRP1 Regulates Peroxisome Biogenesis and Cholesterol Homeostasis in Oligodendrocytes and Promotes CNS Myelin Development and Repair 60
2.1 Abstract 60
2.2 Introduction 60
2.3 Results 62
2.3.1 In adult mice, inducible ablation of Lrp1attenuates CNS white matter repair 62
2.3.2 OL-lineage specific ablation of *Lrp1* impairs timely repair of damaged white matter 63

2.3.3 *Lrp1* is important for proper CNS myelin development and optic nerve conduction 64
2.3.4 Conditional ablation of Lrp1 in the OL-lineage attenuates OPC differentiation 66
2.3.5 Loss of *Lrp1* attenuates OPC differentiation *in vitro* 66
2.3.6 *Lrp1* deficiency in OPCs and OLs causes a reduction in free cholesterol 67
2.3.7 *Lrp1* deficiency impairs peroxisome biogenesis 69
2.3.8 Combination treatment of cholesterol and PPARγ agonist rescues the differentiation block in *Lrp1*-deficient OPCs 70
2.4 Discussion 71
2.5 Materials and Methods 75
2.5.1 Mice 75
2.5.2 Genotyping 76
2.5.3 Stereotaxic injection 77
2.5.4 Histochemistry 77
2.5.5 In situ hybridization 77
2.5.6 Quantification of lesion size and myelin repair 79
2.5.7 Immunostaining 79
2.5.8 Transmission electron microscopy (TEM) 80
2.5.9 Optic nerve recordings 81
2.5.10 OPC/OL primary cultures and drug treatment 81
2.5.11 OPC staining and quantification 82
2.5.12 Western blot analysis 83
2.5.13 Cholesterol measurement 84
2.5.14 Microarray and gene ontology analysis 85
2.5.15 Statistical analysis 85
2.6 Acknowledgements 86
2.7 Author Contribution 86
2.8 Figures 87
2.9 Bibliography 119

CHAPTER III 126

Additional Observations While Examining the Role of LRP1 in CNS Myelin Development and Repair 126

3.1 The study of myelin repair in the LPC demyelination model 126
3.1.1 LPC induced inflammation 126
— LPC injection post a 'find me' signal on the cell surface 126
— Generate local lesion with LPC 127

— Astrocytes from SVZ migrate toward lesion within seven days ... 127
— Nuclei accumulate at the LPC-induced lesion site ... 128
— Proliferative cells in the SVZ and OPCs are present in the naïve brain ... 128
— Myeloid cells are present at the LPC lesion site ... 128
3.1.2 LRP1 expression at the myelin lesion ... 129
3.1.3 LRP1 ablation in myeloid cells affects the size of the LPC induced white matter lesion ... 130
3.1.4 Identification of the LPC-induced myelin lesion ... 131
— Charcoal ... 131
— Cell tracer: CFSE ... 131
— Myelin genes ... 132
3.2 LRP1 in axon-glia interaction and regional myelin diversity ... 133
3.3 Investigate the mechanism of LRP1 in regulating myelin development ... 134
3.3.1 Dissect LRP1 functional domains: RAP peptides and *Lrp1* N2 mice ... 134
— Extracellular domain (ECD) antagonist ... 135
— Intracellular domain (ICD) phospho-dead mutant ... 136
3.3.2 LRP1 as a LDL receptor: cholesterol metabolic pathways ... 137
3.3.3 LRP1 as a transcriptional regulator: miRNA expression ... 138
3.3.4 LRP1 as a novel regulator of organelle trafficking: Myo1D and peroxisome distribution ... 139
— LRP1 regulates Myo1D ... 139
— Study LRP1 and peroxisome subcellular localization ... 140
3.4 Materials and Methods ... 142
3.4.1 Mice ... 142
3.4.2 Genotyping ... 143
3.4.3 Quantitative reverse transcription (qRT)-PCR ... 143
3.4.4 COS-7 cells binding assay ... 144
3.4.5 Histochemistry ... 144
3.4.6 In situ hybridization ... 144
3.4.7 Immunostaining ... 145
3.4.8 Transmission electron microscopy (TEM) ... 146
3.4.9 OPC/OL primary cultures and drug treatment ... 146
3.4.10 Western blot analysis ... 146
3.4.11 Microarray and gene ontology analysis ... 147
3.4.12 Image and statistical analysis ... 147
3.5 Acknowledgements ... 148
3.6 Author contributions ... 148
3.7 Figures ... 149

3.8 Tables 196
3.9 Bibliography 228

CHAPTER IV 230

General Discussion and Future Direction 230

4.1 Abstract 230
4.2 General Discussion 230
4.2.1 How can non-cell-autonomous roles of LRP1 impact CNS remyelination? 231
— Controlled inflammation and demyelination 231
— Myelin debris removal 232
— The heterogeneity of remyelination 233
4.2.2 How can OL-derived LRP1 impact axon diameter, function, and stability 233
— Uncoupled compact myelin formation and OL-axon interaction 233
— Selective myelination and hypomyelination 234
— Search for OL-axon regulator by studying the caliber of axons in vivo 236
4.2.3 How can cholesterol impact myelination and remyelination 237
— As a signaling regulator 237
— As a structural lipid of the membrane 239
4.2.4 How can peroxisome impacts myelin biology 239
— Consider peroxisome as an all-purposed logistic vehicle 240
— A hierarchical role for peroxisomes in cholesterol metabolism? 241
4.2.5 Speculations on how LRP1 impacts myelin biology 242
— LRP1 regulates Myo1d: motor protein trafficking on cytoskeleton 242
4.3 Future Direction 243
— The role of Lrp1 in different cell types and its contribution to myelin repair 243
— Identification of LRP1-PPARγ regulated genes important for CNS myelination 245
— The role of LRP1 in regulating organelle trafficking 246
4.4 Concluding Remarks 247
4.5 Bibliography 249

LIST OF FIGURES

Figure 1.1: CNS myelin anatomy and ultrastructure 8
Figure 1.2: A diagram highlight the top three lipid types in the myelin..... 15
Figure 1.3: Oligodendrocyte lineage commitment and development 21
Figure 1.4: The origin of OPCs under the influence of pattern formation during development 24
Figure 1.5: CNS intercellular metabolic transfer 34
Figure 1.6: The structure of LDL receptor family..... 37
Figure 1.7: The synthesis, maturation, structure, and function of LRP1..... 40
Figure 2.1: Generation of Lrp1 global iKO mice 88
Figure 2.2: In adult mice, global and OL-lineage selective ablation of *Lrp1* attenuates white matter repair 90
Figure 2.3: LPC injection into the corpus callosum leads to focal white matter damage and upregulation of myelin-associated gene products..... 92
Figure 2.4: *Lrp1* ablation in the OL-lineage leads to hypomyelination and nodal defects..... 94
Figure 2.5: *Lrp1* ablation in the OL lineage leads to CNS hypomyelination..... 96
Figure 2.6: Global inducible ablation of *Lrp1* in neonatal mice leads to CNS hypomyelination and reduced axon caliber..... 98
Figure 2.7: Loss of *Lrp1* in the OL lineage leads to faulty optic nerve conduction... 100
Figure 2.8: Loss of *Lrp1* in the OL-lineage attenuates OL differentiation 102
Figure 2.9: Loss of *Lrp1* does not alter optic nerve size and OPC proliferation 104
Figure 2.10: Free cholesterol is reduced in OPCs deficient for *Lrp1* 106
Figure 2.11: *Lrp1* deficient OLs are sensitive to statin treatment but not to bath applied mevalonate 108
Figure 2.12: Gene ontology (GO) analysis of *Lrp1* deficient OPCs revealed enrichment of peroxisomal genes 110

Figure 2.13: In primary OLs, peroxisome density and distribution is regulated by *Lrp1* 112
Figure 2.14: In *Lrp1* deficient OPCs, PPAR γ activation increases peroxisome density but does not promote cell differentiation 114
Figure 2.15: The combined treatment with cholesterol and pioglitazone rescues the differentiation block of *Lrp1* deficient OPCs 116
Figure 2.16: Working model of LRP1 regulated pathways in developing OLs 118
Figure 3.1: LPC induced demyelination, astrogliosis, accumulation of nuclei overtime within the lesion area in the corpus callosum 151
Figure 3.2: LPC induced white matter lesion leads to accumulation of CD68+ myeloid cells and cells in the OL-lineage 153
Figure 3.3: Elevated LRP1 protein and mRNA expression are observed in the LPC induced white matter lesion 155
Figure 3.4: Elevated Lrp1 mRNA is detected in a subset of cells in the OL-lineage. 157
Figure 3.5: Ablation of *Lrp1* in myeloid cells does not impact remyelination. 159
Figure 3.6: Labeling of the LPC induced white matter lesion with the cell tracker CFSE 161
Figure 3.7: Examination of the specificity of RNA probes used for in situ hybridization 163
Figure 3.8: *Lrp1* ablation in the OL-lineage leads to axonal pathology in the optic nerve 165
Figure 3.9: *Lrp1* ablation in the OL-lineage does not impact retina ganglion cells (RGC) density or retinal stratification 167
Figure 3.10: Brain region specific and developmental stage specific regulation of Myelin proteins in Lrp1 cKO CNS tissue 169
Figure 3.11: Bath application of the LRP1 antagonist RAP does not inhibit OPC differentiation 171
Figure 3.12: Characterization of *Lrp1*$^{n2/n2}$ mice carrying a mutation in the distal NPxY phosphorylation site of LRP1 173

Figure 3.13: Analysis of myelin and peroxisome protein expression in P10-14 *Lrp1*$^{n2/n2}$ and *Lrp1* cKO mouse brain tissue fractionated in a sucrose density gradient 175
Figure 3.14: Characterization of myelin protein expression in P19-24 brains of *Lrp1*$^{n2/n2}$ mice in fractions enriched for peroxisomes and light mitochondria 177
Figure 3.15: Gene ontology (GO) analysis of *Lrp1* deficient OPCs revealed enrichment of cholesterol biosynthesis and homeostasis genes 179
Figure 3.16: Validation of genes belonging to the cholesterol metabolism pathway differentially regulated in *Lrp1* control and cKO OPCs 181
Figure 3.17: Validation of the miRNAs that are differentially regulated in *Lrp1* control and cKO OPCs 183
Figure 3.18: Validation of the genes that are differentially regulated in *Lrp1* control and cKO OLs that are O4^{+} 185
Figure 3.19: Gene ontology (GO) analysis of genes that are differentially regulated in *Lrp1* deficient OLs compares to *Lrp1* control OLs. 187
Figure 3.20: LRP1 staining in OLs is closely associated with peroxisomes and lysosomes 189
Figure 3.21: Co-localization analysis of LRP1 and PMP70 in OPCs and mature OLs. 191
Figure 3.22: Co-localization analysis of LRP1 and PMP70 in OPCs, astrocytes, epithelial cells, and neurons 193
Figure 3.23: Image processing rundown for single cell analysis 195
Figure 4.1: Genetic manipulation strategies to study masking effect 244

LIST OF TABLES

Table 1.1: The comparison of CNS myelin composition 16

Table 3.1: List of differentially regulated genes in $O4^+$ OLs upon *Lrp1* ablation..... 227

LIST OF ABBREVIATIONS

A

ACSF	Artificial cerebrospinal fluid
AGC1	Aspartate-glutamate carrier
AKT	Ak strain transforming, aka Protein kinase B (PKB)
AMPA	α-amino-3-hydrozy-5-methyl-4-isoxazole proprionic acid
ANOVA	Analysis of Variance
AP (coordinate)	Anterior-Posterior
AP (substrate)	Alkaline phosphatase
APC	Adenomatous polyposis coli protein
APP	Amyloid precursor protein
Arg-1	Arginase 1
ASPA	Aspartoacylase
ATP	Adenosine triphosphate

B

BACE1	Beta-site APP cleaving enzyme1
BBB	Blood brain barrier
BCIP	5-Bromo-4-Chloro-3-Indoly-Phosphate
BDNF	Brain-derived neurotrophic factor
BMP	Bone morphogenetic protein
BrdU	Bromodeozyuridine
BS	Brain stem

C

CAG	Chicken beta, cytomegalovirus (CMV)
CAPON	Carboxy-terminal PDZ ligand o f nNOS
CAM	Cell adhesion molecule
CamK	Calmodulin-dependent kinase
CAP	Compound Action Potential
Caspr	Contactin-associated protein
CB	Cerebellum
CB1	Cannabinoid type 1 receptor
CC	Corpus Callosum
CD68	Cluster of Differentiation 68
CFSE	Carboxyfluorescein succinimidyl ester
CI-CV repeats	Complement-like repeats
CNPase	2'3'-Cyclic Nucleotide 3'-Phosphodiesterase
CNS	Central Nervous System
CNTP	Ciliary neurotrophic factor
COS-7	CV-1 in Origin with SV40 genes
CR3	Complement receptor 3
CRE	Cre Recombinase
CSF	Cerebral spinal fluid
CTGF	Connective tissue growth factor
CTX	Cortex
CV	Conduction Velocity
Cx32	Connexin32
CX3CR1	CX3C (C-X3-C motif) chemokine receptor 1
CXCL1	Chemokine (C-X-C motif) ligand 1

D

DEPC	Diethyl pyrocarbonate
DM	Differentiation medium
DMSO	Dimethyl sulfoxide
DNA	Deoxyribonucleic acid
DRM	Detergent-resistant membrane
DPI	Days Post Injection

E

EAE	Experimental allergic encephalomyelitis
ECD	Extracellular domain
EDTA	Ethylenediaminetetraacetic acid
ER	Endoplasmic reticulum
ERK	Extracellular signal–regulated kinases
EtBr	Ethidium bromide

F

FcRs	Fc (Fragment, crystallizable) Receptors
FE65	APP binding protein
FGF	Fibroblast growth factor
FISH	Fluorescence in situ hybridization
Flp	Flippase
FM-G	Fluoromyelin-Green
FM-R	Fluoromyelin-Red
FRT	Flippase recognition target

G

GABA	γ-aminobutyric acid
GAIP	G Alpha Interacting Protein
GalC	Galactocerebroside
GAP	GTPase-activating protein
GAPDH	Glyceraldehyde 3-phosphate dehydrogenase
GC	Ganglion cell
GFAP	Glial fibrillary acidic protein
GFP	Green Fluorescent Protein
GIPC	GAIP Interacting Protein C-terminus
GluR	Glutamate receptor
GLUT	Glucose transporter
GM	Growth medium
GO	Gene ontology
GPI	Glycosyl phosphatidylinositol
GPR17	G protein-coupled receptor 17
GSH2/GSX2	Genomic Screened Homeo Box 2
GST	Glutathione S-transferase
GULP	Engulfment Adaptor PTB Domain Containing 1

H

HBS	HEPES-buffered saline
HDAC	Histone deacetylase
HEPES	4-(2-hydroxyethyl)-1-piperazineethanesulfonic acid
HFD	high fat diet
HGF	Hepatocyte growth factor
HIF	Hypoxia-induced factor
HMG-CoA	β-Hydroxy β-methylglutaryl-CoA

I

IACUC	Institutional Animal Care and Use Committee
ICAP1	Integrin cytoplasmic domain–associated protein-1)
ICC	Immunocytochemistry
ICD	Intracellular domain

IGF	Insulin-like growth factor
IHC	Immunohistochemistry
IL-2	Interleukin-2
IN-1	A monoclonal antibody raised against myelin protein, NI-220/250
iNOS	Inducible nitric oxide synthase
INL	Inner nuclear layer
INT	Internode
IPL (myelin)	Interperiod line
IPL (retina)	Inner plexiform layer
ISH	In Situ Hybridization

J

JIP1/2	JNK interacting protein
JNK	c-Jun N-terminal kinases
JXP	Juxtaparanode

K

Ki67	Antibody identified marker of proliferation Ki-67 (MKI67)
KO	Knockout

L

LAMP	Lysosomal Associated Membrane Protein
LDL	Low-Density Lipoprotein
LEs	Late endosomes
LGE	Lateral ganglionic eminence
LINGO-1	Immunoglobin-like domain-containing protein 1
LOX-1	Lectin-type oxidized LDL receptor 1 (Ox-LDLR1)
LPC	Lysophosphatidylcholine, aka lysolecithins
LPS	lipopolysaccharide
LR	Left-Right
LRP1	Low-Density Lipoprotein Receptor Related Protein 1
LXR	liver X receptor
LysM	lysozyme 2
Lys	Lysosomes
LXRE	LXR response elements

M

MAG	Myelin-Associated Glycoprotein
MAP	Mitogen-activated protein
MAPK	Mitogen-activated protein kinase
MBP	Myelin Basic Protein
MCT	Monocarboxy transporter
MDL	Major dense line
MEFs	Mouse Embryonic Fibroblasts
MGE	Medial ganglionic eminence
MGI	Mouse genome informatics
MHC	Major histocompatibility complex
MMPs	Matrix metalloproteinase
MOBP	Myelin-Associated Oligodendrocyte Basic Protein
MOG	Myelin oligodendrocyte protein
MRI	Magnetic resonance spectroscopy
MS	Multiple Sclerosis
mTOR	Mammalian target of rapamycin
MYO1D	Myosin 1d
MYT2	Myelin transcription factor 2

N

NAA	N-acetylaspartate
NBT	Nitro blue tetrazolium
NCAM	Neural cell adhesion molecule

NGF	Nerve growth factor
NKX2.1	NK2 homeobox 1
NMDA	N-methyl-D-aspartate
nNOS	neuronal NO synthase
NO	Nitric oxide
NOGO	Reticulon-4
NRG-1	Neuregulin 1
NSC	Neural stem cells
NT-3	Neurotrophin-3

O

OAP-1	OSP-associated protein
OB	Olfactory bulb
OCT	Optimal cutting temperature
OL	Oligodendrocyte
OLIG2	Oligodendrocyte Transcription Factor
OMP25	Outer-membrane protein 25
ONL	Outer nuclear layer
OPC	Oligodendrocyte Progenitor Cell
OPL	Outer plexiform layer
OSP	Oligodendrocyte-specific protein, aka claudin-11

P

PBDs	Peroxisome biogenesis disorders
PBS	Phosphate-buffered saline
PCR	Polymerase chain reaction
PDGFa	Platelet-Derived Growth Factor
PDZ	Post synaptic density protein (PSD95), Drosophila disc large tumor suppressor (Dlg1), and zonula occludens-1 protein (zo-1) domain
PEXs	Peroxins
PFA	Paraformaldehyde
PGC1a	PPARg-coactivator-1α
PI3K	Phosphatidylinositol 3-kinase
PIP4, 5, kinase	Phosphatidylinositol 4-phosphate (PI4P) 5-kinase
PLP	Proteolipid Protein
PMD	Pelizaeus-Marzbacher disease
PMP70	Peroxisomal Membrane Protein 70kDa
PNL	Paranodal loop
PNS	Peripheral Nervous System
POA	Pre-optic area
POS	Photoreceptor outer segment
PP	Peroxisome Proliferator
PPAR	Peroxisome Proliferation Activated Receptor
PPRE	PPAR-responsive element
PRR	Pattern recognition receptor
PRs	Progesterone receptors
PSA-NCAM	Polysialylated-neural cell adhesion molecule
PSD95	Post synaptic density protein
PS-Rs	Phosphatidylserine receptors
PTEN	Phosphatase and tensin homolog
PVDF	Polyvinylidene fluoride

Q

qRT-PCR	Quantitative reverse transcription polymerase chain reaction

R

RAP	Receptor associated protein
RCT	Reverse cholesterol transport
RE	Recycling endosomes

	RGC	Retinal ganglion cell
	RNA	Ribonucleic acid
	ROS	Reactive oxygen species
	RPE	Retinal pigment epithelium
	RT	Room temperature
	RT-PCR	Reverse transcription-polymerase chain reaction
	RXR	Retinoid X receptor
S		
	S6	Ribosomal protein s6
	SC (cell)	Schwann Cell
	SC (tissue)	Spinal cord
	SCAP	SREBP cleavage-activating protein
	SCI	spinal cord injury
	SDS-PAGE	Sodium dodecyl sulfate–polyacrylamide gel electrophoresis
	SEM	Scanning electron microscope
	SEMCAP-1	M-SemF cytoplasmic domain-associated protein, GIPC
	SQS	Squalene synthase
	Src	Sarcoma, proto-oncogene tyrosine-protein kinase
	SRE	Rterol regulatory element
	SRs	Scavenger Receptors
	SREBP	Sterol-Regulatory Element-Binding Protein
	SSC	Saline-sodium citrate
	SSR	Site-specific recombinase
	STORM	Stochastic Optical Reconstruction Microscopy
	SVZ	Subventricular zone
T		
	TB	Toluidine blue
	TGF	Transforming growth factor
	TH cell	T helper cells
	TC cell	Cytotoxic T cell
	TH	Thalamus
	TSC1	Tuberous sclerosis 1
	TM	Tamoxifen
	TLR-2	Toll-like receptor 2
	TERM2	Triggering receptor expressed on myeloid cells 2
	TNF	Tumor necrosis factor
	THR	Thyroid hormone receptor
	T3	Triidothyronine
	TEM	Transmission Electron Microscopy
U		
V		
	VEGF	Vascular endothelial growth factor
	VLCFAs	Very long chain fatty acids
	VZ	Ventricular zone
W		
	WT	Wildtype
X		
Y		
	YFP	Yellow fluorescent protein
	YY1	Yin Yang 1
Z		
	ZS	Zellweger syndrome

ABSTRACT

Low-density lipoprotein receptor-related protein-1 (LRP1) is one of the most versatile receptors. LRP1 is ubiquitously expressed and best known for its role as a scavenger receptor. The LRP1 extracellular domain binds to and participates in internalization of over 40 different ligands, and thereby regulates myriad cellular functions by recycling components of key pathways. The intracellular domain of LRP1 can undergo phosphorylation at specific tyrosine residues and thereby influence intracellular signaling pathways. In addition, the intracellular domain of LRP1 can be enzymatically processed, translocate to the nucleus, and function as a transcriptional co-regulator. In the developing nervous system, *Lrp1* mRNA expression is highest in oligodendrocyte (OL) progenitor cells and rapidly decreases as OLs mature; however, whether LRP1 plays a role in OL development *in vivo*, remains elusive. Moreover, glial cells bind and internalize myelin breakdown products in an LRP1-dependent manner. As protracted clearance of myelin debris in the CNS is a hallmark of neuronal degeneration and demyelination diseases, the removal of myelin breakdown products through LRP1 might facilitate functional repair. Here we make use of global inducible and tissue-specific *Lrp1* gene ablation in transgenic mice to assess the roles of LRP1 during CNS myelin development and repair. We found that myelin regeneration is attenuated in the absence of *Lrp1*; this defect is likely because of its role in OL maturation and myelin biogenesis. Mechanistic studies revealed that *Lrp1* deficiency disrupts multiple pathways implicated in OL differentiation, including AKT activation, cholesterol homeostasis, PPARγ signaling, and peroxisome biogenesis. Moreover, the subcellular distribution of peroxisomes is altered and accompanied by a thinning of cytosolic spaces in OL processes. The impeded differentiation of cells in the OL lineage of *Lrp1* null mice is largely rescued by bath application of free cholesterol and activation of PPARγ. This combo treatment improves peroxisome distribution into OL processes and

formation of myelin sheets. Collectively, we have identified novel roles of LRP1 during CNS myelin development and white matter repair.

CHAPTER I

Introduction: Myelin, A Matter of Fat

1.1 Abstract

Myelin is by far the most specialized membrane structure in the vertebrate nervous system. This delicate assembly features an exceptionally high lipid to protein ratio. This ratio is critical for providing electrical insulation to axons, through which fast and accurate electrical signal conduction is guaranteed. In the central nervous system (CNS), myelin is generated by mature oligodendrocytes (OLs) through a process called myelination. During myelination, migratory oligodendrocyte progenitor cells (OPCs) become static, exit the cell cycle, differentiate, and mature into myelin-producing OLs. Diseases that disturb the development, maintenance, or replacement of myelin lead to functional deficits. When an OL is elaborating membranes during development, it generates almost 100 times its cell body weight within a short period of time. As this process posts a high metabolic demand, it is conceivable that there is an energy checkpoint for OPCs to determine whether to proceed further. In this chapter, the biogenesis of the myelin building blocks, the challenges faced by glial cells, and their metabolic impacts on CNS health are reviewed.

1.2 Introduction: A Necessary Evil? Myelin—An Energy Expensive Structure

1.2.1 Necessity—Myelin supports biological complexity and protects neurons

More than 160 years ago, the word “myelin” was coined by Rudolf Virchow, in a seminal paper titled “On the extensive presence of a substance analogous to nerve marrow in animal tissues” (Virchow 1854)

. Virchow discovered that “brain fat” is the most widespread ingredient in the vertebrate nervous tissue by heating brains in alcohol (Pearce 2003). The

appearance of “neuroglia” observed by Virchow reminded him of bone “marrow” (Greek, μυελός, muelós) (Verkhratsky & Butt 2013). From then on, the term myelin was proposed and followed to date.

In the CNS, myelin constitutes the white matter, which is readily identified by naked eye due to its white-colored, condensed fatty look in brain specimens. Myelin can be crudely separated into compact and non-compact components based on its morphology. Compact myelin is where membrane fuses and spirally envelops a neuronal axon to ensure saltatory conduction of action potentials. Saltatory conduction is beneficial for evolution as it increased the propagation rate up to ~100 fold compared to non-myelinated axons (Boullerne 2016). On the other hand, non-compact myelin components participate in metabolic support through neuron-glia interaction (Nave 2010a). Pathological deterioration of myelin sheaths often leads to secondary neuronal degeneration in multiple CNS diseases (Franklin 2002), which further supports the necessity for greater understanding of biological mechanisms underlying proper myelin formation and maintenance.

Similar to neurons, myelin is stable with little turnover in the adult brain. The majority of myelin is thought to persist throughout the entire lifespan of vertebrates (Smith & Eng 1965, Yeung et al 2014). In contrast to neurons, CNS myelin can regenerate after insults, such as following virus infection, chemical or physical induced demyelination, and immune attack (Franklin & ffrench-Constant 2008). Subsequent to these insults, the process of new myelin generation is specifically referred to as re-myelination. In the CNS, myelin generation is carried out by a specific type of glial cell called oligodendrocyte (OL). The ability of OLs to proliferate, differentiate, and mature into myelin-producing cells is crucial to maintain or restore a healthy CNS (Franklin & Hinks 1999).

1.2.2 **Evil—Myelin burdens the CNS in disease and in health**

Not all attributes of myelin are positive, just like Albert Camus said, “There is no sun without shadow, and it is essential to know the night.”

— **Myelin debris impede neuron and myelin regeneration**

Ramón y Cajal was the first to suggest that myelin components are inhibitory signals to the CNS repair (Ramon y Cajal 1928). The hindrance on axonal growth and regeneration mediated by myelin breakdown products was first established in 1980s (Berry 1982, Caroni & Schwab 1988). Later, Schwab and colleagues isolated myelin proteins and demonstrated a growth inhibitory effect toward primary neurons. They developed a function-blocking antibody (called IN-1) that neutralized the growth inhibitory activity of mammalian CNS myelin *in vitro* and *in vivo* (Schnell & Schwab 1990, Schwab & Caroni 2008). Initially, the IN-1 antibody was raised against a fraction of myelin components; however, a decade later, the IN-1 antigen was discovered and identified as the reticulon family member Nogo-A (RTN4A) (Chen et al 2000, GrandPre et al 2000, Prinjha et al 2000). From then on, findings unlocked a new and exciting field in the search for molecular mechanisms of myelin-associated inhibitory signals during CNS repair (Filbin 2003, Hannila & Mellado 2017). The detail of this topic has been thoroughly reviewed previously and hence will not be covered in this chapter (Baldwin & Giger 2015).

Similar to neurodegeneration, the lingering of myelin debris is a hallmark of CNS demyelinating diseases, such as multiple sclerosis (MS). At the MS lesion site, myelin-producing OLs are rarely observed despite the presence of numerous OPCs. This suggests that the lesion environment is non-permissive for OPC differentiation and axon myelination (Chang et al 2000, Chang et al 2002, Kuhlmann et al 2008, Wolswijk 1998). Similarly, Miller and colleagues supported a novel concept in the late 1990s, implicating reversible suppression signals sent by neighboring myelin as the key to maintaining the immature OPC pool (Robinson & Miller 1999). In line with this hypothesis, Franklin and colleagues showed the removal rate of myelin debris coincided with the extent of myelin repair (Ruckh et al 2012, Shen et al 2008, Shields et al 1999, Zhao et al 2006). Further evidence showed that purified myelin impairs remyelination *in vivo* (Kotter et al 2006); however, molecular players for the myelin-mediated remyelination block are not clear. Lipase treatment of myelin does not alter the inhibitory properties, suggesting that myelin-associated proteins

might in fact be playing a role (Syed et al 2008). Of note, common myelin-associated axonal regeneration inhibitors, such as Nogo-A, Mag, and OMgP, do not show a negative regulation of myelination *in vitro* (Plemel et al 2013, Syed et al 2008). Instead, these myelin-associated inhibitors, and in particular Nogo-A have been proposed to participate in the precise myelination by altering the lengths of internodes (Chong et al 2012).

— **Myelin clearance triggers excessive inflammatory responses**

While the clearance of myelin debris is beneficial for CNS regeneration, clearance of myelin by microglia and blood-derived macrophages triggers a strong inflammatory response (Wang et al 2015, Williams et al 1994). As myelin debris accumulates over time after fiber injury, the activation of immune cells follows (Gensel & Zhang 2015). For instance, in the case of spinal cord injury (SCI), myelin debris appears within 24 hours (Buss et al 2005, Ek et al 2012, Imai et al 2008), as does the arrival of neutrophils and complement proteins (Kopper & Gensel 2017). The debris then continues to increase for the following seven days, leading to microglia activation and astrogliosis. In the mammalian CNS, myelin debris sometimes persists for years (Becerra et al 1995, Vargas & Barres 2007). While the activation of monocyte-derived macrophages peaks only at the first 1-2 weeks post-SCI prolonged inflammation persist for months. Upon infiltration, immune cells were found to express phagocytotic receptors (Fleming et al 2006), and phagocytes are loaded with myelin debris for weeks (Greenhalgh & David 2014, Vargas & Barres 2007, Wang et al 2015).

There are controversial studies concerning whether myelin loaded immune cells are reparative or pathological for CNS health and function with no clear-cut conclusions (Kopper & Gensel 2017). Without well-identified mechanisms, some studies suggest myelin-laden immune cells can be pro-regenerative through production of anti-inflammatory molecules (Boven et al 2006, Vogel et al 2013) and inhibition of pro-inflammatory genes expression (Spann et al 2012). However, in the case of myelin-triggered pro-inflammatory responses, downstream signaling

following complement activation is suspected to lead to overproduction of cytokines and release of reactive oxygen species (ROS), both of which are destructive. Furthermore, OLs are not mere bystanders, but active generators of immune-regulatory factors to limit pro-inflammatory immune cascades that may result in excessive tissue damage (Peferoen et al 2014). Much like a dominos effect, this prolonged pro-inflammatory signal will lead to progressive demyelination and neuron degeneration, which will ultimately give rise to even more debris. Activated by greater accumulation of myelin debris, more immune cells will infiltrate and get stimulated, therefore igniting a vicious cycle. Collectively, myelin clearance putatively tips the balance of the system and further burdens it with secondary damage.

— **Metabolic vulnerability–an energy price paid to myelinate**

While myelin serves its duty by insulating axons and protecting neurons from extracellular insults, this unique arrange burdens the nervous system. Due to the long length of the axons, it is not energetically efficient to access metabolites and essential organelles from the cell body over a long distances to supply the distal tip. For this reason, local uptake of trophic factors and metabolites becomes a critical alternative in order to meet timely energy requirements (Nave 2010b). Different from the peripheral, the metabolic system in the CNS is largely segregated from the circulation by blood brain barrier (BBB). BBB limits the rate of exchange of certain nutrient or waste. Moreover, the density of capillaries is ~50% less in white matter than in gray matter, which further limits blood-derived nutrient supply to the white matter (Heinzer et al 2008). The scarcity of readily available metabolites becomes an even more pressing issue during active myelination, where rapid production, transport, and use of a massive amount of proteins and lipids are demanded. Based on morphometric analysis, a single rat OL can produce ~50 myelin segments (called internodes), generate 0.1-2 mm^2 of membrane surface area (~1000 times more of its cell body), and synthesize proteins at a rate of ~10^5 molecules per min (Pfeiffer et al 1993). It is speculated that at this synthesis rate to match demands, there is little room and capacity for detection and correction of protein miss-folding or

faulty lipid transportation. If not properly executed, this can lead to OL death and hypomyelination of axons. Moreover, during lipid/protein synthesis, oxidative phosphorylation, or generation of ROS, poses an especially great threat to the health of OPCs (Butts et al 2008). Collectively, myelinated nervous system requires a great deal of energy expenditure, and a delicate balance, maintenance of which is likely susceptible to additional metabolic disturbances.

1.2.3 **Standing Questions: The Focus of This Chapter**

The long-held belief that the vast majority of brain disorders have a neuronal origin is slowly but certainly being replaced by the emerging notion that the major cause may in fact be defects with "neuroglia", including OLs. (Verkhratsky & Butt 2013). This paradigm shift was held dear by Rudolf Virchow, who said "This very interstitial tissue of the brain and spinal marrow is one of the most frequent seats of morbid change" (Virchow 1858). More recently, this hypothesis is further supported by the innumerable body of work, spearheaded by Ben Barres (Liddelow et al 2017, Wang et al 2012). Since all disorders, including demyelinating diseases, can be defined as a form of homeostatic failure in one way or another, understanding how myelin is synthesized, maintained, and repaired in terms of metabolic regulation becomes especially vital. Acknowledging all the presence of extensive literature on neuroglial function is beyond the scope of this work, I will focus on the following aspects: (a) Morphology, composition, and function of myelin; (b) selective protein and lipid components' impact on myelin development and integrity; (c) cell biology of myelin development in health and disease; (d) homeostatic and metabolic regulators and their cross-talk mechanisms during myelin formation.

1.3 **Build the White Matter—Myelin Structure, Composition, and Biology**

1.3.1 **Myelin Morphology**

Myelin structure could not be clearly studied until the advent of the transmission electron microscope (TEM) in the 1950s. The knowledge we gained through studying ultrastructure of myelin by TEM led us to a new era. Even though 2D EM has its limitations to fully describe the complex axon-OL interaction *in vivo*,

the foundation laid by these studies still serves as the foundation of our understanding of myelin morphology. The sub-regions of myelin can be defined by its appearance under the TEM. As shown in Figure 1.1, it can be categorized as electron dense (compact) versus electron light (non-compact) domains; membrane insulated (internode) versus opened (node) areas (Figure 1.1). The general feature of each category and how it impacts the CNS function are described below.

— **Compact myelin**

Compact myelin is formed by a tongue-like cytoplasmic membrane that extends from the cell body and wraps around the axon in a spiral fashion. The leading myelin extension invades inward, squeezes through the gap between axon lamella and previously established myelin, and at the same time expands sideways to accommodate the longitudinal growth of axons (Snaidero et al 2014). Myelin compaction is driven by MBP polymerization by forming a dense meshwork between two cytoplasmic membrane layers, called major dense line (MDL) under TEM (Aggarwal et al 2013). On the contrary, the interface between wraps is called intraperiod line (IPL) (Figure 1.1d-e). Myelin compaction starts from the outmost layer of myelin wraps and delays the leading growing zone for less than four wraps (Snaidero et al 2014, Snaidero & Simons 2014). Each wrap is ~14 nm apart (myelin periodicity) in dehydrated condition (Arroyo & Scherer 2000), and the number of wraps for each axon positively correlates with axon diameter but varies between species and brain regions (Verkhratsky & Butt 2013). In the mouse spinal cord, ~10-60 wraps per axon were observed from axons ranging from 1-6 μm in diameter (Hildebrand & Hahn 1978). A ratio (Greek letter G, Γ) of axon diameter (d^2) divided by fiber diameter (d^1) is commonly used to describe the property of a myelinated axon. This ratio was first introduced back in 1937, now called *g*-ratio (Schmitt & Bear 1937). It is believed that to some extent there exists an optimal *g*-ratio (~0.77 in the CNS) that correlates with fiber conduction velocity and its biological functions (Chomiak & Hu 2009).

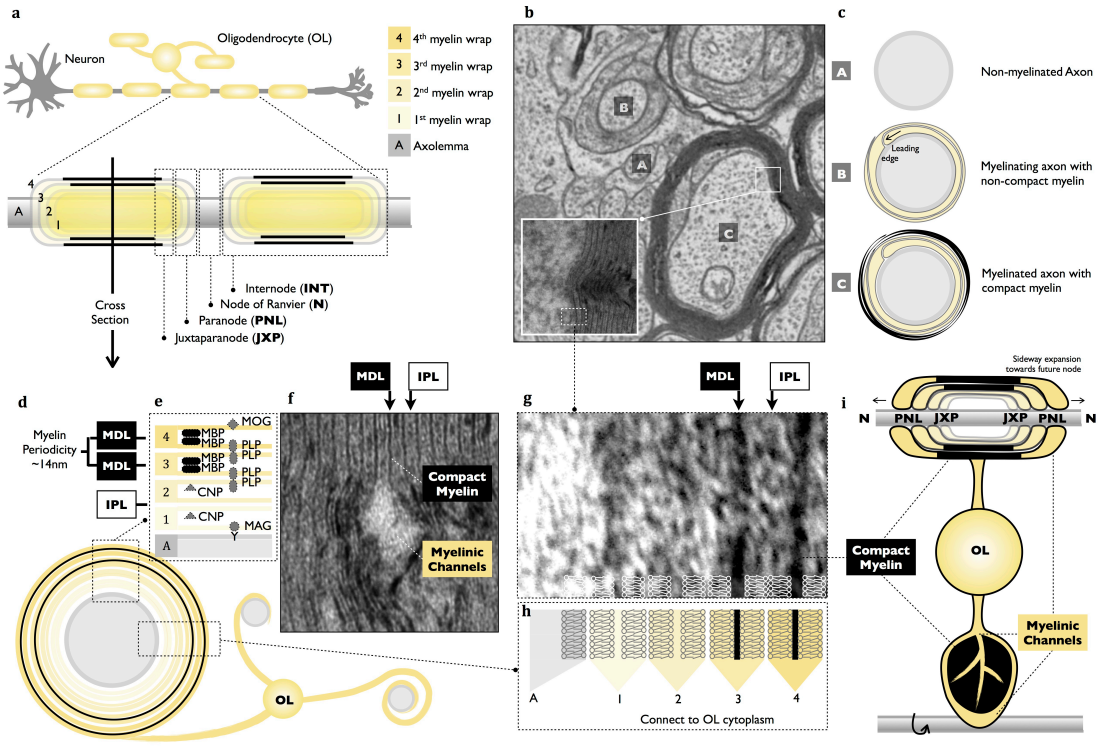

Figure 1.1: CNS myelin anatomy and ultrastructure
(a) Myelinating oligodendrocyte produces myelin sheathes on axons and forms nodal structures including internode (INT), the node of Ranvier (N), paranodal loops (PNL), and juxtaparanode (JXP). An example of the membrane sequence from the interior axolemma (A) to outer myelin wraps (1-4). Cross-sectioned view of an INT shown in d. (b) A TEM image from P21 mouse optic nerve showing non-myelinated axon ('A'), myelinating axon with a few non-compact myelin wraps ('B'), myelinated axon with compact myelin ('C'). The insect is showing a close-up membrane sequence from a myelinated axon. The area of axolemma to the 4th myelin warp is further enlarged in g. (c) Illustration of the axons from b with different myelin status. Myelin compaction delayed the myelin leading edge 2-3 wraps. (d) A cross-section view from a. Myelin periodicity is defined by the repetitive pattern of compact-myelin. Compact myelin appears dark under the TEM, called major dense line (MDL). The interface in between wraps appears light under the TEM, called interperiod line (IPL). The protein composition and membrane organization were enlarged in e and h. (e) The localization of the myelin structural proteins. MOG located at the abaxonal membrane (the outmost wrap of myelin), MBP located in the cytoplasm of myelin sheath to form a dimer and initiating myelin compaction, PLP located in the myelin membrane to form dimer between wraps, CNP anchor to the cytoplasmic membrane in the non-compact myelin, and MAG locate at the adaxomal membrane (the innermost wrap next to axon membrane). (f) An enlarged view of myelin periodicity. (g) An enlarged view of MDL and IPL from d. (h) An illustration depicts the orientation of the lipid bilayer in each wrap aligned with an image from the TEM. (i) A longitudinal section of an INT and an un-rolled myelin sheath. Myelinic channels run within compact myelin during development. This figure was created by Jing-Ping Lin.

Compact myelin is part of the internode, where the number of myelin segments (~20 to 60 internodes) that is generated by a single OL varies in different brain regions and negatively correlates with internodal length (Matthews & Duncan 1971). There is not a uniformed internodal length for each axon; however, evidence shows that it positively correlates with the diameter, the length, and the secondary growth of axons rather than OL intrinsic traits (Fanarraga et al 1998, Gledhill & McDonald 1977, Hildebrand et al 1994, McDonald & Ohlrich 1971, Murray &

Blakemore 1980, Simpson et al 2013). Little is known about which axon and at where along the axon myelination is initiated (Simons & Lyons 2013). However, myelination seems to favor axons that are >0.4 μm in diameter (Lee et al 2012a) and demyelination appears to be more prominent on the smaller axons (Cellerino et al 1997, Lin et al 2017, Samorajski et al 1986, Winters et al 2011). Recently, a two-mode model of myelination was put forward by Simons and colleagues that explained its region-dependent variation. There is possibly a "basal" myelination mode that follows the chronological and topographic sequence, and a "targeted" myelination mode that is responsible for plasticity modification (Snaidero & Simons 2017).

It is believed that compact myelin formation is beneficial evolutionarily. It has been argued that myelin is the last "true invention" of the vertebrates. Myelin enables rapid conduction and economic space occupation, as well as participates in the regulation of complex neuronal activities (Baumann & Pham-Dinh 2001, Nave 2010b). Almost all vertebrates possess compact myelin, except the oldest aganathan cyclostomata, such as ostracoderms—jawless fish (Bullock et al 1984). On the contrary, invertebrates and ostracoderms acquired a form of glial ensheathment that functionally resembles vertebrate myelin (Bullock et al 1984, Zalc 2006). In comparative studies of giant nerves from shrimp or squid to small caliber myelinated axons from mammals, we learned that non-myelinated axons spend much more energy and space to sustain similar firing efficiency (Brady et al 2005, Hartline & Colman 2007, Hildebrand et al 1993). Since it is hard to compare conduction velocity from same-diameter axons, in the same species, with or without myelin, it is only an estimation that there exists a ~100 fold change. Some quantitative insight was provided by Raminsky and colleagues using an induced demyelinating model of un-dissected nerve fibers in rat ventral roots. Their study showed that the integrity of compact myelin determines the conduction speed and correlates with the prolonged response time for the second. It appears that an optimal internodal length of 1mm shows the fastest signal conduction (50m/s) at 37°C. Of the same setting, the velocity slowed down ~25 fold in demyelinated fibers

induced by diphtheria toxin injection (Rasminsky & Sears 1972). Factors that initiate, regulate, or maintain compact myelin stability were clarified to be independent of myelin biogenesis, which is reviewed in the section1.3.2 (Griffiths et al 1998).

— **Node of Ranvier, paranodal junction, and juxtaparanode**

The node of Ranvier is a name given by Louis Ranvier to describe the exposed regions on an axon of the PNS (frog sciatic nerve). Which were thought to be the possible outlets used by neurons to acquire metabolic supports (Barbara 2005, Ranvier 1871). The very existence of equivalent node of Ranvier-like structures for the CNS was debated for decades. It was first depicted and reported by Cajal (Ramon y Cajal 1928), however it took another 20 years to be experimentally confirmed with advanced staining methods using methylene blue (Feindel et al 1948). Nodes typically are found to be wider in the CNS than in the PNS, ranging from ~0.5-5 μm and ~0.25-1.5 μm respectively (Hess & Young 1952, Jacobs 1967, McDonald & Ohlrich 1971). Nodal gap length varies throughout different brain regions and has no significant correlation with axon diameter in the CNS (McDonald & Ohlrich 1971). Nodal gap length, however, negatively correlates with the axon diameter in the PNS (Jacobs 1967). In some cases, these gaps are contacted by astrocytes or OPCs without a fully understood function (Black & Waxman 1988, Butt et al 1994, Butt et al 1999). A cluster of 10nm particles residing at the outer leaflet of the axolemma was observed by freeze-fracture EM. The density of these particles (~1200/μm^2) (Rosenbluth 1976) match the estimated density of sodium channels at the node (Chiu 1980, Waxman & Ritchie 1985). It is well appreciated now that these voltage-gated sodium channels are responsible for membrane depolarization to fire action potentials (APs). A drastic decrease of axolemma particle density (~100/μm^2), synaptic vesicles, microtubules, and mitochondria occur at the paranodal regions, suggesting there is a bottleneck of axonal transport in both directions (Fabricius et al 1993, Rosenbluth 1976, Salzer 1997).

Nodes are guarded by paranodal junctions (PNJ) (Figure 1.1a), through which the subdomains of the axolemma are divided. The morphology of the peripheral PNJ was first described by Robertson about 60 years ago, in which a series of overlapping loops formed by the Schwan cells are in close contacts with axonal membrane adjacent to the node (Robertson 1959). Later in the CNS, similar transverse bands with relatively smooth surfaces were observed, and their role as the physical barrier for particle distribution was suggested (Rosenbluth 1976). Current evidence indicates that PNJ functions in sealing the myelin sheath to axons, blocking the lateral movement of ion channels, and connecting channels to influence nodal activity/metabolites trafficking (Rosenbluth 2009). Paranodal loops formed a septate-like junction with the axolemma, which is the largest intercellular junction that can be found in the body of a vertebrate (Rasband & Peles 2016). It is still unclear if the location of nodal structures is predetermined by glial or axonal signals, but it is believed that the PNJs is capable of adjusting their own position towards the future node to accommodate the lateral growth of the myelin sheath (Dupree et al 1999, Poliak & Peles 2003, Rasband & Peles 2016, Snaidero & Simons 2017). Current knowledge shows that this attachment is carried out by Neurofascin155, Caspr, and Contactin during adjustment (Pedraza et al 2009, Zonta et al 2008), and stabilized by Ankyrin-G at the later stage (Chang et al 2014, Peters et al 1991, Wiley & Ellisman 1980).

The other distinct intramembranous cluster of particles in the CNS were observed by freeze-fracture EM. These particles were found dense at the region adjacent to the PNJ and diffused away towards the internodal area (Rosenbluth 1976). Later, similar "rosette" structures about 10nm in size were found in the PNS and the membrane harbored these rosettes acquired its name, juxtaparanodes, because of its localization (Gledhill & McDonald 1977, Kreusch et al 1998, Murray & Blakemore 1980, Rosenbluth 1976). Juxtaparanode describes a range of ~10-15 μm region at both ends of an internode. It is believed these rosette particles are segregated by PNJ from the sodium channels at the node to carry out distinct functions for electrical signal transduction. Subsequently, evidence showed that

these clusters correspond to the distribution of Kv.1.1 and Kv.1.1 potassium channels (Rasband et al 1998, Vabnick & Shrager 1998, Wang et al 1993, Zhou et al 1998). Current knowledge supports that voltage-gated potassium channels are important in preventing abnormal firing during development (Vabnick et al 1999) and modulating APs in adults by dampening the immediate excitability to repolarizing the AP in myelinated fibers (Hille 1992, Smart et al 1998, Zhou et al 1998).

— **Non-Compact Myelin**

Non-compact myelin components are regions in which myelin membranes do not fuse which harbor cytoplasm which connect to OL cell body. At these cytoplasm pockets the metabolic substances can be exchanged and transported (Figure 1.1i). The nomenclature for these cytosolic tunnels in the CNS was not unified—including the Schmidt-Lanterman Incisure-like tunnels/clefts, the inner/outer/lateral tongues/lips, the radial components, and the paranodal loops (Lazzarini 2004). However, these "myelinic tunnels" are crucial with their influence on neuronal function (Nave & Werner 2014). The existence and morphology of these cytosolic tunnels in the compact myelin were debated for a long time, as they were rarely found in the adult CNS, as opposed to PNS Schmidt-Lanterman Incisures that persist into adulthood. This ultrastructure was first reported by Peters 50 years ago; he reported dense lines radially arranged thoroughly or partially across the thickness of the myelin sheath in a cross-sectioned optic nerve (Peters 1961). These arrangements looked like tight junctions, and later work found that they contained caludin-11/oligodendrocyte-specific protein (OSP), a family of tight junction proteins (Bronstein et al 1997, Gow et al 1999, Morita et al 1999).

Given that myelinic tunnels are hard to visualize, their structural details were not revealed until recent technical advancements in EM and live imaging of myelin. Traditional EM studies often result in a collapse of intracellular spaces during sample preparation, specifically fixing with glutaraldehyde and dehydration of tissue. The new high-pressure freezing EM method allowed fixation-free sample

preparation, and therefore improved tissue preservation and helped maintain its native architecture (Mobius et al 2010). Recently, by combining 3D EM reconstructive techniques, evidence showed that these tunnels are largely present during myelin development and disappear after myelin compaction (Snaidero et al 2014, Snaidero & Simons 2014). Microinjection of Lucifer Yellow into OL or myelin sheaths further demonstrated that these tunnels are connected to the cell body and allow small substances to pass (Velumian et al 2011). Furthermore, we learned that the myelinic tunnels are maintained by the expression of CNP, which counteract MBP-mediated myelin compaction. It is suggested that the preservation of these myelinic tunnels is the key to make myelin dynamic possible and impact metabolite exchange during axon-OL interactions (Snaidero & Simons 2017, Snaidero et al 2017).

1.3.2 **Myelin Building blocks**

Lipids and proteins compose the majority of myelin after water. The lipid portion is much higher in myelin (~80%) compared to plasma membrane (<50%) when measured in dry weight (Norton & Poduslo 1973, Rumsby 1978). While myelin proteins constitute the lower proportion, they greatly impact myelin morphology and structure due to their special conformation and surface charge. Generally, PMP22 and P0 are expressed exclusively in the PNS myelin while MOG and MOBP are only found in the CNS myelin. The fact that MAG, MBP, and PLP/DM20 are expressed both in the PNS and CNS myelin, but in different proportions is worth noting (Nave & Werner 2014). Selective myelin lipids and proteins will be highlighted in the following sections, where Table 1.1 lists some of this information with more available in previous reviews (Brady et al 2005, Martenson 1992).

1.3.2.1 **Myelin Lipids**

Lipids are “the center, life and chemical soul of all bioplasm.”—Thudichum, 1884.

More than hundred years have passed after this statement was uttered without losing its validity, especially for myelin biochemistry. Due to its high lipid abundance, the brain is the host region for discovery of many of the complex lipid structures Generally, lipids can be classified into simple, complex, and derived lipids based on their constitution (Figure 1.2). Lipids can also be categorized by their biological function as energy storage (triglycerides), structural components of membrane, or signaling messengers (steroid hormones and inositides). There are no myelin-specific lipids; however, some lipids have a heavy content of myelin. When dry weight is measured, phospholipids are the most abundant (~40%) lipid in myelin, but they are not as prevalent when compared to the dry weight composition of gray matter (~70%) (Martenson 1992). However, when molecular numbers are the unit of measurement, the ratio amongst cholesterol, phospholipids, and galactolipids is 4:3:2 in myelin differing from any other cell membrane composition (Rumsby 1978). Myelin lipids are qualitatively similar among species and between PNS and CNS with regional variations. For example, a higher lipid ratio was found in the spinal cord compared to the brain, glycolipids are exclusively located at the outer-monolayer of a lipid-bilayer, and sphingolipids are absent from mitochondria and low in ER membrane. Readers are directed to Table 1.1 and previous reviews for detail information (Lazzarini 2004, Martenson 1992, Morell & Norton 1980).

— **Cerebroside**

During early brain development, the synthesis rate of galactosylcerebroside well predicted the accumulation progress of the myelin. Cerebroside together with cerebroside sulfate (sulfatide), composes ~30% of total lipids in the myelin brain. Given the distribution specificity and quantity, it was recognized as an essential lipid for CNS myelin biogenesis. Surprisingly, in a null mice line that was generated to block the terminal step of cerebroside biosynthesis, the gross structure of myelin turned out to be largely normal. However, progressive neurological abnormalities were present and got worsened as these mice aged. Specifically, deformed paranodal loops (intercellular tight junctions) were prominent, leading to the

conclusion that cerebrosides are important for axon-glial interaction. Further studies showed that this cell-cell and cell-substratum interaction impacts nerve regeneration (Brady et al 2005).

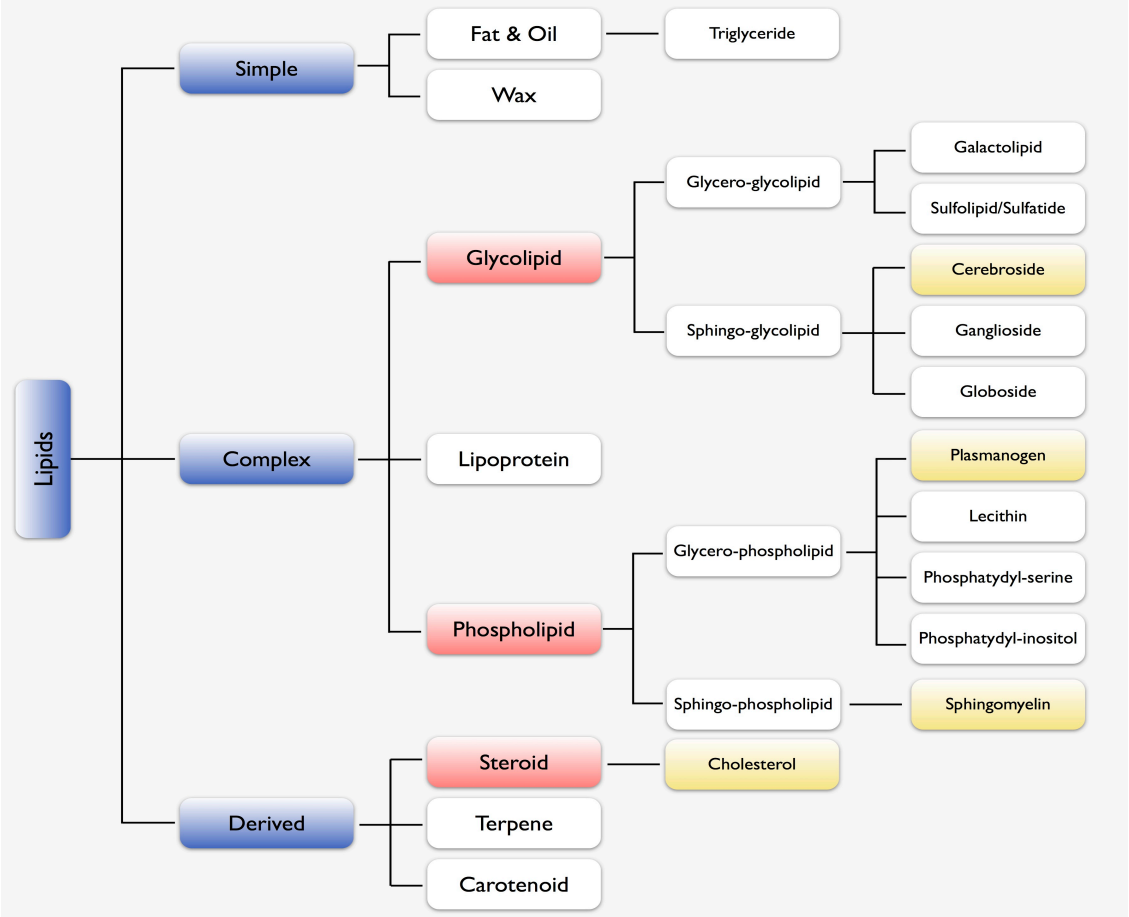

Figure 1.2: A diagram highlight the top three lipid types in the myelin
This figure was created by Jing-Ping Lin.

— **Plasmanogen/Sphingomyelin**

Plasmanogen and sphingomyelin fall under the class of phospholipids, which compose >40% of total lipids in myelin. Phospholipids in myelin have similar roles as in other plasma membranes, and serve as structural components and in some cases signaling messengers. Plasmanogen constitutes ~30% of the myelin phospholipids. It is synthesized in peroxisomes and is important for myelin development (Di Biase et al 1990, Horrocks 1967, Linington et al 1980).

	CNS Myelin			Myelin		White Matter	Gray Matter	
Sample	% of total myelin protein dry weight			**Human[c]**	**Rat[c]**	**Human[c]**	**Human[c]**	**Rat[c]**
				% of total myelin dry weight				
Protein				**30.0%**	29.5%	39%	55.4%	56.9%
	PLP	50% [a]	17% [b]					
	MBP	35% [a]	8% [b]					
	CNP	5% [a]	4% [b]					
	MAG	1% [a]	1% [b]					
	MOG	n/a	1% [b]					
	Others	~10% [a]	67% [b]					
Lipid				**70.0%**	70.5%	54.9%	32.7%	37%
	Cholesterol			**27.7**	27.3	27.5	22.0	23.0
	Total Galactolipids			**27.5**	31.5	26.4	22.0	23.0
	Cerebroside			22.7	23.7	19.8	5.4	14.6
	Sulfatide			3.8	7.1	5.4	1.7	4.8
	Total Phospholipids			43.1	44	45.9	69.5	57.6
	Plasmalogen			12.3	14.1	11.2	8.8	11.6
	Lecithin			11.2	11.3	12.8	26.7	22.0
	Sphigomyelin			7.9	3.2	7.7	6.9	3.8
	Phosphatidylserine			4.8	7.0	7.9	8.7	7.2
	Phosphatidylinositol			0.6	1.2	0.9	2.7	2.4

a. (Deber & Reynolds 1991, Morell & Norton 1980, Norton & Poduslo 1973, Rumsby 1978)

b. (Jahn et al 2009)

c. (Lazzarini 2004, Martenson 1992, Rumsby 1978)

Table 1.1: The comparison of CNS myelin composition
Each percentage indicated percentage of total myelin protein dry weight or total myelin dry weight as indicated. The information are gathered from several reviews as noted with a, b, and c. This table was consolidated by Jing-Ping Lin.

— Cholesterol

Cholesterol comprises ~30% of total lipids in the myelin and is enriched at the extracellular face of the bilayer. Particularly, cholesterol is the key molecule to form lipid rafts that serve as information signaling platforms and mediate membrane curvature during fusing events. Other than its contribution in membrane structure, cholesterol is considered a critical element, especially during CNS development (Herz & Farese 1999). More specifically, high cholesterol level has been found to act as a critical rate-limiting factor for myelin production. Genetic or pharmacological manipulation of cholesterol synthesis, trafficking, or uptake has been shown to perturb myelin formation both *in vitro* and *in vivo* significantly (Saher & Stumpf 2015, Schmitt et al 2015). Therefore, dysregulation of cholesterol

homeostasis is associated with a wide spectrum of CNS neurodegenerative and myelin disorders (Courtney & Landreth 2016, Saher & Stumpf 2015). While we cannot emphasize enough the importance of cholesterol homeostasis to the brain, only recently did we start to understand the regulation of cholesterol in the CNS at a cellular level. Since cholesterol is toxic, more is not better. The fine regulation of transcriptionally controlled biosynthetic pathways, cellular uptake, esterified storage, and cellular efflux needs to be considered to maintain a healthy nervous system. Cholesterol homeostasis and how it impacts the CNS myelination are further reviewed and discussed in Chapter IV.

1.3.2.2 **Myelin Proteins**

Myelin proteins, except for MBP, are neither dissolvable in aqueous solution nor easy to extract. The initial characterization of the constitution was from a cytoskeletal/lipid matrix that is extracted from myelin using nonionic detergents (Martenson 1992). It is believed that myelin structural proteins (such as PLP, MBP, CNP, and MAG) constitute >90% of myelin proteins in the CNS (Table 1.1, left)(Rumsby 1978). However, recent proteomic data corrected the relative abundance of previously defined proteins to comprise ~35% of total myelin-associated proteins with the advance of technology (Jahn et al 2009). In this section, the general feature of each myelin protein and their impact on the health of the CNS are reviewed. Specific protein trafficking and assembly are discussed in Chapter IV.

— **PLP/DM20: Proteolipid Protein**

PLP (30kDa) is the most prevalent protein in CNS myelin. Together with its alternative splice form DM20 (M_r 20,000), PLP is embedded in the myelin membrane to stabilize IPL. Abnormally condensed IPL was observed in both PLP knockout mice and PLP mutants (*jimpy* mice). PLP is transcriptionally regulated by myelin transcription factor 2 (MYT2), Yin Yang 1 (YY1), thyroid hormone receptor (THR), and peroxisome proliferator-activated receptor (PPAR) (Lazzarini 2004). The mRNA of DM20 is expressed early in the OPCs before the onset of myelination has an unknown function. Myelinating OLs express PLP/DM20 proteins and thus

they were used as mature OL markers. However, PLP/DM20 are dispensable for the formation of compact myelin. Knockout mice showed relatively normal myelin, motor function, and lifespan. Later in life, the integrity of myelin decreased following osmotic shock, axons appeared swollen, and neuron degeneration occurred. Over-expression of mutant PLP, on the other hand, showed severe hypomyelination and early death in both mouse model and human patient (Pelizaeus-Marzbacher Disease, PMD). Interestingly, the protein structure of PLP resembles that of a channel protein family, lipophilin, suggesting that PLP may serve as a "pore" protein to exchange charged molecules on the myelin membrane. Cultured cells that express PLP, but not DM20, showed a decreased pH in the media, supporting the idea that PLP can sense and regulate the extracellular ionic environment (Lazzarini 2004).

— **MBP: Myelin Basic Protein**

MBP mRNA is alternatively spliced, resulting in protein isoforms that are 21.5, 18.5, 17.2, 17, and 14 kDa in size. MBP is localized at the cytoplasmic surface of the bilayer to form MDL (Figure 1.1) after myelin compaction. The positive surface charge of MBP gives its name, and no specific tertiary structure and folding were found. The mRNA of MBP has a peri-nuclear distribution in OPCs; however, MBP mRNA is transported to OL processes and locally translated during myelination. Spontaneously derived MBP mutant mice (*shiverer* mice) showed hypomyelination and problematic myelin compaction (Chernoff 1981). Recently, it was shown that MBPs form a meshwork to serve as a size filter leaving out large molecular weight proteins such as CNP and MAG (Aggarwal et al 2013, Aggarwal et al 2011, Simons et al 2012). Overexpression of MBP leads to premature myelin compaction. Although there had been no previous established correlation of MBP with human disease, a recent study showed variation of the MBP gene predicts MS disease progression (Zhou et al 2017).

— **CNP: 2’3’-cyclic nucleotide 3’-phosphodiesterase**

CNP mRNA is alternatively spliced, giving rise to two proteins detected at 46 and 48 kDa molecular weight in the CNS myelin. CNP acquires its name by the structural similarity with phosphodiesterases; however, if the enzymatic function of CNP has a physiological role in the vertebrate myelin (Myllykoski et al 2016, Raasakka & Kursula 2014). CNP is not localized at compact myelin; instead, it is a crucial component for the maintenance of non-compact myelin channels. It has been shown that CNP binds to cytoskeletal elements (tubulin and actin) to promote cellular growth. Of note, CNP amino acids exhibit a similarity to RNA-processing enzymes with an unknown function. The mRNA of CNP is detected in OPCs, whereas the protein’s expression starts with pre-myelinating OLs and persists throughout the consecutive stages. For this reason, CNP is used as an OL differentiation marker. Similar to PLP-null mice, CNP-null mice showed relatively normal myelin formation in young animals. Later in life, axon swelling, neuron degeneration, and premature death were observed. Interestingly, CNP overexpression led to myelin defect in transgenic mice, and the following potential mechanism is recently proposed: CNP antagonizes the function of MBP to prevent premature myelin compaction. CNP preserves cytosolic space in myelin, such as paranodal loops, to ensure the possibility of substances exchange (Snaidero et al 2014). The balance between protein level of CNP and MBP determines the integrity of myelin structure (Snaidero et al 2017).

— **MAG: Myelin-associated Glycoprotein**

MAG was first found in myelin of rats that were injected with radially labeled fucose 45 years ago when they search for glycoproteins (Quarles et al 1973). MAG mRNA is alternatively spliced to two forms, one with a long C-terminal tail (L-MAG, 72kDa) and one with a short tail (S-MAG, 67 kDa). These two forms are developmentally regulated in rodents. The young and adult animals are dominant in L- and S-form, respectively (Inuzuka et al 1991, Lai et al 1987, Pedraza et al 1991, Tropak et al 1988, Tropak & Roder 1997). MAG appears to be 100kDa in size with glycosylation and is low at the CNS myelin. The extracellular portion of MAG

contained five Ig domains, and it showed high morphological similarity with neural cell adhesion molecule (NCAM). MAG is not present in compact myelin, but is localized at the adaxonal membrane where it connects myelin sheath to the axolemma. Similar to other myelin protein deletion, MAG-null mice show relatively normal myelination. However, there were increased incidents of repeated myelination in the same axon (multiple concentric wrapping), excessive out-folded myelin, smaller axons in caliber, and decreased oligodendrocyte in aging animals, suggesting that MAG might be involved in the axon-glial interaction of sensing the repulsive signals from axons for the efficiency during myelination (Li et al 1994, Montag et al 1994). There is a naturally occurring hypomyelinated mutant (*quaking* mice) that leads to abnormal MAG glycosylation (Sidman et al 1964). Further studies showed that MAG is functionally associated with Fyn. Severe hypomyelination was observed in Fyn null mice, suggesting the involvement of MAG in regulating myelin formation (Lazzarini 2004, Umemori et al 1994).

— **MOG: Myelin Oligodendrocyte Glycoprotein**

MOG is another glycoprotein associated with myelin, first found as the M2 antigen inducing EAE in guinea pig. MOG is only expressed in mammals and can be detected by surface labeling. MOG has one Ig-like domain on the extracellular surface of myelin sheaths. The expression of MOG correlates with the late stage of OL maturation. MOG is the only CNS antigen that can induce both B-cell and T-cell response in EAE model. The myelin structure is grossly normal in MOG null (Lazzarini 2004).

— **Other myelin proteins**

Other than PLP, MBP, CNP, MAG, and MOG, it was thought that there are less than 10% myelin proteins yet to be characterized. With the advance of profiling methods, additional information was gathered from cell-cytometry, proteomics, and RNA sequencing data. There are actually more proteins (~67% of total myelin protein) that were found to have a potential link to myelin/OL (Jahn et al 2009). For review of other myelin proteins that are oligodendrocyte-associated rather than

myelin-associated, such as OSP/claudin-11, OAP-1, Sirtuin2, Integrin, Connexin-32, Neurofascin-155, Caspr, AMPA and NMDA receptors, enzymes that are involved in lipid metabolism, readers are directed to the references listed below (Baumann & Pham-Dinh 2001, Lazzarini 2004, Martenson 1992, Morell 2012, Nave & Werner 2014).

1.3.3 **Myelin Cell Biology—Oligodendrocyte**

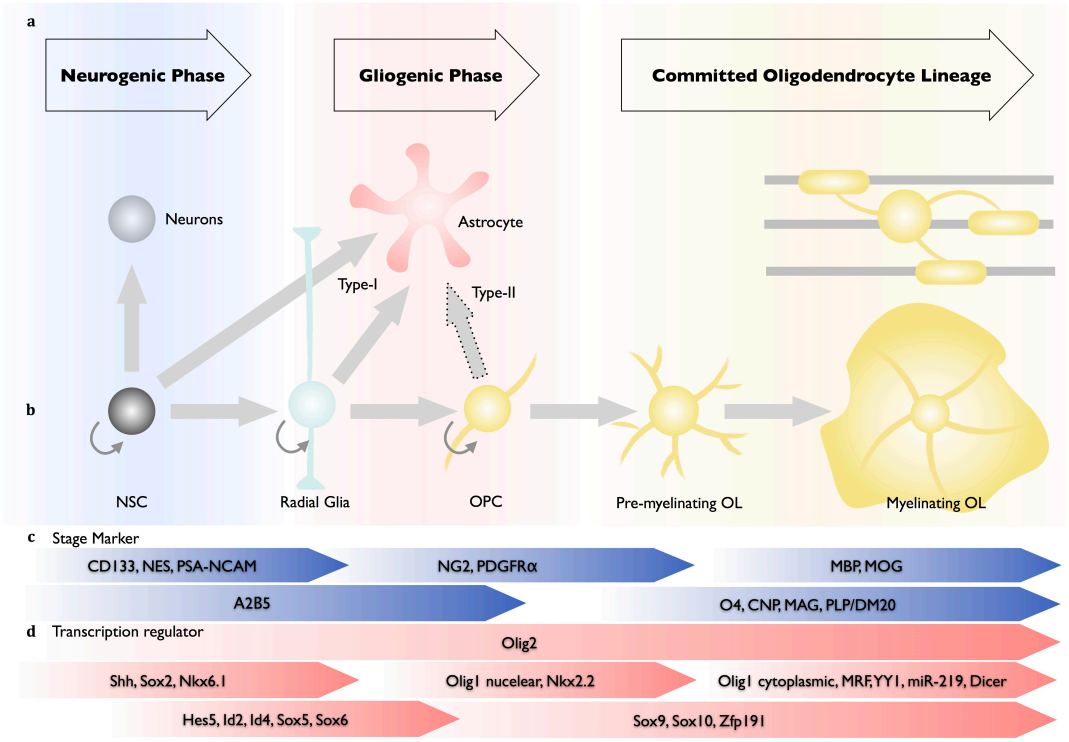

Figure 1.3: Oligodendrocyte lineage commitment and development
(a) CNS progenitors cells go through the neurogenic phase, gliogenic phase, and committed OL lineage. (b) Neural stem cells (NSCs) at the ventricular zone (VZ) give rise to neurons, astrocytes, and radial glia cells at the subventricular zone (SVZ). Radial glia cells give rise to astrocytes and OPCs that are committed to OL-lineage. OPCs differentiate to type-II astrocytes (in culture condition) or pre-myelinating OLs. Pre-myelinating OLs then mature to become myelinating OLs. (c) Progenitor cells can be crudely categorized by the expression of surface selection markers or stage markers with overlapping phases. (d) Lineage commitment is under the control of different waves of transcription factors that gradually changes their levels across developmental stages. This figure was created by Jing-Ping Lin.

Before the era of TEM, Cajal misinterpreted CNS myelin as an organ derived from axon (Ramon y Cajal 1928). It was due to the limitation of light microscopy, which would be still impossible to achieve the required resolution. With the advancement of technology, however, now it is clear to us that a group of cells, that is OL-lineage, undergo dramatic changes to form myelin in the CNS throughout life.

Based on the current nomenclature, myelin biogenesis during development is called myelination, and myelin synthesis after losing pre-established myelin is called remyelination. Although myelination and remyelination are similar in many ways, discovery of the key differences between the two processes critically shaped our understanding of the myelin plasticity. In this section, general overview of myelination, differences during remyelination, and our current understanding of myelin dynamics are addressed.

1.3.3.1 **Myelination: *De Novo* Synthesis**

— **OL-lineage fate commitment**

In neural phylogeny, a neural stem cell (NSC) goes through the neurogenic phase, the gliogenic phase, and then commits to the OL-lineage (Rowitch & Kriegstein 2010). This process is achieved by the influence of transcription factors in a temporal- and spatial- regulated sequence (Figure 1.3). It begins by down-regulation of neuroepithelial factor (*Sox2*), followed by up-regulation of glial-lineage factor (*Sox9*), and the expression of OL-lineage factors (*Nkx2.2*, *Olig1*, and *Olig2*). OL-lineage transcription factors then lead to the expression of PDGFRa, the key marker in OPC ontogeny as it is only expressed by OPCs. From then on, OPCs proliferate and migrate to populate the whole brain, differentiate under the control of extrinsic and intrinsic signals, and become myelin-producing OLs (Zuchero & Barres 2013). From current knowledge, OL-lineage can be sorted based on its expression of surface epitopes, nuclear transcription factors, mitotic and self-renewal potential, and morphology. Of note, OPCs also express less specific antigens, A2B5 and NG2. Additionally, A2B5 is also expressed by neuronal and glial progenitors, and NG2 is also found on pericytes. (Goldman & Kuypers 2015)

— **OPC pool origins**

Not all OPC populations resemble one another. Different subclasses of OPCs are found in the brain and spinal cord, and can be traced to different progenitor domains, where they are influenced by pattern formation signals, including ventral derived (Shh) and dorsal secreted (BMP). Although the origins of the OL-lineage

have been debated for decades, the currently accepted paradigm crudely divides OPCs into three temporal competing waves (OPC1, OPC2, and OPC3) from partially overlapping areas (Figure 1.4). These waves of OPCs are functionally redundant, as they can replace each other and carry out myelination similarly (Kessaris et al 2006, Nery et al 2001, Orentas et al 1999). In the bran, OPC1 is driven by the ventral derived Shh signal during embryonic stage. The *Nkx2.1* expressing OPC1 (Tekki-Kessaris et al 2001) migrates dorsally from the medial ganglionic eminence (MGE) and pre-optic area (POA) to settle throughout the brain (Kessaris et al 2006, Klämbt 2009). Days later, OPC2 expresses *Gsh2/Gsx2* (Chapman et al 2013), originates from the lateral ganglionic eminence (LGE), and migrates dorsally to the cortex (where BMP signal is dominant) to colonize the forebrain (Kessaris et al 2006, Klämbt 2009, Rowitch & Kriegstein 2010). Closer to birth, under the control of *Emx1* (Kessaris et al 2006), OPC3 migrates from the subventricular zone (SVZ) toward the corpus callosum and cortex, integrates with OPC1 and OPC2 populations, and later replaces them to become the main population by postnatal day (P) 10 (Kessaris et al 2006). A pool of OPCs remains as progenitor cells throughout adult life, so that adult OPCs can participate in myelin turnover when needed and have functions independent of myelin biogenesis (De Biase et al 2010). OPCs express AMPA receptors, sodium channels, and form close contact with nodes (Butt et al 1999, Faivre-Sarrailh & Devaux 2013, Rasband et al 1999, Salzer 1997), which may have a physiological role in regulating electrical activities.

— **OPC proliferation / apoptosis**

The number of OPCs to axon ratio is under tight control. During myelin development, excess of OPCs are generated and subsequently eliminated by apoptosis (Barres & Raff 1994, Raff et al 1993, Trapp et al 1997). OPCs compete for the limited source of survival signals such as PDGF-A, FGF-2, IGF-1, NT-3, and CNTF to proliferate and maintain (Barres et al 1994) (Miller 2002). Electric signals (Gibson et al 2014) are also shown to promote OPC proliferation. Sexual dimorphism plays a role in OL proliferation and apoptosis. Whereas more OLs were found in male mice, OPC proliferation is more active in female (Cerghet 2006).

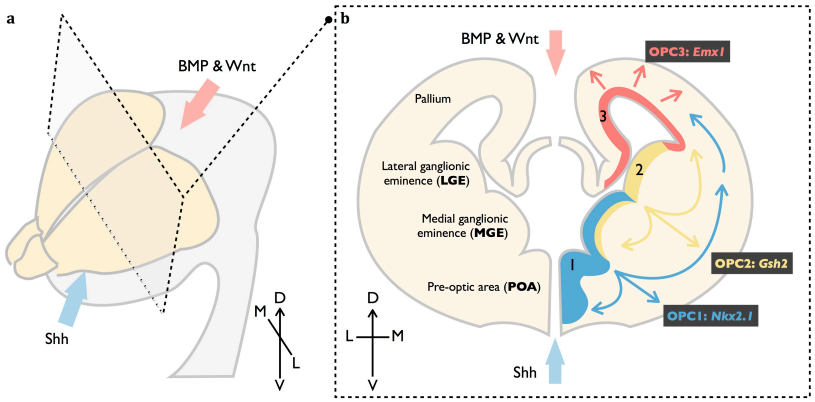

Figure 1.4: The origin of OPCs under the influence of pattern formation during development
(a) Ventral derived Shh signal and dorsal originated BMP/Wnt signals direct the development of CNS progenitor cells. Cross-sectioned view shown in b. (b) Three waves of OPCs migrate to colonize the whole brain following a temporal sequence. Shh: sonic hedgehog; BMP: bone morphogenetic proteins; LGE: lateral ganglionic eminence; MGE: medial ganglionic eminence; POA: Pre-optic area; OPC: oligodendrocyte progenitor cell. This figure was created by Jing-Ping Lin.

— OPC migration

The CNS is built by the long journey of neuronal cells that move radially and tangentially from their place of origin. Compared to neurons and astrocytes, OPCs migrate most extensively and disperse evenly in space to tile the entire brain (Bergles & Richardson 2015, Goldman & Kuypers 2015, Levine et al 2001, Richardson et al 2006, Trotter et al 2010). Both secreted (growth factors: PDGF, FGF, and HGF; chemotropic molecules: netrin and secreted semaphorins; chemokine: CXCL1) and contact-based (extracellular matrix or cell surface molecules) signals have been found to guide OPC migration. However, it was not until recently that we could directly visualize OPC movement. It was demonstrated beautifully by cortical slice culture showing that OPCs migrate towards their future destination by crawling along and jumping between vasculatures (Tsai et al 2016). A defect in vasculature structure but not pericytes hindered the movement of OPCs. Mechanistic studies further showed that Wnt-Cxcr4 signaling is critical in regulating OPC-endothelial interactions. Imaging studies showed that OPCs are constantly "sampling" the environment by extending and retracting cellular processes during migration before they settle for myelination (Hughes 2013, Kirby et al 2006).

— **OPC differentiation/maturation**

160 years after the discovery of myelin, it is still unclear at where the first myelin segment is initiated on the axon, how a single OL myelinates different axons at the same time, and what factors decide the volume of the myelin generated per OL to accommodate the needs of each axon. Instead of a mechanism derived by the internal clock, OPC differentiation is considered to result from the release of local suppressor cues (Emery 2010). Further evidence indicated that OPC differentiation is influenced by neuron electrical activity (Gibson et al 2014), spatial density of OPCs, cues from astrocyte/microglia/macrophage, but less relies on the axonal molecular signals. This discovery is certainly surprising, as the myelin differentiation strongly correlates with neuronal development. On the contrary, this is indeed the case for the PNS; the abundance of neuronal neuregulin-1 (NRG1) type III is detected by ErbB receptor on the Schwann cell to trigger myelination and to determine the thickness of myelin. However, this interaction is not critical in the CNS, as NRG1 or ErbB null animals showed normal myelination. Thus far, no equivalent CNS molecule has been found.

With advances in mouse genetic tools and transcriptional profiling, more molecules are found to be involved in OPC differentiation. Among them, the discovery of neuron- or myelin-associated differentiation inhibitors (Notch, Wnt, PSA-NCAM, LINGO1, NGF, Semaphorins, and GPR17) enabled greater understanding on regional specification during myelination (Budde et al 2010, Dugas et al 2010, Fancy et al 2009, Kim et al 2010, Shin et al 2005, Tawk et al 2011, Zhao et al 2010). For example, studying the signals that prevent repeated myelination of the same axon, preserving nodal gaps, and repelling myelination at the cell bodies or synapses will greatly improve our understanding of myelin coordination. The discovery of inhibitory signals can further lead to developing novel strategies to release OPCs from “repressed” state and promote remyelination or myelin remodeling. On the other end of the spectrum, we learned that hypermyelination can be achieved by inactivating PTEN or overexpressing Akt to ultimately promote PI3K/Akt/mTOR

signaling that leads to OL differentiation (Flores et al 2008, Harrington et al 2010, Narayanan et al 2009).

1.3.3.2 **Remyelination: Re-program development**

Unlike neuronal regeneration, spontaneous remyelination takes place naturally in the naïve CNS. As we try to recapitulate this process through virus infection, immune-mediated inflammation, or physical/chemical-induced injuries, we found that before myelin can be replaced, myelin debris must be cleaned up. For the past ten years, remyelination is considered to be "re-development." Remyelination, sometimes referred to as myelin repair, mimics intricate processes of *de novo* myelin biogenesis. During this process, OPCs need to exit quiescence state from the reserved pool, proliferate, differentiate, and ensheath denuded axons. However, combining multiple controversial studies in a unified hypothesis is still an ongoing effort (Franklin & Hinks 1999, Franklin 2002, Franklin & ffrench-Constant 2008, Franklin & Gallo 2014). The models to study remyelination, the differences of myelination versus remyelination, and the standing questions are reviewed as follows.

— **Systems for Studying Remyelination**

To study remyelination, establish a condition that is non-myelinated or demyelinated as baseline is important. I listed several systems that are commonly used to study remyelination, what do we learn about remyelination from each method, and their limits are noted as follows.

Nonmyelinated Tracts: Although axons in an adult mammalian optic nerve can reach as high as 99% myelination rate, the intraretinal segments of ganglion cell axons are not myelinated in most rodents (Perry & Hayes 1985). In humans, dogs, rabbits, and chickens, these bundles are myelinated by OLs. Intra-ocular transplantation of Schwann cells resulted in limited myelination, while transplanted OPCs reached 25% coverage in the retina (Huang et al 1991, Laeng et al 1996).

Neonatal animals/myelin mutants: Since active myelination happens post-natally in mammalian organisms, neonatal counterparts can serve as a solid receiver. Through engraftment studies, we learned that remyelination can readily occur in the CNS. By engrafting PNS nerve, we learned the extent of permissiveness of this extracellular milieu, where CNS axons can enter the transplants, and are myelinated by Schwann cells . Additionally, myelination can be triggered by transplanting CNS fragments into myelin-defected brain, such as *Shiverer* mice (Franklin & Blakemore 1990, Gout & Dubois-Dalcq 1993, Gout et al 1988).

Myelin Toxins in Adult Animals: Toxin-mediated demyelination can be conducted by focal tissue injection, intrathecal injection, or chow feeding. Local myelin lesions can be generated by the injection of demyelinating reagents including lysolecithin/lysophosphatidyl choline (LPC), Ethidium bromide (EtBr), anti-galactocerebroside antibodies, and complement. X-irradiation can also eliminate local remyelination capacity. Diffused myelin lesions can be generated by the injection of viral constructs or Cholera toxin B, ingestion of cuprizone infused chow, and induction experimental allergic encephalomyelitis (EAE). Of note, each method generates a slightly different local environment, leading to a different remyelination potential. As a result, one needs to take precaution when interpreting data from these studies. For example, cuprizone damages axons in addition to OLs, LPC spares astrocytes and OPCs, and EtBr kills all dividing cells (Blakemore & Franklin 2008, Lazzarini 2004).

— **Identifying Remyelination**

There is no unique molecular marker for remyelination. The most commonly used method to analyze remyelination is to use EM or to quantify histological changes indirectly. Axon ultrastructures indicative of non-compacted myelin, thinner sheaths (higher g-ratio), or shorter internodes that resemble immature myelin during development are indirectly assumed as undergoing remyelination. Additionally, since similar features were observed in degenerating tissue, distinguishing morphologies of degenerating or regenerating myelin becomes a

challenging undertaking. One proposal puts forth that the thickness of myelin and the number of internodes in remyelinated axons are not correlated with axon caliber, and can never reach the level of its un-affected counterpart. However, this observation is biased, since in the case where myelin is completely regenerated, there is no way to discriminate it from the un-affected normal tissue. With the improvements of technology, an elegant imaging study demonstrated that remyelinated axon exhibited indistinguishable myelin thickness, and that the internodal length is approaching that of uninjured controls after 6 months. This was done by YFP labeling of adult $NG2^+$ OPCs using retrovirus injection in adult mice with a spinal cord contusion injury (Powers et al 2013).

— **Removing Myelin Debris**

Before OPCs can initiate the remyelination process, creating a permissive environment is essential. Debris from myelin breakdown accumulates following injury, and failure of debris removal correlates with the poor myelin repair. Myelin can be removed through both opsonized and non-opsonized pathways by microglia/macrophages. Opsonized clearance is regulated by pattern recognition receptor (PRR) and complement receptor 3 (CR3/CD11b/MAC-1) (Kopper & Gensel 2017, Rotshenker 2003). Microglia are polarized and recruited to the lesion by extracellular ATP through purinergic receptors within 1-2 days following injury. Whereas some microglia can be neurotoxic, some microglia can be neuroprotective by down-regulating pro-inflammatory signals (TNF-a and IL-1b) and increasing anti-inflammatory signals (IGF-1, BDNF, IL-10, and TGF-b). Phagocytosis can also take place with or without inflammation, the latter being toxic for neuronal survival and OPC remyelinating capacity. Ongoing investigations focus on pro-inflammatory responses mediated by TLRs and FcRs, as well as anti-inflammation responses mediated by TREM2, PRs, PS-R, SRs, and subtypes of FcRs will be informative. (Haider 2015, Kopper & Gensel 2017, Neumann et al 2009)

— **Recruiting and Differentiating Adult OPCs**

Starting from CNS developmental stages, OPCs evenly tiled the whole brain and persist into adulthood of animals. New OPCs in adult animal can be generated from SVZ-residing progenitors. Both pre-exist and newly committed adult OPCs migrate and cycle slower than perinatal OPCS (Levine et al 2001, Talbott et al 2005). The capability of myelin replacement by adult OPCs varies among different brain regions, declines with age, and is weaker in males (Li et al 2006). Robust myelin repair is often observed in rodent demyelination models; however, in humans, this capacity is greatly reduced. Our understanding of key steps of remyelination comes from studies with post-mortem MS brain tissue. OPCs were found to be sparse in about 30% of the un-myelinated MS lesions, and another 70% of MS lesion showed an abundance of OPCs, which however, remained in an immature state and failed to repair myelin lesions (Chang et al 2000, Martin et al 2008, Wolswijk 1998). Together, these studies suggest that disturbances in either OPC recruitment or differentiation lead to remyelination failure. From then on, the main focus has been on investigating the signals known to promote OPC migration or differentiation in animal models of demyelinating disorders. Semaphorin (Sema) 3F and PDGF signals in the OPCs and reactive astrocytes derived CXCL1, 8, and 10 signals at the lesion border were found to positively regulate OPC recruitment. Sema3A, on the other hand, correlates with reduced OPCs at the lesion and poor repair. Much like *de novo* OL differentiation, inhibitory signals such as Lingo-1 (Li et al 2007, Mi et al 2005), Notch (Genoud et al 2002, Zhang et al 2009), Wnt (Fancy et al 2009, Feigenson et al 2009), myelin products (Plemel et al 2013), and PSA-NCAM (Charles et al 2002) hinder myelin repair. Additionally, BMP-mediated astrogliosis leads to hyaluronan deposition at the lesion. Hyaluronan most likely blocks differentiation through TLR-2 expression and activation by OPCs (Back et al 2005, Sloane et al 2010). Different signals are required during development and repair; for example Olig1 signal can be compensated by Olig2 during development, but is required during remyelination.

— **Failing at Remyelination**

As mentioned, remyelination required adult OPCs to differentiate and mature into myelinating OLs. While spontaneous remyelination is considered to be robust and not easily prone to failure, multiple lines of evidence show that OPCs stall in an immature state at the border of MS lesions (Chang et al 2000). Moreover, mechanistic studies sometimes do not agree with each other in different remyelination models. To reconcile these observations, local signaling environments are considered to weigh more than OPC intrinsic potential. Franklin articulated a "dysregulation model" 15 years ago to explain possible reasons for remyelination failure (Franklin 2002). In this model, OPCs are locked at a quiescent immature state, not necessarily due to the prolonged inhibitory signals, but rather due to missing a critical window for differentiation. Chronic MS lesions are relatively non-inflammatory and surrounded by non-reactive scarring astrocytes; these conditions might not be permissive for myelin repair. In addition, decreased HDAC recruitment to the lesion cannot modify the profile of transcription factors and leading to a failure in becoming differentiation profile, further explaining remyelination failure. Our knowledge to promote successful remyelination in diseases is rather still elementary. Therefore, future work that validates targets that regulate OPC differentiation, integrates current knowledge to create a conceptual framework, considers non-genetic regulatory level processes such as epigenetics, and access to human tissue will provide valuable insights (Chang et al 2002, Gilson & Blakemore 1993, Imai et al 2008, Kotter et al 2011, Kuhlmann et al 2008, Levine et al 2001, Maki et al 2013, Taveggia et al 2010).

1.3.3.3 **Myelin Turnover: Dynamic Myelination**

Myelin has been especially studied for its exceptional stability with little to no turn over. The half-life of myelin components range from weeks to several years, and some are too long to be traced by pulse-chased isotope labeling (Toyama et al 2013, Yeung et al 2014). This working hypothesis was further corroborated when dissections revealed that the ultrastructure of 5000-yr-old myelin from a Tyrolean Iceman was grossly intact (Hess et al 1998). However, recent evidence showed that

myelin is under constant remodeling in adulthood (Young et al 2013), and can be influenced by local functional activity. Adult OPCs slowly, but constantly, proliferate and differentiate to generate shorter but more frequent internodes in the mouse optic nerve. It was proposed that these shorter myelin sheaths open up the possibility of refining neuronal functions (Lasiene et al 2009, Young et al 2013).

The total volume of myelin generated by one single OL seems to be constant; however, myelin density, internodal length, thickness, and segment number were found to be heterogeneous in different brain regions. More myelin wraps per internode or longer internodal length is often associated with fewer segments (Simons & Nave 2016), suggesting there is plasticity during myelination. It is speculated that this variability between various brain regions attributing to differential functions of the brain. Further evidence showed that even environmental stimuli could shape the morphology of myelin (Fields 2008, Liu et al 2012, Makinodan et al 2012, Mangin et al 2012, Young et al 2013). For example, social isolation and lack of visual stimulation negatively impacts myelination (Liu et al 2012, Makinodan et al 2012). On the other hand, reading, learning, and motor skill training stimulate myelination in a region-dependent manner (Bengtsson et al 2005, Keller & Just 2009, Liu et al 2012, Sampaio-Baptista et al 2013, Scholz et al 2009). The underlying molecular mechanisms remain largely elusive; however, this adaptive myelination mode seems to be independent of the OPC intrinsic feature.

Clearly, searching for the molecular regulators of dynamic myelination is important, as it might lead to discovering ways to intervene in myelin repair. Recently, the association between myelin membrane alterations and increase of myelin volume was investigated by PTEN ablation in adult mice. PTEN loss of function leads to activation of the Akt/mTOR pathway, which triggered active myelination. The active myelination is associated with the morphological changes which myelinic channels are resumed (Snaidero et al 2014). As mentioned previously, myelinic channels are regulated by the expression of CNP. CNP functioned in antagonizing MBP to maintain myelinic channels, ensuring metabolic

exchange between OL and axons (Snaidero et al 2017). Interestingly, in CNP null mice myelination is spared, but axon integrity is compromised with age. Normal aging impairs myelin integrity, differentially affecting myelin proteins including CNP. Further studies, focusing on the epigenetic changes during cognitive activities and considering intercellular metabolic exchange will greatly improve our understanding of the emerging picture.

1.4 The More the Merrier? Precise Myelination Matters

1.4.1 To Myelinate or Not, That is the Question

From studies in the past, we learned that not all myelin structures are generated equally. As mentioned before, they in fact differ from one brain region to another to meet specific activity requirements. A constant g-ratio for each axon diameter was found, suggesting that myelin wraps are associated with a specific axon caliber. Myelin dynamically alters its structure to adapt to new neuronal activities, such as learning. To perform complex function, precise coordination of electrical signal transductions from neighboring inputs is required. Therefore, unrestricted myelin thickening (leads to uncontrolled increasing signal transduction speed) is not necessarily better. In addition, myelin is an energy expensive structure. It was argued that the amount of ATP spent to maintain myelin structure is actually more than what is conserved when axons fire action potentials (Harris & Attwell 2012). Nave and colleagues argued that defective myelin-mediated metabolism do more harm than good—even the myelin structure remains grossly intact (Nave 2010a, Nave 2010b, Nave & Trapp 2008, Simons & Nave 2016). It was speculated that myelin ensheathment confines the access of outer energy source exchange to the nodes, defective myelin with deformed nodal structure often leads to axon degeneration. Many myelin proteins, such as CNP, MAG, and PLP were found to be crucial in supporting axonal integrity rather than functioning in myelin biogenesis.

In a large projection neuron, up to 99% of the cytoplasm is in the axon and 1% in the cell body. As neurons possess axons up to a meter in length, the timely

supply of metabolites to axons and synapses, far away from the cell body, is a formidable challenge. To understand the metabolic stringency of neurons due to their length, a scale up model is discussed. Consider a cortical neuron with a 1 μm diameter axon width and a 100 cm axon in the corticospinal tract; this is equivalent to traveling on a 4 m wide highway from the University of Michigan to the East Coast (~2500 miles away) (Nave 2010a). Molecular transport in fast bound (5 μm/s) cytoskeleton-associated vesicles, such as mitochondria, would take 2-3 days (Zala et al 2013). However, if traveled through slow bound diffusion (2 mm/day), such as soluble enzymes, it would take years to reach the distal part of the axon. This time scale is way beyond the stability of a protein (Brady & Lasek 1981, Oblinger et al 1988, Yuan et al 1999). In either case, the response time is way slower than the metabolic demand for neuronal activities. Therefore, a route of transferring nearby metabolites through axon-glia interactions is crucial.

For successful remyelination, myelin degeneration and regeneration must happen sequentially. Inflammation is important for myelin debris removal; however it can also induce apoptosis of the myelinating OLs. Future studies for signaling regulators that coordinate these events are required.

1.4.2 **Lateral Transfer of Metabolites**

— **Energy Cooperation**

Glucose is the major source of energy in the brain. Endothelial cells at the capillary take up glucose and pass it on to neuronal cells through glucose transporters (GLUTs). Glucose then can either be stored as glycogen in the astrocyte, or undergo glycolysis to generate lactate or pyruvate in glia cells (Wiesinger et al 1997). Mitochondria oxidize lactate and pyruvate to generate ATP in neuronal cells. Lactate and pyruvate can be transferred between astrocytes and OLs via monocarboxy transporters (MCTs) and gap junctions (connexins, Cx). During myelination, OLs consume astrocyte-derived lactate to generate ATP or synthesize myelin lipids (Rinholm et al 2011, Sánchez-Abarca et al 2001). Interestingly, OLs do not rely on functional mitochondria to maintain their myelin,

nor do OL mitochondria impact axon integrity *in vivo* (Fünfschilling et al 2012). One explanation for this came with the observation that mitochondrial traffic is fast along the axon, but stalled at the nodes of Ranvier (Misgeld et al 2007).

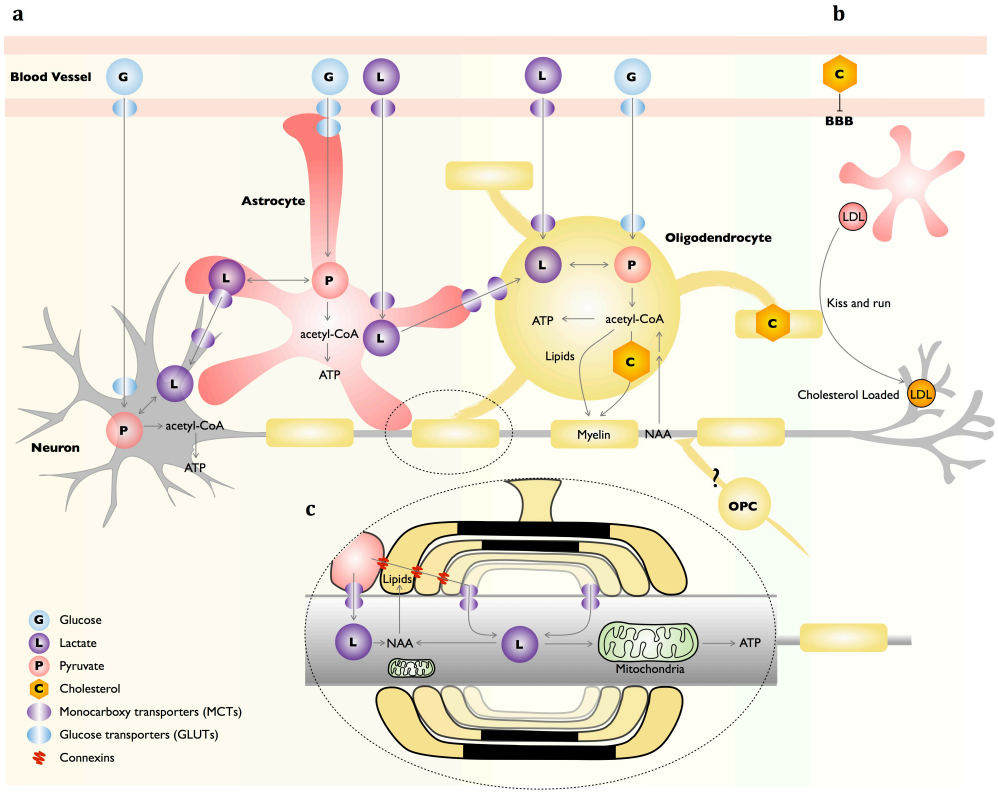

Figure 1.5: CNS intercellular metabolic transfer
(a) Glucose is the major energy source of the brain. Glucose passes through BBB and goes into the cells through GLUTs. Glucose is transformed to pyruvate and to lactate. Lactate can be transfered between neurons, astrocytes, and OLs through MCTs to be the energy source for mitochondria to create ATPs. Neuronal axons provide metabolic support for OLs by NAA transfer through myelinic channels. OL utilize NAA to synthesize myelin lipids and cholesterol. (b) Cholesterol cannot pass BBB of the CNS and can only be synthesized locally. Cholesterol can be transferred in between cells. Astrocyte derived LDL load cholesterol through membrane contacts with OLs to meet local demands of neuronal synapse. LDL, low-density lipoprotein; BBB, blood brain barrier; GLUT, glucose transporter; MCT, monocarboxy transporter; NAA, N-acetylaspartate; ATP, Adenosine triphosphate. This figure was created by Jing-Ping Lin.

Additionally, selective MCT1 ablation in glial cells leads to axon degeneration and neuronal loss (Lee et al 2012b), suggesting that lactate may be transported from OLs to axons at the nodes for axonal mitochondria to generate ATP. It was also speculated that OLs support axons through energy generated by breakdown of myelin lipids in OL peroxisomes, which are accumulated at the paranodal loops (Kassmann 2014). However, astrocytes also express MCT1 (Rinholm et al 2011),

shown by their capability of passing lactate to neurons at the synapses (Suzuki et al 2011), and formaing close contacts with nodes. Future cell-type specific deletion is required to dissect this specific relationship. On the other hand, neurons support OLs by providing N-acetylaspartate (NAA) to synthesize myelin lipids. The NAA catabolic enzyme, aspartoacylase (ASPA), strictly resides in OLs (Namboodiri et al 2006). Defects in ASPA in the OLs, as well as the aspartate-glutamate carrier (AGC1), an enzyme shuttle for NAA precursor to the cytosol, in the neuronal mitochondria lead to hypomyelination (Jalil et al 2005, Kaul et al 1993, Mersmann et al 2011, Wiame et al 2009, Wibom et al 2009). As illustrated in Figure 1.5, the bidirectional metabolic exchange amongst neurons, astrocytes, and OLs fulfills the energy demand for brain function.

— **Cholesterol homeostasis**

CNS cholesterol is separated from the circulation by the blood brain barrier (BBB) (Björkhem & Meaney 2004), The BBB prevents fluctuations of cholesterol levels caused by dietary uptake. Distinct from the cholesterol dynamic in the periphery, over 95% of cholesterol in the mammalian brain is locally synthesized *de novo* by CNS resident cells (Dietschy & Turley 2001, Jurevics & Morell 1995). In addition, over 99.5% of cholesterol in the CNS exists as un-esterified, free form (Björkhem & Meaney 2004), and is stable with a half-life of 0.5-5 years (Andersson et al 1990). Cholesterol is transferrable between CNS cell types via a process called reverse cholesterol transport (RCT) (Courtney & Landreth 2016) (Figure 1.5). Notably, OLs synthesize the majority of cholesterol cell-autonomously, and this constitutes ~80% of the total cholesterol in the CNS (Muse et al 2000). Interestingly, astrocytes collaboratively produce the majority of lipoprotein particles in adult CNS, (DeMattos et al 2001, Xu et al 2006) which serve as cholesterol shuttles between cells (Dietschy & Turley 2004, Han 2007). In order to meet local needs of forming/remodeling synapses and axonal growth, neurons uptake additional cholesterol containing lipoproteins that are generated from neighboring glial cells. This uptake is mediated at lease in part by the family members of the low-density lipoprotein (LDL) receptor, including LDL receptor receptor-related protein 1

(LRP1) (de Chaves et al 1997, Hayashi et al 2004, Mauch et al 2001, Posse De Chaves et al 2000).

1.4.3 **Signaling Coordinator-LRP1**

With the advances in "omic" profiling studies, more myelin/OL candidate genes were found (Zhang et al 2014). Among them, low-density lipoprotein receptor-related protein 1 (LRP1) caught our attention. LRP1 is also known as CD91 and the α-2-macroglobulin receptor. LRP1 was discovered based on its structural and biochemical similarity to LDL family members (Figure 1.6). A potential role in lipoprotein trafficking was first postulated in the 1980s (Herz et al 1988). Family members include core members (LDLR, VLDLR, LRP1, LRP1b, LRP2, LRP4, and LRP8), distant members (LRP5, LRP6, and LRP11), and far members (LRP3, LRP10, LRP12) (He et al 2004, Lillis et al 2008). All members contain two or more cysteine-rich complement-like repeats, also called ligand binding repeats. LRP1B with high sequence similarity that has overlapping ligand-binding ability with LRP1. LRP1B undergoes endocytosis in a slower rate than LRP1, therefore it antagonizes the function of LRP1 (Causevic et al 2003, Chappell et al 1993, Chappell et al 1994). Similarly, LRP2 functions in ligand uptake in epithelial cells of the kidney (Cathcart et al 1991). The structures of LDLR, VLDLR, and LRP8 are similar, these receptors function in reelin signaling rather than lipoprotein endocytosis (Chazaud et al 2002). LRP4 structurally resembles a portion of LRP1. LRP4 is a receptor for Agrin, a protein that modulates the formation of neuromuscular synapses and functions in limb patterning (Christensen et al 1996, Chrzanowska-Wodnicka & Burridge 1996). The structure of LRP5/6 are more diverse than for the principal LDL family members (Chu et al 1994), they serve as co-receptors for Wnt signaling. LRP11 functions in intracellular protein trafficking (Chu et al 1994). Interestingly, *Lrp1* gene deletion is embryonic-lethal in mice (Herz et al 1992), indicating that *Lrp1* deficiency cannot be compensated by other LDL family members albeit their structural similarity.

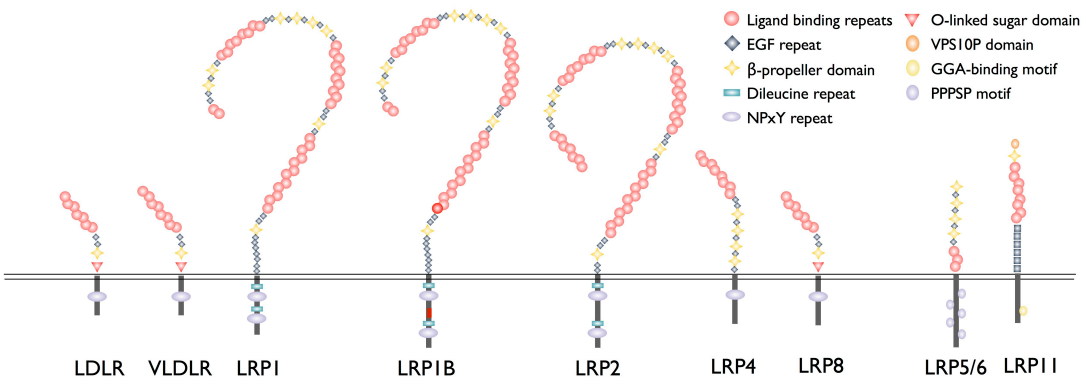

Figure 1.6: The structure of LDL receptor family
The core and distant LDL family members are shown. The differences in structure between LRP1 and LRP1B are labeled in red on LRP1B, including one extra ligand binding repeats and a 33 amino acids insertion at intracellular domain. The identity of the amino acid sequence is 59% between LRP1 and LRP1B. EGF, epidermal growth factor; VPS10P, Vacuolar protein sorting 10 protein; GGA-binding motif, Golgi-localized, gamma adaptin ear-containing, ARF-binding; PPPSP motif, proline proline proline serine proline motif. This figure was created by Jing-Ping Lin.

LRP1 is one of the largest family members with an extracellular α-chain (515 kDa) non-covalently attached to a single pass transmembrane β-chain (85 kDa). The *Lrp1* gene is activated by sterol regulatory element binding protein 2 (SREBP2), hypoxia-induced factor 1α (HIF1α), and nitric oxide-dependent transcription factors. *Lrp1* is blocked by a naturally occurring anti-sense RNA that is reversely transcribed from *Lrp1* gene exons 5 and 6 (Auderset et al 2016). A chaperone, receptor associated protein (RAP), binds to LRP1 protein precursor to prevent misfolding and premature ligand binding in the ER. LRP1 precursor is then transported to the Golgi through the regulation of its NPxY domain (Auderset et al 2016). The dissociation of LRP1-RAP complex is triggered by low pH in the trans-Golgi network. Furin proteases cleave LRP1 precursor at the consensus sequence (RxKR or RxRR) to generate the α- and β-chains. These two chains remain attached as a functional unit when the receptor is inserted into plasma membrane at the cell surface. On the cell surface, LRP1 can be processed by sheddases, such as beta-site APP cleaving enzyme1 (BACE1) and matrix metalloproteinase (MMPs), to form a soluble extracellular domain (sLRP1). sLRP1 is detected in plasma and cerebral spinal fluid (CSF) in the forms of α-chain and 55kDa β-chain (Auderset et al 2016, Gonias & Campana 2014). The intracellular domain of LRP1 can be processed by γ-

secretase to release a 15k Da LRP-ICD, which serves as a transcription regulator (Figure 1.7).

There are four ligand-binding repeats in LRP1, most of the ligands bind to cluster II and IV (CI and CIV). Crystal structural studies of this complement-like repeat revealed that it forms a cage for Ca^{2+} to stabilize the structure of LRP1 (Fass et al 1997). Additionally, LRP1 contains EGF precursor homologous regions, which consists of two cysteine-rich EGF repeats and β-propeller domain (YWTD repeats) (Jeon et al 2001, Springer 1998). Mutants at the EGF precursor homologous region lead to failure of ligand releasing in the low pH endosomal compartments (Davis et al 1987, Mikhailenko et al 1999, Rudenko et al 2002). LRP1 contains a single-pass transmembrane and a cytoplasmic domain consists of 100 amino acids. There are two dileucine (LL) motifs and two NPxY motifs in the cytoplasmic domain. The distal NPxY motif is phosphorylated by PDGFR-β through CTGF and v-Src signaling (Barnes et al 2003, Boucher et al 2002, Yang et al 2004). The cytoplasmic domain of LRP1 interacts with various adaptor proteins, such as Disabled-1, Shc, PKCα, FE65, PSD95, SEMCAP-1, JIP1/2, GULP, Talin-like protein, OMP25, CAPON, PIP4,5, kinase like protein, ICAP1, and Cb1 (Lillis et al 2008).

Over the past 20 years, our knowledge of LRP1 has expanded remarkably. We learned that it is one of the most multifunctional endocytic scavenger receptors. LRP1 binds to over 40 different ligands, and is involved in regulating a broad spectrum of cellular physiology in our body (Pieper-Fürst & Lammert 2013). By recycling components functioned in other pathways, LRP1 indirectly regulated physiological functions. By its intracellular domain phosphorylation, LRP1 directly pass down extracellular signals to influence signaling pathways inside the cells. Given there is a broad spectrum of ligands bind to LRP1, the role of LRP1 as a sensor of the cellular microenvironment was proposed (Gonias & Campana 2014). LRP1 is ubiquitously expressed in various cell types. The roles of LRP1 in vasculature protection, cancer progression, apoptotic cell phagocytosis, immune responses, lipid homeostasis in adipocytes, BBB functions, nervous system development, amyloid

clearance, and so on have been intensively reviewed (Lillis et al 2008) (Auderset et al 2016, Boucher & Herz 2011, Bu 2009, Gaultier et al 2008, Gaultier et al 2010, Gonias & Campana 2014, Gorovoy et al 2010, Kanekiyo & Bu 2014, Kanekiyo et al 2013, Liu et al 2007a, Spuch et al 2012, Zlokovic et al 2008). Following I focus on several aspects that are most relevant to my studies (Chapter II and III). Additional relevant information about LRP1 is briefly summarized as I describing and discussing my new findings in later chapters.

Previously, LRP1 has been found to bind and internalize detrimental myelin debris (Fernandez-Castaneda et al 2013, Stiles et al 2013), which suggests its role in facilitating neuron and myelin regeneration. In the process of RCT, *Lrp1* transcripts are expressed in all neuronal cells, as well as showing the highest level in OPCs. As OLs mature, *Lrp1* transcript levels decrease drastically, coinciding with the decreasing rate of cholesterol biosynthesis during myelination (Muse et al 2000, Quan et al 2003). Furthermore, selective deletion of *Lrp1* in the forebrain under the αCaMKII driver significantly lowers cholesterol levels in the adult mouse brains (Liu et al 2010). On the other hand, conditional deletion of cholesterol synthesis enzyme (SQS) in OLs under CNP driver increased LRP1 level in adult mice spinal cord (Saher et al 2005). Cholesterol-induced axonal regeneration was abolished by LRP1 antagonist *in vitro* (Hayashi et al 2004). However, the level of cholesterol uptake is not affected upon LRP1 deletion in OLs (Safina et al 2016). Collectively, these findings imply the possibility that LRP1 is more than a cholesterol transporter in OPCs/OLs. Albeit recent work shedding light on the requirement of LRP1 in oligodendrogenesis (Hennen et al 2013, Safina et al 2016), the role of LRP1 in OL cholesterol homeostasis, and how it affects myelination during development and injury repair *in vivo* remain to be elucidated.

To bridge these gaps, in the following chapters, first I answer if LRP1 has a role in CNS myelin development and repair. Then I ask if LRP1 participates in myelin repair, if it is through similar pathways as during myelin development.

Following I ask which stage of OL development is LRP1 involved and what is the potential mechanisms.

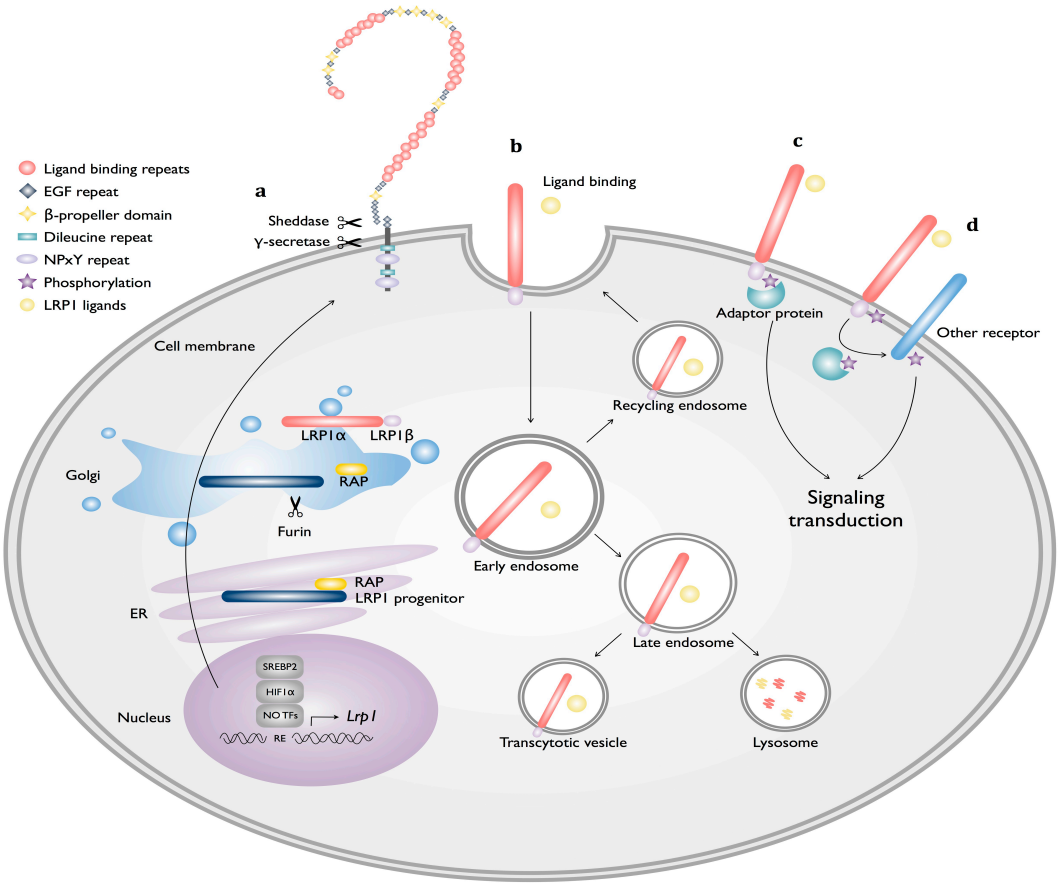

Figure 1.7: The synthesis, maturation, structure, and function of LRP1
(a) LRP1 progenitor is bound by RAP in the ER, matured in golgi by Furin processing, and transported to cell surface. At the surface it can further be processed by sheddase and γ-secretase to generate sLRP1 and LRP1-ICD. (b) LRP1 endocytose ligands to enter endosomes. (c) LRP1 transduces signals through intracellular phosphorylation or (d) trans-activate nearby receptors. RAP, receptor associated protein; EGF, epidermal growth factor. This figure was created by Jing-Ping Lin.

1.5 **Bibliography**

Aggarwal S, Snaidero N, Pähler G, Frey S, Sánchez P, et al. 2013. Myelin Membrane Assembly Is Driven by a Phase Transition of Myelin Basic Proteins Into a Cohesive Protein Meshwork. In *PLoS Biol.*, pp. e1001577

Aggarwal S, Yurlova L, Snaidero N, Reetz C, Frey S, et al. 2011. A Size Barrier Limits Protein Diffusion at the Cell Surface to Generate Lipid-Rich Myelin-Membrane Sheets. In *Developmental Cell*, pp. 445-56: Elsevier Inc.

Andersson M, Elmberger PG, Edlund C, Kristensson K, Dallner G. 1990. Rates of cholesterol, ubiquinone, dolichol and dolichyl-P biosynthesis in rat brain slices. In *FEBS Lett.*, pp. 15-18

Arroyo EJ, Scherer SS. 2000. On the molecular architecture of myelinated fibers. In *Histochem. Cell Biol.*, pp. 1-18

Auderset L, Landowski LM, Foa L, Young KM. 2016. Low Density Lipoprotein Receptor Related Proteins as Regulators of Neural Stem and Progenitor Cell Function. In *Stem Cells Int*, pp. 2108495

Back SA, Tuohy TMF, Chen H, Wallingford N, Craig A, et al. 2005. Hyaluronan accumulates in demyelinated lesions and inhibits oligodendrocyte progenitor maturation. In *Nat Med*, pp. 966-72

Baldwin KT, Giger RJ. 2015. Insights into the physiological role of CNS regeneration inhibitors. In *Front Mol Neurosci*, pp. 23

Barbara JG. 2005. Les étranglements annulaires de Louis Ranvier (1871). In *Lettre des Neurosciences*

Barnes H, Ackermann EJ, van der Geer P. 2003. v-Src induces Shc binding to tyrosine 63 in the cytoplasmic domain of the LDL receptor-related protein 1. In *Oncogene*, pp. 3589-97

Barres BA, Raff MC. 1994. Control of oligodendrocyte number in the developing rat optic nerve. In *Neuron*, pp. 935-42

Barres BA, Raff MC, Gaese F, Bartke I, Dechant G, Barde YA. 1994. A crucial role for neurotrophin-3 in oligodendrocyte development. In *Nature*, pp. 371-75

Baumann N, Pham-Dinh D. 2001. Biology of oligodendrocyte and myelin in the mammalian central nervous system. In *Physiological Reviews*, pp. 871-927

Becerra JL, Puckett WR, Hiester ED, Quencer RM, Marcillo AE, et al. 1995. MR-pathologic comparisons of wallerian degeneration in spinal cord injury. In *AJNR Am J Neuroradiol*, pp. 125-33

Bengtsson SL, Nagy Z, Skare S, Forsman L, Forssberg H, Ullén F. 2005. Extensive piano practicing has regionally specific effects on white matter development. In *Nat. Neurosci.*, pp. 1148-50

Bergles DE, Richardson WD. 2015. Oligodendrocyte Development and Plasticity. In *Cold Spring Harb Perspect Biol*, pp. a020453

Berry M. 1982. Post-injury myelin-breakdown products inhibit axonal growth: an hypothesis to explain the failure of axonal regeneration in the mammalian central nervous system. In *Bibl Anat*, pp. 1-11

Björkhem I, Meaney S. 2004. Brain cholesterol: long secret life behind a barrier. In *Arterioscler. Thromb. Vasc. Biol.*, pp. 806-15

Black JA, Waxman SG. 1988. The perinodal astrocyte. In *Glia*, pp. 169-83

Blakemore WF, Franklin RJM. 2008. Remyelination in experimental models of toxin-induced demyelination. In *Curr. Top. Microbiol. Immunol.*, pp. 193-212

Boucher P, Herz J. 2011. Signaling through LRP1: Protection from atherosclerosis and beyond. In *Biochem. Pharmacol.*, pp. 1-5: Elsevier Inc.

Boucher P, Liu P, Gotthardt M, Hiesberger T, Anderson RGW, Herz J. 2002. Platelet-derived growth factor mediates tyrosine phosphorylation of the cytoplasmic domain of the low Density lipoprotein receptor-related protein in caveolae. In *J. Biol. Chem.*, pp. 15507-13

Boullerne AI. 2016. The history of myelin. In *Exp Neurol*, pp. 431-45: Elsevier Inc.

Boven LA, Van Meurs M, Van Zwam M, Wierenga-Wolf A, Hintzen RQ, et al. 2006. Myelin-laden macrophages are anti-inflammatory, consistent with foam cells in multiple sclerosis. In *Brain*, pp. 517-26

Brady S, Siegel G, Albers RW, Price D. 2005. Basic Neurochemistry. In *Molecular, Cellular and Medical Aspects*, pp. 1016: Elsevier

Brady ST, Lasek RJ. 1981. Nerve-specific enolase and creatine phosphokinase in axonal transport: soluble proteins and the axoplasmic matrix. In *Cell*, pp. 515-23

Bronstein JM, Micevych PE, Chen K. 1997. Oligodendrocyte-specific protein (OSP) is a major component of CNS myelin. In *J. Neurosci. Res.*, pp. 713-20

Bu G. 2009. Apolipoprotein E and its receptors in Alzheimer's disease: pathways, pathogenesis and therapy. In *Nat. Rev. Neurosci.*, pp. 333-44

Budde H, Schmitt S, Fitzner D, Opitz L, Salinas-Riester G, Simons M. 2010. Control of oligodendroglial cell number by the miR-17-92 cluster. In *Development*, pp. 2127-32

Bullock TH, Moore JK, Fields RD. 1984. Evolution of myelin sheaths: both lamprey and hagfish lack myelin. In *Neurosci Lett*, pp. 145-48

Buss A, Pech K, Merkler D, Kakulas BA, Martin D, et al. 2005. Sequential loss of myelin proteins during Wallerian degeneration in the human spinal cord. In *Brain*, pp. 356-64

Butt AM, Duncan A, Berry M. 1994. Astrocyte associations with nodes of Ranvier: ultrastructural analysis of HRP-filled astrocytes in the mouse optic nerve. In *J. Neurocytol.*, pp. 486-99

Butt AM, Duncan A, Hornby MF, Kirvell SL, Hunter A, et al. 1999. Cells expressing the NG2 antigen contact nodes of Ranvier in adult CNS white matter. In *Glia*, pp. 84-91

Butts BD, Houde C, Mehmet H. 2008. Maturation-dependent sensitivity of oligodendrocyte lineage cells to apoptosis: implications for normal development and disease. In *Cell Death Differ*, pp. 1178-86

Caroni P, Schwab ME. 1988. Two membrane protein fractions from rat central myelin with inhibitory properties for neurite growth and fibroblast spreading. In *The Journal of Cell Biology*, pp. 1281-88

Cathcart MK, McNally AK, Chisolm GM. 1991. Lipoxygenase-mediated transformation of human low density lipoprotein to an oxidized and cytotoxic complex. In *J. Lipid Res.*, pp. 63-70

Causevic M, Ramoz N, Haroutunian V, Davis KL, Buxbaum JD. 2003. Lack of association between the levels of the low-density lipoprotein receptor-

related protein (LRP) and either Alzheimer dementia or LRP exon 3 genotype. In *J. Neuropathol. Exp. Neurol.*, pp. 999-1005

Cellerino A, Carroll P, Thoenen H, Barde YA. 1997. Reduced size of retinal ganglion cell axons and hypomyelination in mice lacking brain-derived neurotrophic factor. In *Mol. Cell. Neurosci.*, pp. 397-408

Cerghet M. 2006. Proliferation and Death of Oligodendrocytes and Myelin Proteins Are Differentially Regulated in Male and Female Rodents. In *Journal of Neuroscience*, pp. 1439-47

Chang A, Nishiyama A, Peterson J, Prineas J, Trapp BD. 2000. NG2-positive oligodendrocyte progenitor cells in adult human brain and multiple sclerosis lesions. In *J. Neurosci.*, pp. 6404-12

Chang A, Tourtellotte WW, Rudick R, Trapp BD. 2002. Premyelinating oligodendrocytes in chronic lesions of multiple sclerosis. In *N Engl J Med*, pp. 165-73

Chang K-J, Zollinger DR, Susuki K, Sherman DL, Makara MA, et al. 2014. Glial ankyrins facilitate paranodal axoglial junction assembly. In *Nat. Neurosci.*, pp. 1673-81: Nature Publishing Group

Chapman H, Waclaw RR, Pei Z, Nakafuku M, Campbell K. 2013. The homeobox gene Gsx2 controls the timing of oligodendroglial fate specification in mouse lateral ganglionic eminence progenitors. In *Development*, pp. 2289-98

Chappell DA, Fry GL, Waknitz MA, Muhonen LE, Pladet MW, et al. 1993. Lipoprotein lipase induces catabolism of normal triglyceride-rich lipoproteins via the low density lipoprotein receptor-related protein/alpha 2-macroglobulin receptor in vitro. A process facilitated by cell-surface proteoglycans. In *J. Biol. Chem.*, pp. 14168-75

Chappell DA, Inoue I, Fry GL, Pladet MW, Bowen SL, et al. 1994. Cellular catabolism of normal very low density lipoproteins via the low density lipoprotein receptor-related protein/alpha 2-macroglobulin receptor is induced by the C-terminal domain of lipoprotein lipase. In *J. Biol. Chem.*, pp. 18001-06

Charles P, Reynolds R, Seilhean D, Rougon G, Aigrot MS, et al. 2002. Re-expression of PSA-NCAM by demyelinated axons: an inhibitor of remyelination in multiple sclerosis? In *Brain*, pp. 1972-79

Chazaud B, Ricoux R, Christov C, Plonquet A, Gherardi RK, Barlovatz-Meimon G. 2002. Promigratory effect of plasminogen activator inhibitor-1 on invasive breast cancer cell populations. In *Am. J. Pathol.*, pp. 237-46

Chen MS, Huber AB, van der Haar ME, Frank M, Schnell L, et al. 2000. Nogo-A is a myelin-associated neurite outgrowth inhibitor and an antigen for monoclonal antibody IN-1. In *Nature*, pp. 434-39

Chernoff GF. 1981. Shiverer: an autosomal recessive mutant mouse with myelin deficiency. In *J. Hered.*, pp. 128

Chiu SY. 1980. Asymmetry currents in the mammalian myelinated nerve. In *J. Physiol. (Lond.)*, pp. 499-519

Chomiak T, Hu B. 2009. What is the optimal value of the g-ratio for myelinated fibers in the rat CNS? A theoretical approach. In *PLoS ONE*, pp. e7754

Chong SYC, Rosenberg SS, Fancy SPJ, Zhao C, Shen Y-AA, et al. 2012. Neurite outgrowth inhibitor Nogo-A establishes spatial segregation and extent of oligodendrocyte myelination. In *Proc. Natl. Acad. Sci. U.S.A.*, pp. 1299-304

Christensen L, Wiborg Simonsen AC, Heegaard CW, Moestrup SK, Andersen JA, Andreasen PA. 1996. Immunohistochemical localization of urokinase-type plasminogen activator, type-1 plasminogen-activator inhibitor, urokinase receptor and alpha(2)-macroglobulin receptor in human breast carcinomas. In *Int. J. Cancer*, pp. 441-52

Chrzanowska-Wodnicka M, Burridge K. 1996. Rho-stimulated contractility drives the formation of stress fibers and focal adhesions. In *The Journal of Cell Biology*, pp. 1403-15

Chu CT, Oury TD, Enghild JJ, Pizzo SV. 1994. Adjuvant-free in vivo targeting. Antigen delivery by alpha 2-macroglobulin enhances antibody formation. In *J Immunol*, pp. 1538-45

Courtney R, Landreth GE. 2016. LXR Regulation of Brain Cholesterol: From Development to Disease. In *Trends Endocrinol. Metab.*, pp. 404-14

Davis CG, Goldstein JL, Südhof TC, Anderson RG, Russell DW, Brown MS. 1987. Acid-dependent ligand dissociation and recycling of LDL receptor mediated by growth factor homology region. In *Nature*, pp. 760-65

De Biase LM, Nishiyama A, Bergles DE. 2010. Excitability and synaptic communication within the oligodendrocyte lineage. In *J. Neurosci.*, pp. 3600-11

de Chaves EI, Rusiñol AE, Vance DE, Campenot RB, Vance JE. 1997. Role of lipoproteins in the delivery of lipids to axons during axonal regeneration. In *J. Biol. Chem.*, pp. 30766-73

Deber CM, Reynolds SJ. 1991. Central nervous system myelin: structure, function, and pathology. In *Clin. Biochem.*, pp. 113-34

DeMattos RB, Brendza RP, Heuser JE, Kierson M, Cirrito JR, et al. 2001. Purification and characterization of astrocyte-secreted apolipoprotein E and J-containing lipoproteins from wild-type and human apoE transgenic mice. In *Neurochem Int*, pp. 415-25

Di Biase A, Salvati S, Serlupi Crescenzi G. 1990. Lipid profile of rat myelin subfractions. In *Neurochem Res*, pp. 519-22

Dietschy JM, Turley SD. 2001. Cholesterol metabolism in the brain. In *Current Opinion in Lipidology*, pp. 105-12

Dietschy JM, Turley SD. 2004. Thematic review series: brain Lipids. Cholesterol metabolism in the central nervous system during early development and in the mature animal. In *J. Lipid Res.*, pp. 1375-97

Dugas JC, Cuellar TL, Scholze A, Ason B, Ibrahim A, et al. 2010. Dicer1 and miR-219 Are required for normal oligodendrocyte differentiation and myelination. In *Neuron*, pp. 597-611

Dupree JL, Girault JA, Popko B. 1999. Axo-glial interactions regulate the localization of axonal paranodal proteins. In *The Journal of Cell Biology*, pp. 1145-52

Ek CJ, Habgood MD, Dennis R, Dziegielewska KM, Mallard C, et al. 2012. Pathological changes in the white matter after spinal contusion injury in the rat. In *PLoS ONE*, pp. e43484

Emery B. 2010. Transcriptional and post-transcriptional control of CNS myelination. In *Current Opinion in Neurobiology*, pp. 601-07

Fabricius C, Berthold CH, Rydmark M. 1993. Axoplasmic organelles at nodes of Ranvier. II. Occurrence and distribution in large myelinated spinal cord axons of the adult cat. In *J. Neurocytol.*, pp. 941-54

Faivre-Sarrailh C, Devaux JJ. 2013. Neuro-glial interactions at the nodes of Ranvier: implication in health and diseases. In *Front. Cell. Neurosci.*, pp. 196

Fanarraga ML, Griffiths IR, Zhao M, Duncan ID. 1998. Oligodendrocytes are not inherently programmed to myelinate a specific size of axon. In *J Comp Neurol*, pp. 94-100

Fancy SPJ, Baranzini SE, Zhao C, Yuk D-I, Irvine K-A, et al. 2009. Dysregulation of the Wnt pathway inhibits timely myelination and remyelination in the mammalian CNS. In *Genes Dev.*, pp. 1571-85

Fass D, Blacklow S, Kim PS, Berger JM. 1997. Molecular basis of familial hypercholesterolaemia from structure of LDL receptor module. In *Nature*, pp. 691-93

Feigenson K, Reid M, See J, Crenshaw EB, Grinspan JB. 2009. Wnt signaling is sufficient to perturb oligodendrocyte maturation. In *Mol. Cell. Neurosci.*, pp. 255-65

Feindel WH, Allison AC, Weddell G. 1948. Intravenous methylene blue for experimental studies on the central nervous system. In *Journal of neurology*

Fernandez-Castaneda A, Arandjelovic S, Stiles TL, Schlobach RK, Mowen KA, et al. 2013. Identification of the Low Density Lipoprotein (LDL) Receptor-related Protein-1 Interactome in Central Nervous System Myelin Suggests a Role in the Clearance of Necrotic Cell Debris. In *Journal of Biological Chemistry*, pp. 4538-48

Fields RD. 2008. Oligodendrocytes changing the rules: action potentials in glia and oligodendrocytes controlling action potentials. In *Neuroscientist*, pp. 540-43

Filbin MT. 2003. Myelin-associated inhibitors of axonal regeneration in the adult mammalian CNS. In *Nat. Rev. Neurosci.*, pp. 703-13

Fleming JC, Norenberg MD, Ramsay DA, Dekaban GA, Marcillo AE, et al. 2006. The cellular inflammatory response in human spinal cords after injury. In *Brain*, pp. 3249-69

Flores AI, Narayanan SP, Morse EN, Shick HE, Yin X, et al. 2008. Constitutively active Akt induces enhanced myelination in the CNS. In *J. Neurosci.*, pp. 7174-83

Franklin RJ, Blakemore WF. 1990. The peripheral nervous system-central nervous system regeneration dichotomy: a role for glial cell transplantation. In *Journal of Cell Science*, pp. 185-90

Franklin RJ, Hinks GL. 1999. Understanding CNS remyelination: clues from developmental and regeneration biology. In *J. Neurosci. Res.*, pp. 207-13

Franklin RJM. 2002. Why does remyelination fail in multiple sclerosis? In *Nat. Rev. Neurosci.*, pp. 705-14

Franklin RJM, ffrench-Constant C. 2008. Remyelination in the CNS: from biology to therapy. In *Nat. Rev. Neurosci.*, pp. 839-55

Franklin RJM, Gallo V. 2014. The translational biology of remyelination: Past, present, and future. In *Glia*, pp. n/a-n/a

Fünfschilling U, Supplie LM, Mahad D, Boretius S, Saab AS, et al. 2012. Glycolytic oligodendrocytes maintain myelin and long-term axonal integrity. In *Nature*, pp. 517-21

Gaultier A, Arandjelovic S, Li X, Janes J, Dragojlovic N, et al. 2008. A shed form of LDL receptor-related protein-1 regulates peripheral nerve injury and neuropathic pain in rodents. In *J. Clin. Invest.*, pp. 161-72

Gaultier A, Simon G, Niessen S, Dix M, Takimoto S, et al. 2010. LDL receptor-related protein 1 regulates the abundance of diverse cell-signaling proteins in the plasma membrane proteome. In *J. Proteome Res.*, pp. 6689-95

Genoud S, Lappe-Siefke C, Goebbels S, Radtke F, Aguet M, et al. 2002. Notch1 control of oligodendrocyte differentiation in the spinal cord. In *The Journal of Cell Biology*, pp. 709-18

Gensel JC, Zhang B. 2015. Macrophage activation and its role in repair and pathology after spinal cord injury. In *Brain Res*, pp. 1-11

Gibson EM, Purger D, Mount CW, Goldstein AK, Lin GL, et al. 2014. Neuronal activity promotes oligodendrogenesis and adaptive myelination in the mammalian brain. In *Science*, pp. 1252304

Gilson J, Blakemore WF. 1993. Failure of remyelination in areas of demyelination produced in the spinal cord of old rats. In *Neuropathol. Appl. Neurobiol.*, pp. 173-81

Gledhill RF, McDonald WI. 1977. Morphological characteristics of central demyelination and remyelination: A single-fiber study. In *Ann Neurol.*, pp. 552-60

Goldman SA, Kuypers NJ. 2015. How to make an oligodendrocyte. In *Development*, pp. 3983-95

Gonias SL, Campana WM. 2014. LDL Receptor-Related Protein-1. In *Am. J. Pathol.*, pp. 18-27: American Society for Investigative Pathology

Gorovoy M, Gaultier A, Campana WM, Firestein GS, Gonias SL. 2010. Inflammatory mediators promote production of shed LRP1/CD91, which regulates cell signaling and cytokine expression by macrophages. In *Journal of Leukocyte Biology*, pp. 769-78

Gout O, Dubois-Dalcq M. 1993. Directed migration of transplanted glial cells toward a spinal cord demyelinating lesion. In *Int. J. Dev. Neurosci.*, pp. 613-23

Gout O, Gansmuller A, Baumann N, Gumpel M. 1988. Remyelination by transplanted oligodendrocytes of a demyelinated lesion in the spinal cord of the adult shiverer mouse. In *Neurosci Lett*, pp. 195-99

Gow A, Southwood CM, Li JS, Pariali M, Riordan GP, et al. 1999. CNS myelin and sertoli cell tight junction strands are absent in Osp/claudin-11 null mice. In *Cell*, pp. 649-59

GrandPre T, Nakamura F, Vartanian T, Strittmatter SM. 2000. Identification of the Nogo inhibitor of axon regeneration as a Reticulon protein. In *Nature*, pp. 439-44

Greenhalgh AD, David S. 2014. Differences in the phagocytic response of microglia and peripheral macrophages after spinal cord injury and its effects on cell death. In *J. Neurosci.*, pp. 6316-22

Griffiths I, Klugmann M, Anderson T, Yool D, Thomson C, et al. 1998. Axonal swellings and degeneration in mice lacking the major proteolipid of myelin. In *Science*, pp. 1610-13

Haider L. 2015. Inflammation, Iron, Energy Failure, and Oxidative Stress in the Pathogenesis of Multiple Sclerosis. In *Oxid Med Cell Longev*, pp. 1-10

Han X. 2007. Potential mechanisms contributing to sulfatide depletion at the earliest clinically recognizable stage of Alzheimer's disease: a tale of shotgun lipidomics. In *J. Neurochem.*, pp. 171-79

Hannila S, Mellado W. 2017. Editorial: Myelin-Mediated Inhibition of Axonal Regeneration: Past, Present, and Future. In *Front Mol Neurosci*, pp. 113

Harrington EP, Zhao C, Fancy SPJ, Kaing S, Franklin RJM, Rowitch DH. 2010. Oligodendrocyte PTEN is required for myelin and axonal integrity, not remyelination. In *Ann Neurol.*, pp. 703-16

Harris JJ, Attwell D. 2012. The energetics of CNS white matter. In *J. Neurosci.*, pp. 356-71

Hartline DK, Colman DR. 2007. Rapid Conduction and the Evolution of Giant Axons and Myelinated Fibers. In *Current Biology*, pp. R29-R35

Hayashi H, Campenot RB, Vance DE, Vance JE. 2004. Glial lipoproteins stimulate axon growth of central nervous system neurons in compartmented cultures. In *J. Biol. Chem.*, pp. 14009-15

He X, Semenov M, Tamai K, Zeng X. 2004. LDL receptor-related proteins 5 and 6 in Wnt/beta-catenin signaling: arrows point the way. In *Development*, pp. 1663-77

Heinzer S, Kuhn G, Krucker T, Meyer E, Ulmann-Schuler A, et al. 2008. Novel three-dimensional analysis tool for vascular trees indicates complete micro-networks, not single capillaries, as the angiogenic endpoint in mice overexpressing human VEGF(165) in the brain. In *Neuroimage*, pp. 1549-58

Hennen E, Safina D, Haussmann U, Wörsdörfer P, Edenhofer F, et al. 2013. A LewisX Glycoprotein Screen Identifies the Low Density Lipoprotein Receptor-related Protein 1 (LRP1) as a Modulator of Oligodendrogenesis in Mice. In *Journal of Biological Chemistry*, pp. 16538-45

Herz J, Clouthier DE, Hammer RE. 1992. LDL receptor-related protein internalizes and degrades uPA-PAI-1 complexes and is essential for embryo implantation. In *Cell*, pp. 411-21

Herz J, Farese RV. 1999. The LDL receptor gene family, apolipoprotein B and cholesterol in embryonic development. In *J. Nutr.*, pp. 473S-75S

Herz J, Hamann U, Rogne S, Myklebost O, Gausepohl H, Stanley KK. 1988. Surface location and high affinity for calcium of a 500-kd liver membrane protein closely related to the LDL-receptor suggest a physiological role as lipoprotein receptor. In *EMBO J.*, pp. 4119-27

Hess A, Young JZ. 1952. The nodes of Ranvier. In *Proc. R. Soc. Lond., B, Biol. Sci.*, pp. 301-20

Hess MW, Kirschning E, Pfaller K, Debbage PL, Hohenberg H, Klima G. 1998. 5000-year-old myelin: uniquely intact in molecular configuration and fine structure. In *Curr. Biol.*, pp. R512-3

Hildebrand C, Bowe CM, Remahl IN. 1994. Myelination and myelin sheath remodelling in normal and pathological PNS nerve fibres. In *Prog. Neurobiol.*, pp. 85-141

Hildebrand C, Hahn R. 1978. Relation between myelin sheath thickness and axon size in spinal cord white matter of some vertebrate species. In *J. Neurol. Sci.*, pp. 421-34

Hildebrand C, Remahl S, Persson H, Bjartmar C. 1993. Myelinated nerve fibres in the CNS. In *Prog. Neurobiol.*, pp. 319-84

Hille B. 1992. Ionic Channels of Excitable Membranes. pp. 607: Sinauer Associates Incorporated

Horrocks LA. 1967. Composition of myelin from peripheral and central nervous systems of the squirrel monkey. In *J. Lipid Res.*, pp. 569-76

Huang PP, Alliquant B, Carmel PW, Friedman ED. 1991. Myelination of the rat retina by transplantation of oligodendrocytes into 4-day-old hosts. In *Exp Neurol*, pp. 291-300

Hughes V. 2013. Mapping brain networks: Fish-bowl neuroscience. In *Nature*, pp. 466-68

Imai M, Watanabe M, Suyama K, Osada T, Sakai D, et al. 2008. Delayed accumulation of activated macrophages and inhibition of remyelination after spinal cord injury in an adult rodent model. In *J Neurosurg Spine*, pp. 58-66

Inuzuka T, Fujita N, Sato S, Baba H, Nakano R, et al. 1991. Expression of the large myelin-associated glycoprotein isoform during the development in the mouse peripheral nervous system. In *Brain Res*, pp. 173-75

Jacobs JM. 1967. Experimental diphtheritic neuropathy in the rat. In *Br J Exp Pathol*, pp. 204-16

Jahn O, Tenzer S, Werner HB. 2009. Myelin Proteomics: Molecular Anatomy of an Insulating Sheath. In *Mol Neurobiol*, pp. 55-72

Jalil MA, Begum L, Contreras L, Pardo B, Iijima M, et al. 2005. Reduced N-acetylaspartate levels in mice lacking aralar, a brain- and muscle-type mitochondrial aspartate-glutamate carrier. In *J. Biol. Chem.*, pp. 31333-39

Jeon H, Meng W, Takagi J, Eck MJ, Springer TA, Blacklow SC. 2001. Implications for familial hypercholesterolemia from the structure of the LDL receptor YWTD-EGF domain pair. In *Nat. Struct. Biol.*, pp. 499-504

Jurevics H, Morell P. 1995. Cholesterol for synthesis of myelin is made locally, not imported into brain. In *J. Neurochem.*, pp. 895-901

Kanekiyo T, Bu G. 2014. The low-density lipoprotein receptor-related protein 1 and amyloid-β clearance in Alzheimer's disease. In *Frontiers in Aging Neuroscience*, pp. 93: Frontiers Media S.A.

Kanekiyo T, Cirrito JR, Liu CC, Shinohara M, Li J, et al. 2013. Neuronal Clearance of Amyloid- by Endocytic Receptor LRP1. In *J. Neurosci.*, pp. 19276-83

Kassmann CM. 2014. Myelin peroxisomes - essential organelles for the maintenance of white matter in the nervous system. In *Biochimie*, pp. 111-18

Kaul R, Gao GP, Balamurugan K, Matalon R. 1993. Cloning of the human aspartoacylase cDNA and a common missense mutation in Canavan disease. In *Nat Genet*, pp. 118-23

Keller TA, Just MA. 2009. Altering cortical connectivity: remediation-induced changes in the white matter of poor readers. In *Neuron*, pp. 624-31

Kessaris N, Fogarty M, Iannarelli P, Grist M, Wegner M, Richardson WD. 2006. Competing waves of oligodendrocytes in the forebrain and postnatal elimination of an embryonic lineage. In *Nat. Neurosci.*, pp. 173-79

Kim JY, Shen S, Dietz K, He Y, Howell O, et al. 2010. HDAC1 nuclear export induced by pathological conditions is essential for the onset of axonal damage. In *Nat. Neurosci.*, pp. 180-89

Kirby BB, Takada N, Latimer AJ, Shin J, Carney TJ, et al. 2006. In vivo time-lapse imaging shows dynamic oligodendrocyte progenitor behavior during zebrafish development. In *Nat. Neurosci.*, pp. 1506-11

Klämbt C. 2009. Modes and regulation of glial migration in vertebrates and invertebrates. In *Nat. Rev. Neurosci.*, pp. 769-79

Kopper TJ, Gensel JC. 2017. Myelin as an inflammatory mediator: Myelin interactions with complement, macrophages, and microglia in spinal cord injury. In *J. Neurosci. Res.*

Kotter MR, Li W-W, Zhao C, Franklin RJM. 2006. Myelin impairs CNS remyelination by inhibiting oligodendrocyte precursor cell differentiation. In *Journal of Neuroscience*, pp. 328-32

Kotter MR, Stadelmann C, Hartung H-P. 2011. Enhancing remyelination in disease--can we wrap it up? In *Brain*, pp. 1882-900

Kreusch A, Pfaffinger PJ, Stevens CF, Choe S. 1998. Crystal structure of the tetramerization domain of the Shaker potassium channel. In *Nature*, pp. 945-48

Kuhlmann T, Miron V, Cui Q, Cuo Q, Wegner C, et al. 2008. Differentiation block of oligodendroglial progenitor cells as a cause for remyelination failure in chronic multiple sclerosis. In *Brain*, pp. 1749-58

Laeng P, Molthagen M, Yu EG, Bartsch U. 1996. Transplantation of oligodendrocyte progenitor cells into the rat retina: extensive myelination of retinal ganglion cell axons. In *Glia*, pp. 200-10

Lai C, Brow MA, Nave KA, Noronha AB, Quarles RH, et al. 1987. Two forms of 1B236/myelin-associated glycoprotein, a cell adhesion molecule for postnatal neural development, are produced by alternative splicing. In *Proc. Natl. Acad. Sci. U.S.A.*, pp. 4337-41

Lasiene J, Matsui A, Sawa Y, Wong F, Horner PJ. 2009. Age-related myelin dynamics revealed by increased oligodendrogenesis and short internodes. In *Aging Cell*, pp. 201-13

Lazzarini RA. 2004. Myelin Biology and Disorders. Academic Press

Lee S, Leach MK, Redmond SA, Chong SYC, Mellon SH, et al. 2012a. A culture system to study oligodendrocyte myelination processes using engineered nanofibers. In *Nat. Methods*, pp. 917-22

Lee Y, Morrison BM, Li Y, Lengacher S, Farah MH, et al. 2012b. Oligodendroglia metabolically support axons and contribute to neurodegeneration. In *Nature Publishing Group*, pp. 443-48

Levine JM, Reynolds R, Fawcett JW. 2001. The oligodendrocyte precursor cell in health and disease. In *Trends in Neurosciences*, pp. 39-47

Li C, Tropak MB, Gerlai R, Clapoff S, Abramow-Newerly W, et al. 1994. Myelination in the absence of myelin-associated glycoprotein. In *Nature*, pp. 747-50

Li QM, Tep C, Yune TY, Zhou XZ, Uchida T, et al. 2007. Opposite regulation of oligodendrocyte apoptosis by JNK3 and Pin1 after spinal cord injury. In *J. Neurosci.*, pp. 8395-404

Li W-W, Penderis J, Zhao C, Schumacher M, Franklin RJM. 2006. Females remyelinate more efficiently than males following demyelination in the aged but not young adult CNS. In *Exp Neurol*, pp. 250-54

Liddelow SA, Guttenplan KA, Clarke LE, Bennett FC, Bohlen CJ, et al. 2017. Neurotoxic reactive astrocytes are induced by activated microglia. In *Nature Publishing Group*, pp. 481-87: Nature Publishing Group

Lillis AP, Van Duyn LB, Murphy-Ullrich JE, Strickland DK. 2008. LDL Receptor-Related Protein 1: Unique Tissue-Specific Functions Revealed by Selective Gene Knockout Studies. In *Physiological Reviews*, pp. 887-918

Lin J-P, Mironova YA, Shrager P, Giger RJ. 2017. LRP1 regulates peroxisome biogenesis and cholesterol homeostasis in oligodendrocytes and is required for proper CNS myelin development and repair. In *Elife*

Linington C, Waehneldt TV, Neuhoff V. 1980. The lipid composition of light and heavy myelin subfractions isolated from rabbit sciatic nerve. In *Neurosci Lett*, pp. 211-15

Liu J, Dietz K, DeLoyht JM, Pedre X, Kelkar D, et al. 2012. Impaired adult myelination in the prefrontal cortex of socially isolated mice. In *Nat. Neurosci.*, pp. 1621-23

Liu Q, Trotter J, Zhang J, Peters MM, Cheng H, et al. 2010. Neuronal LRP1 knockout in adult mice leads to impaired brain lipid metabolism and progressive, age-dependent synapse loss and neurodegeneration. In *J. Neurosci.*, pp. 17068-78

Liu Q, Zerbinatti CV, Zhang J, Hoe H-S, Wang B, et al. 2007a. Amyloid Precursor Protein Regulates Brain Apolipoprotein E and Cholesterol Metabolism through Lipoprotein Receptor LRP1. In *Neuron*, pp. 66-78

Maki T, Liang AC, Miyamoto N, Lo EH, Arai K. 2013. Mechanisms of oligodendrocyte regeneration from ventricular-subventricular zone-derived progenitor cells in white matter diseases. In *Front. Cell. Neurosci.*, pp. 275

Makinodan M, Rosen KM, Ito S, Corfas G. 2012. A critical period for social experience-dependent oligodendrocyte maturation and myelination. In *Science*, pp. 1357-60

Mangin J-M, Li P, Scafidi J, Gallo V. 2012. Experience-dependent regulation of NG2 progenitors in the developing barrel cortex. In *Nat. Neurosci.*, pp. 1192-94

Martenson RE. 1992. Myelin. In *Biology and Chemistry*, pp. 958: CRC PressI Llc

Martin AM, Kuhlmann C, Trossbach S, Jaeger S, Waldron E, et al. 2008. The functional role of the second NPXY motif of the LRP1 beta-chain in tissue-type plasminogen activator-mediated activation of N-methyl-D-aspartate receptors. In *J. Biol. Chem.*, pp. 12004-13

Matthews MA, Duncan D. 1971. A quantitative study of morphological changes accompanying the initiation and progress of myelin production in the dorsal funiculus of the rat spinal cord. In *J Comp Neurol*, pp. 1-22

Mauch DH, Nägler K, Schumacher S, Göritz C, Müller EC, et al. 2001. CNS synaptogenesis promoted by glia-derived cholesterol. In *Science*, pp. 1354-57
McDonald WI, Ohlrich GD. 1971. Quantitative anatomical measurements on single isolated fibres from the cat spinal cord. In *J. Anat.*, pp. 191-202
Mersmann N, Tkachev D, Jelinek R, Röth PT, Mobius W, et al. 2011. Aspartoacylase-lacZ knockin mice: an engineered model of Canavan disease. In *PLoS ONE*, pp. e20336
Mi S, Miller RH, Lee X, Scott ML, Shulag-Morskaya S, et al. 2005. LINGO-1 negatively regulates myelination by oligodendrocytes. In *Nat. Neurosci.*, pp. 745-51
Mikhailenko I, Considine W, Argraves KM, Loukinov D, Hyman BT, Strickland DK. 1999. Functional domains of the very low density lipoprotein receptor: molecular analysis of ligand binding and acid-dependent ligand dissociation mechanisms. In *Journal of Cell Science*, pp. 3269-81
Miller RH. 2002. Regulation of oligodendrocyte development in the vertebrate CNS. In *Prog. Neurobiol.*, pp. 451-67
Misgeld T, Kerschensteiner M, Bareyre FM, Burgess RW, Lichtman JW. 2007. Imaging axonal transport of mitochondria in vivo. In *Nat. Methods*, pp. 559-61
Mobius W, Cooper B, Kaufmann WA, Imig C, Ruhwedel T, et al. 2010. Electron microscopy of the mouse central nervous system. In *Methods Cell Biol*, pp. 475-512
Montag D, Giese KP, Bartsch U, Martini R, Lang Y, et al. 1994. Mice deficient for the myelin-associated glycoprotein show subtle abnormalities in myelin. In *Neuron*, pp. 229-46
Morell P. 2012. Myelin second edition. pp. 1-557: Springer Science & Business Media
Morell P, Norton WT. 1980. Myelin. In *Sci. Am.*, pp. 88-90- 92- 96 passim
Morita K, Sasaki H, Fujimoto K, Furuse M, Tsukita S. 1999. Claudin-11/OSP-based tight junctions of myelin sheaths in brain and Sertoli cells in testis. In *The Journal of Cell Biology*, pp. 579-88
Murray JA, Blakemore WF. 1980. The relationship between internodal length and fibre diameter in the spinal cord of the cat. In *J. Neurol. Sci.*, pp. 29-41
Muse ED, Jurevics H, Toews AD, Matsushima GK, Morell P. 2000. Parameters related to lipid metabolism as markers of myelination in mouse brain. In *J. Neurochem.*, pp. 77-86
Myllykoski M, Seidel L, Muruganandam G, Raasakka A, Torda AE, Kursula P. 2016. Structural and functional evolution of 2',3'-cyclic nucleotide 3'-phosphodiesterase. In *Brain Res*, pp. 64-78
Namboodiri AMA, Peethambaran A, Mathew R, Sambhu PA, Hershfield J, et al. 2006. Canavan disease and the role of N-acetylaspartate in myelin synthesis. In *Mol. Cell. Endocrinol.*, pp. 216-23
Narayanan SP, Flores AI, Wang F, Macklin WB. 2009. Akt signals through the mammalian target of rapamycin pathway to regulate CNS myelination. In *J. Neurosci.*, pp. 6860-70
Nave K-A. 2010a. Myelination and support of axonal integrity by glia. In *Nature*, pp. 244-52
Nave K-A. 2010b. Myelination and the trophic support of long axons. In *Nat. Rev. Neurosci.*, pp. 275-83: Nature Publishing Group

Nave K-A, Trapp BD. 2008. Axon-glial signaling and the glial support of axon function. In *Annu. Rev. Neurosci.*, pp. 535-61
Nave K-A, Werner HB. 2014. Myelination of the Nervous System: Mechanisms and Functions. In *Annu. Rev. Cell Dev. Biol.*, pp. 503-33
Nery S, Wichterle H, Fishell G. 2001. Sonic hedgehog contributes to oligodendrocyte specification in the mammalian forebrain. In *Development*, pp. 527-40
Neumann H, Kotter MR, Franklin RJM. 2009. Debris clearance by microglia: an essential link between degeneration and regeneration. In *Brain*, pp. 288-95
Norton WT, Poduslo SE. 1973. Myelination in rat brain: changes in myelin composition during brain maturation. In *J. Neurochem.*, pp. 759-73
Oblinger MM, Foe LG, Kwiatkowska D, Kemp RG. 1988. Phosphofructokinase in the rat nervous system: regional differences in activity and characteristics of axonal transport. In *J. Neurosci. Res.*, pp. 25-34
Orentas DM, Hayes JE, Dyer KL, Miller RH. 1999. Sonic hedgehog signaling is required during the appearance of spinal cord oligodendrocyte precursors. In *Development*, pp. 2419-29
Pearce J. 2003. Fragments of Neurological History.
Pedraza L, Frey AB, Hempstead BL, Colman DR, Salzer JL. 1991. Differential expression of MAG isoforms during development. In *J. Neurosci. Res.*, pp. 141-48
Pedraza L, Huang JK, Colman D. 2009. Disposition of axonal caspr with respect to glial cell membranes: Implications for the process of myelination. In *J. Neurosci. Res.*, pp. 3480-91
Peferoen L, Kipp M, van der Valk P, van Noort JM, Amor S. 2014. Oligodendrocyte-microglia cross-talk in the central nervous system. In *Immunology*, pp. 302-13
Perry VH, Hayes L. 1985. Lesion-induced myelin formation in the retina. In *J. Neurocytol.*, pp. 297-307
Peters A. 1961. A radial component of central myelin sheaths. In *J Biophys Biochem Cytol*, pp. 733-35
Peters A, Palay SL, Webster Hd. 1991. The fine structure of the nervous system. In *neurons and their supporting cells*, pp. 494: Oxford University Press, USA
Pfeiffer SE, Warrington AE, Bansal R. 1993. The oligodendrocyte and its many cellular processes. In *Trends in Cell Biology*, pp. 191-97
Pieper-Fürst U, Lammert F. 2013. Low-density lipoprotein receptors in liver: old acquaintances and a newcomer. In *Biochim. Biophys. Acta*, pp. 1191-98
Plemel JR, Manesh SB, Sparling JS, Tetzlaff W. 2013. Myelin inhibits oligodendroglial maturation and regulates oligodendrocytic transcription factor expression. In *Glia*, pp. 1471-87
Poliak S, Peles E. 2003. The local differentiation of myelinated axons at nodes of Ranvier. In *Nat. Rev. Neurosci.*, pp. 968-80
Posse De Chaves EI, Vance DE, Campenot RB, Kiss RS, Vance JE. 2000. Uptake of lipoproteins for axonal growth of sympathetic neurons. In *J. Biol. Chem.*, pp. 19883-90

Powers BE, Sellers DL, Lovelett EA, Cheung W, Aalami SP, et al. 2013. Remyelination reporter reveals prolonged refinement of spontaneously regenerated myelin. In *Proc. Natl. Acad. Sci. U.S.A.*, pp. 4075-80

Prinjha R, Moore SE, Vinson M, Blake S, Morrow R, et al. 2000. Inhibitor of neurite outgrowth in humans. In *Nature*, pp. 383-84

Quan G, Xie C, Dietschy JM, Turley SD. 2003. Ontogenesis and regulation of cholesterol metabolism in the central nervous system of the mouse. In *Brain Res. Dev. Brain Res.*, pp. 87-98

Quarles RH, Everly JL, Brady RO. 1973. Evidence for the close association of a glycoprotein with myelin in rat brain. In *J. Neurochem.*, pp. 1177-91: Blackwell Publishing Ltd

Raasakka A, Kursula P. 2014. The myelin membrane-associated enzyme 2',3'-cyclic nucleotide 3'-phosphodiesterase: on a highway to structure and function. In *Neurosci Bull*, pp. 956-66

Raff MC, Barres BA, Burne JF, Coles HS, Ishizaki Y, Jacobson MD. 1993. Programmed cell death and the control of cell survival: lessons from the nervous system. In *Science*, pp. 695-700

Ramon y Cajal S. 1928. Degeneration and regeneration of the nervous system. In *Degeneration and regeneration of the nervous system.*: Clarendon Press SN -

Ranvier L. 1871. Sur les éléments conjonctifs de la moelle épinière. In *Comptes Rendus de l'Académie des Sciences.*, pp. 1168-71: Comptes Rendus de l'Académie des Sciences.

Rasband MN, Peles E. 2016. The Nodes of Ranvier: Molecular Assembly and Maintenance. In *Cold Spring Harb Perspect Biol*, pp. a020495

Rasband MN, Peles E, Trimmer JS, Levinson SR, Lux SE, Shrager P. 1999. Dependence of nodal sodium channel clustering on paranodal axoglial contact in the developing CNS. In *J. Neurosci.*, pp. 7516-28

Rasband MN, Trimmer JS, Schwarz TL, Levinson SR, Ellisman MH, et al. 1998. Potassium channel distribution, clustering, and function in remyelinating rat axons. In *J. Neurosci.*, pp. 36-47

Rasminsky M, Sears TA. 1972. Internodal conduction in undissected demyelinated nerve fibres. In *J. Physiol. (Lond.)*, pp. 323-50

Richardson WD, Kessaris N, Pringle N. 2006. Oligodendrocyte wars. In *Nat. Rev. Neurosci.*, pp. 11-18

Rinholm JE, Hamilton NB, Kessaris N, Richardson WD, Bergersen LH, Attwell D. 2011. Regulation of Oligodendrocyte Development and Myelination by Glucose and Lactate. In *J. Neurosci.*, pp. 538-48

Robertson JD. 1959. Preliminary observations on the ultrastructure of nodes of Ranvier. In *Cell Tissue Res.*, pp. 553-60

Robinson S, Miller RH. 1999. Contact with central nervous system myelin inhibits oligodendrocyte progenitor maturation. In *Dev. Biol.*, pp. 359-68

Rosenbluth J. 1976. Intramembranous particle distribution at the node of Ranvier and adjacent axolemma in myelinated axons of the frog brain. In *J. Neurocytol.*, pp. 731-45

Rosenbluth J. 2009. Multiple functions of the paranodal junction of myelinated nerve fibers. In *J. Neurosci. Res.*, pp. 3250-58

Rotshenker S. 2003. Microglia and macrophage activation and the regulation of complement-receptor-3 (CR3/MAC-1)-mediated myelin phagocytosis in injury and disease. In *J Mol Neurosci*, pp. 65-72

Rowitch DH, Kriegstein AR. 2010. Developmental genetics of vertebrate glial-cell specification. In *Nature*, pp. 214-22

Ruckh JM, Zhao J-W, Shadrach JL, van Wijngaarden P, Rao TN, et al. 2012. Rejuvenation of Regeneration in the Aging Central Nervous System. In *Stem Cell*, pp. 96-103: Elsevier Inc.

Rudenko G, Henry L, Henderson K, Ichtchenko K, Brown MS, et al. 2002. Structure of the LDL receptor extracellular domain at endosomal pH. In *Science*, pp. 2353-58

Rumsby MG. 1978. Organization and structure in central-nerve myelin. In *Biochem. Soc. Trans.*, pp. 448-62

Safina D, Schlitt F, Romeo R, Pflanzner T, Pietrzik CU, et al. 2016. Low-density lipoprotein receptor-related protein 1 is a novel modulator of radial glia stem cell proliferation, survival, and differentiation. In *Glia*, pp. 1363-80

Saher G, Brugger B, Lappe-Siefke C, Mobius W, Tozawa R-i, et al. 2005. High cholesterol level is essential for myelin membrane growth. In *Nat. Neurosci.*, pp. 468-75

Saher G, Stumpf SK. 2015. Cholesterol in myelin biogenesis and hypomyelinating disorders. In *BBA - Molecular and Cell Biology of Lipids*, pp. 1083-94: Elsevier B.V.

Salzer JL. 1997. Clustering sodium channels at the node of Ranvier: close encounters of the axon-glia kind. In *Neuron*, pp. 843-46

Samorajski T, Lancaster F, Wiggins RC. 1986. Fetal ethanol exposure: a morphometric analysis of myelination in the optic nerve. In *Int. J. Dev. Neurosci.*, pp. 369-74

Sampaio-Baptista C, Khrapitchev AA, Foxley S, Schlagheck T, Scholz J, et al. 2013. Motor skill learning induces changes in white matter microstructure and myelination. In *J. Neurosci.*, pp. 19499-503

Sánchez-Abarca LI, Tabernero A, Medina JM. 2001. Oligodendrocytes use lactate as a source of energy and as a precursor of lipids. In *Glia*, pp. 321-29

Schmitt FO, Bear RS. 1937. The optical properties of vertebrate nerve axons as related to fiber size. In *J. Cell. Comp. Physiol.*, pp. 261-73: The Wistar Institute of Anatomy and Biology

Schmitt S, Castelvetri LC, Simons M. 2015. Metabolism and functions of lipids in myelin. In *Biochim. Biophys. Acta*, pp. 999-1005

Schnell L, Schwab ME. 1990. Axonal regeneration in the rat spinal cord produced by an antibody against myelin-associated neurite growth inhibitors. In *Nature*, pp. 269-72

Scholz J, Klein MC, Behrens TEJ, Johansen-Berg H. 2009. Training induces changes in white-matter architecture. In *Nat. Neurosci.*, pp. 1370-71

Schwab ME, Caroni P. 2008. Antibody against myelin-associated inhibitor of neurite growth neutralizes nonpermissive substrate properties of CNS white matter. In *Neuron*, pp. 404-05

Shen S, Sandoval J, Swiss VA, Li J, Dupree J, et al. 2008. Age-dependent epigenetic control of differentiation inhibitors is critical for remyelination efficiency. In *Nat. Neurosci.*, pp. 1024-34

Shields SA, Gilson JM, Blakemore WF, Franklin RJ. 1999. Remyelination occurs as extensively but more slowly in old rats compared to young rats following gliotoxin-induced CNS demyelination. In *Glia*, pp. 77-83

Shin J-Y, Fang Z-H, Yu Z-X, Wang C-E, Li S-H, Li X-J. 2005. Expression of mutant huntingtin in glial cells contributes to neuronal excitotoxicity. In *The Journal of Cell Biology*, pp. 1001-12

Sidman RL, Dickie MM, Appel SH. 1964. Mutant mice (quaking and jimpy) with deficient myelination in the central nervous system. In *Science*, pp. 309-11

Simons M, Lyons DA. 2013. Axonal selection and myelin sheath generation in the central nervous system. In *Curr Opin Cell Biol*, pp. 512-19

Simons M, Nave K-A. 2016. Oligodendrocytes: Myelination and Axonal Support. In *Cold Spring Harb Perspect Biol*, pp. a020479

Simons M, Snaidero N, Aggarwal S. 2012. Cell polarity in myelinating glia: From membrane flow to diffusion barriers. In *BBA - Molecular and Cell Biology of Lipids*, pp. 1146-53: Elsevier B.V.

Simpson AH, Gillingwater TH, Anderson H, Cottrell D, Sherman DL, et al. 2013. Effect of limb lengthening on internodal length and conduction velocity of peripheral nerve. In *J. Neurosci.*, pp. 4536-39

Sloane JA, Batt C, Ma Y, Harris ZM, Trapp B, Vartanian T. 2010. Hyaluronan blocks oligodendrocyte progenitor maturation and remyelination through TLR2. In *Proc. Natl. Acad. Sci. U.S.A.*, pp. 11555-60

Smart SL, Lopantsev V, Zhang CL, Robbins CA, Wang H, et al. 1998. Deletion of the K(V)1.1 potassium channel causes epilepsy in mice. In *Neuron*, pp. 809-19

Smith ME, Eng LF. 1965. The turnover of the lipid components of myelin. In *J Am Oil Chem Soc*, pp. 1013-18

Snaidero N, Mobius W, Czopka T, Hekking LHP, Mathisen C, et al. 2014. Myelin membrane wrapping of CNS axons by PI(3,4,5)P3-dependent polarized growth at the inner tongue. In *Cell*, pp. 277-90

Snaidero N, Simons M. 2014. Myelination at a glance. In *J. Cell. Sci.*, pp. 2999-3004

Snaidero N, Simons M. 2017. The logistics of myelin biogenesis in the central nervous system. In *Glia*, pp. 1021-31

Snaidero N, Velte C, Myllykoski M, Raasakka A, Ignatev A, et al. 2017. Antagonistic Functions of MBP and CNP Establish Cytosolic Channels in CNS Myelin. In *Cell Rep*, pp. 314-23: ElsevierCompany.

Spann NJ, Garmire LX, McDonald JG, Myers DS, Milne SB, et al. 2012. Regulated accumulation of desmosterol integrates macrophage lipid metabolism and inflammatory responses. In *Cell*, pp. 138-52

Springer TA. 1998. An extracellular beta-propeller module predicted in lipoprotein and scavenger receptors, tyrosine kinases, epidermal growth factor precursor, and extracellular matrix components. In *Journal of Molecular Biology*, pp. 837-62

Spuch C, Ortolano S, Navarro C. 2012. LRP-1 and LRP-2 receptors function in the membrane neuron. Trafficking mechanisms and proteolytic processing in Alzheimer's disease. In *Front Physiol*, pp. 1-14

Stiles TL, Dickendesher TL, Gaultier A, Fernandez-Castaneda A, Mantuano E, et al. 2013. LDL receptor-related protein-1 is a sialic-acid-independent receptor for myelin-associated glycoprotein that functions in neurite outgrowth inhibition by MAG and CNS myelin. In *Journal of Cell Science*, pp. 209-20

Suzuki A, Stern SA, Bozdagi O, Huntley GW, Walker RH, et al. 2011. Astrocyte-neuron lactate transport is required for long-term memory formation. In *Cell*, pp. 810-23

Syed YA, Baer AS, Lubec G, Hoeger H, Widhalm G, Kotter MR. 2008. Inhibition of oligodendrocyte precursor cell differentiation by myelin-associated proteins. In *Neurosurg Focus*, pp. E5

Talbott JF, Loy DN, Liu Y, Qiu MS, Bunge MB, et al. 2005. Endogenous Nkx2.2+/Olig2+ oligodendrocyte precursor cells fail to remyelinate the demyelinated adult rat spinal cord in the absence of astrocytes. In *Exp Neurol*, pp. 11-24

Taveggia C, Feltri ML, Wrabetz L. 2010. Signals to promote myelin formation and repair. In *Nat Rev Neurol*, pp. 276-87

Tawk M, Makoukji J, Belle M, Fonte C, Trousson A, et al. 2011. Wnt/beta-catenin signaling is an essential and direct driver of myelin gene expression and myelinogenesis. In *J. Neurosci.*, pp. 3729-42

Tekki-Kessaris N, Woodruff R, Hall AC, Gaffield W, Kimura S, et al. 2001. Hedgehog-dependent oligodendrocyte lineage specification in the telencephalon. In *Development*, pp. 2545-54

Toyama BH, Savas JN, Park SK, Harris MS, Ingolia NT, et al. 2013. Identification of long-lived proteins reveals exceptional stability of essential cellular structures. In *Cell*, pp. 971-82

Trapp BD, Nishiyama A, Cheng D, Macklin W. 1997. Differentiation and death of premyelinating oligodendrocytes in developing rodent brain. In *The Journal of Cell Biology*, pp. 459-68

Tropak MB, Johnson PW, Dunn RJ, Roder JC. 1988. Differential splicing of MAG transcripts during CNS and PNS development. In *Brain Res*, pp. 143-55

Tropak MB, Roder JC. 1997. Regulation of myelin-associated glycoprotein binding by sialylated cis-ligands. In *J. Neurochem.*, pp. 1753-63

Trotter J, Karram K, Nishiyama A. 2010. NG2 cells: Properties, progeny and origin. In *Brain Res Rev*, pp. 72-82

Tsai H-H, Niu J, Munji R, Davalos D, Chang J, et al. 2016. Oligodendrocyte precursors migrate along vasculature in the developing nervous system. In *Science*, pp. 379-84

Umemori H, Sato S, Yagi T, Aizawa S, Yamamoto T. 1994. Initial events of myelination involve Fyn tyrosine kinase signalling. In *Nature*, pp. 572-76

Vabnick I, Shrager P. 1998. Ion channel redistribution and function during development of the myelinated axon. In *J. Neurobiol.*, pp. 80-96

Vabnick I, Trimmer JS, Schwarz TL, Levinson SR, Risal D, Shrager P. 1999. Dynamic potassium channel distributions during axonal development prevent aberrant firing patterns. In *J. Neurosci.*, pp. 747-58

Vargas ME, Barres BA. 2007. Why is Wallerian degeneration in the CNS so slow? In *Annu. Rev. Neurosci.*, pp. 153-79

Velumian AA, Samoilova M, Fehlings MG. 2011. Visualization of cytoplasmic diffusion within living myelin sheaths of CNS white matter axons using microinjection of the fluorescent dye Lucifer Yellow. In *Neuroimage*, pp. 27-34

Verkhratsky A, Butt AM. 2013. Glial Physiology and Pathophysiology Ch5. pp. 560: John Wiley & Sons

Virchow R. 1854. Ueber das ausgebreitete Vorkommen einer dem Nervenmark analogen Substanz in den thierischen Geweben. In *Archiv für pathologische Anatomie und Physiologie und für klinische Medicin*, pp. 562-72

Virchow R. 1858. Die Cellularpathologie in ihrer Begründung auf physiologische und pathologische Gewebelehre. In *Vorlesungen uber Pathologie. - Berlin : Hirschwald*: Hirschwald

Vogel DYS, Vereyken EJF, Glim JE, Heijnen PDAM, Moeton M, et al. 2013. Macrophages in inflammatory multiple sclerosis lesions have an intermediate activation status. In *J Neuroinflammation*, pp. 35

Wang H, Kunkel DD, Martin TM, Schwartzkroin PA, Tempel BL. 1993. Heteromultimeric K+ channels in terminal and juxtaparanodal regions of neurons. In *Nature*, pp. 75-79

Wang JT, Medress ZA, Barres BA. 2012. Axon degeneration: Molecular mechanisms of a self-destruction pathway. In *The Journal of Cell Biology*, pp. 7-18

Wang X-M, Yik WY, Zhang P, Lu W, Huang N, et al. 2015. Induced pluripotent stem cell models of Zellweger spectrum disorder show impaired peroxisome assembly and cell type-specific lipid abnormalities. In *Stem Cell Res Ther*, pp. 158

Waxman SG, Ritchie JM. 1985. Organization of ion channels in the myelinated nerve fiber. In *Science*, pp. 1502-07

Wiame E, Tyteca D, Pierrot N, Collard F, Amyere M, et al. 2009. Molecular identification of aspartate N-acetyltransferase and its mutation in hypoacetylaspartia. In *Biochem. J.*, pp. 127-36

Wibom R, Lasorsa FM, Töhönen V, Barbaro M, Sterky FH, et al. 2009. AGC1 deficiency associated with global cerebral hypomyelination. In *N Engl J Med*, pp. 489-95

Wiesinger H, Hamprecht B, Dringen R. 1997. Metabolic pathways for glucose in astrocytes. In *Glia*, pp. 22-34

Wiley CA, Ellisman MH. 1980. Rows of dimeric-particles within the axolemma and juxtaposed particles within glia, incorporated into a new model for the paranodal glial-axonal junction at the node of Ranvier. In *The Journal of Cell Biology*, pp. 261-80

Williams K, Ulvestad E, Waage A, Antel JP, McLaurin J. 1994. Activation of adult human derived microglia by myelin phagocytosis in vitro. In *J. Neurosci. Res.*, pp. 433-43

Winters JJ, Ferguson CJ, Lenk GM, Giger-Mateeva VI, Shrager P, et al. 2011. Congenital CNS hypomyelination in the Fig4 null mouse is rescued by neuronal expression of the PI(3,5)P(2) phosphatase Fig4. In *J. Neurosci.*, pp. 17736-51

Wolswijk G. 1998. Chronic stage multiple sclerosis lesions contain a relatively quiescent population of oligodendrocyte precursor cells. In *J. Neurosci.*, pp. 601-09

Xu Q, Bernardo A, Walker D, Kanegawa T, Mahley RW, Huang Y. 2006. Profile and regulation of apolipoprotein E (ApoE) expression in the CNS in mice with targeting of green fluorescent protein gene to the ApoE locus. In *J. Neurosci.*, pp. 4985-94

Yang M, Huang H, Li J, Li D, Wang H. 2004. Tyrosine phosphorylation of the LDL receptor-related protein (LRP) and activation of the ERK pathway are required for connective tissue growth factor to potentiate myofibroblast differentiation. In *FASEB J.*, pp. 1920-21

Yeung MSY, Zdunek S, Bergmann O, Bernard S, Salehpour M, et al. 2014. Dynamics of oligodendrocyte generation and myelination in the human brain. In *Cell*, pp. 766-74

Young KM, Psachoulia K, Tripathi RB, Dunn S-J, Cossell L, et al. 2013. Oligodendrocyte dynamics in the healthy adult CNS: evidence for myelin remodeling. In *Neuron*, pp. 873-85

Yuan A, Mills RG, Bamburg JR, Bray JJ. 1999. Cotransport of glyceraldehyde-3-phosphate dehydrogenase and actin in axons of chicken motoneurons. In *Cell Mol Neurobiol*, pp. 733-44

Zala D, Hinckelmann M-V, Yu H, Lyra da Cunha MM, Liot G, et al. 2013. Vesicular glycolysis provides on-board energy for fast axonal transport. In *Cell*, pp. 479-91

Zalc B. 2006. The acquisition of myelin: a success story. In *Novartis Found. Symp.*, pp. 15-21- discussion 21-5- 54-7- 275-81

Zhang Y, Argaw AT, Gurfein BT, Zameer A, Snyder BJ, et al. 2009. Notch1 signaling plays a role in regulating precursor differentiation during CNS remyelination. In *Proc. Natl. Acad. Sci. U.S.A.*, pp. 19162-67

Zhang Y, Chen K, Sloan SA, Bennett ML, Scholze AR, et al. 2014. An RNA-sequencing transcriptome and splicing database of glia, neurons, and vascular cells of the cerebral cortex. In *J. Neurosci.*, pp. 11929-47

Zhao C, Li W-W, Franklin RJM. 2006. Differences in the early inflammatory responses to toxin-induced demyelination are associated with the age-related decline in CNS remyelination. In *Neurobiol. Aging*, pp. 1298-307

Zhao X, Pan Z, Wu J, Zhou G, Zeng Y. 2010. Automatic identification and morphometry of optic nerve fibers in electron microscopy images. In *Comput Med Imaging Graph*, pp. 179-84

Zhou L, Zhang CL, Messing A, Chiu SY. 1998. Temperature-sensitive neuromuscular transmission in Kv1.1 null mice: role of potassium channels under the myelin sheath in young nerves. In *J. Neurosci.*, pp. 7200-15

Zhou Y, Simpson S, Charlesworth JC, van der Mei I, Lucas RM, et al. 2017. Variation within MBP gene predicts disease course in multiple sclerosis. In *Brain Behav*, pp. e00670

Zlokovic BV, Deane R, Sagare AP, Bell RD, Winkler EA. 2008. Low-density lipoprotein receptor-related protein-1: a serial clearance homeostatic mechanism controlling Alzheimer's amyloid β-peptide elimination from the brain. In *Sci Signal*, pp. ra15-ra15

Zonta B, Tait S, Melrose S, Anderson H, Harroch S, et al. 2008. Glial and neuronal isoforms of Neurofascin have distinct roles in the assembly of nodes of Ranvier in the central nervous system. In *The Journal of Cell Biology*, pp. 1169-77

Zuchero JB, Barres BA. 2013. Intrinsic and extrinsic control of oligodendrocyte development. In *Current Opinion in Neurobiology*, pp. 914-20: Elsevier Ltd

CHAPTER II

LRP1 Regulates Peroxisome Biogenesis and Cholesterol Homeostasis in Oligodendrocytes and Promotes CNS Myelin Development and Repair

2.1 Abstract

Low-density lipoprotein receptor-related protein-1 (LRP1) is a large endocytic and signaling molecule broadly expressed by neurons and glia. In adult mice, global inducible (*Lrp1*$^{flox/flox}$*;CAG-CreER*) or oligodendrocyte (OL)-lineage specific ablation (*Lrp1*$^{flox/flox}$*;Pdgfra-CreER*) of *Lrp1* attenuates repair of damaged white matter. In oligodendrocyte progenitor cells (OPCs), *Lrp1* is required for cholesterol homeostasis and differentiation into mature OLs. *Lrp1*-deficient OPC/OLs show a strong increase in the sterol-regulatory element-binding protein-2 yet are unable to maintain normal cholesterol levels, suggesting more global metabolic deficits. Mechanistic studies revealed a decrease in peroxisomal biogenesis factor-2 and fewer peroxisomes in OL processes. Treatment of*Lrp1*$^{-/-}$ OPCs with cholesterol or activation of peroxisome proliferator-activated receptor-γ with pioglitazone alone is not sufficient to promote differentiation; however, when combined, cholesterol and pioglitazone enhance OPC differentiation into mature OLs. Collectively, our studies reveal a novel role for *Lrp1* in peroxisome biogenesis, lipid homeostasis, and OPC differentiation during white matter development and repair

2.2 Introduction

In the central nervous system (CNS), the myelin-producing cell is the oligodendrocyte (OL). Mature OLs arise from oligodendrocyte progenitor cells (OPCs), a highly migratory pluripotent cell type (Rowitch & Kriegstein 2010, Zuchero & Barres 2013). OPCs that commit to differentiate along the OL-lineage undergo a tightly regulated process of maturation, membrane expansion, and axon

myelination (Emery et al 2009, Hernandez & Casaccia 2015, Li & Yao 2012, Simons & Lyons 2013). Even after developmental myelination is completed, many OPCs persist as stable CNS resident cells that participate in normal myelin turnover and white matter repair following injury or disease (Fancy et al 2011, Franklin & ffrench-Constant 2008).

LRP1 is a member of the LDL receptor family with prominent functions in endocytosis, lipid metabolism, energy homeostasis, and signal transduction (Boucher & Herz 2011). *Lrp1* is broadly expressed in the CNS and abundantly found in OPCs (Auderset et al 2016, Zhang et al 2014). Global deletion of *Lrp1* is embryonically lethal (Herz et al 1992) and conditional deletion revealed numerous tissue specific functions in neural and non-neural cell types (Lillis et al 2008). In the PNS, *Lrp1* regulates Schwann cell survival, myelin thickness, and morphology of Remak bundles (Campana et al 2006, Mantuano et al 2010, Orita et al 2013). In the CNS, *Lrp1* influences neural stem cell proliferation (Auderset et al 2016), synaptic strength (Gan et al 2014, Nakajima et al 2013), axonal regeneration (Landowski et al 2016, Stiles et al 2013, Yoon et al 2013), and clearance of amyloid beta amyloid beta (Kanekiyo et al 2013, Kim et al 2014, Liu et al 2010, Zlokovic et al 2008). Recent evidence shows that neurospheres deficient for*Lrp1* produce more $GFAP^+$ astrocytes at the expense of $O4^+$ OLs and $TuJ1^+$ neurons (Hennen et al 2013, Safina et al 2016). Whether LRP1 is required for proper CNS myelinogenesis, nerve conduction, or repair of damaged adult CNS white matter, however, has not yet been examined. Moreover, the molecular basis of how LRP1 influences OPC differentiation remains poorly understood.

LRP1 is a large type-1 membrane protein comprised of a ligand binding 515-kDa α chain non-covalently linked to an 85kDa β chain that contains the transmembrane domain and cytoplasmic portion. Through its α chain, LRP1 binds over 40 different ligands with diverse biological functions (Fernandez-Castaneda et al 2013, Lillis et al 2008). LRP1 mediates endocytotic clearance of a multitude of extracellular ligands (May et al 2003, Tao et al 2016) and participates in cell

signaling, including activation of the Ras/MAPK and AKT pathways (Fuentealba et al 2009, Martin et al 2008, Muratoglu et al 2010). The LRP1β chain can be processed by γ-secretase and translocate to the nucleus where it associates with transcription factors to regulate gene expression (Carter 2007, May et al 2002).

Here, we combine conditional *Lrp1* gene ablation with ultrastructural and electrophysiological approaches to show that*Lrp1* is important for myelin development, nerve conduction, and adult CNS white matter repair. Gene expression analysis in *Lrp1*-deficient OPCs identified a reduction in peroxisomal gene products. We show that *Lrp1* deficiency decreases production of peroxisomal proteins and disrupts cholesterol homeostasis. Mechanistic studies uncover a novel role for *Lrp1* in PPARγ-mediated OPC differentiation, peroxisome biogenesis, and CNS myelination.

2.3 Results

2.3.1 In adult mice, inducible ablation of Lrp1attenuates CNS white matter repair

To study the role of *Lrp1* in CNS myelin repair, we pursued a mouse genetic approach. *Lrp1* global knockout through the germline results in embryonic lethality (Herz et al 1992). To circumvent this limitation, we generated *Lrp1*$^{flox/flox}$*;CAG-CreER*^{TM} mice (*Lrp1* iKO) that allow tamoxifen (TM)-inducible global gene ablation. As control, *Lrp1* mice harboring at least one wild-type or non-recombined *Lrp1* allele were injected with TM and processed in parallel (Figure 2.1). TM injection into P56 mice resulted in an approximately 50% decrease of LRP1 in brain without noticeable impact on white matter structure (Figure 2.1). One month after TM treatment, *Lrp1* iKO and control mice were subjected to unilateral injection of 1% lysophosphatidylcholine (LPC) into the corpus callosum. The contralateral side was injected with isotonic saline (PBS) and served as control. Brains were collected 10 and 21 days after LPC/PBS injection and the extent of white matter damage and repair were analyzed (Figure 2.2a). Serially cut sections were stained with Fluoromyelin-Green (FM-G) and anti-GFAP (Figure 2.3a and b) or subjected to *in*

situ hybridization (ISH) for the myelin-associated gene products *Mbp*, *Mag, Plp1* and the OPC marker *Pdgfra* (Figure 2.2b, Figure 2.3c and d). Independent of *Lrp1* genotype, at 10 days following LPC injection, similar-sized white matter lesions (area devoid of FM-G labeling) and comparable astrogliosis were observed (Figure 2.3b). At 21 DPI, however, astrogliosis was increased and the lesion area larger in LPC injected *Lrp1* iKO mice (Figure 2.3b). ISH revealed no changes in *Mbp, Mag, Plp1,* or *Pdgfra* expression on the PBS injected side (Figure 2.3c); however, LPC injection resulted in a strong increase in *Mag, Plp1,* and *Mbp1* (Figure 2.3c and d). Because *Mbp* mRNA is strongly upregulated in myelin producing OLs and transported into internodes (Ainger 1993), we used *Mpb* ISH to find the white matter lesion (Figure 2.2b). The section with the largest circumference of the intensely labeled Mbp^{+}area was defined as the lesion center and subjected to quantification (Figure 2.2c). The extent of white matter lesion, the outer rim of elevated *Mbp* labeling (white dotted line), was comparable between*Lrp1* control and iKO mice (Figure 2.2d). As shown in Figure 2.2c, the area that failed to undergo repair, the inner rim of elevated *Mbp* labeling (yellow solid line), was larger in *Lrp1* iKO mice (Figure 2.2c). Quantification of lesion repair revealed a significant decrease in *Lrp1* iKO mice compared to *Lrp1* control mice (Figure 2.2e). As an independent assessment, serial sections were stained for *Pdgfra*, *Plp1,* and *Mag* transcripts and revealed fewer labeled cells within the lesion of iKO mice (Figure 2.3e). Together these studies indicate that in adult mice, *Lrp1* is required for the timely repair of a chemically induced white matter lesion. When coupled with the broad expression of *Lrp1* in different neural cell types (Zhang et al 2014), this prompted further studies to examine whether *Lrp1* function in the OL lineage is important for CNS white matter repair.

2.3.2 OL-lineage specific ablation of *Lrp1* impairs timely repair of damaged white matter

To determine the cell autonomy of *Lrp1* in adult white matter repair, we generated $Lrp1^{flox/flox}$;*Pdgfra-CreER*^{TM} (*Lrp1* iKO^{OL}) mice that allow inducible gene ablation selectively in OPCs in adult mice. At P56 *Lrp1* iKO^{OL} mice were injected with

TM and one month later subjected to unilateral injection of LPC into the corpus callosum and PBS on the contralateral side. *Lrp1* control mice, harboring at least one wildtype or non-recombined *Lrp1* allele, were processed in parallel. Twenty-one days post LPC/PBS injection (21 DPI), brains were collected and serially sectioned (Figure 2.2f). Detection of the initial white matter lesion and quantification of the extent of white matter repair was assessed as described above (Figure 2.2b). The initial size of the LPC inflicted white matter lesion was comparable between *Lrp1* control and iKO^{OL} mice (Figure 2.2g and h). However, the extent of lesion repair was significantly decreased in *Lrp1* iKO^{OL} mice (Figure 2.2g and i). This demonstrates an OL-linage-specific role for *Lrp1* in the timely repair of a chemically induced white matter lesion.

2.3.3 *Lrp1* is important for proper CNS myelin development and optic nerve conduction

To examine whether *Lrp1* is required for proper CNS myelin development, we generated *Lrp1$^{flox/flox}$;Olig2-Cre* mice (*Lrp1*cKO^{OL}) (Figure 2.5a). *Lrp1* cKO^{OL} pups are born at the expected Mendelian frequency and show no obvious abnormalities at the gross anatomical level (data not shown). LRP1 protein levels in the brains of P10, P21, and P56 *Lrp1* control and cKO^{OL} mice were analyzed by Western blot analysis and revealed a partial loss of LRP1β (Figure 2.5b). The partial loss of LRP1β in brain lysates of *Lrp1* cKO^{OL} mice is due to *Lrp1*expression in several other neural cell types. *Olig2-Cre* mice express cre recombinase under the endogenous *Olig2* promoter, rendering mice haploinsufficient for *Olig2*. Loss of one allele of *Olig2* has been shown to reduce *Mbp* mRNA expression in neonatal mouse spinal cord (Liu et al 2007b). Therefore, we examined whether the presence of the *Olig2-Cre* allele influences LRP1β, MAG, CNP, or MBP in P21 brain lysates. Quantification of protein levels revealed no differences between *Lrp1$^{flox/+}$* and *Lrp1$^{flox/+}$;Olig2-Cre* mice (Figure 2.5c). However, LRP1β is reduced in P10 and P21 *Lrp1$^{flox/flox}$;Olig2-Cre* mice, compared to *Lrp1$^{flox/flox}$* or *Lrp1$^{flox/+}$;Olig2-Cre* mice (Figure 2.5d). Similar results were showed with *Lrp1$^{flox/flox}$; CAG-CreER^{TM}* (Figure 2.6).

To examine whether *Lrp1* cKO^{OL} mice exhibit defects in myelin development, optic nerves were isolated at P10, the onset of myelination; at P21, near completion of myelination; and at P56, when myelination is completed. Ultrastructural analysis at P10 revealed no significant difference in myelinated axons between *Lrp1* control (17 ± 6%) and cKO^{OL} (7 ± 2%) optic nerves. At P21 and P56, the percentile of myelinated axons in the optic nerve of cKO^{OL} mice (49 ± 4% and 66 ± 5%, respectively) is significantly reduced compared to controls (70 ± 2% and 88 ± 1%, respectively) (Figure 2.4a and b). In *Lrp1* cKO^{OL} mice, hypomyelination is preferentially observed in intermediate to small caliber axons (Figure 2.5f-n). As an independent assessment of fiber structure, the g-ratio was determined. At P10, P21, and P56 the average g-ratio of *Lrp1* cKO^{OL} optic fibers is significantly larger than in age-matched *Lrp1* control mice (Figure 2.4c and Figure 2.5e). Western blot analysis of adult *Lrp1* cKO^{OL} brain lysates revealed a significant reduction in CNP, MAG, and MBP (Figure 2.5o and p). Together, these studies show that in the OL lineage *Lrp1* functions in a cell-autonomous manner and is required for proper CNS myelinogenesis.

To examine whether *Lrp1* in OLs is required for nodal organization, optic nerve sections of P21 *Lrp1* control and cKO^{OL} mice were immunostained for sodium channels (PanNaCh) and the paranodal axonal protein (Caspr). Nodal density, the number of PanNaCh^{+} clusters in longitudinal optic nerve sections is significantly reduced in *Lrp1* cKO^{OL} mice (Figure 2.4d and g). In addition, an increase in nodal structural defects, including elongated nodes, heminodes, and nodes in which sodium channel staining is missing, was observed in mutant nerves. Quantification revealed an increase of nodal structural defects from 13.7 ± 1.3% in *Lrp1* control mice to 33.4 ± 2.9% in cKO^{OL} optic nerves (Figure 2.4e and h). Sodium channel staining associated with large caliber (>1 μm) axons was increased and staining associated with small (<0.5 μm) caliber axons was reduced (Figure 2.4f and i). The density of optic nerve axons does not change between *Lrp1* control and cKO^{OL} mice (Figure 2.5q-s).

To assess whether structural defects observed in optic nerve of *Lrp1*cKO^{OL} mice are associated with impaired nerve conduction, we used electrophysiological methods to measure compound action potentials (CAPs) in acutely isolated nerves (Figure 2.7). Recordings revealed a modest but significant delay in a subpopulation of myelinated optic nerve axons. The observed changes in conduction in *Lrp1* cKO^{OL} nerves fit well with defects at the ultrastructural level and aberrant node assembly.

2.3.4 Conditional ablation of Lrp1 in the OL-lineage attenuates OPC differentiation

CNS hypomyelination in *Lrp1* cKO^{OL} mice may be the result of reduced OPC production or impaired OPC differentiation into myelin producing OLs. To distinguish between these two possibilities, optic nerve cross-sections were stained with anti-PDGFRα, a marker for OPCs; anti-Olig2, to account for all OL lineage cells; and anti-CC1, a marker for mature OLs. No change in OPC density was observed, but the number of mature OLs was significantly reduced in *Lrp1* cKO^{OL} mice (Figure 2.8a and c). Optic nerve ISH for *Pdgfra* revealed no reduction in labeled cells in *Lrp1*cKO^{OL} mice, a finding consistent with anti-PDGFRα immunostaining. The density of *Plp* and *Mag* expressing cells, however, is significantly reduced in the optic nerve cross-sections and longitudinal-sections of *Lrp1* cKO^{OL} mice (Figure 2.8b and d). The optic nerve cross-sectional area is not different between *Lrp1*control and cKO^{OL} mice (Figure 2.9a). Together these studies show that OPCs are present at normal density and tissue distribution in *Lrp1* cKO^{OL} mice, but apparently fail to generate sufficient numbers of mature, myelin-producing OLs.

2.3.5 Loss of *Lrp1* attenuates OPC differentiation *in vitro*

To independently assess the role of *Lrp1* in OL differentiation, we isolated OPCs from brains of *Lrp1* control and cKO^{OL} pups (Figure 2.8e). OPCs were kept in PDGF-AA containing growth medium (GM) or switched to differentiation medium (DM) containing triiodothyronine (T3). Staining for the proliferation marker Ki67 did not reveal any change in OPC proliferation in *Lrp1* cKO^{OL} cultures after 1 or 2

days in GM (Figure 2.9d-f). After 3 days in DM, the number of $NG2^+$ and CNP^+ OLs was comparable between *Lrp1* control and cKO^{OL} cultures (Figure 2.8f and h). An abundant signal for LRP1β was detected in *Lrp1* control lysate, but LRP1 was not detectable in *Lrp1* cKO^{OL} cell lysate, demonstrating efficient gene deletion in the OL linage (Figure 2.8g). Moreover, a significant reduction in CNP, MAG, and PLP was detected in *Lrp1*cKO^{OL} cell lysates (Figure 2.9g and i). Importantly, halplosufficiency for Olig2 in cultures prepared from$Lrp1^{flox/+}$ and $Lrp1^{flox/+}$*;Olig2-Cre* pups did not reveal any difference in MAG, PLP, or LRP1β protein (Figure 2.9b and c). As LRP1 signaling is known to regulate ERK1/2 and AKT activity (Yoon et al 2013), immunoblots were probed for pAKT (S473) and pErk1/2. When normalized to total AKT, levels of pAKT are reduced in *Lrp1* cKO^{OL} lysate, while pERK1/2 levels are comparable between *Lrp1* control and cKO^{OL} lysates (Figure 2.9h and j). Extended culture of*Lrp1*-deficient OLs in DM for 5 days is not sufficient to restore myelin protein levels. Compared to *Lrp1* control cultures, mutants show significantly fewer MAG^+, PLP^+, and MBP^+ cells (Figure 2.8i and k) and immunoblotting of cell lysates revealed a reduction in total CNP, MAG, PLP, and MBP (Figure 2.8j and l). Collectively, our studies demonstrate a cell-autonomous function for *Lrp1* in the OL lineage, important for OPC differentiation into myelin sheet producing OLs.

2.3.6 *Lrp1* deficiency in OPCs and OLs causes a reduction in free cholesterol

While LRP1 has been implicated in cholesterol uptake and homeostasis in non-neural cell types (van de Sluis et al 2017), a role in cholesterol homeostasis in the OL-lineage has not yet been investigated. We find that $Lrp1^{-/-}$ OPCs, prepared from$Lrp1^{flox/flox}$*;Olig2-Cre*, have reduced levels of free cholesterol compared to *Lrp1* control OPCs (Figure 2.10a and b). Levels of cholesteryl-ester are very low in the CNS (Björkhem & Meaney 2004) and near the detection limit in *Lrp1* control and $Lrp1^{-/-}$ OPCs (Figure 2.10c). Morphological studies with MBP^+ OLs revealed a significant reduction in myelin-like membrane sheet expansion in$Lrp1^{-/-}$ OLs (Figure 2.10d and e), reminiscent of wildtype OLs cultures treated with statins to inhibit HMG-CoA reductase, the rate limiting enzyme in the cholesterol biosynthetic pathway (Maier et al 2009, Paintlia et al 2010, Smolders et al 2010). To assess

cholesterol distribution in primary OLs, cultures were stained with filipin. In *Lrp1* control OLs, staining was observed on myelin sheets and was particularly strong near the cell soma. In *Lrp1*$^{-/-}$ OLs, filipin and MBP staining were significantly reduced (Figure 2.10f). Reduced filipin staining is not simply a reflection of smaller cell size, as staining intensity was decreased when normalized to myelin sheet surface area (Figure 2.10g). Thus, independent measurements revealed a dysregulation of cholesterol homeostasis in *Lrp1*$^{-/-}$ OPCs/OLs.

Cellular lipid homeostasis is regulated by a family of membrane-bound basic helix-loop-helix transcription factors, called sterol-regulatory element-binding proteins (SREBPs). To assess whether*Lrp1* deficiency leads to an increase in SREBP2, OLs were cultured for 3 days in DM and analyzed by immunoblotting. OL cultures prepared from *Lrp1*$^{flox/+}$ and *Lrp1*$^{flox/+}$*;Olig2-cre* pups showed very similar levels of SREBP2. In marked contrast, we observed a strong upregulation of SREBP2 in *Lrp1*$^{-/-}$ cultures (Figure 2.10i, Figure 2.11a and b). Elevated SREBP2 in mutant cultures can be reversed by exogenous cholesterol directly added to the culture medium (Figure 2.10i and j). This shows the existence of LRP1-independent cholesterol uptake mechanisms in *Lrp1*$^{-/-}$ OLs and a normal physiological response to elevated levels of cellular cholesterol. In *Lrp1* control cultures, bath application of cholesterol leads to a small, yet significant decrease in SREBP2 (Figure 2.10j). Given the importance of cholesterol in OL maturation (Kramer-Albers et al 2006, Mathews et al 2014, Saher et al 2005), we examined whether the differentiation block can be rescued by bath-applied cholesterol. Remarkably, cholesterol treatment of *Lrp1*$^{-/-}$OLs for 3 days failed to augment PLP, MAG or CNP to control levels (Figure 2.10k-n). While cholesterol treated *Lrp1*$^{-/-}$ OLs showed a modest increase in PLP, levels remained below *Lrp1* controls. Moreover, prolonged cholesterol treatment for 5 days failed to increase PLP levels (Figure 2.10o and p) or the number of MBP^{+} OLs in *Lrp1*$^{-/-}$ cultures (Figure 2.10q and r). Although differentiation of*Lrp1*$^{-/-}$ OLs cannot be 'rescued' by bath-applied cholesterol, cells are highly sensitive to a further reduction in cholesterol, as shown by bath-applied simvastatin (Figure 2.10e and f). Since cholesterol is only one of many lipid derivatives produced by the

cholesterol biosynthetic pathway (Figure 2.11c), we asked whether treatment with mevalonate improves differentiation of *Lrp1*$^{-/-}$ OPC. However, similar to cholesterol, mevalonate fails to increase differentiation (Figure 2.11g and h). Taken together, *Lrp1* deficiency in the OL-lineage leads to a drop in cellular cholesterol and arrest in differentiation that cannot be rescued by cholesterol or mevalonate supplementation. Our data suggest that in addition to cholesterol homeostasis, LRP1 regulates other biological processes important for OPC differentiation.

2.3.7 *Lrp1* deficiency impairs peroxisome biogenesis

To further investigate what type of biological processes might be dysregulated by *Lrp1* deficiency, we performed transcriptomic analyses of OPCs acutely isolated from *Lrp1* control and cKO^{OL}pups. Gene ontology (GO) analysis identified differences in 'peroxisome organization' and 'peroxisome proliferation-associated receptor (PPAR) signaling pathway' (Figure 2.12a). Six gene products regulated by *Lrp1* belong to peroxisome and PPAR GO terms, including *Pex2*, *Pex5l*, *Hrasls*, *Ptgis*, *Mavs*, and *Stard10* (Figure 2.12b). Western blot analysis of*Lrp1*$^{-/-}$ OLs further revealed a significant reduction in PEX2 after 5 days in DM (Figure 2.12c and d). Because PEX2 has been implicated in peroxisome biogenesis (Gootjes et al 2004), and peroxisome biogenesis disorders (PBDs) are typically associated with impaired lipid metabolism and CNS myelin defects (Krause et al 2006), this prompted us to further explore a potential link between LRP1 and peroxisomes. To assess whether the observed reduction in PEX2 impacts peroxisome density in primary OLs, MBP^{+} OLs were stained with anti-PMP70, an ATP-binding cassette transporter enriched in peroxisomes (Figure 2.13a). In *Lrp1*$^{-/-}$ OLs, we observed reduced PMP70 staining (Figure 2.13b) and a decrease in the total number of peroxisomes (Figure 2.13c). Normalization of peroxisome counts to cell size revealed that the reduction in *Lrp1*$^{-/-}$OLs is not simply a reflection of smaller cells (Figure 2.13d). The subcellular localization of peroxisomes is thought to be important for ensuring a timely response to metabolic demands (Berger et al 2016). This prompted us to analyze the distribution of peroxisomes in primary OLs. Interestingly, while the number of PMP70 positive puncta near the cell soma is comparable

between *Lrp1* control and*Lrp1*$^{-/-}$ OLs, we observed a significant drop in peroxisomes along radial processes of MBP^{+} OLs (Figure 2.13e-h).

2.3.8 Combination treatment of cholesterol and PPARγ agonist rescues the differentiation block in *Lrp1*-deficient OPCs

In endothelial cells, the LRP1-ICD functions as a co-activator of PPARγ, a key regulator of lipid and glucose metabolism (Mao et al 2017). Activated PPARγ moves into the nucleus to control gene expression by binding to PPAR-responsive elements (PPREs) on numerous target genes, including *Lrp1* (Gauthier et al 2003). In addition, PPREs are found in genes important for lipid and glucose metabolism, and peroxisome biogenesis (Fang et al 2016, Hofer et al 2017). *In vitro*, a 5-day treatment of *Lrp1* control OPCs with pioglitazone, an agonist of PPARγ, results in elevated LRP1 (Figure 2.14a and b) and accelerated differentiation into MBP^{+} OLs (Figure 2.14c and d) (Bernardo et al 2009). This stands in marked contrast to*Lrp1*$^{-/-}$ cultures, where pioglitazone treatment fails to accelerate OPC differentiation (Figure 2.14c and d). Moreover, pioglitazone does not regulate PMP70 staining intensity in MBP^{+} *Lrp1* control or*Lrp1*$^{-/-}$ OLs, nor does it have any effect on total peroxisome counts per cell (Figure 2.14e-i). However, pioglitazone leads to a modest but significant increase in the number of peroxisomes located in cellular processes of *Lrp1*$^{-/-}$ OLs (Figure 2.14j and k). Treatment of *Lrp1*control OPCs with the PPARγ antagonist GW9662 blocks differentiation into MBP^{+} OLs (Roth et al 2003), but does not lead to a further reduction in MBP^{+} cells in *Lrp1*$^{-/-}$ OL cultures (Figure 2.14l and m). This suggests that in *Lrp1*$^{-/-}$ OLs PPARγ is not active.

Given LRP1's multifunctional receptor role, we asked whether simultaneous treatment with pioglitazone and cholesterol is sufficient to rescue the differentiation block of *Lrp1*$^{-/-}$ OPCs (Figure 2.15a). This is indeed the case, as the number of MBP^{+} cells in *Lrp1*$^{-/-}$cultures is significantly increased by the combination treatment (Figure 2.15b and c). Moreover, the size of MBP^{+} *Lrp1*$^{-/-}$ OLs increased (Figure 2.15d and f) and peroxisome counts are elevated (Figure 2.15e and g), however the anti-MBP staining intensity was only partially rescued (Figure 2.15h). Quantification of

peroxisome distribution in *Lrp1*$^{-/-}$ OPC/OL cultures subjected to combo treatment revealed a marked increase in PMP70^{+} peroxisomes in OL processes (Figure 2.15i and j). Together, these findings indicate that LRP1 regulates multiple metabolic functions important for OL differentiation. In addition to its known role in cholesterol homeostasis, LRP1 regulates expression of PEX2 and thereby metabolic functions associated with peroxisomes.

2.4 **Discussion**

LRP1 function in the OL-lineage is necessary for proper CNS myelin development and the timely repair of a chemically induced focal white matter lesion *in vivo*. Optic nerves of *Lrp1* cKO^{OL} show fewer myelinated axons, thinning of myelin sheaths, and an increase in nodal structural defects. Morphological alterations have a physiological correlate, as *Lrp1* cKO^{OL} mice exhibit faulty nerve conduction. Mechanistically, *Lrp1* deficiency disrupts multiple signaling pathways implicated in OL differentiation, including AKT activation, cholesterol homeostasis, PPARγ signaling, peroxisome biogenesis and subcellular distribution. The pleiotropic roles of LRP1 in OPC differentiation are further underscored by the fact that restoring cholesterol homeostasis or activation of PPARγ alone is not sufficient to drive differentiation. Only when cholesterol supplementation is combined with PPARγ activation, is differentiation of *Lrp1*$^{-/-}$ OPC into MBP^{+} OLs significantly increased. Taken together, our studies identify a novel role for LRP1 in peroxisome function and suggest that broad metabolic dysregulation in *Lrp1*-deficient OPCs attenuates differentiation into mature OLs (Figure 2.16).

In the embryonic neocortex, LRP1 is strongly expressed in the ventricular zone and partially overlaps with nestin^{+} neural stem and precursor cells (Hennen et al 2013). In *Lrp1*$^{flox/flox}$ neurospheres, conditional gene ablation reduces cell proliferation, survival, and negatively impacts differentiation into neurons and O4^{+} OLs (Safina et al 2016). Consistent with these observations, *Lrp1* cKO^{OL} mice show reduced OPC differentiation *in vivo*. Studies with purified OPCs *in vitro* and OL-linage specific gene ablation *in vivo*, suggest a cell-autonomous role for *Lrp1* in OPC

maturation. Non-cell-autonomous functions for LRP1 following white matter lesion are likely, since LRP1 is upregulated in astrocytes and myeloid cells near multiple sclerosis lesions (Chuang et al 2016). Moreover, deletion of *Lrp1* in microglia worsens the course of experimental autoimmune encephalomyelitis and has been proposed to promote a proinflammatory milieu associated with disease exacerbation (Chuang et al 2016). Studies with *Lrp1 iKO*^{OL} mice show that *Lrp1*in the OL linage is necessary for the timely repair of a focal myelin lesion. This suggests that similar to OPCs in the developing brain, OPCs in the adult brain depend on *Lrp1* for rapid differentiation into myelin producing OLs. Since white matter repair was analyzed by repopulation of the lesion area with *Mbp*$^{+}$ cells, additional studies, including electron microscopy, will be needed to demonstrate a requirement for *Lrp1* in remyelination of denuded axons.

Cholesterol does not cross the blood-brain-barrier (Saher & Stumpf 2015) and CNS resident cells need to either synthesize their own cholesterol or acquire it through horizontal transfer from neighboring cells, including astrocytes (Camargo et al 2017). In the OL-lineage cholesterol is essential for cell maturation, including myelin gene expression, myelin protein trafficking, and internode formation (Kramer-Albers et al 2006, Mathews et al 2014, Saher et al 2005). Sterol biosynthesis is in part accomplished by peroxisomes. Specifically, the pre-squalene segment of the cholesterol biosynthetic pathway takes place in peroxisomes. However, cholesterol is only one of many lipid derivatives produced by this pathway (Faust & Kovacs 2014). A drop in intracellular cholesterol leads to an increase in SREBPs, a family of transcription factors that regulate expression of gene products involved in cholesterol and fatty acid synthesis (Faust & Kovacs 2014, Goldstein et al 2006). In Schwann cells, SREBPs and the SREBP-activating protein SCAP are required for AKT/mTOR-dependent lipid biosynthesis, myelin membrane synthesis, and normal PNS myelination (Norrmén et al 2014, Verheijen et al 2009). In the OL linage blockage of SREBP inhibits CNS myelination (Camargo et al 2017, Monnerie et al 2017). Blocking of SREBP processing in primary OLs leads to a drop in cholesterol and inhibits cell differentiation and membrane expansion. This can be rescued by

cholesterol added to the culture medium (Monnerie et al 2017). In primary OLs, *Lrp1* deficiency leads to activation of SREBP2, yet cells are unable to maintain cholesterol homeostasis, suggesting more global metabolic deficits. The cholesterol sensing apparatus in*Lrp1*-deficient OPCs appears to be largely intact, as bath applied cholesterol restores SREBP2 to control levels. Since SREBP2 can be induced by ER stress (Faust & Kovacs 2014), reversibility by bath applied cholesterol suggests that *Lrp1* cKO^{OL} cultures upregulate SREBP2 due to cholesterol deficiency and not elevated ER stress (Faust & Kovacs 2014). Significantly, restoring cellular cholesterol homeostasis in *Lrp1*$^{-/-}$ OPCs is not sufficient to overcome the differentiation block, suggesting more widespread functional deficits.

Members of the PPAR subfamily, including PPARα, PPARβ/δ, and PPARγ, are ligand-activated transcription factors that belong to the nuclear hormone receptor family (Michalik et al 2006). PPARs regulate transcription through heterodimerization with the retinoid X receptor (RXR). When activated by a ligand, the dimer modulates transcription via binding to a PPRE motif in the promoter region of target genes (Michalik et al 2006). PPARs-regulated gene expression controls numerous biochemical pathways implicated in lipid, glucose and energy metabolism (Berger & Moller 2002, Han et al 2017). A critical role for PPARγ in OL differentiation is supported by the observation that activation with pioglitazone or rosiglitazone accelerates OPC differentiation into mature OLs (Bernardo et al 2009, Bernardo et al 2013, De Nuccio et al 2011, Roth et al 2003, Saluja et al 2001) and inhibition with GW9662 blocks OL differentiation (Bernardo et al 2017). Deficiency for the PPARγ-coactivator-1 alpha (PGC1a) leads to impaired lipid metabolism, including an increase in very long chain fatty acids (VLCFAs) and disruption of cholesterol homeostasis (Camacho et al 2013, Xiang et al 2011). In addition, PGC1a deficiency results in defects of peroxisome-related gene function, suggesting the increase in VLCFAs and drop in cholesterol reflects impaired peroxisome function (Baes & Aubourg 2009). Following γ-secretase-dependent processing, the LRP1 ICD can translocate to the nucleus where it associates with transcriptional regulators (Carter 2007, May et al 2002). In endothelial cells, the LRP1-ICD binds directly to

the nuclear receptor PPARγ to regulate gene products that function in lipid and glucose metabolism (Mao et al 2017). Treatment of *Lrp1*$^{-/-}$ OPCs with pioglitazone leads to an increase in peroxisomes in OL processes but fails to promote differentiation into myelin sheet producing OLs. In the absence of the LRP1-ICD, pioglitazone may fail to fully activate PPARγ (Mao et al 2017), but the observed increase in PMP70^{+} peroxisomes in OL processes of*Lrp1* deficient cultures suggests that mutant cells still respond to pioglitazone. Because *Lrp1* cKO^{OL} cultures are cholesterol deficient and the LRP1-ICD participates in PPARγ regulated gene expression, we examined whether a combination treatment rescues the differentiation block in *Lrp1* deficient OPCs/OLs. This was indeed the case, suggesting that *Lrp1* deficiency leads to dysregulation of multiple pathways important for OPC differentiation.

The importance of peroxisomes in the human nervous system is underscored by inherited disorders caused by complete or partial loss of peroxisome function, collectively described as Zellweger spectrum disorders (Berger et al 2016, Waterham et al 2016). *PEX* genes encode peroxins, proteins required for normal peroxisome assembly. Defects in *PEX* genes can cause peroxisome biogenesis disorder (PBD), characterized by a broad range of symptoms, including aberrant brain development, white matter abnormalities, and neurodegeneration (Berger et al 2016). The genetic basis for PBD is a single gene mutation in one of the 14 PEX genes, typically leading to deficiencies in numerous metabolic functions carried out by peroxisomes (Adam et al 1993, Steinberg et al 2006). Mounting evidence points to a close interaction of peroxisomes with other organelles, mitochondria in particular, and disruption of these interactions may underlie the far reaching metabolic defects observed in PBD and genetically manipulated model organisms deficient for a single PEX (Fransen et al 2017, Wangler et al 2017). In developing OLs, *Lrp1* deficiency leads to a decrease in peroxisomal gene products, most prominently a ~50% reduction in PEX2, an integral membrane protein that functions in the import of peroxisomal matrix proteins. Mice deficient for *Pex2* lack normal peroxisomes but do assemble empty peroxisome membrane ghosts (Faust &

Hatten 1997). *Pex2* mutant mice show significantly lower plasma cholesterol levels and in the brain the rate of cholesterol synthesis is significantly reduced (Faust & Kovacs 2014); brain size is reduced, cerebellar development impaired, and depending on the genetic background death occurs in early postnatal life (Faust 2003). Mutations in human *PEX2* cause Zellweger spectrum disorder but have no apparent impact on white matter appearance (Mignarri et al 2012). In mice, *CNP-Cre*mediated ablation of *Pex5* in OLs disrupts peroxisome function and integrity of myelinated fibers, but does not impair CNS myelinogenesis (Kassmann et al 2007). This suggests that defects in CNS myelinogenesis observed in *Lrp1* cKO^{OL} mice are likely not only a reflection of reduced peroxisome biogenesis or transport into internodes. Rather we provide evidence that *Lrp1* deficiency in OPCs leads to dysregulation of additional pathways implicated in myeliogenesis, including AKT, SREBP2, and PAPRγ. We propose that the combined action of these deficits attenuates OPC differentiation.

In sum, our studies show that *Lrp1* is required in the OL lineage for proper CNS myelin development and the timely repair of a chemically induced white matter lesion *in vivo*. Mechanistic studies with primary OPCs revealed that loss of *Lrp1* causes differentiation block that can be rescued by bath application of cholesterol combined with pharmacological activation of PPARγ.

2.5 Materials and Methods

2.5.1 Mice

All animal handling and surgical procedures were performed in compliance with local and national animal care guidelines and were approved by the Institutional Animal Care and Use Committee (IACUC). *Lrp1*$^{flox/flox}$ mice were obtained from Steven Gonias (Stiles et al 2013) and crossed with *Olig2-Cre* (Schüller et al 2008),*CAG-CreER*^{TM} (Jackson Laboratories, #004682, Bar Harbor, ME), and *Pdgfra-CreER*^{TM} (Kang et al 2010) mice. For inducible gene ablation in adult male and female mice, three intraperitoneal (i.p.) injections of tamoxifen (75 mg/kg) were given every 24 hr. Tamoxifen (10 mg/ml) was prepared in a mixture of 9%

ethanol and 91% sunflower oil. Mice were kept on a mixed background of C57BL/6J and 129SV. Throughout the study, male and female littermate animals were used. *Lrp1* 'control' mice harbor at least one functional *Lrp1* allele. Any of the following genotypes $Lrp1^{+/+}$, $Lrp1^{+/flox}$, $Lrp1^{flox/flox}$, or $Lrp1^{flox/+};Cre^{+}$ served as *Lrp1* controls.

2.5.2 **Genotyping**

To obtain genomic DNA (gDNA), tail biopsies were collected, boiled for 30 min in 100 µl alkaline lysis buffer (25 mM NaOH and 0.2 mM EDTA in ddH_2O) and neutralized by adding 100 µl of 40 mM Tris-HCI (pH 5.5). For PCR genotyping, 1–5 µl of gDNA was mixed with 0.5 µl of 10 mM dNTP mix (Promega, C1141, Madison, WI), 10 µl of 25 mM $MgCl_2$, 5 µl of 5X Green GoTaq Buffer (Promega, M791A), 0.2 µl of GoTaq DNA polymerase (Promega, M3005), 0.15 µl of each PCR primer stock (90 µM each), and ddH_2O was added to a total volume of 25 µl. The following cycling conditions were used: DNA denaturing step (94°C for 3 min) 1X, amplification steps (94°C for 30 s, 60°C for 1 min, and 72°C for 1 min) 30X, followed by an elongation step (72°C for 10 min) then kept at 4°C for storage. The position of PCR primers used for genotyping is shown in Figure 2.1. *Lrp1* WT and loxP-flanked (floxed) alleles were amplified with the forward primer [Lrp1tF10290, F2] 5'-CAT ACC CTC TTC AAA CCC CTT G-3' and the reverse primer [Lrp1tR10291, R2] 5'-GCA AGC TCT CCT GCT CAG ACC TGG A-3'. The WT allele yields a 291 bp product and the floxed allele yields a 350 bp product. The recombined *Lrp1* allele was amplified with the forward primer [Lrp1rF, F1] 5'- CCC AAG GAA ATC AGG CCT CGG C-3' and the reverse primer [R2], resulting in a 400 bp product (Hennen et al 2013). For detection of *Cre*, the forward primer [oIMR1084, CreF] 5'-GCG GTC TGG CAG TAA AAA CTA TC-3' and reverse primer [oIMR1085, CreR] 5'-GTG AAA CAG CAT TGC TGT CAC TT-3' were used, resulting in a ~ 200 bp product. As a positive control, the forward primer [oIMR7338, Il-2pF] 5'-CTA GGC CAC AGA ATT GAA AGA-3' and the reverse primer [oIMR7339, Il-2pR] 5'-GTA GGT GGA AAT TCT AGC ATC-3' were mixed with CreF and CreR primers in the same reaction, this reaction yields a 324 bp product (The Jackson laboratory).

2.5.3 **Stereotaxic injection**

Male and female mice at postnatal-day (P) 42–56 were used for stereotaxic injection of L-α-Lysophosphatidylcholine (LPC) (Sigma, L4129, Mendota Heights, MN) into the corpus callosum. Mice were anesthetized with 4% isoflurane mixed with oxygen, mounted on a Stoelting stereotaxic instrument (51730D, Wood Dale, IL), and kept under 2% isoflurane anesthesia during surgery. A 5µl-hamilton syringe was loaded with 1% LPC in PBS (Gibco, 10010023, Gaithersburg, MD), mounted on a motorized stereotaxic pump (Stoelting Quintessential Stereotaxic injector, 53311) and used for intracranial injection at the following coordinates, AP: 1.25 mm, LR: ±1 mm, D: 2.25 mm. Over duration of 1 min, 0.5 µl of 1% LPC solution was injected on the ipsilateral site and 0.5 µl PBS on the contralateral side. After the injection was completed, the needle was kept in place for 2 min before retraction. Following surgery, mice were treated with three doses of 70 µl of buprenorphine (0.3 mg/ml) every 12 hr. Brains were collected at day 10, and 21 post injection.

2.5.4 **Histochemistry**

Animals were deeply anesthetized with a mixture of ketamine/xylazine (25 mg/ml ketamine and 2.5 mg/ml xylazine in PBS) and perfused trans-cardially with ice-cold PBS for 5 min, followed by ice-cold 4% paraformaldehyde in PBS (4%PFA/PBS) for 5 min. Brains were harvested and post-fixed for 2 hr in perfusion solution. Optic nerves were harvested separately and post-fixed for 20 min in perfusion solution. Brains and optic nerves were cryoprotected overnight in 30% sucrose/PBS at 4°C, embedded in OCT (Tissue-Tek, 4583, Torrance, CA), and flash frozen in powderized dry ice. Serial sections were cut at 20 µm (brains) and 10 µm (optic nerves) at −20°C using a Leica CM 3050S Cryostat. Serial sections were mounted onto Superfrost^{+} microscope slides (Fisherbrand, 12-550-15, Pittsburgh, PA) and stored at −20°C.

2.5.5 **In situ hybridization**

Tissue sections mounted on microscope slides were post-fixed overnight in 4%PFA/PBS at 4°C. Sections were then rinsed 3 times for 5 min each in PBS and the

edge of microscope slides was demarcated with a DAKO pen (DAKO, S2002, Denmark). Sections were subsequently incubated in a series of ethanol/water mixtures: 100% for 1 min, 100% for 1 min, 95% for 1 min, 70% for 1 min, and 50% for 1 min. Sections were then rinsed in 2x saline-sodium citrate (SSC, 150 mM NaCl, and 77.5 mM sodium citrate in ddH_2O, pH7.2) for 1 min, and incubated at 37°C for 30 min in proteinase K solution (10 µg/ml proteinase K, 100 mM Tris-HCl pH8.0, and 0.5 mM EDTA in ddH_2O). Proteinase digestion was stopped by rinsing sections in ddH_2O and then in PBS for 5 min each. To quench RNase activity, slides were incubated in 1% triethanolamine (Sigma, 90278) and 0.4% acetic anhydride (Sigma, 320102) mixture in ddH_2O for 10 min at room temperature, rinsed once in PBS for 5 min and once in 2X SSC for another 5 min. To reduce non-specific binding of cRNA probes, sections were pre-incubated with 125 µl hybridization buffer (10% Denhardts solution, 40 mg/ml baker's yeast tRNA, 5 mg/ml sheared herring sperm DNA, 5X SSC, and 50% formamide in ddH_2O) for at least 2 hr at room temperature. Digoxigenin-labeled cRNA probes were generated by run-off *in vitro* transcription as described (Winters et al 2011). Anti-sense and sense cRNA probes were diluted in 125 µl pre-hybridization buffer to ~200 ng/ml, denatured for 5 min at 85°C, and rapidly cooled on ice for 2 min. Probes were applied to tissue sections, microscope slides covered with parafilm, and incubated at 55°C overnight in a humidified and sealed container. The next morning slides were rinsed in 5X SSC for 1 min at 55°C, 2X SSC for 5 mins at 55°C, and incubated in 0.2X SSC/50% formamide for 30 min at 55°C. Sections were rinsed in 0.2X SSC at room temperature for 5 min then rinsed with Buffer1 (100 mM Tris-HCl pH7.5, and 1.5M NaCl in ddH_2O) for 5 min. A 1% blocking solution was prepared by dissolving 1 g blocking powder (Roche, 11096176001, Switzerland) in Buffer1 at 55°C, cooled to room temperature (RT), and applied to slides for 1 hr at RT. Slides were rinsed in Buffer1 for 5 min and 125 µl anti-Digoxigenin-AP antibody (Roche, 11093274910, 1:2500) in Buffer1 was applied to each slide for 1.5 hr at RT. Sections were rinsed in Buffer1 for 5 min, then rinsed in Buffer2 (100 mM Tris-HCl pH9.5, 100 mM NaCl, and 5 mM $MgCl_2$ in ddH_2O) for 5 min, and incubated in alkaline phosphatase (AP) substrate (Roche, 11681451001, 1:50) in Buffer2. The color reaction was developed

for 1–48 hr and stopped by rinsing sections in PBS for 10 min. Sections were incubated in Hoechst dye 33342 (Life technology, H3570, Pittsburgh, PA) for 5 min, air dried, mounted with Fluoromount-G (SouthernBiotech, 0100–01), and dried overnight before imaging under bright-field. The following cRNA probes were used, *Pdgfra* and *Plp* (DNA templates were kindly provided by Richard Lu (Dai et al 2014)), *Mag* (Winters et al 2011), and *Mbp*(a 650 bp probe based on template provided in the Allen Brain Atlas).

2.5.6 **Quantification of lesion size and myelin repair**

Serial sections of the corpus callosum, containing the LPC and PBS injection sites were mounted onto glass coverslips and stained by ISH with digoxigenin-labeled cRNA probes specific for *Mbp, Mag, Plp,* and *Pdgfra*. For quantification of the white matter lesion area, the same intensity cutoff was set by Image J threshold for all brain sections and used to measure the size of the lesion. The outer rim of the strongly Mbp^+ region ($lesion^{out}$) was traced with the ImageJ freehand drawing tool. The inner rim facing the Mbp^- region ($lesion^{in}$) was traced as well. For each animal examined, the size of the initial lesion area ($lesion^{out}$) in μm^2 and remyelinated area ($lesion^{out}$-$lesion^{in}$) in μm^2 was calculated by averaging the measurement from two sections at the lesion core. The lesion core was defined as the section with the largest lesion area ($lesion^{out}$). To determine remyelination, the ratio of ($lesion^{out}$-$lesion^{in}$)/($lesion^{out}$) in percent was calculated. As an initial lesion depth control, criteria of $lesion^{out}$ area must cover the center of the corpus callosum in each serial section set. If a $lesion^{out}$ area was not located within the corpus callosum, the animal and corresponding brain sections were excluded from the analysis.

2.5.7 **Immunostaining**

Tissue sections mounted onto microscope slides were rehydrated in PBS for 5 min, permeabilized in 0.1% TritonX-100, and blocked in PHT (1% horse serum and 0.1% TritonX-100 in PBS) for 1 hr at RT. Primary antibodies were diluted in PHT and applied overnight at 4°C. Sections were rinsed in PBS 3 times for 5 min each and appropriate secondary antibodies were applied (Life technologies, Alexa-

fluorophore 405, 488, 555, 594, or 647 nm, 1:1000). Slides were rinsed in PBS 3 times for 5 min each and mounted with ProLong Gold antifade reagent (Life technologies, P36930). For quantification of nodal structures, randomly selected fields of view in each nerve were imaged at 96X magnification with an Olympus IX71 microscope, a maximum projection of 6 Z-stacked images of each region was generated, and the stacked images were used for quantification. As axons run in and out of the plane within longitudinal sections, criteria were set to exclude structures in which Caspr staining was unpaired to reduce 'false positive' as nodal defect. The following primary antibodies were used: rabbit anti-Olig2 (Millipore, AB9610, Burlington, MA, 1:500), rat anti-PDGFRα (BD Pharmingen, 558774, San Jose, CA, 1:500), rabbit anti-GFAP (Dako, Nr. A 0334, 1:2000), mouse anti-APC (Calbiochem, OP80, Clone CC1, San Diego, CA, 1:500), rabbit anti-Caspr (1:1000, [Peles, 1997 #57]), mouse anti-Na Channel (1:75, [Rasband, 1999 #58]). For myelin staining, sections were incubated in Fluoromyelin-Green (Life technologies, F34651 1:200) reagent for 15 min.

2.5.8 **Transmission electron microscopy (TEM)**

Tissue preparation and image acquisition were carried out as described by (Winters et al 2011). Briefly, mice at P10, P21, and P56 were perfused trans-cardially with ice cold PBS for 1 min, followed by a 10 min perfusion with a mixture of 3% PFA and 2.5% glutaraldehyde in 0.1M Sorensen's buffer. Brains and optic nerves were dissected and post-fixed in perfusion solution overnight at 4°C. Post-fixed brain tissue and optic nerves were rinsed and transferred to 0.1M Sorensen's buffer and embedded in resin by the University of Michigan Imaging Laboratory Core. Semi-thin (0.5 μm) sections were cut and stained with toluidine blue and imaged by light microscopy. Ultra-thin (75 nm) sections were cut and imaged with a Philips CM-100 or a JEOL 100CX electron microscope. For each genotype and age, at least three animals were processed and analyzed. For each animal, over 1000 axons in the optic nerve were measured and quantified by ImageJ. For each optic nerve, 10 images at 13,500x magnification were randomly taken and quantified to calculate the g-ratio and the fraction of myelinated axons. The inner ($area^{in}$) and outer

($area^{out}$) rim of each myelin sheath was traced with the ImageJ freehand drawing tool and the area within was calculated. We then derived axon caliber and fiber caliber (2 r) by the following: $area^{in} = r^2\pi$. The g-ratios were calculated as such: $\frac{\sqrt{area^{in}}}{\sqrt{area^{out}}}$. The g-ratio is only accurate if the compact myelin and axon outline can clearly be traced. Individual fibers with not clearly defined features were excluded from the quantification.

2.5.9 **Optic nerve recordings**

Compound action potentials were recorded as described elsewhere (Carbajal et al 2015, Winters et al 2011). Briefly, optic nerves were acutely isolated from P21 mice and transferred into oxygenated ACSF buffer (125 mM NaCl, 1.25 mM NaH_2PO_4, 25 mM glucose, 25 mM $NaHCO_3$, 2.5 mM $CaCl_2$, 1.3 mM $MgCl_2$, 2.5 mM KCl) for 45 min at RT before transferring into a recording chamber at 37 ± 0.4°C. Suction pipette electrodes were used for stimulation and recording of the nerve (Figure 2.7a). A computer-driven (Axon pClamp10.3 software) stimulus isolation unit (WPI, FL) was used to stimulate the optic nerve with 2 mA/50 µs pulses. The recording electrode was connected to a differential AC amplifier (custom-made). A stimulus artifact-subtracting pipette was placed near the recording pipette. A data acquisition system (Axon digidata 1440A, Axon pClamp 10.3, Molecular Devices, Sunnyvale, CA) was used to digitize the signals. Conduction velocity was calculated from the length of the nerve and the time to peak of each component of the CAP. Amplitudes were normalized to a resistance ratio of 1.7, as described (Fernandes et al 2014). Raw traces were fitted with four Gaussian curves with Origin9.1 software for analysis of individual components of the CAP. Due to limitations in the resolution of individual peaks in short nerves, CAP recordings from nerves that were shorter than 1 mm in length were excluded from the analysis.

2.5.10 **OPC/OL primary cultures and drug treatment**

OPCs were isolated from P6-P9 mouse pups by rat anti-PDGFRα (BD Pharmingen, 558774) immunopanning as described (Mironova et al 2016). For

plating of cells, 5–7.5 × 10^3 cells (for 12 mm cover glass) or 3–5 × 10^4 (12-well plastic plate) were seeded onto PDL pre-coated surface. Primary OPCs were kept in a 10% CO_2 incubator at 37°C. To maintain OPCs in a proliferative state, growth medium (20 ng/ml PDGF-AA (Peprotech, 100-13A, Rocky Hill, NJ), 4.2 µg/ml Forskolin (Sigma, F6886), 10 ng/ml CNTF (Peprotech, 450–02), and 1 ng/ml NT-3 (Peprotech, 450–03) in SATO) were added to the culture. To induce OPC differentiation, differentiation medium was constituted by adding (4.2 µg/ml Forskolin, 10 ng/ml CNTF, and 4 ng/ml T3 (Sigma, T6397) in SATO) to the culture. For drug treatment, all compounds were mixed with differentiation medium at the desired concentration, and the compound-containing medium was replaced every other day. Stock and working solutions including 20 mg/ml cholesterol (Sigma, C8667) in 100% EtOH were kept at RT and warmed up to 37°C before use, then diluted in differentiation medium to 5 µg/ml; 10 mM pioglitazone (Sigma, E6910) in DMSO was kept at −20°C and diluted in differentiation medium to 1 µM; 10 mM simvastatin (Sigma, S6196) in DMSO was kept at −20°C and diluted in differentiation medium to 0.5 µM; 10 mM GW9662 (Sigma, M6191) in DMSO was kept at −20°C and diluted in differentiation medium to 1 µM.

2.5.11 **OPC staining and quantification**

At different stages of development, OPC/OL cultures were fixed for 15 min in 4%PFA/PBS. Cells were rinsed three times in PBS and permeabilized with 0.1% Triton/PBS solution for three mins. Cells were then rinsed in PBS and incubated in blocking solution (3% BSA/PBS) for 1 hr at RT. Primary antibodies were prepared in blocking solution. For immunostaining, 35 µl were dropped onto a sheet of parafilm, the coverslips were inverted onto the primary antibody drop, and incubated overnight at 4°C. The following day, coverslips were transferred back to a 24-well-plate and rinsed with PBS 3 times for 5 min each. Secondary antibody ±filipin (Sigma, F9765, 0.1 mg/ml) was prepared in blocking solution, 350 µl were added to each well, and the coverslips were incubated for 2 hr at RT. Coverslips then were rinsed in PBS three times for 5 min each and stained with Hoechst (1:50,000) for 10 s. Coverslips then were rinsed in ddH_2O and mounted in

ProLong Gold antifade reagent. For quantification in Figure 2.8, the percent of OL markers$^+$/Hoechst$^+$cells was calculated from 10 images that were taken from randomly selected areas in each coverslip at 20X magnification with an Olympus IX71 microscope. For quantification in Figure 2.10 and after, the percent of OL markers$^+$/Hoechst$^+$ cells was calculated from 25 images that were taken from randomly selected areas in each coverslip at 10X magnification with a Zeiss Axio-Observer microscope. For single-cell intensity and size measurement in Figure 2.10-Figure 2.15, individual cell images were taken at 40X magnification with a Zeiss Axio-Observer microscope with Apotom.2. For quantification, the same intensity cutoff was set by Image J threshold to all cells and binary images were generated to define each cell outline. The individual cell outline was applied to original images to measure the intensity of filipin, MBP, or PMP70 staining per cell. For PMP70 puncta distribution analysis, the coordinates of each PMP70$^+$ center were acquired by the process >find maxima function in ImageJ, the cell center coordinate was defined by point selection function, and the distance of each PMP70$^+$ dot to the cell center was then calculated. The data were then binned from 1 to 25 μm at 1 μm divisions, and plotted. Primary antibodies included: rat anti-PDGFRα (BD pharmingen, 558774, 1:500), rabbit anti-CNPase (Aves Labs, 27490 R12-2096, Tigard, OR, 1:500), mouse anti-MAG (Millipore, MAB1567, 1:500), rat anti-MBP (Millipore, MAB386, 1:1000), chicken anti-PLP (Aves Labs, 27592, 1:500), mouse anti-GFAP (Sigma, G3893, 1:1000), chicken anti-GFAP (Aves Labs, GFAP, 1:500), rabbit anti-NG2 (Millipore, AB5320, 1:500), rabbit anti-LRP1β (Abcam, ab92544, 1:500), rabbit anti-PMP70 (Thermo, PA1-650, Waltham, MA, 1:1000), and rabbit anti-Ki67 (Abcam, ab15580, 1:1000).

2.5.12 **Western blot analysis**

Protein lysates were separated by SDS-PAGE and transferred onto PVDF membranes for immunoblotting. Depending on the application, 2 to 10 μg of total protein were loaded per well. 2% Blotting-Grade Blocker (Bio-Rad, #170–6404, Hercules, CA) or 2% BSA fraction V (Fisher, BP1600-100) in 0.1%TBST buffer (0.1% Tween-20, 3M NaCl, 200 mM Tris-HCl pH7.4) were used as blocking solutions

and membranes were incubated for 1 hr at RT. Primary antibodies were diluted in blocking buffer and used for incubation at 4°C overnight. For protein detection and densitometric analysis, membranes were incubated in Super Signal West Pico substrate (Thermo, 34080), WesternSure PREMIUM Chemiluminescent Substrate (LI-COR Biosciences, 926–95000, Lincoln, NE), or Super Signal West Femto substrate (Thermo, 34095) followed by scanning on a C-DiGit blot scanner (LI-COR, P/N 3600–00). Images were quantified with Image Studio Lite Western Blot Analysis Software, relative to loading controls. Blots were used for quantification only when the loading control signals were comparable between groups and signals between technical repeats were similar. Primary antibodies included: rabbit anti-LRP1β 85 kDa (Abcam, ab92544, United Kingdom, 1:2000), mouse anti-βIII tubulin (Promega, G7121, 1:5000), mouse anti-β-actin (Sigma, AC-15 A5441, 1:5000), rat anti-MBP (Millipore, MAB386, 1:1000), rabbit anti-MAG (homemade serum, 1:1000), rabbit anti-PLP (Abcam, ab28486, 1:1000), rat anti-PLP/DM20 (Wendy Macklin AA3 hybridoma, 1:500) rabbit anti-Olig2 (Millipore, AB9610, 1:1000), mouse anti-GFAP (Sigma, G3893, 1:1000), mouse anti-CNPase (Abcam, ab6319, 1:1000), rabbit anti-PXMP3 (PEX2) (One world lab, AP9179c, San Diego, CA, 1:250), rabbit anti-SREBP2 (One world lab, 7855, 1:500), rabbit anti-pAKT (S473, Cell signaling, 4060S, 1:1000), rabbit anti-Erk1/2 (Cell signaling, 4695S, 1:1000), and (Cell signaling, 4376S, 1:1000).

2.5.13 **Cholesterol measurement**

OPCs were isolated by immunopanning as described above. OPCs bound to panning plates were collected by scraping with a Scraper (TPP, TP99002) in 250 µl of ice-cold PBS and sonicated in an ice-cold water bath (Sonic Dismembrator, Fisher Scientific, Model 500) at 50% amplitude three times for 5 s with a 5-s interval. The sonicated cell suspensions were immediately used for cholesterol measurement following the manufacturer's instructions (Chemicon, 428901). For colorimetric detection and quantification of cholesterol, absorbance was measured at 570 nm with a Multimode Plate Reader (Molecular Devices, SpectraMax M5^{e}). Results were

normalized to total protein concentration measured by DC™Protein Assay according to the manufacturer's manual (Bio-Rad, 5000112).

2.5.14 **Microarray and gene ontology analysis**

OPCs were isolated by immunopanning as described above and RNA was isolated with the RNeasy Micro Kit (Qiagen, 74004, Germany). To compare *Lrp1* control and cKO^{OL} RNA expression profiles, the Mouse Gene ST2.1 Affymetrix array was used. Differentially expressed genes, with a p-value<0.05 set as cutoff, were subjected to gene ontology (GO) analysis. Go terms were quarried from Mouse Genome Informatics (MGI) GO browser. The fold enrichment was calculated by dividing the number of genes associated with the GO term in our list by the number of genes associated with the GO term in the database.

2.5.15 **Statistical analysis**

There was no pre-experimental prediction of the difference between control and experimental groups when the study was designed. Therefore, we did not use computational methods to determine sample size a priori. Instead, we use the minimum of mice per genotype and experimental treatment for a total of at least three independent experiments to achieve the statistical power discussed by (Gauch 2006). We used littermate *Lrp1* control or *Lrp1* cKO or iKO mice for comparison throughout the study. All independent replicas were biological replicas, rather than technical replicas. For each experiment, the sample size (n) is specified in the figure legend. Throughout the study, independent replicas (n) indicate biological replica. Technical replicas were used to control for the quality of each measurement and were averaged before quantification and the average value was used as (n = 1) biological replica. Unless indicated otherwise, results are represented as mean value ±SEM. For single pairwise comparison, Student's *t*-test was used and a p-value<0.05 was considered statistically significant. For multiple comparisons, two-way ANOVA followed by post hoc *t*-test were used. Numbers and R software (see source code file for details) were used for determining statistical significance and graph plotting. For detailed raw data and statistical report, see source data files for

each figure. For image processing and quantification, ImageJ 1.47 v software was used for threshold setting, annotation, and quantification.

2.6 Acknowledgements

This chapter was modified from Lin et. al., 2017 under the Creative Commons license (CC BY 40) agreement. The original references are as follows:

Lin JP, Mironova YA, Shrager P, Giger RJ. "LRP1 Regulates Peroxisome Biogenesis and Cholesterol Homeostasis in Oligodendrocytes and is Required in CNS Myelin Development and Repair" 2017 bioRxiv doi: https://doi.org/10.1101/189563.

Lin JP, Mironova YA, Shrager P, Giger RJ. "LRP1 Regulates Peroxisome Biogenesis and Cholesterol Homeostasis in Oligodendrocytes and is Required for Proper in CNS Myelin Development and Repair" 2017 eLife doi: 10.7554/eLife.30498.

We thank Giger lab members for their feedback during the study. We thank Andy Lieberman for providing *CAG-CreER*^{TM} mice, Ben Barres for providing *Olig2-Cre* mice, and Richard Lu for *Plp1* and *Mbp* plasmid DNA. We thank Chang-Ting Lin, Wei-Chin Ho, and Chih-Hsu Lin for bioinformatics consulting. This work was supported by a Bradley Merrill Patten Fellowship (J-PL), the Training Program in Organogenesis T32HD007505 and NIH Cellular and Molecular Biology Training Grant T32-GM007315 (YAM), R01 NS081281 (PS and RJG), the Schmitt Program on Integrative Brain Research (PS), and the Dr. Miriam and Sheldon G. Adelson Medical Foundation on Neural Repair and Rehabilitation (RJG).

2.7 Author Contribution

Jing-Ping Lin, Yevgeniya Mironova, Peter Shrager, and Roman Giger designed research. Jing-Ping Lin, Yevgeniya Mironova, and Roman Giger performed research. Jing-Ping Lin and Roman Giger wrote the paper.

2.8 Figures

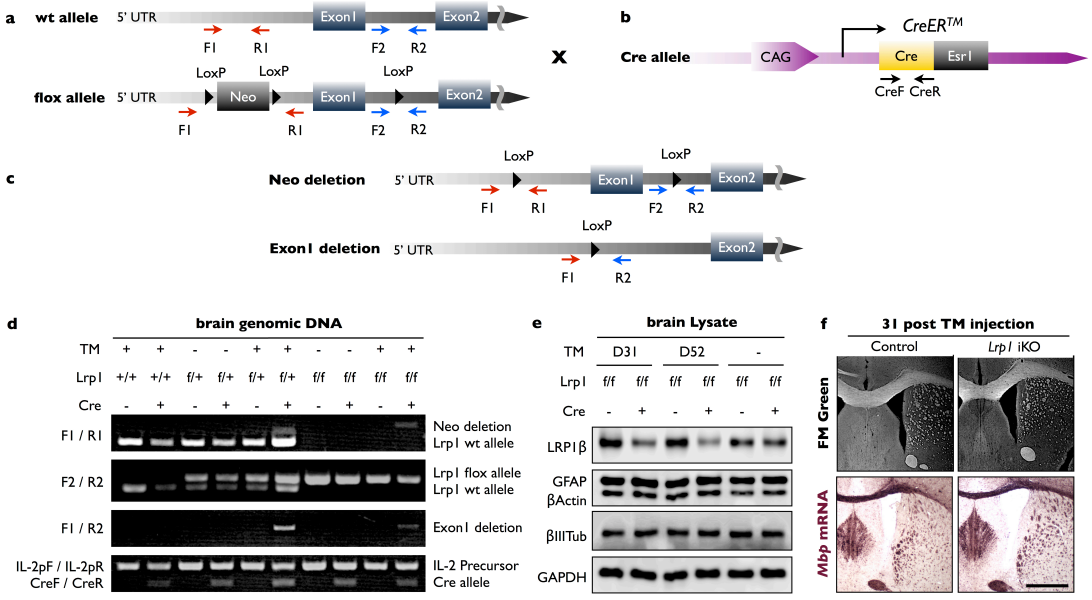
a
wt allele
5' UTR
Exon1
Exon2
F1
R1
F2
R2
flox allele
LoxP
Neo
b
Cre allele
CAG
CreER™
Cre
Esr1
CreF CreR
c
Neo deletion
Exon1 deletion
d
brain genomic DNA
TM
Lrp1
Cre
F1 / R1
F2 / R2
Neo deletion
Lrp1 wt allele
Lrp1 flox allele
Exon1 deletion
IL-2pF / IL-2pR
CreF / CreR
IL-2 Precursor
Cre allele
e
brain Lysate
D31
D52
LRP1β
GFAP
βActin
βIIITub
GAPDH
f
31 post TM injection
Control
Lrp1 iKO
FM Green
Mbp mRNA

Figure 2.1: Generation of Lrp1 global iKO mice
(a) Lrp1 wildtype (wt) and conditional, LoxP flanked (floxed), alleles. The location of PCR primers used for genotyping, the neomycin cassette (Neo), and LoxP sites are shown. (b) For global inducible gene ablation, the CAG-CreERTM mouse line was used, in which the Cre recombinase is fused with a tamoxifen (TM) responsive estrogen receptor (Ers1) and expressed under the control of a ubiquitous chicken β-actin-CMV hybrid (CAG) promoter. (c) Following TM administration, recombination can lead to deletion of Neo only or deletion of Neo and exon 1. (d) PCR genotyping of brain genomic DNA. Analysis of PCR products amplified from of Lrp1+/+ mice with (+) or without (-) the cre allele; Lrp1flox/+ mice ±Cre allele and ±TM treatment; Lrp1flox/flox mice ±Cre allele and ±TM treatment. The F1/R1 primer pair amplifies a ~300 bp PCR product from the wt Lrp1 allele and a ~400 bp PCR product if the Neo cassette is deleted. The F2/R2 primer pair amplifies a 291 bp PCR product from wt Lrp1 allele and a 350 bp PCR product from Lrp1 flox allele. The F1/R2 primer pair amplifies a ~500 bp PCR product if exon1 in deleted. The IL-2pF/IL-2pR primer pair amplifies a 324 bp fragment and served as internal PCR quality control. The CreF/CreR primer pair amplifies a ~200 bp PCR product if Cre is present. (e) Immunoblots of whole brain lysates prepared from Lrp1flox/flox;CAG-CreERTM mice 31 and 52 days after TM (+) or vehicle (-) treatment. Representative blots probed with anti-LRP1β, anti-GFAP, anti-β-actin, anti-β-III tubulin, and anti-GAPDH. (f) Coronal-sections of adult Lrp1 control and iKO mice 31 days after i.p. TM administration. Sections were stained with FM Green or probed for Mpb mRNA by in situ hybridization. Scale bar= 1mm.

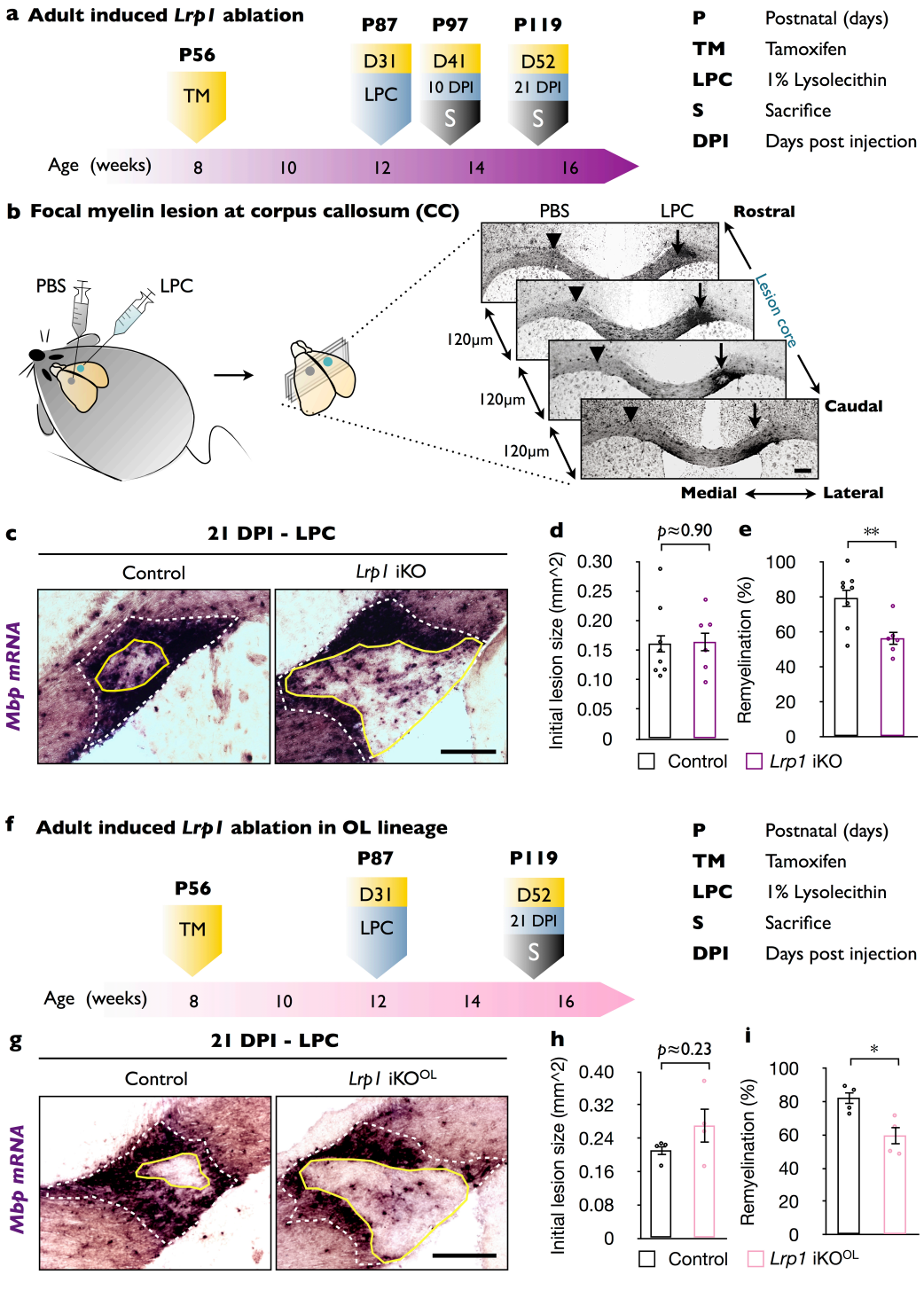
a Adult induced Lrp1 ablation
P56
TM
P87
D31
LPC
P97
D41
10 DPI
S
P119
D52
21 DPI
S
Age (weeks)
8
10
12
14
16
P Postnatal (days)
TM Tamoxifen
LPC 1% Lysolecithin
S Sacrifice
DPI Days post injection
b Focal myelin lesion at corpus callosum (CC)
PBS
LPC
Rostral
Lesion core
120µm
120µm
120µm
Caudal
Medial
Lateral
c
21 DPI - LPC
Control
Lrp1 iKO
Mbp mRNA
d
p≈0.90
Initial lesion size (mm^2)
0.30
0.25
0.20
0.15
0.10
0.05
0
e
**
Remyelination (%)
100
80
60
40
20
0
Control
Lrp1 iKO
f Adult induced Lrp1 ablation in OL lineage
P56
TM
P87
D31
LPC
P119
D52
21 DPI
S
Age (weeks)
8
10
12
14
16
P Postnatal (days)
TM Tamoxifen
LPC 1% Lysolecithin
S Sacrifice
DPI Days post injection
g
21 DPI - LPC
Control
Lrp1 iKOOL
Mbp mRNA
h
p≈0.23
Initial lesion size (mm^2)
0.40
0.32
0.24
0.16
0.08
0
i
*
Remyelination (%)
100
80
60
40
20
0
Control
Lrp1 iKOOL

Figure 2.2: In adult mice, global and OL-lineage selective ablation of *Lrp1* attenuates white matter repair

(a) Timeline in weeks indicating when *Lrp1* ablation was induced (*Lrp1*$^{flox/flox}$*;CAG-CreER*^{TM}, *Lrp1* iKO), lysolecithin (LPC) injected, and animals sacrificed. (b) Cartoon showing unilateral injection of LPC in the corpus callosum (CC) and PBS into the contralateral side. Coronal brain sections (series of 6, each 120 µm apart) probed for *Mbp* by *in situ* hybridization (ISH). Brain sections containing the lesion center were identified and subjected to quantification. (c) Coronal brain sections through the CC 21 days post LPC injection (21 DPI). The outer rim of the lesion area (lesion^{out}) is demarcated by the elevated *Mbp* signal (white dashed line). The non-myelinated area of the lesion is defined by the inner rim of elevated *Mbp* signal (lesion^{in}) and delineated by a solid yellow line. Scale bar= 200µm. (d) Quantification of the initial lesion size (lesion^{out}) in *Lrp1* control (n= 8) and iKO (n= 6) mice. (e) Quantification of white matter repair in *Lrp1* control (n= 8) and iKO (n= 6) mice. The extent of repair was calculated as the percentile of (lesion^{out} - lesion^{int})/(lesion^{out}) x 100. (f) Timeline in weeks showing when OL-lineage specific *Lrp1* ablation (*Lrp1*$^{flox/flox}$*;Pdgfra-CreER*^{TM}, *Lrp1* iKO^{OL}) was induced, LPC injected, and animals sacrificed. (g) Coronal brain sections through the CC at 21 days post LPC injection of *Lrp1* control and iKO^{OL} mice. The initial lesion area is demarcated by a white dashed-line. A solid yellow line delineates the non-myelinated area. Scale bar= 200µm. (h) Quantification of the initial lesion size in *Lrp1* control (n= 4) and iKO^{OL} (n= 4) mice. (i) Quantification of white matter repair in *Lrp1* control (n= 4) and iKO^{OL} (n= 4) mice. Results are shown as mean ± SEM, *p<0.05, **p<0.01, and ***p<0.001, Student's *t*-test.

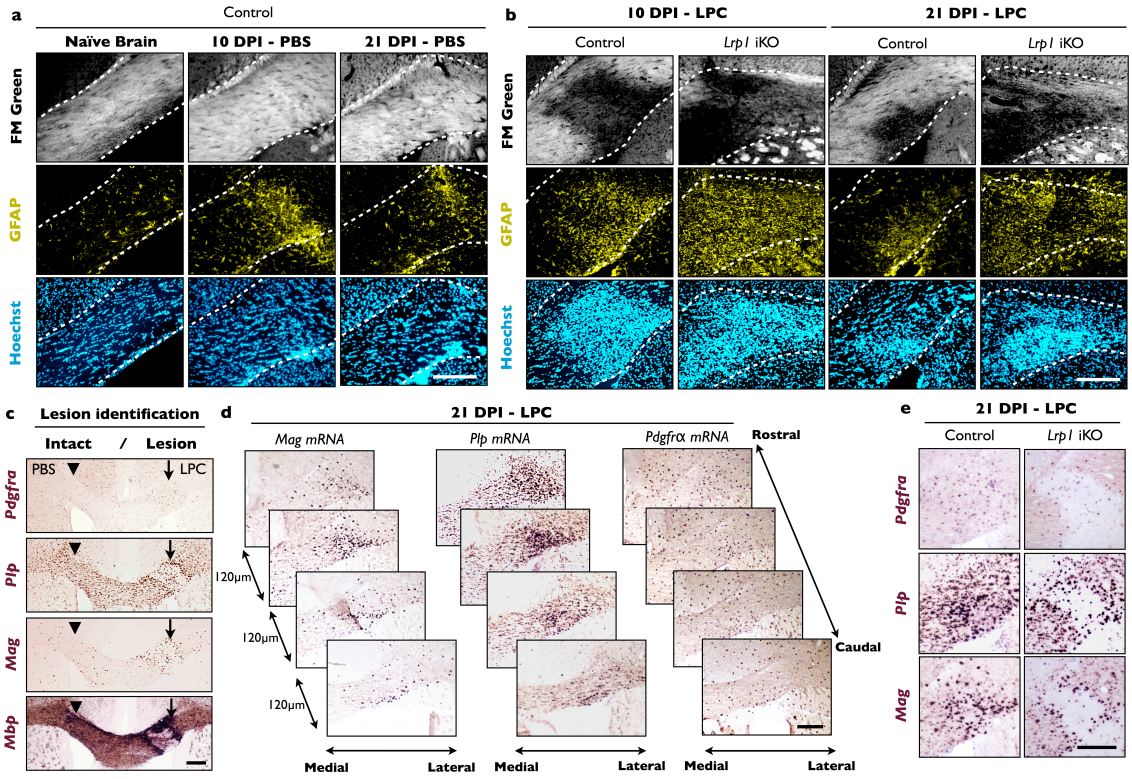
a
Control
Naïve Brain
10 DPI - PBS
21 DPI - PBS
FM Green
GFAP
Hoechst
b
10 DPI - LPC
21 DPI - LPC
Control
Lrp1 iKO
Control
Lrp1 iKO
FM Green
GFAP
Hoechst
c
Lesion identification
Intact / Lesion
PBS
LPC
Pdgfra
Plp
Mag
Mbp
d
21 DPI - LPC
Mag mRNA
Plp mRNA
Pdgfrα mRNA
Rostral
Caudal
120µm
120µm
120µm
Medial
Lateral
Medial
Lateral
Medial
Lateral
e
21 DPI - LPC
Control
Lrp1 iKO
Pdgfra
Plp
Mag

Figure 2.3: LPC injection into the corpus callosum leads to focal white matter damage and upregulation of myelin-associated gene products
(a) Coronal forebrain sections of adult *Lrp1* control (naïve) mice and mice subjected to stereotaxic injection of PBS into the corpus callosum. At 10 days post injection (10 DPI) and 21 DPI of PBS, brains were collected, serially sectioned and stained with FM Green, anti-GFAP and Hoechst dye33342. The white dotted lines demarcate the corpus callosum. The injection site is readily identified by the elevated GFAP immunoreactivity. (b) Coronal forebrain sections of *Lrp1* control and iKO mice at 10 DPI and 21 DPI of LPC stained with FM Green, anti-GFAP, and Hoechst dye33342. White dotted lines demarcate the corpus callosum. The white matter lesion is identified by the absence of FM Green labeling. Scale bar= 200μm. (c) Serial coronal-sections of adult brain after PBS and LPC injection in the corpus callosum, probed for *Pdgfra*, *Plp1*, *Mag*, and *Mbp* mRNA expression to identify the lesion area and to examine gene expression changes in the OL lineage. The site injected with PBS is marked by an arrowhead and the LPC injection site is marked by an arrow. The lesion boarder shows elevated staining for *Plp1*, *Mag* and *Mbp*. Scale bar= 200μm. (d) Serial brain sections of adult *Lrp1* control mice injected with LPC at 21 DPI. Serial sections through the lesion area (120 μm apart) were probed for *Mag, Plp1*, and *Pdgfra*, mRNA expression. Scale bar= 200μm. (e) Coronal brain sections through the CC including the lesion center of *Lrp1* control and *Lrp1* iKO mice injected with LPC at 21 DPI. Serial sections were probed for *Pdgfra*, *Plp1*, and *Mag* mRNA expression. Scale bar= 200μm.

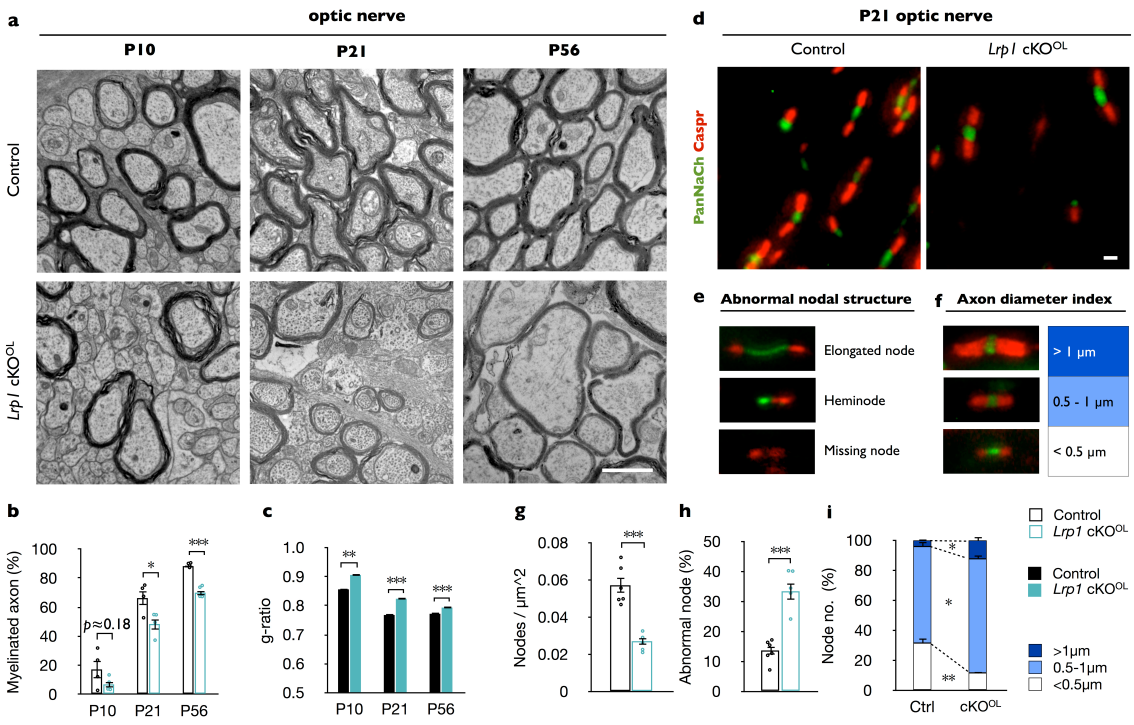
a
optic nerve
P10
P21
P56
Control
Lrp1 cKOOL
d
P21 optic nerve
Control
Lrp1 cKOOL
PanNaCh Caspr
e
Abnormal nodal structure
Elongated node
Heminode
Missing node
f
Axon diameter index
> 1 µm
0.5 - 1 µm
< 0.5 µm
b
Myelinated axon (%)
p≈0.18
P10 P21 P56
c
g-ratio
P10 P21 P56
g
Nodes / µm^2
h
Abnormal node (%)
i
Node no. (%)
Ctrl
cKOOL
Control
Lrp1 cKOOL
Control
Lrp1 cKOOL
>1µm
0.5-1µm
<0.5µm

Figure 2.4: *Lrp1* ablation in the OL-lineage leads to hypomyelination and nodal defects

(a) Ultrastructural images of optic nerve cross-sections from P10, P21, and P56 control and *Lrp1*$^{flox/flox}$*;Olig2-Cre* conditional knockout mice (*Lrp1* cKO^{OL}). Scale bar= 1μm. (b) Quantification of myelinated axons in the optic nerve of *Lrp1* control and cKO^{OL} mice at P10, P21 and P56 (n= 4 mice per genotype for each three time point). (c) Averaged g-ratio of *Lrp1* control and cKO^{OL} optic nerve fibers from 4 mice per genotype for each of the three time points. At P10, n= 488 myelinated axons for control and n= 261 for cKO^{OL}; at P21, n= 1015 for control and n= 997 for cKO^{OL}; at P56, n= 1481 for control and n= 1020 for cKO^{OL} mice. (d) Nodes of Ranvier in P21 optic nerves of *Lrp1* control and cKO^{OL} mice were labeled by anti-PanNaCh (green, node) and anti-Caspr (red, paranode) staining. Scale bar= 1μm. (e) Nodal defects detected include elongated node, heminode, and missing node (Na^+ channels absent). (f) Representative nodal staining categorized by axon diameter. (g) Quantification of nodal density in P21 *Lrp1* control (n= 6) and cKO^{OL} (n= 5) optic nerves. (h) Quantification of abnormal nodes of Ranvier in *Lrp1* control (n= 6) and cKO^{OL} (n= 5) optic nerves. (i) Quantification of nodes associated with large (> 1 μm), intermediate (0.5-1 μm), and small caliber fibers (< 0.5 μm) in *Lrp1* control (n= 6) and cKO^{OL} (n= 5) optic nerves. Results are shown as mean ± SEM, *p<0.05, **p<0.01, and ***p<0.001, Student's *t*-test.

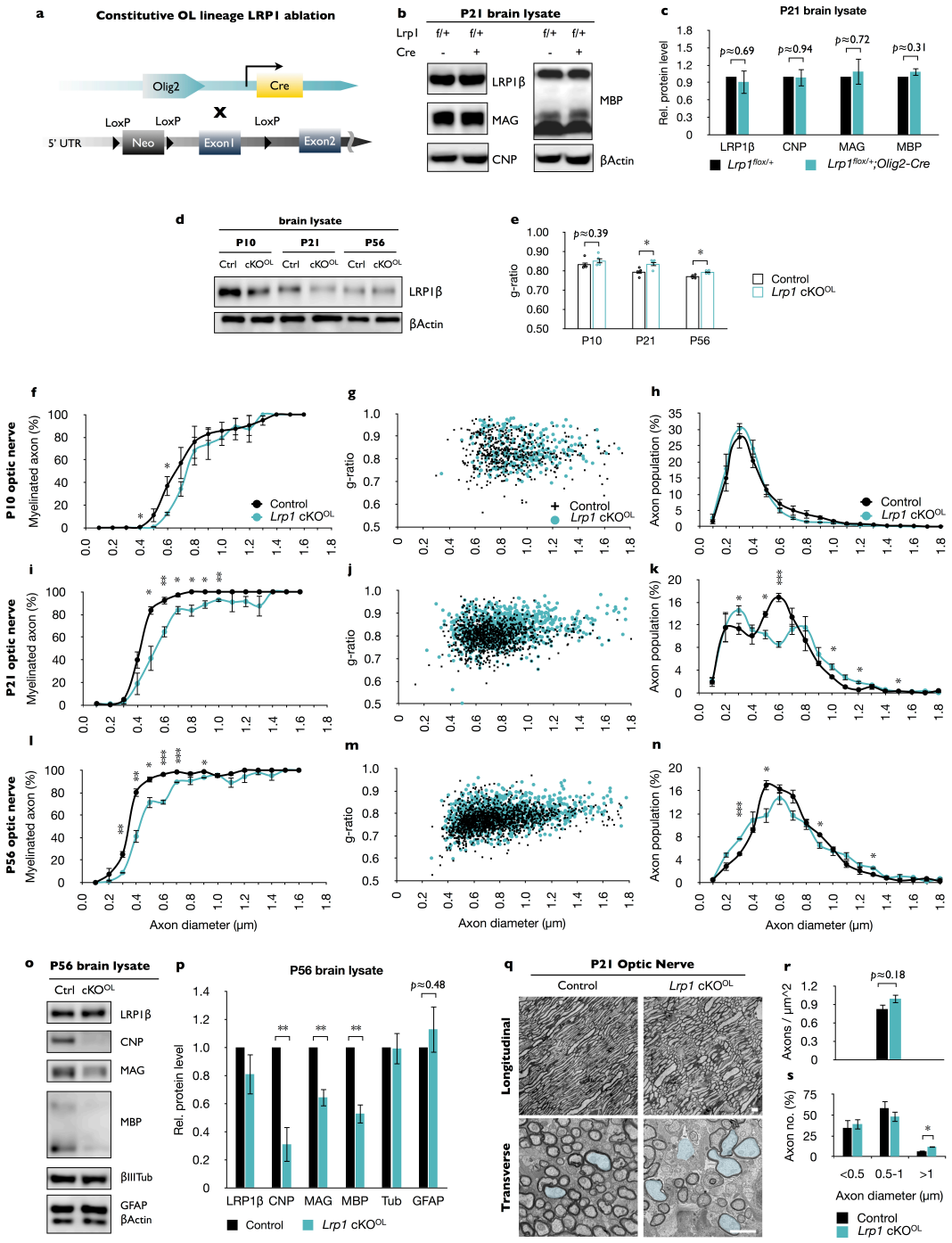
a
Constitutive OL lineage LRP1 ablation
Olig2
Cre
X
LoxP
LoxP
LoxP
5' UTR
Neo
Exon1
Exon2
b
P21 brain lysate
Lrp1
Cre
f/+
f/+
f/+
f/+
-
+
-
+
LRP1β
MAG
CNP
MBP
βActin
c
P21 brain lysate
Rel. protein level
p≈0.69
p≈0.94
p≈0.72
p≈0.31
LRP1β
CNP
MAG
MBP
Lrp1flox/+
Lrp1flox/+;Olig2-Cre
d
brain lysate
P10
P21
P56
Ctrl
cKOOL
LRP1β
βActin
e
g-ratio
p≈0.39
P10
P21
P56
Control
Lrp1 cKOOL
f
P10 optic nerve
Myelinated axon (%)
g
g-ratio
h
Axon population (%)
i
P21 optic nerve
Myelinated axon (%)
j
g-ratio
k
Axon population (%)
l
P56 optic nerve
Myelinated axon (%)
Axon diameter (μm)
m
g-ratio
Axon diameter (μm)
n
Axon population (%)
Axon diameter (μm)
Control
Lrp1 cKOOL
o
P56 brain lysate
Ctrl
cKOOL
LRP1β
CNP
MAG
MBP
βIIITub
GFAP
βActin
p
P56 brain lysate
Rel. protein level
p≈0.48
LRP1β
CNP
MAG
MBP
Tub
GFAP
Control
Lrp1 cKOOL
q
P21 Optic Nerve
Control
Lrp1 cKOOL
Longitudinal
Transverse
r
Axons / μm^2
p≈0.18
s
Axon no. (%)
<0.5
0.5-1
>1
Axon diameter (μm)
Control
Lrp1 cKOOL

Figure 2.5: *Lrp1* ablation in the OL lineage leads to CNS hypomyelination
(a) *Lrp1*$^{flox/flox}$ mice were crossed with *Olig2-Cre* mice to conditionally ablate *Lrp1* in OL lineage (cKO^{OL}). (b) To ensure that the presence of the *Olig2-Cre* allele does not lead to altered expression of myelin-associated proteins or LRP1, P21 brains of *Lrp1*$^{flox/+}$ and *Lrp1*$^{flox/+}$*;Olig2-Cre* mice were lysed and subjected to SDS-PAGE. Representative Western blots probed with anti-LRP1β, anti-MAG, anti-CNP, anti-MBP, and anti-β-actin are shown. (c) Quantification of protein levels detected by Western blotting of *Lrp1*$^{flox/+}$ (n= 3) and *Lrp1*$^{flox/+}$*;Olig2-Cre* (n= 3) brain lysates revealed no differences in the presence or absence of the *Olig2-Cre* allele. (d) Immunoblotting of whole brain lysates prepared from P10, P21, and P56 of *Lrp1* control (Ctrl) and cKO^{OL} mice. Representative blots probed with anti-LRP1β and anti-β-Actin. (e) Average g-ratio of myelinated optic nerve axons of *Lrp1* control and cKO^{OL} mice, n= 4 mice per genotype for each of the three time points. (f, i, and l) Graphs show the percentage of myelinated axons in the optic nerve at P10, P21 and P56 as a function of axon caliber in *Lrp1* control (n= 4 for each time point) and cKO^{OL} (n= 4 for each time point) mice. Axon calibers were binned into 9 groups of 0.2 μm intervals, ranging from 0.1 to 1.7 μm. (g, j, and m) Scatter plot showing the distribution of g ratios for individual fibers in the optic nerve at P10, P21 and P56 of *Lrp1* control and cKO^{OL} mice. P10, n= 488 axons from *Lrp1* control mice and n= 261 axons from cKO^{OL} mice; P21, n= 1015 axons from *Lrp1* control mice and n= 997 axons from 4 cKO^{OL} mice; P56, n= 1481 axons from *Lrp1* control mice and n= 1020 axons from 4 cKO^{OL} mice. (h, k, and n) Morphometric assessment of axon caliber distribution in P10, P21 and P56 optic nerves of *Lrp1* control (n= 4) and cKO^{OL} (n= 4) mice. Measurements of axon diameter were made from electron microscopy images. (o) Immunoblotting of whole brain lysates prepared from P56 *Lrp1* control (Ctrl) and cKO^{OL} mice. Representative blots probed with anti-LRP1β, anti-CNP, anti-MAG, anti-MBP, anti-β-III tubulin, anti-GFAP, and anti-β-actin. (p) Quantification of protein levels detected by Western blotting of *Lrp1* control (n= 3) and cKO^{OL} (n= 3) brain lysates. (q) Electron microscopy images of optic nerve cross- and longitudinal-sections acquired from P21 *Lrp1* control and cKO^{OL} mice. Axons that are >1μm in diameter are colored in light blue. Scale bar= 1μm. (r) Quantification of axon density in the P21 optic nerve for *Lrp1* control (n= 4) and cKO^{OL} (n=4) mice. (s) Quantification of optic nerve axons smaller than < 0.5μm, between 0.5-1.0μm and larger than 1μm in *Lrp1* control (n= 4) and cKO^{OL} (n= 4) mice. Results are presented as the mean ± SEM, **p*<0.05, ***p*<0.01, and ****p*<0.001, Student's *t*-test.

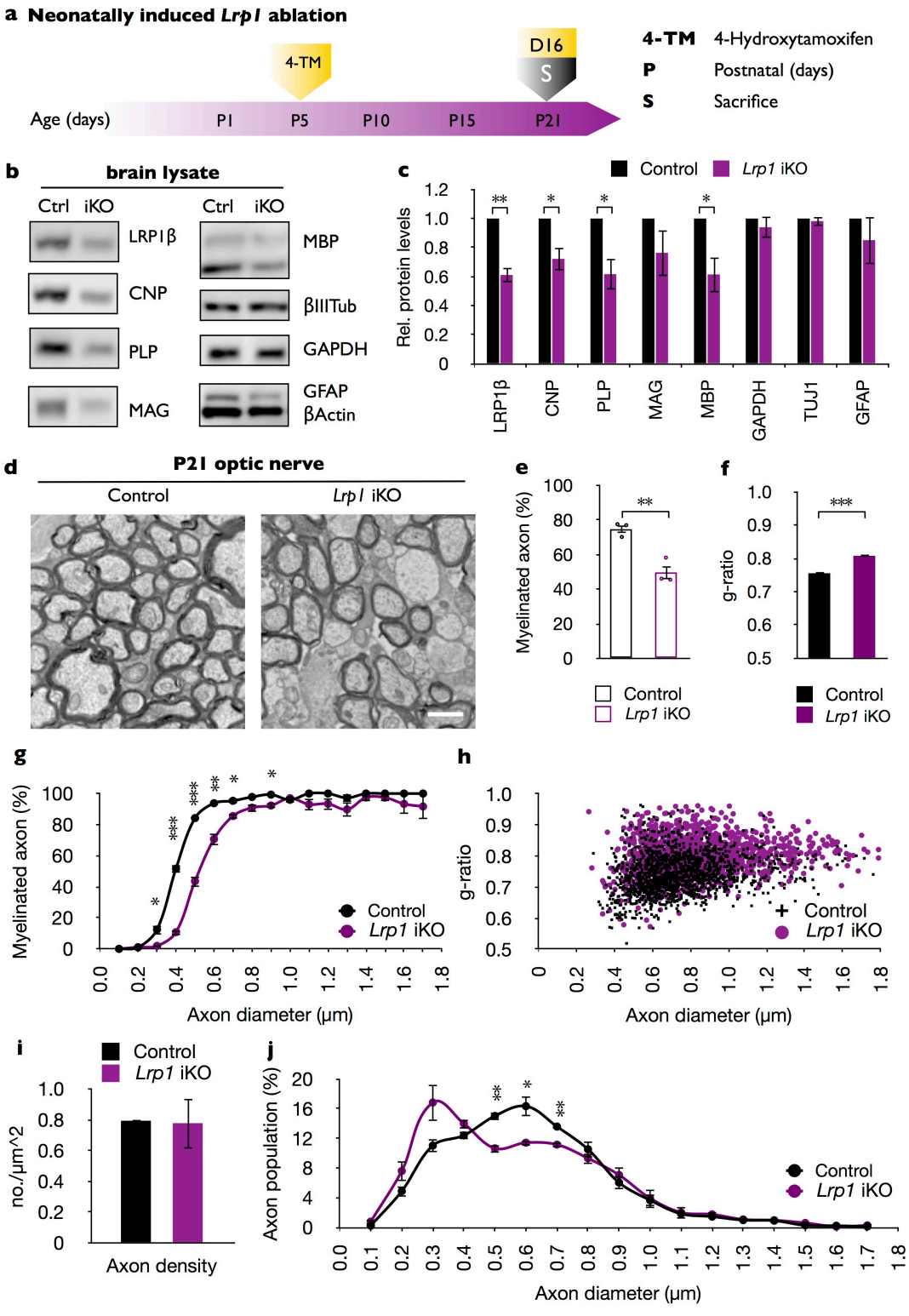
a Neonatally induced Lrp1 ablation
4-TM
D16
S
Age (days)
P1
P5
P10
P15
P21
4-TM 4-Hydroxytamoxifen
P Postnatal (days)
S Sacrifice
b
brain lysate
Ctrl iKO
Ctrl iKO
LRP1β
CNP
PLP
MAG
MBP
βIIITub
GAPDH
GFAP
βActin
c
Control
Lrp1 iKO
Rel. protein levels
LRP1β
CNP
PLP
MAG
MBP
GAPDH
TUJ1
GFAP
d
P21 optic nerve
Control
Lrp1 iKO
e
Myelinated axon (%)
Control
Lrp1 iKO
f
g-ratio
Control
Lrp1 iKO
g
Myelinated axon (%)
Control
Lrp1 iKO
Axon diameter (μm)
h
g-ratio
Control
Lrp1 iKO
Axon diameter (μm)
i
Control
Lrp1 iKO
no./μm^2
Axon density
j
Axon population (%)
Control
Lrp1 iKO
Axon diameter (μm)

Figure 2.6: Global inducible ablation of *Lrp1* in neonatal mice leads to CNS hypomyelination and reduced axon caliber

(a) Timeline in days showing when *Lrp1* ablation was induced and when mice were sacrificed. (b) Immunoblotting of whole brain lysates prepared from *Lrp1* control (Ctrl) and *Lrp1* inducible knockout (*Lrp1*$^{flox/flox}$*;CAG-CreER*^{TM}, *Lrp1* iKO) mice. Representative blots probed with anti-LRP1β, anti-CNP, anti-PLP, anti-MAG, anti-MBP, anti-β-III tubulin, anti-GAPDH, anti-GFAP, and anti-β-actin are shown. (c) Quantification of protein levels detected in brain lysates of *Lrp1* control (n= 3) and iKO (n= 3) mice. (d) Ultrastructural images of optic nerve cross-sections from P21 *Lrp1* control and iKO mice. Scale bar= 1μm. (e) Quantification of myelinated axons in *Lrp1* control (n= 3) and iKO (n= 3) mice. (f) Averaged g-ratio of optic nerve fibers of *Lrp1* control (n= 1932 axons, 3 mice) and iKO (n= 2461 axons, 3 mice) mice. Scale bar= 1 μm. (g) Graph showing the percentage of myelinated axons in the optic nerve of P21 mice as a function of axon caliber. Axon calibers of *Lrp1* control (n= 3) and iKO (n= 3) mice were binned into 9 groups of 0.2 μm intervals, ranging from 0.1 to 1.7 μm. The percentile of myelination is not significantly different for axons <0.3μm, significantly different for axons between 0.3-0.9μm, and not significantly different for axons between 1.0-1.7μm. (h) Scatter plot showing the distribution of g-ratios for individual fibers in the optic nerve of P21 *Lrp1* control (n= 2461 axons, 3 mice) and iKO (n= 1934 axons, 3 mice). (i) Quantification of axon density per μm^2 in P21 optic nerve cross sections of *Lrp1* control (n= 3) and iKO (n= 3) mice. (j) Morphometric assessment of axon caliber distribution in P21 optic nerves of *Lrp1* control (n= 3) and iKO (n= 3) mice. Axon diameters were measured on electron microscopy images and quantification revealed a shift toward smaller-sized axons in *Lrp1* iKO mice. Results are presented as the mean ± SEM, *p<0.05, **p<0.01, and ***p<0.001, Student's *t*-test.

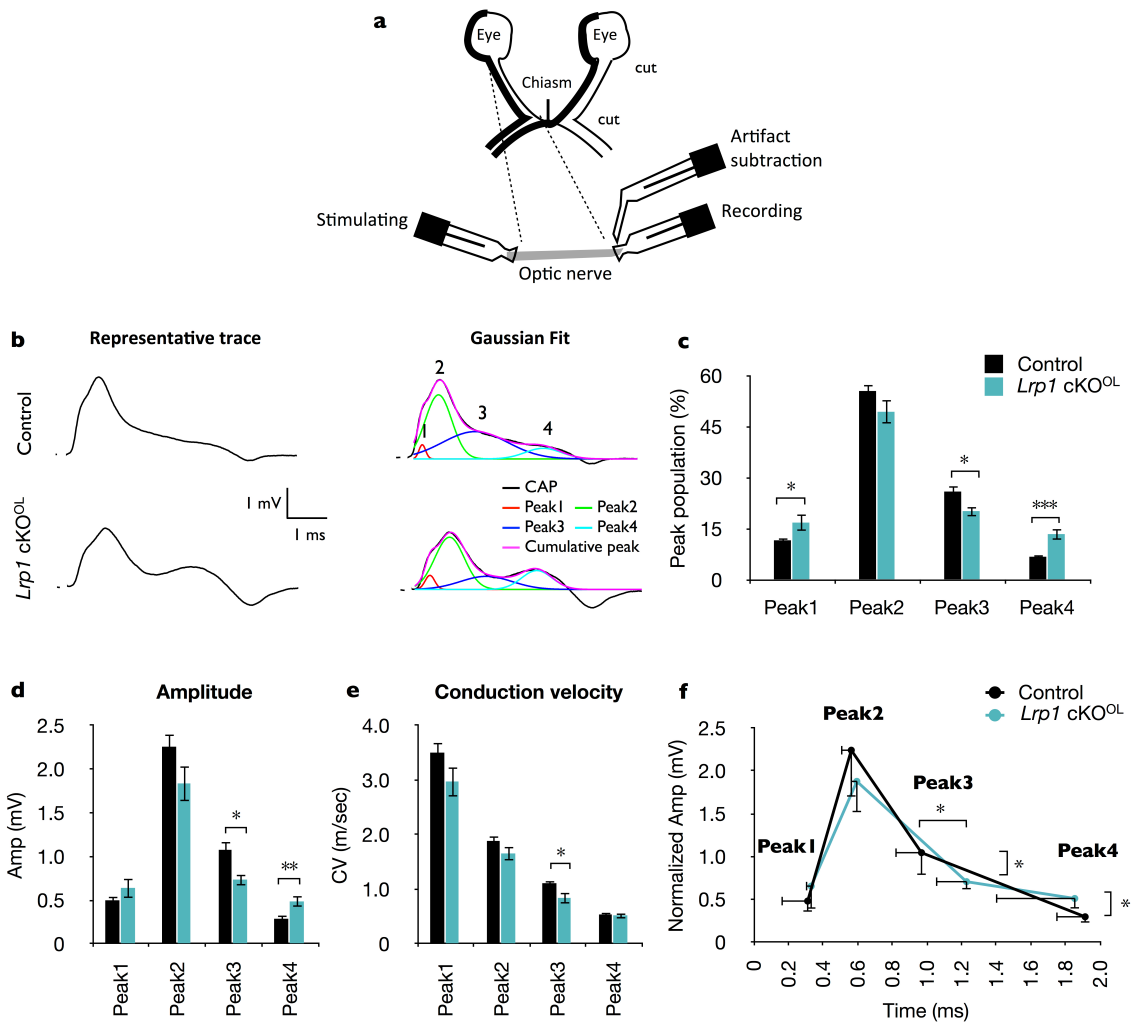
a
Eye
Eye
Chiasm
cut
cut
Artifact subtraction
Recording
Stimulating
Optic nerve
b
Representative trace
Gaussian Fit
Control
Lrp1 cKOOL
1 mV
1 ms
2
3
4
CAP
Peak1
Peak2
Peak3
Peak4
Cumulative peak
c
Control
Lrp1 cKOOL
Peak population (%)
60
45
30
15
0
*
*
***
Peak1
Peak2
Peak3
Peak4
d
Amplitude
Amp (mV)
2.5
2.0
1.5
1.0
0.5
0
*
**
Peak1
Peak2
Peak3
Peak4
e
Conduction velocity
CV (m/sec)
4.0
3.0
2.0
1.0
0
*
Peak1
Peak2
Peak3
Peak4
f
Control
Lrp1 cKOOL
Peak2
Peak3
Peak1
Peak4
*
*
*
Normalized Amp (mV)
2.5
2.0
1.5
1.0
0.5
0
0
0.2
0.4
0.6
0.8
1.0
1.2
1.4
1.6
1.8
2.0
Time (ms)

Figure 2.7: Loss of *Lrp1* in the OL lineage leads to faulty optic nerve conduction
(a) Scheme depicting the orientation of an optic nerve prepared for compound action potential (CAP) recordings. Positions of the stimulating electrode, the recording electrode, and artifact subtraction electrode are shown. (b) Left: representative raw CAP traces of P21 optic nerves. Right: For each recording, traces were fitted with 4 Gaussians representing peak 1 (red), peak 2 (green), peak 3 (blue), peak 4 (cyan), and the sum of the four peaks (magenta). (c) The distribution of peak populations in *Lrp1* control and cKO^{OL} mice. (d) Quantification of amplitudes (mV) of peaks 1, 2, 3 and 4 in *Lrp1* control and cKO^{OL} optic nerves. (e) Quantification of conduction velocities (m/sec) of peaks 1, 2, 3 and 4 in *Lrp1* control and cKO^{OL} optic nerves. (f) Reconstituted averaged peak 1-4 amplitude as a function of time. *Lrp1* control (n= 21 nerves/ 14 mice) and cKO^{OL} (n= 9 nerves/ 7 mice). Results are presented as the mean ±SEM, *p<0.05, **p<0.01, and ***p<0.001, Student's t-test.

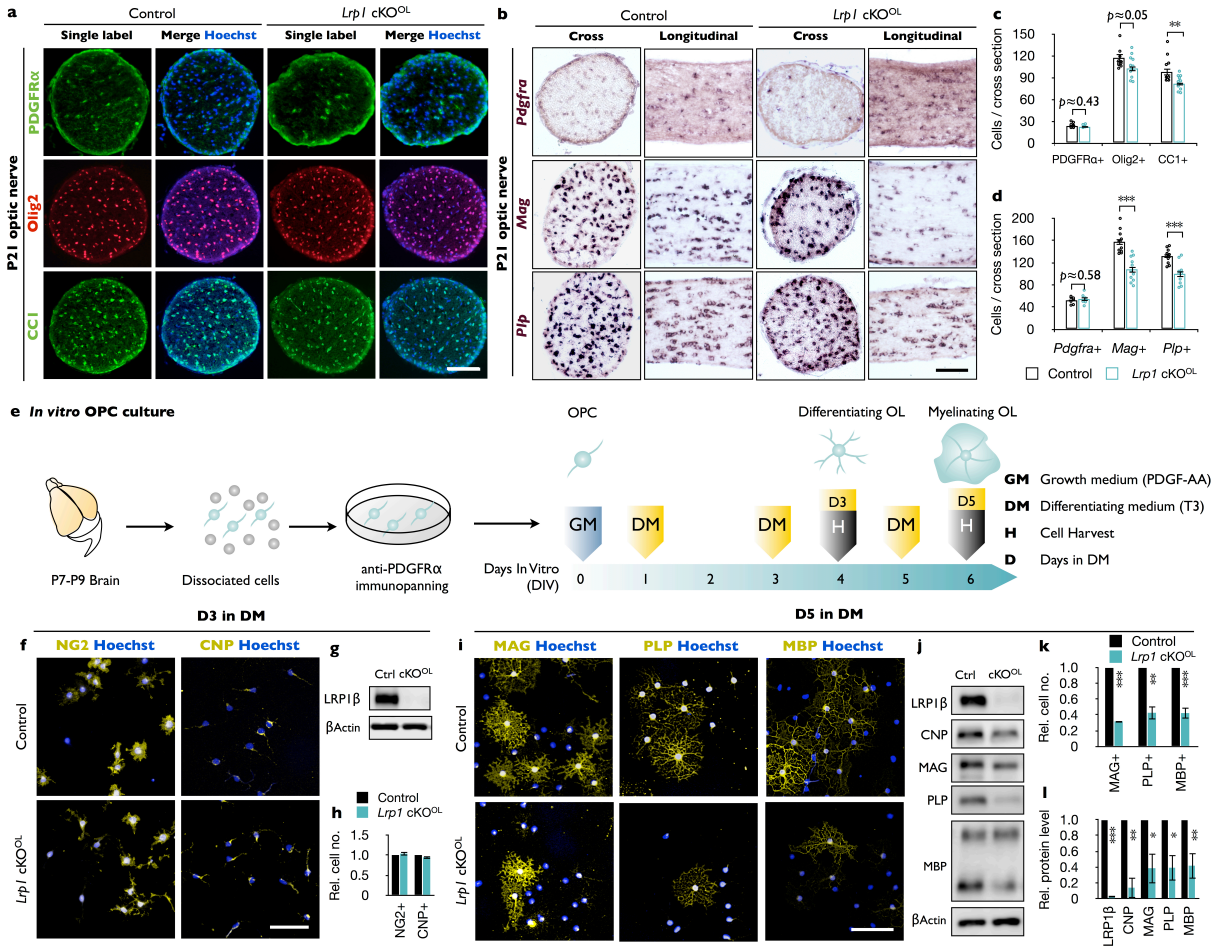
a
Control
Lrp1 cKOOL
Single label
Merge Hoechst
P21 optic nerve
PDGFRα
Olig2
CC1
b
Cross
Longitudinal
Pdgfra
Mag
Plp
c
Cells / cross section
p≈0.43
p≈0.05
PDGFRα+
Olig2+
CC1+
d
p≈0.58
Pdgfra+
Mag+
Plp+
Control
Lrp1 cKOOL
e In vitro OPC culture
P7-P9 Brain
Dissociated cells
anti-PDGFRα immunopanning
Days In Vitro (DIV)
OPC
Differentiating OL
Myelinating OL
GM
DM
H
D3
D5
GM Growth medium (PDGF-AA)
DM Differentiating medium (T3)
H Cell Harvest
D Days in DM
D3 in DM
f
NG2 Hoechst
CNP Hoechst
g
Ctrl cKOOL
LRP1β
βActin
h
Rel. cell no.
NG2+
CNP+
D5 in DM
i
MAG Hoechst
PLP Hoechst
MBP Hoechst
j
CNP
MAG
PLP
MBP
k
Rel. cell no.
MAG+
PLP+
MBP+
l
Rel. protein level
LRP1β
CNP
MAG
PLP
MBP

Figure 2.8: Loss of *Lrp1* in the OL-lineage attenuates OL differentiation
(a) Cross-sections of *Lrp1* control and cKO^{OL} optic nerves stained with anti-PDGFRα (OPC marker), anti-Olig2 (pan-OL marker), anti-CC1 (mature OL marker), and Hoechst dye33342. Scale bar= 100μm. (b) Cross- and longitudinal-sections of *Lrp1* control and cKO^{OL} optic nerves probed for *Pdgfra*, *Mag*, and *Plp* mRNA expression. Scale bar= 100μm. (c) Quantification of labeled cells per nerve cross-section. Anti-PDGFRα in control (n= 8) and cKO^{OL} (n= 6) mice; anti-Olig2 and anti-CC1 in control (n=11) and cKO^{OL} (n= 12) mice. (d) Quantification of labeled cells per nerve cross-section. *Pdgfra*, control (n= 8) and cKO^{OL} (n= 6) mice; *Mag*, control (n= 11) and cKO^{OL} (n= 11) mice; *Plp*, control (n= 11) and cKO^{OL} (n= 10) mice. (e) Workflow for OPC isolation and culturing with timeline when growth medium (GM) or differentiation medium (DM) was added and cells were harvested. (f) OPC/OL cultures after 3 days in DM stained with anti-NG2 (premyelinating marker), anti-CNP (differentiating OL marker), and Hoechst dye33342. Scale bar= 100μm. (g) Immunoblot of OL lysates prepared from *Lrp1* control and cKO^{OL} cultures after 3 days in DM probed with anti-LRP1β and anti-β-actin. (h) Quantification of NG2^{+} (n= 3) and CNP^{+} (n= 3) cells in *Lrp1* control and cKO^{OL} cultures. (i) Control and *Lrp1* deficient OL cultures after 5 days in DM stained with anti-MAG, anti-PLP, and anti-MBP. Scale bar= 100μm. (j) Immunoblotting of OL lysates prepared from *Lrp1* control and cKO^{OL} cultures after 5 days in DM probed with anti-LRP1β, anti-CNP, anti-MAG, anti-PLP, anti-MBP, and anti-β-actin. (k) Quantification of MAG^{+}, PLP^{+}, and MBP^{+} cells in *Lrp1* control (n= 3) and cKO^{OL} (n= 3) cultures. (l) Quantification of protein levels in OL lysates detected by immunoblotting. Anti-LRP1, CNP, and PLP, n= 3 per condition; anti-MAG, n= 4 per condition; anti-MBP n= 5 per condition. Results are shown as mean values ±SEM, *p<0.05, **p<0.01, and ***p<0.001, Student's *t*-test.

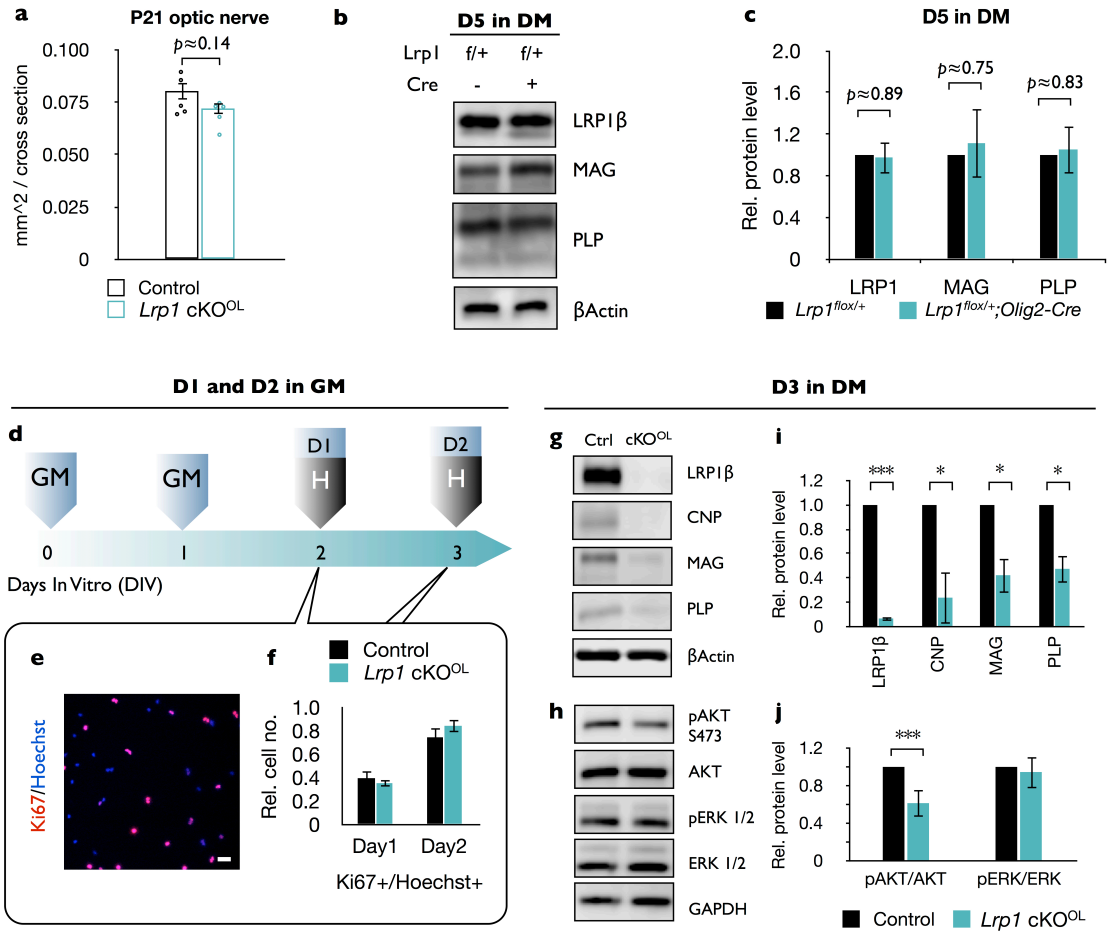
a
P21 optic nerve
p≈0.14
mm^2 / cross section
0.100
0.075
0.050
0.025
0
Control
Lrp1 cKOOL
b
D5 in DM
Lrp1 f/+ f/+
Cre - +
LRP1β
MAG
PLP
βActin
c
D5 in DM
Rel. protein level
2.0
1.6
1.2
0.8
0.4
0
p≈0.89
p≈0.75
p≈0.83
LRP1
MAG
PLP
Lrp1flox/+
Lrp1flox/+;Olig2-Cre
D1 and D2 in GM
d
GM
GM
D1
H
D2
H
0
1
2
3
Days In Vitro (DIV)
e
Ki67/Hoechst
f
Control
Lrp1 cKOOL
Rel. cell no.
1.0
0.8
0.6
0.4
0.2
0
Day1
Day2
Ki67+/Hoechst+
D3 in DM
g
Ctrl cKOOL
LRP1β
CNP
MAG
PLP
βActin
i
Rel. protein level
1.2
1.0
0.8
0.6
0.4
0.2
0
***
*
*
*
LRP1β
CNP
MAG
PLP
h
pAKT S473
AKT
pERK 1/2
ERK 1/2
GAPDH
j
Rel. protein level
1.2
0.8
0.4
0
***
pAKT/AKT
pERK/ERK
Control
Lrp1 cKOOL

Figure 2.9: Loss of *Lrp1* does not alter optic nerve size and OPC proliferation
(a) Quantification of optic nerve diameter in *Lrp1* control (n= 5) and cKO (n= 5) mice. (b) To ensure that the presence of the *Olig2-Cre* allele does not lead to altered expression of myelin-associated proteins or LRP1, in primary OPCs/OLs prepared from *Lrp1*$^{flox/+}$ or *Lrp1*$^{flox/+}$*;Olig2-Cre* pups, cells were lysed and subjected to Western blot analysis. OPCs/OLs were cultured for 5 days in differentiation medium (DM). Cell lysates were separated by SDS-PAGE and protein blots probed with anti-LRP1β, anti-CNP, anti-MAG, anti-PLP and anti-β-actin. Equal amounts of total protein were loaded per lane. (c) Quantification of LRP1, MAG, and PLP protein levels detected by immunoblotting of *Lrp1*$^{flox/+}$ and *Lrp1*$^{flox/+}$*;Olig2-Cre* OPC/OL culture lysates (n= 3 per genotype) revealed no differences in the presence or absence of the *Olig2-cre* allele. (d) Timeline in days indicating when growth medium (GM) was added to cells and when cells were harvested (H) to assess proliferation. (e) OPC/OL culture after 1 or 2 days in GM stained with anti-Ki67 (proliferation marker) and Hoechst dye33342. Scale bar= 100μm. (f) Quantification of cell proliferation in OPC/OL cultures prepared from *Lrp1* control and cKO^{OL} mice. The percentile of Ki67^{+}/Hoechst^{+} cells was calculated on day 1 for *Lrp1* control (n= 5) and cKO^{OL} (n= 5) cultures and on day 2 for *Lrp1* control (n= 4) and cKO^{OL} (n = 4) cultures. (g) Immunoblots of cell lysates prepared from *Lrp1* control and cKO^{OL} OPC/OL cultures after 3 days in differentiation medium (DM). Blots were probed with anti-LRP1β, anti-CNP, anti-MAG, anti-PLP, and anti-β-actin. (h) Immunoblots of lysates prepared from *Lrp1* control and cKO^{OL} OPC/OL cultures after 3 days in DM. Representative blots were probed with anti-pAKT (S473), anti-AKT, anti-pERK (1/2), anti-ERK (1/2), and anti-GAPDH. (i) Quantification of protein levels detected by immunoblotting of *Lrp1* control and cKO^{OL} cell culture lysate. Anti-LRP1β (n= 3), anti-MAG (n=3), anti-CNP (n= 4) and anti-PLP (n=4) per genotype. (j) Quantification of protein levels detected by immunoblotting of *Lrp1* control and cKO^{OL} cell lysates. pAKT/AKT, n= 5 for *Lrp1* control and cKO^{OL} cultures; pERK/ERK, n= 3 for *Lrp1* control and cKO^{OL} cultures. Results are presented as the mean ± SEM, *p<0.05, **p<0.01, and ***p<0.001, Student's *t*-test.

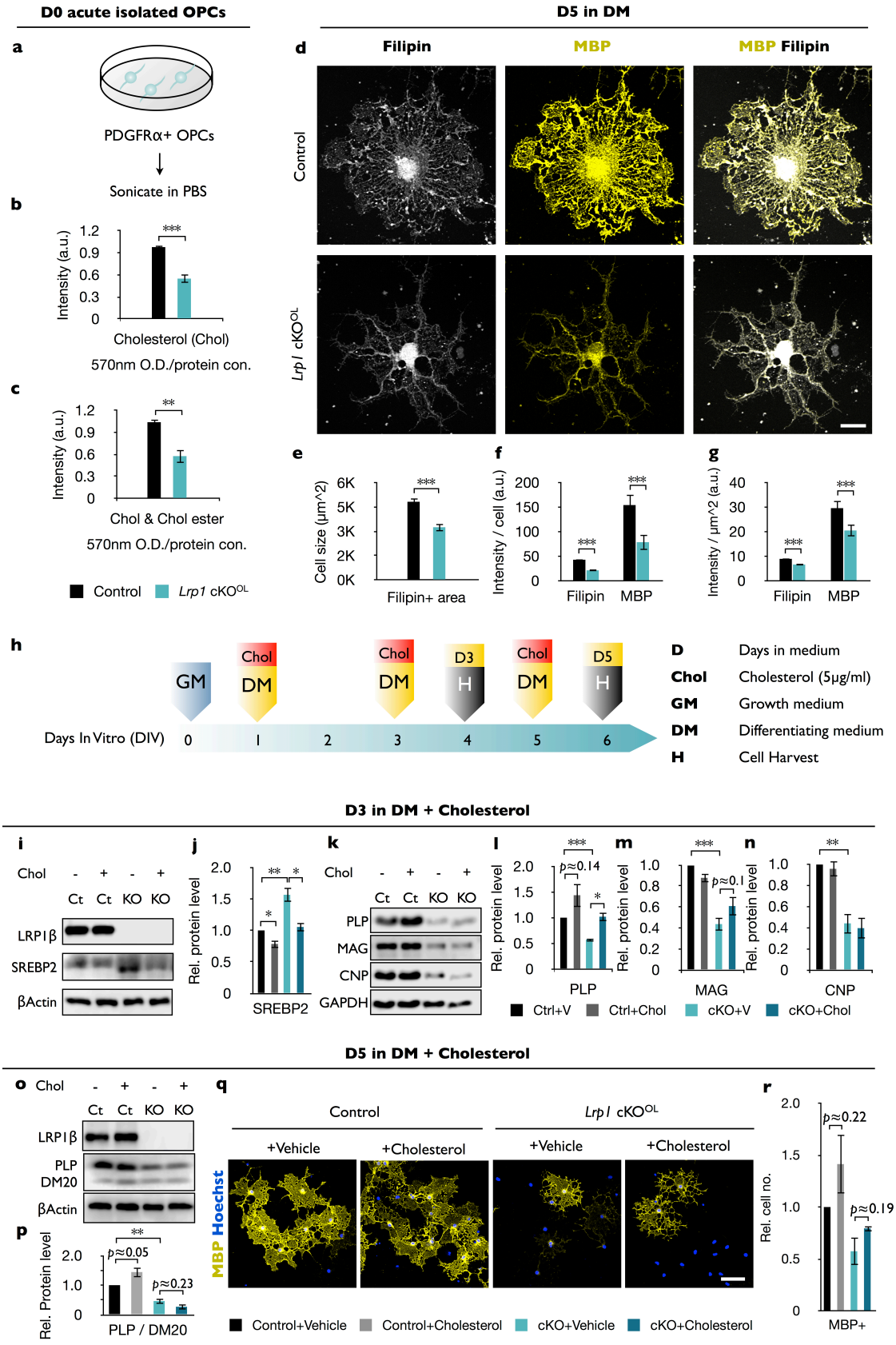
D0 acute isolated OPCs
D5 in DM
a
PDGFRα+ OPCs
Sonicate in PBS
b
Intensity (a.u.)
Cholesterol (Chol)
570nm O.D./protein con.
c
Chol & Chol ester
570nm O.D./protein con.
Control
Lrp1 cKOOL
d
Filipin
MBP
MBP Filipin
e
Cell size (μm^2)
Filipin+ area
f
Intensity / cell (a.u.)
g
Intensity / μm^2 (a.u.)
h
GM
DM
H
Days In Vitro (DIV)
D Days in medium
Chol Cholesterol (5μg/ml)
GM Growth medium
DM Differentiating medium
H Cell Harvest
D3 in DM + Cholesterol
i
LRP1β
SREBP2
βActin
j
Rel. protein level
k
PLP
MAG
CNP
GAPDH
l
m
n
p≈0.14
p≈0.1
PLP
MAG
CNP
Ctrl+V
Ctrl+Chol
cKO+V
cKO+Chol
D5 in DM + Cholesterol
o
PLP
DM20
p
p≈0.05
p≈0.23
PLP / DM20
q
+Vehicle
+Cholesterol
MBP Hoechst
Control+Vehicle
Control+Cholesterol
cKO+Vehicle
cKO+Cholesterol
r
p≈0.22
p≈0.19
Rel. cell no.
MBP+

Figure 2.10: Free cholesterol is reduced in OPCs deficient for *Lrp1*
(a) OPCs were isolated from P8 brains by anti-PDGFRα immunopanning, sonicated and subjected to measurement of cholesterol (Chol). (b and c) Quantification of free Chol (b) and total Chol (Chol & Chol ester) (c) in OPCs isolated from *Lrp1* control (n= 5) and cKO^{OL} (n= 5) mouse pups. (d) *Lrp1* control and cKO^{OL} OLs after 5 days in DM stained with filipin and anti-MBP. Scale bar= 10μm. (e-g) Quantification of OL size in μm^2 (e), the intensity of filipin and MBP labeling per cell (f), and the intensity of filipin and MBP staining per μm^2 (g). For *Lrp1* control and cKO^{OL} OLs, n= 29 cells from 3 mice in each group. (h) Timeline in days showing when growth medium (GM) or differentiation medium (DM) with (+) or without (-) Chol was added and when cells were harvested. (i and k) Immunoblotting of OL lysates prepared from *Lrp1* control and cKO^{OL} cultures after 3 days in DM. Representative blots were probed with anti-LRP1β, anti-SREBP2, anti-β-actin, anti-PLP, anti-MAG, anti-CNP, and anti-GAPDH. (j, l-n) Quantification of SREBP2 (j), PLP (l), MAG (m), and CNP (n) in *Lrp1* control and cKO^{OL} cultures ±bath applied Chol. Number of independent immunoblots: anti-PLP and MAG, n= 3 per condition; anti-SREBP2 and anti-CNP, n= 4 per condition. (o) Immunoblotting of OL lysates prepared from *Lrp1* control and cKO^{OL} cultures after 5 days in DM ±bath applied Chol. Representative blots were probed with anti-LRP1β, anti-PLP/DM20, and anti-β-actin. (p) Quantification of PLP (n=4 per condition) in *Lrp1* control and cKO^{OL} cultures ±bath applied Chol (q) Immunostaining of OLs after 5 days in DM ±bath applied Chol. Primary OLs stained with anti-MBP and Hoechst dye33342. Scale bar= 100μm. (r) Quantification showing relative number of MBP$^+$ cells in *Lrp1* control and cKO^{OL} cultures (n= 3-5 per condition). Results are shown as mean values ± SEM, *p<0.05, **p<0.01, and ***p<0.001, 2-way ANOVA, post hoc *t*-test.

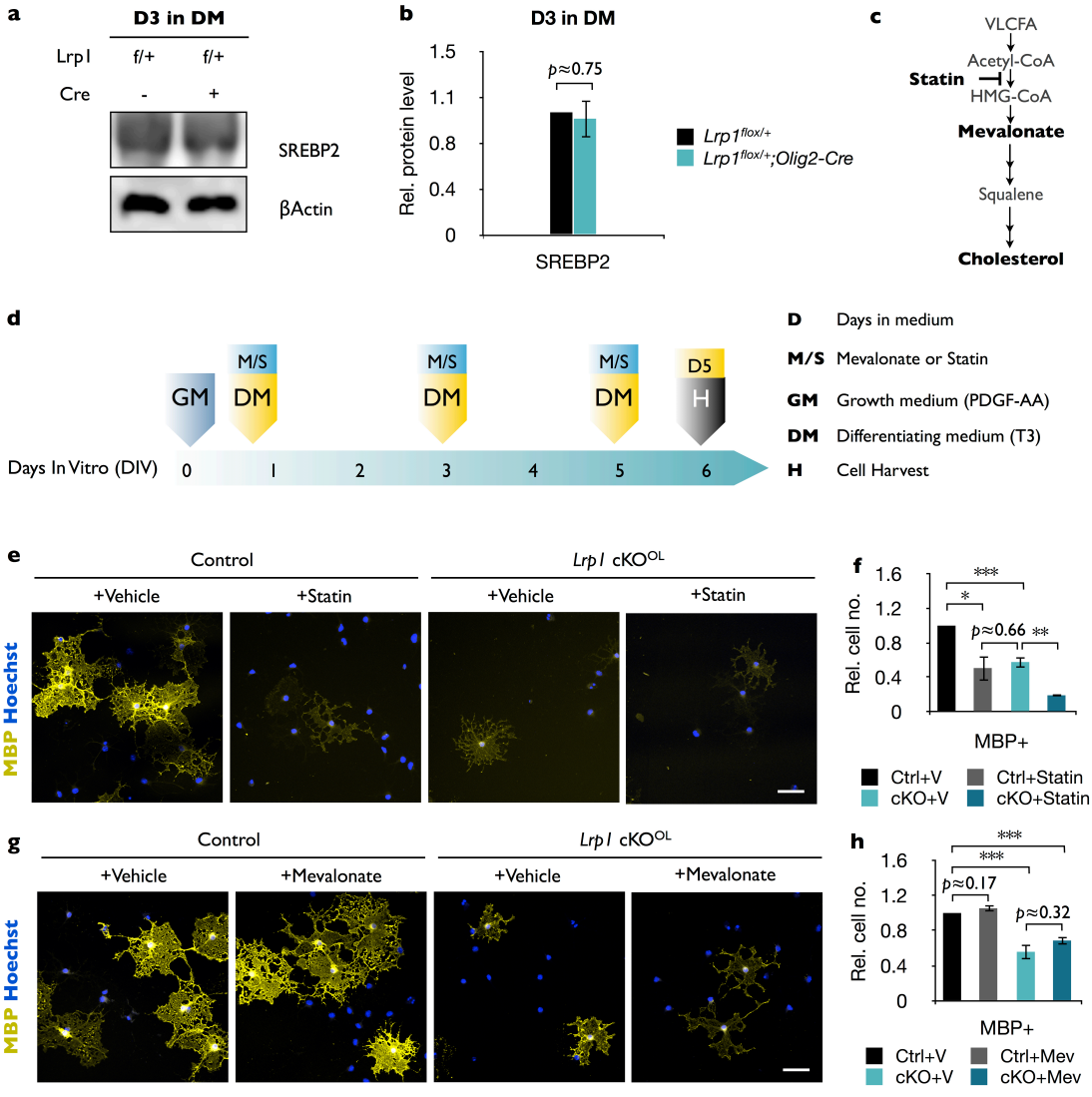
a
D3 in DM
Lrp1
f/+
f/+
Cre
-
+
SREBP2
βActin
b
D3 in DM
p≈0.75
Rel. protein level
1.5
1.1
0.8
0.4
0
SREBP2
Lrp1flox/+
Lrp1flox/+;Olig2-Cre
c
VLCFA
Acetyl-CoA
Statin
HMG-CoA
Mevalonate
Squalene
Cholesterol
d
GM
M/S
DM
M/S
DM
M/S
DM
D5
H
Days In Vitro (DIV)
0
1
2
3
4
5
6
D Days in medium
M/S Mevalonate or Statin
GM Growth medium (PDGF-AA)
DM Differentiating medium (T3)
H Cell Harvest
e
Control
Lrp1 cKOOL
+Vehicle
+Statin
+Vehicle
+Statin
MBP Hoechst
f
Rel. cell no.
1.6
1.2
0.8
0.4
0
***
*
p≈0.66
**
MBP+
Ctrl+V
Ctrl+Statin
cKO+V
cKO+Statin
g
Control
Lrp1 cKOOL
+Vehicle
+Mevalonate
+Vehicle
+Mevalonate
MBP Hoechst
h
Rel. cell no.
1.6
1.2
0.8
0.4
0
***
***
p≈0.17
p≈0.32
MBP+
Ctrl+V
Ctrl+Mev
cKO+V
cKO+Mev

Figure 2.11: *Lrp1* deficient OLs are sensitive to statin treatment but not to bath applied mevalonate

(a) Primary OPCs were isolated by anti-PDGFRα immunopanning from *Lrp1*$^{flox/+}$ and *Lrp1*$^{flox/+}$*;Olig2-Cre* pups and cultured for 3 days in differentiation medium (D3 in DM). Cells were lysed and subjected to immunoblotting with anti-SREBP2 and anti-β-actin. (b) Quantification of SREBP2 protein levels in cell lysates of *Lrp1*$^{flox/+}$ (n= 4) and *Lrp1*$^{flox/+}$*;Olig2-Cre* (n= 4) cultures revealed comparable levels. This demonstrates that the presence or absence of the *Olig2-Cre* allele does not affect SREBP2 levels. (c) Cholesterol biosynthetic pathway and site of action of statins (simvastatin), which function as inhibitors of 3-hydroxy-3methyl-glutaryl-coenzyme A reductase (HMG-CoA), the rate controlling enzyme of the mevalonate pathway. (d) Timeline in days showing when growth medium (GM) and differentiation medium (DM), either containing simvastatin or mevalonate (M/S) were added to cultures and when cells were harvested (H) for immunofluorescence labeling. (e) Immunostaining of control and *Lrp1* deficient OL cultures after 5 days in DM treated with vehicle or statin. Cell cultures were labeled with anti-MBP and Hoechst dye33342. Scale bar= 50μm. (f) Quantification of MBP$^+$ cells in *Lrp1* control cultures treated with vehicle (n= 4), *Lrp1* control cultures treated with statin (n= 3), *Lrp1* cKO^{OL} cultures treated with vehicle (n= 4), and *Lrp1* cKO^{OL} cultures treated with statin (n= 3). (g) Immunostaining of control and *Lrp1* deficient OL cultures after 5 days in DM treated with vehicle or mevalonate. Cell cultures were labeled with anti-MBP and Hoechst dye33342. Scale bar= 50μm. (h) Quantification of MBP$^+$ cells in *Lrp1* control cultures treated with vehicle (n= 3), *Lrp1* control cultures treated with mevalonate (n= 3), *Lrp1* cKO^{OL} cultures treated vehicle (n= 3), and *Lrp1* cKO^{OL} cultures treated with mevalonate (n= 3). Results are shown as mean values ±SEM, *p<0.05, **p<0.01, and ***p<0.001, 2-way ANOVA, post hoc t-test.

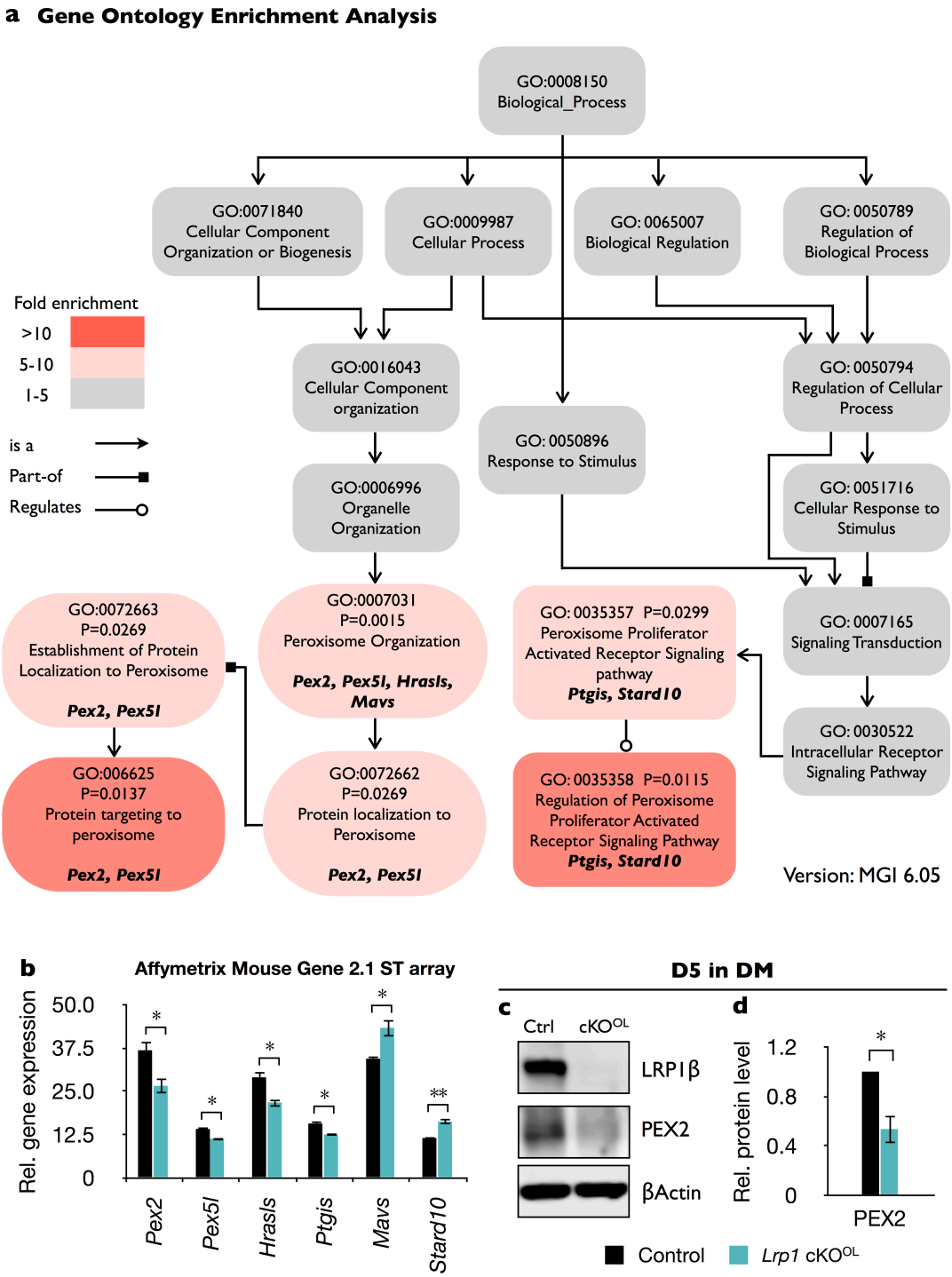
a Gene Ontology Enrichment Analysis
GO:0008150
Biological_Process
GO:0071840
Cellular Component
Organization or Biogenesis
GO:0009987
Cellular Process
GO: 0065007
Biological Regulation
GO: 0050789
Regulation of
Biological Process
Fold enrichment
>10
5-10
1-5
is a
Part-of
Regulates
GO:0016043
Cellular Component
organization
GO: 0050794
Regulation of Cellular
Process
GO: 0050896
Response to Stimulus
GO:0006996
Organelle
Organization
GO: 0051716
Cellular Response to
Stimulus
GO:0072663
P=0.0269
Establishment of Protein
Localization to Peroxisome
Pex2, Pex5l
GO:0007031
P=0.0015
Peroxisome Organization
Pex2, Pex5l, Hrasls,
Mavs
GO: 0035357 P=0.0299
Peroxisome Proliferator
Activated Receptor Signaling
pathway
Ptgis, Stard10
GO: 0007165
Signaling Transduction
GO: 0030522
Intracellular Receptor
Signaling Pathway
GO:006625
P=0.0137
Protein targeting to
peroxisome
Pex2, Pex5l
GO:0072662
P=0.0269
Protein localization to
Peroxisome
Pex2, Pex5l
GO: 0035358 P=0.0115
Regulation of Peroxisome
Proliferator Activated
Receptor Signaling Pathway
Ptgis, Stard10
Version: MGI 6.05
b
Affymetrix Mouse Gene 2.1 ST array
Rel. gene expression
50.0
37.5
25.0
12.5
0
Pex2
Pex5l
Hrasls
Ptgis
Mavs
Stard10
D5 in DM
c
Ctrl
cKOOL
LRP1β
PEX2
βActin
d
Rel. protein level
1.2
0.8
0.4
0
PEX2
Control
Lrp1 cKOOL

Figure 2.12: Gene ontology (GO) analysis of *Lrp1* deficient OPCs revealed enrichment of peroxisomal genes

Acutely isolated OPCs from *Lrp1*$^{+/+}$ and *Lrp1*$^{flox/flox}$*;Olig2-Cre* mouse pups were subjected to microarray analysis. (a) GO structure of biological process module related to peroxisome function. Each box shows the GO term ID, *p*-value, GO term, and the genes from the input list associated with the GO term. The color of each box shows the level of enrichment for each GO term. Specific GO terms were queried with the Mouse Genome Informatics (MGI) GO browser. *P*-values were calculated by Fisher's exact test. The fold-enrichment was calculated by dividing the ratio of genes that are associated with each GO term from the input list by the ratio of genes that are expected in the database. (b) Quantification of relative expression levels of gene products that are associated with specific GO terms listed in (a). mRNA was prepared from acutely isolated OPCs of *Lrp1* controls (n= 4) and cKO^{OL} (n =4) pups and analyzed with the Affymetrix mouse gene 2.1 ST array. Differentially regulated gene products include *Pex2* (peroxisomal biogenesis factor 2), *Pex5l* (peroxisomal biogenesis factor 5 like), *Hrasls* (hRas-like suppressor), *Ptgis* (prostaglandin I2 synthase), *Mavs* (Mitochondrial antiviral signaling), and *Stard10* (StAR-related lipid transfer protein 10). (c) Immunoblotting of lysates prepared from *Lrp1* control and cKO^{OL} OL cultures after 5 days in DM. Representative blots probed with anti-LRP1β, anti-PEX2, and anti-β-actin. (d) Quantification of PEX2 in *Lrp1* control (n= 3) and cKO^{OL} (n= 3) cultures. Results are shown as mean values ±SEM, *p<0.05 and **p<0.01, Student's *t*-test.

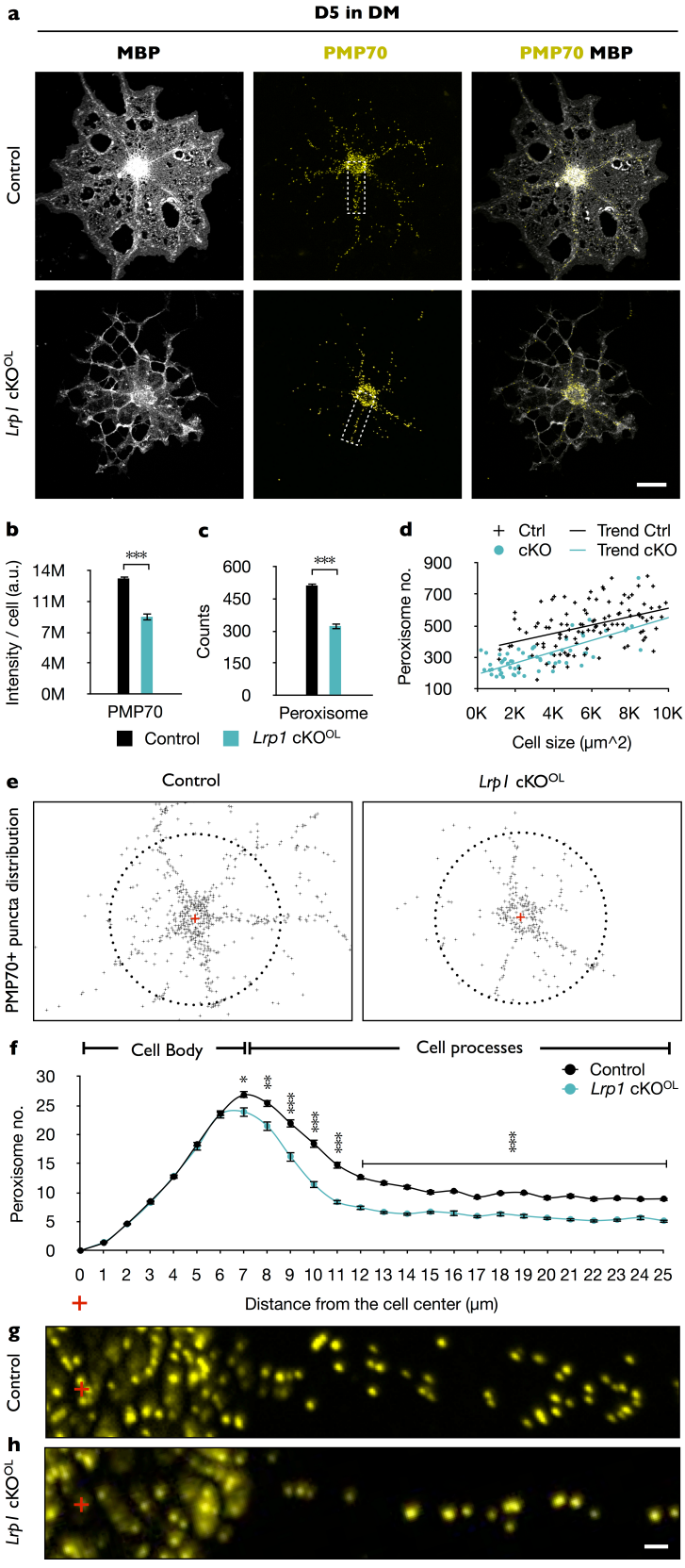
a
D5 in DM
MBP
PMP70
PMP70 MBP
Control
Lrp1 cKOOL
b
Intensity / cell (a.u.)
14M
11M
7M
4M
0M
***
PMP70
c
Counts
600
450
300
150
0
***
Peroxisome
Control
Lrp1 cKOOL
d
Ctrl
cKO
Trend Ctrl
Trend cKO
Peroxisome no.
900
700
500
300
100
0K 2K 4K 6K 8K 10K
Cell size (μm^2)
e
Control
Lrp1 cKOOL
PMP70+ puncta distribution
f
Cell Body
Cell processes
Control
Lrp1 cKOOL
Peroxisome no.
30
25
20
15
10
5
0
0 1 2 3 4 5 6 7 8 9 10 11 12 13 14 15 16 17 18 19 20 21 22 23 24 25
Distance from the cell center (μm)
g
Control
h
Lrp1 cKOOL

Figure 2.13: In primary OLs, peroxisome density and distribution is regulated by *Lrp1*

(a) Primary OLs prepared from *Lrp1* control and cKO^{OL} OL pups, cultured for 5 days in DM were stained with anti-MBP and anti-PMP70. Scale bar= 10μm. (b-d) Quantification of PMP70 labeling intensity per cell (b), PMP70^{+} puncta per cell (c), and scatter plot showing the number of PMP70^{+} peroxisomes as a function of cell size for MBP^{+} OLs of *Lrp1* control and *Lrp1* cKO^{OL} cultures (d). For *Lrp1* control OLs, n= 112 cells from 3 mice. For *Lrp1* cKO^{OL} OLs, n= 60 cells from 3 mice. (e) Representative distribution of PMP70^{+} puncta of *Lrp1* control and cKO^{OL} OL. For quantification, the center of the cell was marked with a red cross. Puncta within a 25μm radius from the center (dashed circle) were subjected to quantification. (f) Quantification of peroxisome number plotted against the distance from the center of *Lrp1* control (n= 113 cells, 3 mice) and cKO^{OL} (n= 63 cells, 3 mice) OLs. (g and h) Representative high-magnification views of PMP70^{+} puncta from areas boxed in panel (a). Scale bar= 1μm. Results are shown as mean values ± SEM, *$p<0.05$, **$p<0.01$, and ***$p<0.001$, Student's *t*-test.

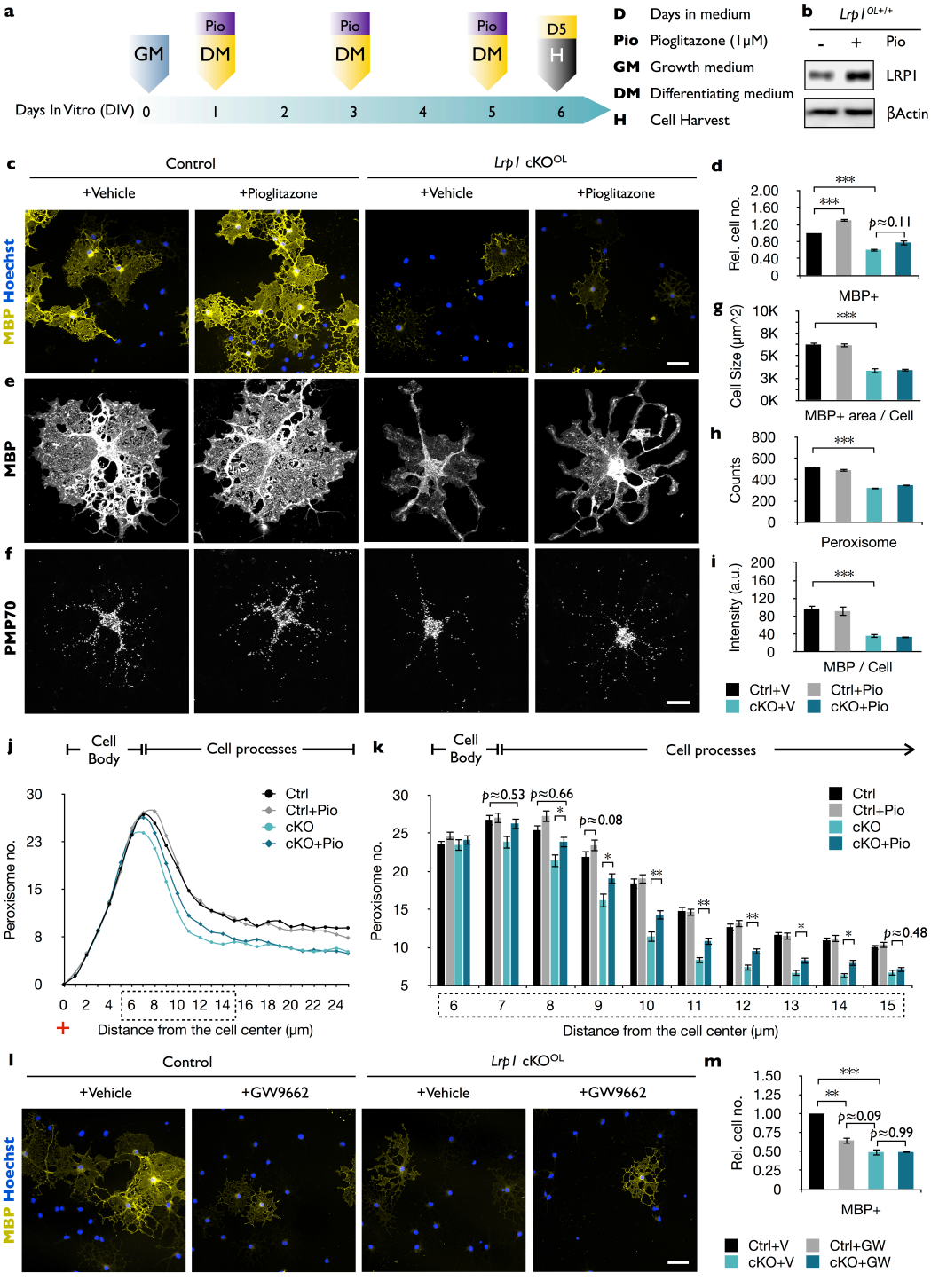
a
GM
Pio
DM
Pio
DM
Pio
DM
D5
H
Days In Vitro (DIV) 0 1 2 3 4 5 6
D Days in medium
Pio Pioglitazone (1μM)
GM Growth medium
DM Differentiating medium
H Cell Harvest
b
Lrp1 OL+/+
- + Pio
LRP1
βActin
c
Control
Lrp1 cKOOL
+Vehicle
+Pioglitazone
+Vehicle
+Pioglitazone
MBP Hoechst
e
MBP
f
PMP70
d
Rel. cell no.
2.00
1.60
1.20
0.80
0.40
0
***
***
p≈0.11
MBP+
g
Cell Size (μm^2)
10K
8K
5K
3K
0K
***
MBP+ area / Cell
h
Counts
800
600
400
200
0
***
Peroxisome
i
Intensity (a.u.)
200
160
120
80
40
0
***
MBP / Cell
Ctrl+V
Ctrl+Pio
cKO+V
cKO+Pio
j
Cell Body
Cell processes
Peroxisome no.
30
23
15
8
0
Ctrl
Ctrl+Pio
cKO
cKO+Pio
0 2 4 6 8 10 12 14 16 18 20 22 24
Distance from the cell center (μm)
k
Cell Body
Cell processes
Peroxisome no.
30
25
20
15
10
5
p≈0.53
p≈0.66
p≈0.08
p≈0.48
Ctrl
Ctrl+Pio
cKO
cKO+Pio
6 7 8 9 10 11 12 13 14 15
Distance from the cell center (μm)
l
Control
Lrp1 cKOOL
+Vehicle
+GW9662
+Vehicle
+GW9662
MBP Hoechst
m
Rel. cell no.
1.50
1.25
1.00
0.75
0.50
0.25
0
***
**
p≈0.09
p≈0.99
MBP+
Ctrl+V
Ctrl+GW
cKO+V
cKO+GW

Figure 2.14: In *Lrp1* deficient OPCs, PPARγ activation increases peroxisome density but does not promote cell differentiation

(a) Timeline in days showing when growth medium (GM) or differentiation medium (DM) with pioglitazone (Pio) were supplied and cells were harvested for analysis. (b) Immunoblots of OL lysates prepared from *Lrp1* wildtype cultures after 5 days in DM with (+) or without (-) Pio, probed with anti-LRP1β. Anti-β-actin is shown as loading control. (c) Immunostaining of *Lrp1* control and cKO^{OL} cultures after 5 days in DM. Representative cell cultures stained with anti-MBP and Hoechst dye 33342. Scale bar= 50μm. (d) Quantification of MBP^+ cells in *Lrp1* control cultures with vehicle (n= 6), *Lrp1* control cultures with Pio (n= 6), cKO^{OL} cultures with vehicle (n= 4), and cKO^{OL} cultures with Pio (n= 4). (e-f) Primary OLs probed with anti-MBP and anti-PMP70. Scale bar= 10μm. (g-i) Quantification of OL size in μm^2 (g), the number of $PMP70^+$ puncta (h), and the intensity of MBP staining per cell (i). (j) Distribution of peroxisomes as a function of distance from the cell center in *Lrp1* control and cKO^{OL} OLs treated ±Pio. The number of $PMP70^+$ peroxisomes between 6-15μm in *Lrp1* control and cKO^{OL} cultures was subjected to statistical analysis in (k). *Lrp1* control (n= 112 cells, 3 mice), *Lrp1* control cultures with Pio (n= 180 cells, 3 mice), cKO^{OL} (n= 60 cells, 3 mice), and cKO^{OL} cultures with Pio. (n= 110 cells, 3 mice) (k). (l) Immunostaining of OLs after 5 days in DM ±GW9662, probed with anti-MBP and Hoechst dye33342. Scale bar= 50μm. (m) Quantification of MBP^+ cells under each of the 4 different conditions (n=3 per condition). Results are shown as mean values ± SEM, *p<0.05, **p<0.01, and ***p<0.001, 2-way ANOVA, post hoc *t*-test.

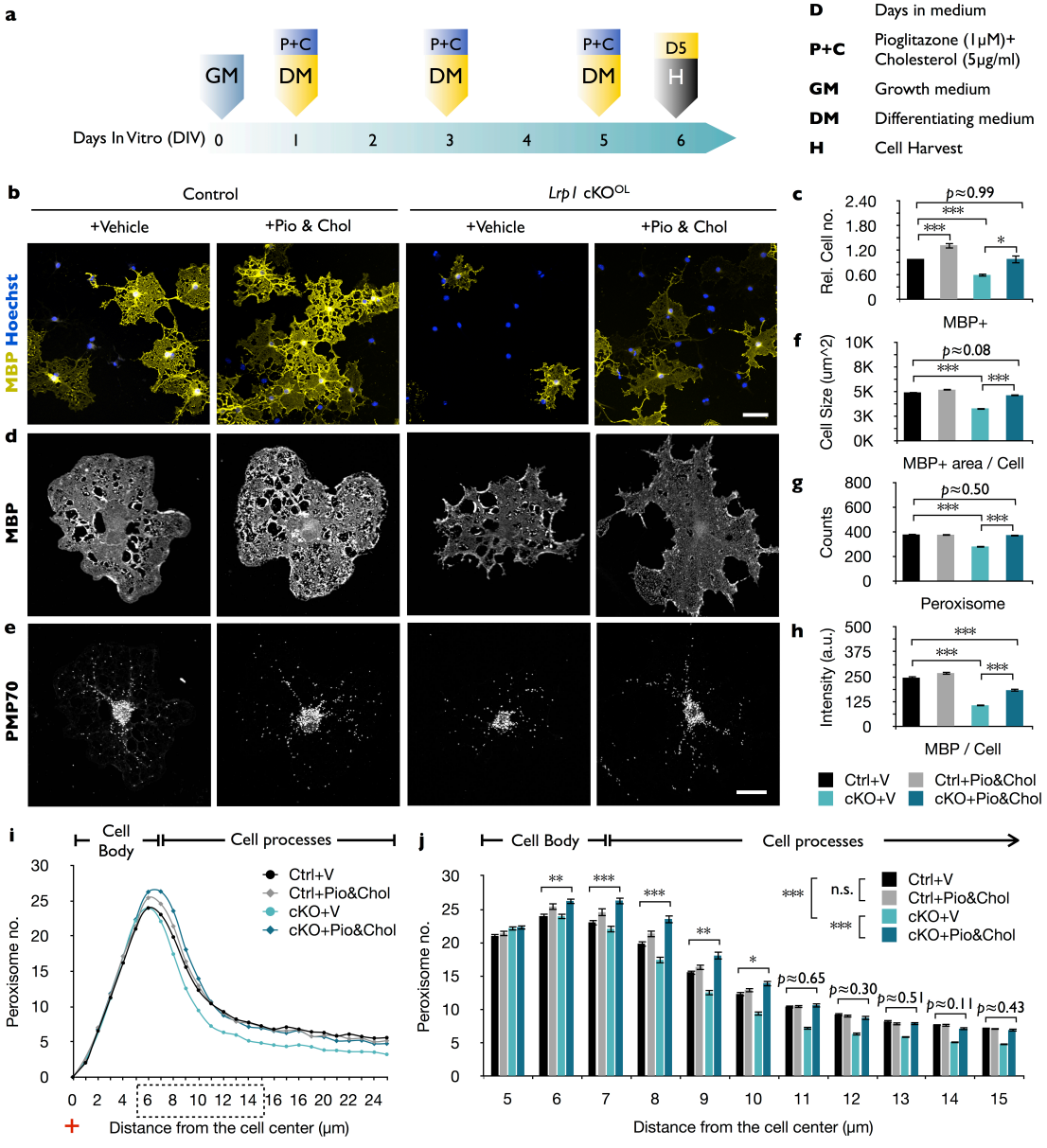
a
GM
P+C
DM
P+C
DM
P+C
DM
D5
H
Days In Vitro (DIV) 0 1 2 3 4 5 6
D Days in medium
P+C Pioglitazone (1μM)+ Cholesterol (5μg/ml)
GM Growth medium
DM Differentiating medium
H Cell Harvest
b
Control
Lrp1 cKOOL
+Vehicle
+Pio & Chol
+Vehicle
+Pio & Chol
MBP Hoechst
d
MBP
e
PMP70
c
Rel. Cell no.
p≈0.99
MBP+
f
Cell Size (um^2)
p≈0.08
MBP+ area / Cell
g
Counts
p≈0.50
Peroxisome
h
Intensity (a.u.)
MBP / Cell
Ctrl+V
Ctrl+Pio&Chol
cKO+V
cKO+Pio&Chol
i
Cell Body
Cell processes
Peroxisome no.
Distance from the cell center (μm)
j
Cell Body
Cell processes
Peroxisome no.
n.s.
p≈0.65
p≈0.30
p≈0.51
p≈0.11
p≈0.43
Distance from the cell center (μm)

Figure 2.15: The combined treatment with cholesterol and pioglitazone rescues the differentiation block of *Lrp1* deficient OPCs

(a) Timeline in days showing when growth medium (GM) or differentiation medium (DM) with pioglitazone (Pio) and cholesterol (Chol) was supplied and cells were harvested for analysis. (b) Immunostaining of *Lrp1* control and cKO^{OL} cultures after 5 days in DM, probed with anti-MBP and Hoechst dye 33342. Scale bar= 50µm. (c) Quantification of MBP^+ cells in *Lrp1* control cultures treated with vehicle (n= 4), *Lrp1* control cultures treated with Pio & Chol (n= 3), cKO^{OL} cultures treated with vehicle (n= 4), and cKO^{OL} cultures treated with Pio & Chol (n= 3). (d and e) Primary OLs probed with anti-MBP and anti-PMP70. Scale bar= 10µm. (f-h) Quantification of OL size in μm^2 (f), the number of $PMP70^+$ puncta and (g), the intensity of MBP staining per cell (h). (i) Distribution of peroxisomes as a function of distance from the cell center in *Lrp1* control and cKO^{OL} cultures with (+) or without (-) Pio & Chol combo-treatment. The number of $PMP70^+$ peroxisomes between 5-15µm in *Lrp1* control and cKO^{OL} cultures was subjected to statistical analysis in (j). *Lrp1* control cultures with vehicle (n= 210 cells, 3 mice), *Lrp1* control cultures treated with Pio & Chol (n= 208 cells, 3 mice), cKO^{OL} cultures treated wtih vehicle (n= 199 cells, 3 mice), and cKO^{OL} cultures treated wtih Pio & Chol (n= 190 cells, 3 mice) (k). Results are shown as mean values ± SEM, *$p<0.05$, **$p<0.01$, and ***$p<0.001$, 2-way ANOVA, post hoc *t*-test.

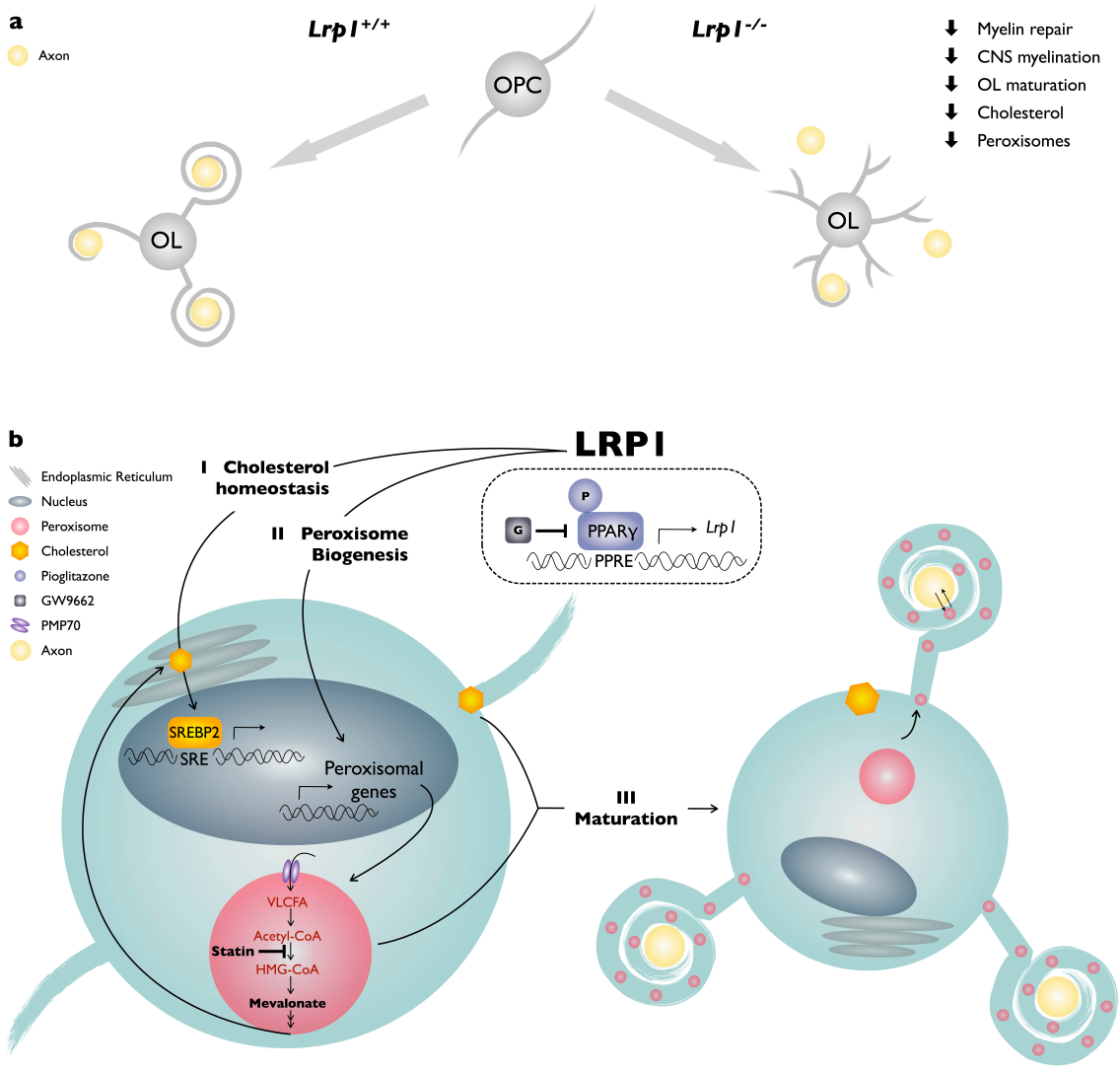
a
Axon
Lrp1 +/+
Lrp1 -/-
OPC
OL
OL
Myelin repair
CNS myelination
OL maturation
Cholesterol
Peroxisomes
b
Endoplasmic Reticulum
Nucleus
Peroxisome
Cholesterol
Pioglitazone
GW9662
PMP70
Axon
LRP1
I Cholesterol homeostasis
II Peroxisome Biogenesis
P
G
PPARγ
Lrp1
PPRE
SREBP2
SRE
Peroxisomal genes
III Maturation
VLCFA
Acetyl-CoA
Statin
HMG-CoA
Mevalonate
Oligodendrocyte Progenitor Cell
Oligodendrocyte

Figure 2.16: Working model of LRP1 regulated pathways in developing OLs
(a) LRP1 function in the OL-lineage is necessary for proper CNS myelin development and the timely repair of a chemically induced focal white matter lesion. In OPCs, Lrp1 deficiency leads to dysregulation of cholesterol homeostasis and impaired peroxisome biogenesis. (b) LRP1 is a key regulator of multiple pathways important for OPC differentiation into mature myelin producing OLs: I) LRP1 regulates cholesterol homeostatsis; II) LRP1 regulates peroxisome biogenesis; and III) the combined treatment of Lrp1 deficient primary OPCs with cholesterol and pioglitazone is sufficient to drive maturation into MBP+ myelin sheet producing OLs.

2.9 **Bibliography**

Adam MP, Ardinger HH, Pagon RA, Wallace SE, Bean LJ, et al. 1993. Zellweger Spectrum Disorder. In *GeneReviews*®: University of Washington, Seattle

Ainger K. 1993. Transport and localization of exogenous myelin basic protein mRNA microinjected into oligodendrocytes. In *The Journal of Cell Biology*, pp. 431-41: Rockefeller University Press

Auderset L, Landowski LM, Foa L, Young KM. 2016. Low Density Lipoprotein Receptor Related Proteins as Regulators of Neural Stem and Progenitor Cell Function. In *Stem Cells Int*, pp. 2108495

Baes M, Aubourg P. 2009. Peroxisomes, myelination, and axonal integrity in the CNS. In *Neuroscientist*, pp. 367-79

Berger J, Dorninger F, Forss-Petter S, Kunze M. 2016. Peroxisomes in brain development and function. In *BBA - Molecular Cell Research*, pp. 934-55: The Authors

Berger J, Moller DE. 2002. The mechanisms of action of PPARs. In *Annu. Rev. Med.*, pp. 409-35

Bernardo A, Bianchi D, Magnaghi V, Minghetti L. 2009. Peroxisome proliferator-activated receptor-gamma agonists promote differentiation and antioxidant defenses of oligodendrocyte progenitor cells. In *J. Neuropathol. Exp. Neurol.*, pp. 797-808

Bernardo A, De Simone R, De Nuccio C, Visentin S, Minghetti L. 2013. The nuclear receptor peroxisome proliferator-activated receptor-gamma promotes oligodendrocyte differentiation through mechanisms involving mitochondria and oscillatory Ca2+ waves. In *Biol Chem*, pp. 1607-14

Bernardo A, Giammarco ML, De Nuccio C, Ajmone-Cat MA, Visentin S, et al. 2017. Docosahexaenoic acid promotes oligodendrocyte differentiation via PPAR-gamma signalling and prevents tumor necrosis factor-alpha-dependent maturational arrest. In *Biochim. Biophys. Acta*, pp. 1013-23

Björkhem I, Meaney S. 2004. Brain cholesterol: long secret life behind a barrier. In *Arterioscler. Thromb. Vasc. Biol.*, pp. 806-15

Boucher P, Herz J. 2011. Signaling through LRP1: Protection from atherosclerosis and beyond. In *Biochem. Pharmacol.*, pp. 1-5: Elsevier Inc.

Camacho A, Huang JK, Delint-Ramirez I, Yew Tan C, Fuller M, et al. 2013. Peroxisome proliferator-activated receptor gamma-coactivator-1 alpha coordinates sphingolipid metabolism, lipid raft composition and myelin protein synthesis. In *Eur J Neurosci*, pp. 2672-83

Camargo N, Goudriaan A, van Deijk A-LF, Otte WM, Brouwers JF, et al. 2017. Oligodendroglial myelination requires astrocyte-derived lipids. In *PLoS Biol.*, pp. e1002605

Campana WM, Li X, Dragojlovic N, Janes J, Gaultier A, Gonias SL. 2006. The low-density lipoprotein receptor-related protein is a pro-survival receptor in Schwann cells: possible implications in peripheral nerve injury. In *J. Neurosci.*, pp. 11197-207

Carbajal KS, Mironova Y, Ulrich-Lewis JT, Kulkarni D, Grifka-Walk HM, et al. 2015. Th Cell Diversity in Experimental Autoimmune Encephalomyelitis and Multiple Sclerosis. In *The Journal of Immunology*, pp. 2552-59

Carter CJ. 2007. Convergence of genes implicated in Alzheimer's disease on the cerebral cholesterol shuttle: APP, cholesterol, lipoproteins, and atherosclerosis. In *Neurochem Int*, pp. 12-38

Chuang T-Y, Guo Y, Seki SM, Rosen AM, Johanson DM, et al. 2016. LRP1 expression in microglia is protective during CNS autoimmunity. In *Acta Neuropathol Commun*, pp. 1-12

Dai ZM, Sun S, Wang C, Huang H, Hu X, et al. 2014. Stage-Specific Regulation of Oligodendrocyte Development by Wnt/ -Catenin Signaling. In *Journal of Neuroscience*, pp. 8467-73

De Nuccio C, Bernardo A, De Simone R, Mancuso E, Magnaghi V, et al. 2011. Peroxisome proliferator-activated receptor γ agonists accelerate oligodendrocyte maturation and influence mitochondrial functions and oscillatory Ca(2+) waves. In *J. Neuropathol. Exp. Neurol.*, pp. 900-12

Emery B, Agalliu D, Cahoy JD, Watkins TA, Dugas JC, et al. 2009. Myelin Gene Regulatory Factor Is a Critical Transcriptional Regulator Required for CNS Myelination. In *Cell*, pp. 172-85: Elsevier Ltd

Fancy SPJ, Chan JR, Baranzini SE, Franklin RJM, Rowitch DH. 2011. Myelin regeneration: a recapitulation of development? In *Annu. Rev. Neurosci.*, pp. 21-43

Fang L, Zhang M, Li Y, Liu Y, Cui Q, Wang N. 2016. PPARgene: A Database of Experimentally Verified and Computationally Predicted PPAR Target Genes. In *PPAR Res*, pp. 1-6

Faust PL. 2003. Abnormal cerebellar histogenesis in PEX2 Zellweger mice reflects multiple neuronal defects induced by peroxisome deficiency. In *J Comp Neurol*, pp. 394-413

Faust PL, Hatten ME. 1997. Targeted deletion of the PEX2 peroxisome assembly gene in mice provides a model for Zellweger syndrome, a human neuronal migration disorder. In *The Journal of Cell Biology*, pp. 1293-305

Faust PL, Kovacs WJ. 2014. Cholesterol biosynthesis and ER stress in peroxisome deficiency. In *Biochimie*, pp. 75-85: Elsevier Masson SAS

Fernandes KA, Harder JM, John SW, Shrager P, Libby RT. 2014. DLK-dependent signaling is important for somal but not axonal degeneration of retinal ganglion cells following axonal injury. In *Neurobiology of Disease*, pp. 108-16: Elsevier Inc.

Fernandez-Castaneda A, Arandjelovic S, Stiles TL, Schlobach RK, Mowen KA, et al. 2013. Identification of the Low Density Lipoprotein (LDL) Receptor-related Protein-1 Interactome in Central Nervous System Myelin Suggests a Role in the Clearance of Necrotic Cell Debris. In *Journal of Biological Chemistry*, pp. 4538-48

Franklin RJM, ffrench-Constant C. 2008. Remyelination in the CNS: from biology to therapy. In *Nat. Rev. Neurosci.*, pp. 839-55

Fransen M, Lismont C, Walton P. 2017. The Peroxisome-Mitochondria Connection: How and Why? In *IJMS*, pp. 1126

Fuentealba RA, Liu Q, Kanekiyo T, Zhang J, Bu G. 2009. Low Density Lipoprotein Receptor-related Protein 1 Promotes Anti-apoptotic Signaling in Neurons by Activating Akt Survival Pathway. In *Journal of Biological Chemistry*, pp. 34045-53

Gan M, Jiang P, McLean P, Kanekiyo T, Bu G. 2014. Low-Density Lipoprotein Receptor-Related Protein 1 (LRP1) Regulates the Stability and Function of GluA1 α -Amino-3-Hydroxy-5-Methyl-4-Isoxazole Propionic Acid (AMPA) Receptor in Neurons. In *PLoS ONE*, pp. e113237

Gauch J, H G. 2006. Winning the Accuracy Game Three statistical strategies—replicating, blocking and modeling—can help scientists improve accuracy and accelerate …. American Scientist

Gauthier A, Vassiliou G, Benoist F, McPherson R. 2003. Adipocyte Low Density Lipoprotein Receptor-related Protein Gene Expression and Function Is Regulated by Peroxisome Proliferator-activated Receptor γ. In *Journal of Biological Chemistry*, pp. 11945-53

Goldstein JL, DeBose-Boyd RA, Brown MS. 2006. Protein Sensors for Membrane Sterols. In *Cell*, pp. 35-46

Gootjes J, Elpeleg O, Eyskens F, Mandel H, Mitanchez D, et al. 2004. Novel Mutations in the PEX2 Gene of Four Unrelated Patients with a Peroxisome Biogenesis Disorder. In *Pediatr Res*, pp. 431-36

Han L, Shen W-J, Bittner S, Kraemer FB, Azhar S. 2017. PPARs: regulators of metabolism and as therapeutic targets in cardiovascular disease. Part I: PPAR-α. In *Future Cardiol*, pp. 259-78

Hennen E, Safina D, Haussmann U, Wörsdörfer P, Edenhofer F, et al. 2013. A LewisX Glycoprotein Screen Identifies the Low Density Lipoprotein Receptor-related Protein 1 (LRP1) as a Modulator of Oligodendrogenesis in Mice. In *Journal of Biological Chemistry*, pp. 16538-45

Hernandez M, Casaccia P. 2015. Interplay between transcriptional control and chromatin regulation in the oligodendrocyte lineage. In *Glia*, pp. 1357-75

Herz J, Clouthier DE, Hammer RE. 1992. LDL receptor-related protein internalizes and degrades uPA-PAI-1 complexes and is essential for embryo implantation. In *Cell*, pp. 411-21

Hofer DC, Pessentheiner AR, Pelzmann HJ, Schlager S, Madreiter-Sokolowski CT, et al. 2017. Critical role of the peroxisomal protein PEX16 in white adipocyte development and lipid homeostasis. In *BBA - Molecular and Cell Biology of Lipids*, pp. 358-68: The Author(s)

Kanekiyo T, Cirrito JR, Liu CC, Shinohara M, Li J, et al. 2013. Neuronal Clearance of Amyloid- by Endocytic Receptor LRP1. In *J. Neurosci.*, pp. 19276-83

Kang SH, Fukaya M, Yang JK, Rothstein JD, Bergles DE. 2010. NG2+ CNS Glial Progenitors Remain Committed to the Oligodendrocyte Lineage in Postnatal Life and following Neurodegeneration. In *Neuron*, pp. 668-81: Elsevier Inc.

Kassmann CM, Lappe-Siefke C, Baes M, Brugger B, Mildner A, et al. 2007. Axonal loss and neuroinflammation caused by peroxisome-deficient oligodendrocytes. In *Nat Genet*, pp. 969-76

Kim J, Yoon H, Basak J, Kim J. 2014. Apolipoprotein E in Synaptic Plasticity and Alzheimer's Disease: Potential Cellular and Molecular Mechanisms. In *Molecules and Cells*, pp. 767-76

Kramer-Albers EM, Gehrig-Burger K, Thiele C, Trotter J, Nave KA. 2006. Perturbed Interactions of Mutant Proteolipid Protein/DM20 with Cholesterol and Lipid Rafts in Oligodendroglia: Implications for Dysmyelination in Spastic Paraplegia. In *J. Neurosci.*, pp. 11743-52

Krause C, Rosewich H, Thanos M, Gärtner J. 2006. Identification of novel mutations in PEX2, PEX6, PEX10, PEX12, and PEX13in Zellweger spectrum patients. In *Hum. Mutat.*, pp. 1157-57

Landowski LM, Pavez M, Brown LS, Gasperini R, Taylor BV, et al. 2016. Low-density Lipoprotein Receptor-related Proteins in a Novel Mechanism of Axon Guidance and Peripheral Nerve Regeneration. In *Journal of Biological Chemistry*, pp. 1092-102

Li J-S, Yao Z-X. 2012. MicroRNA patents in demyelinating diseases: a new diagnostic and therapeutic perspective. In *Recent Pat DNA Gene Seq*, pp. 47-55

Lillis AP, Van Duyn LB, Murphy-Ullrich JE, Strickland DK. 2008. LDL Receptor-Related Protein 1: Unique Tissue-Specific Functions Revealed by Selective Gene Knockout Studies. In *Physiological Reviews*, pp. 887-918

Liu Q, Trotter J, Zhang J, Peters MM, Cheng H, et al. 2010. Neuronal LRP1 knockout in adult mice leads to impaired brain lipid metabolism and progressive, age-dependent synapse loss and neurodegeneration. In *J. Neurosci.*, pp. 17068-78

Liu Z, Hu X, Cai J, Liu B, Peng X, et al. 2007b. Induction of oligodendrocyte differentiation by Olig2 and Sox10: evidence for reciprocal interactions and dosage-dependent mechanisms. In *Dev. Biol.*, pp. 683-93

Maier O, De Jonge J, Nomden A, Hoekstra D, Baron W. 2009. Lovastatin induces the formation of abnormal myelin-like membrane sheets in primary oligodendrocytes. In *Glia*, pp. 402-13

Mantuano E, Jo M, Gonias SL, Campana WM. 2010. Low Density Lipoprotein Receptor-related Protein (LRP1) Regulates Rac1 and RhoA Reciprocally to Control Schwann Cell Adhesion and Migration. In *Journal of Biological Chemistry*, pp. 14259-66

Mao H, Lockyer P, Li L, Ballantyne CM, Patterson C, et al. 2017. Endothelial LRP1 regulates metabolic responses by acting as a co-activator of PPARγ. In *Nature Communications*, pp. 1-11: Nature Publishing Group

Martin AM, Kuhlmann C, Trossbach S, Jaeger S, Waldron E, et al. 2008. The functional role of the second NPXY motif of the LRP1 beta-chain in tissue-type plasminogen activator-mediated activation of N-methyl-D-aspartate receptors. In *J. Biol. Chem.*, pp. 12004-13

Mathews ES, Mawdsley DJ, Walker M, Hines JH, Pozzoli M, Appel B. 2014. Mutation of 3-hydroxy-3-methylglutaryl CoA synthase I reveals requirements for

isoprenoid and cholesterol synthesis in oligodendrocyte migration arrest, axon wrapping, and myelin gene expression. In *J. Neurosci.*, pp. 3402-12
May P, Bock HH, Herz J. 2003. Integration of endocytosis and signal transduction by lipoprotein receptors. In *Sci. STKE*, pp. PE12
May P, Reddy YK, Herz J. 2002. Proteolytic Processing of Low Density Lipoprotein Receptor-related Protein Mediates Regulated Release of Its Intracellular Domain. In *Journal of Biological Chemistry*, pp. 18736-43
Michalik L, Auwerx J, Berger JP, Chatterjee VK, Glass CK, et al. 2006. International Union of Pharmacology. LXI. Peroxisome proliferator-activated receptors. In *Pharmacol. Rev.*, pp. 726-41
Mignarri A, Vinciguerra C, Giorgio A, Ferdinandusse S, Waterham H, et al. 2012. Zellweger Spectrum Disorder with Mild Phenotype Caused by PEX2 Gene Mutations. In *JIMD Rep*, pp. 43-46
Mironova YA, Lenk GM, Lin J-P, Lee SJ, Twiss JL, et al. 2016. PI(3,5)P2 biosynthesis regulates oligodendrocyte differentiation by intrinsic and extrinsic mechanisms. In *Elife*, pp. 1-29
Monnerie H, Romer M, Jensen BK, Millar JS, Jordan-Sciutto KL, et al. 2017. Reduced sterol regulatory element-binding protein (SREBP) processing through site-1 protease (S1P) inhibition alters oligodendrocyte differentiation in vitro. In *J. Neurochem.*, pp. 53-67
Muratoglu SC, Mikhailenko I, Newton C, Migliorini M, Strickland DK. 2010. Low Density Lipoprotein Receptor-related Protein 1 (LRP1) Forms a Signaling Complex with Platelet-derived Growth Factor Receptor- β in Endosomes and Regulates Activation of the MAPK Pathway. In *Journal of Biological Chemistry*, pp. 14308-17
Nakajima C, Kulik A, Frotscher M, Herz J, Schäfer M, et al. 2013. LDL receptor-related protein 1 (LRP1) modulates N-methyl-D-aspartate (NMDA) receptor-dependent intracellular signaling and NMDA-induced regulation of postsynaptic protein complexes. In *Journal of Biological Chemistry*
Norrmén C, Figlia G, Lebrun-Julien F, Pereira JA, Trötzmüller M, et al. 2014. mTORC1 controls PNS myelination along the mTORC1-RXR γ -SREBP-lipid biosynthesis axis in Schwann cells. In *Cell Rep*, pp. 646-60
Orita S, Henry K, Mantuano E, Yamauchi K, De Corato A, et al. 2013. Schwann Cell LRP1 Regulates Remak Bundle Ultrastructure and Axonal Interactions to Prevent Neuropathic Pain. In *J. Neurosci.*, pp. 5590-602
Paintlia AS, Paintlia MK, Singh AK, Orak JK, Singh I. 2010. Activation of PPAR- γ and PTEN cascade participates in lovastatin-mediated accelerated differentiation of oligodendrocyte progenitor cells. In *Glia*, pp. 1669-85
Roth AD, Leisewitz AV, Jung JE, Cassina P, Barbeito L, et al. 2003. PPAR gamma activators induce growth arrest and process extension in B12 oligodendrocyte-like cells and terminal differentiation of cultured oligodendrocytes. In *J. Neurosci. Res.*, pp. 425-35
Rowitch DH, Kriegstein AR. 2010. Developmental genetics of vertebrate glial-cell specification. In *Nature*, pp. 214-22

Safina D, Schlitt F, Romeo R, Pflanzner T, Pietrzik CU, et al. 2016. Low-density lipoprotein receptor-related protein 1 is a novel modulator of radial glia stem cell proliferation, survival, and differentiation. In *Glia*, pp. 1363-80

Saher G, Brugger B, Lappe-Siefke C, Mobius W, Tozawa R-i, et al. 2005. High cholesterol level is essential for myelin membrane growth. In *Nat. Neurosci.*, pp. 468-75

Saher G, Stumpf SK. 2015. Cholesterol in myelin biogenesis and hypomyelinating disorders. In *BBA - Molecular and Cell Biology of Lipids*, pp. 1083-94: Elsevier B.V.

Saluja I, Granneman JG, Skoff RP. 2001. PPAR delta agonists stimulate oligodendrocyte differentiation in tissue culture. In *Glia*, pp. 191-204

Schüller U, Heine VM, Mao J, Kho AT, Dillon AK, et al. 2008. Acquisition of Granule Neuron Precursor Identity Is a Critical Determinant of Progenitor Cell Competence to Form Shh-Induced Medulloblastoma. In *Cancer Cell*, pp. 123-34

Simons M, Lyons DA. 2013. Axonal selection and myelin sheath generation in the central nervous system. In *Curr Opin Cell Biol*, pp. 512-19

Smolders I, Smets I, Maier O, vandeVen M, Steels P, Ameloot M. 2010. Simvastatin interferes with process outgrowth and branching of oligodendrocytes. In *J. Neurosci. Res.*, pp. 3361-75

Steinberg SJ, Dodt G, Raymond GV, Braverman NE, Moser AB, Moser HW. 2006. Peroxisome biogenesis disorders. In *Biochim. Biophys. Acta*, pp. 1733-48

Stiles TL, Dickendesher TL, Gaultier A, Fernandez-Castaneda A, Mantuano E, et al. 2013. LDL receptor-related protein-1 is a sialic-acid-independent receptor for myelin-associated glycoprotein that functions in neurite outgrowth inhibition by MAG and CNS myelin. In *Journal of Cell Science*, pp. 209-20

Tao W, Moore R, Smith ER, Xu X-X. 2016. Endocytosis and Physiology: Insights from Disabled-2 Deficient Mice. In *Front. Cell Dev. Biol.*, pp. 1311

van de Sluis B, Wijers M, Herz J. 2017. News on the molecular regulation and function of hepatic low-density lipoprotein receptor and LDLR-related protein 1. In *Current Opinion in Lipidology*, pp. 241-47

Verheijen MHG, Camargo N, Verdier V, Nadra K, de Preux Charles A-S, et al. 2009. SCAP is required for timely and proper myelin membrane synthesis. In *Proc. Natl. Acad. Sci. U.S.A.*, pp. 21383-88

Wangler MF, Chao Y-H, Bayat V, Giagtzoglou N, Shinde AB, et al. 2017. Peroxisomal biogenesis is genetically and biochemically linked to carbohydrate metabolism in Drosophila and mouse. In *PLoS Genet.*, pp. e1006825

Waterham HR, Ferdinandusse S, Wanders RJA. 2016. Human disorders of peroxisome metabolism and biogenesis. In *Biochim. Biophys. Acta*, pp. 922-33

Winters JJ, Ferguson CJ, Lenk GM, Giger-Mateeva VI, Shrager P, et al. 2011. Congenital CNS hypomyelination in the Fig4 null mouse is rescued by neuronal expression of the PI(3,5)P(2) phosphatase Fig4. In *J. Neurosci.*, pp. 17736-51

Xiang Z, Valenza M, Cui L, Leoni V, Jeong H-K, et al. 2011. Peroxisome-proliferator-activated receptor gamma coactivator 1 alpha contributes to dysmyelination

in experimental models of Huntington's disease. In *J. Neurosci.*, pp. 9544-53

Yoon C, Van Niekerk EA, Henry K, Ishikawa T, Orita S, et al. 2013. Low-density Lipoprotein Receptor-related Protein 1 (LRP1)-dependent Cell Signaling Promotes Axonal Regeneration. In *Journal of Biological Chemistry*, pp. 26557-68

Zhang Y, Chen K, Sloan SA, Bennett ML, Scholze AR, et al. 2014. An RNA-sequencing transcriptome and splicing database of glia, neurons, and vascular cells of the cerebral cortex. In *J. Neurosci.*, pp. 11929-47

Zlokovic BV, Deane R, Sagare AP, Bell RD, Winkler EA. 2008. Low-density lipoprotein receptor-related protein-1: a serial clearance homeostatic mechanism controlling Alzheimer’s amyloid β-peptide elimination from the brain. In *Sci Signal*, pp. ra15-ra15

Zuchero JB, Barres BA. 2013. Intrinsic and extrinsic control of oligodendrocyte development. In *Current Opinion in Neurobiology*, pp. 914-20: Elsevier Ltd

CHAPTER III

Additional Observations While Examining the Role of LRP1 in CNS Myelin Development and Repair

In Chapter II I showed that LRP1 promotes CNS myelin repair and development, using a combination of *in vitro* and *in vivo* strategies. Here, I summarize several pilot experiments, hanging thoughts, and experimental methods needed to facilitate follow up studies. In addition, I briefly discuss rationales, conclusions, and limitations on data interpretation. For in-depth discussion of future directions and research questions I refer to Chapter IV.

3.1 The study of myelin repair in the LPC demyelination model

3.1.1 LPC induced inflammation

Below I summarized several observations and notes for future studies. Collectively, I developed an injection protocol to generate a local myelin lesion and found that 21 DPI can be used to analyze myelin repair. I found that the pool of proliferative progenitors at the SVZ and OPCs are present in the native state and are available to assist in remyelination. Astrocytes migrate from the SVZ toward the lesion followed by a cell population I have yet to identify. Brief analyses of these dense nuclei present at the lesion site showed that they were at least in part from $GFAP^+$, $Olig2^+$, and $CD68^+$ cells.

— LPC injection post a 'find me' signal on the cell surface

Lysophosphatidylcholine (LPC) is a lipid with a dominant hydrophilic group; therefore it is positively curved to form a monolayer micelle (Thiam et al 2013). Since 1972 LPC has been used as a demyelinating reagent (Hall 1972), in which LPC specifically targets myelinating OLs but spares OPCs, astrocytes, and neurons (Blakemore & Franklin 2008, Lazzarini 2004). LPC-mediated demyelination showed

a limited amount of inflammation in the lesion, while recovery rate is age dependent (Shields et al 1999). LPC is one of the four well-characterized recruitment signals ('find-me' signal) for apoptotic cells requiring engulfment. LPC is the only lysophospholipid to induced phagocyte chemotaxis, and its release is Caspase-3 and ABCA1 dependent (Lauber et al 2003, Peter et al 2012). It has been speculated that the duration of the 'find-me' signal will affect the extent of the 'eat-me' landscape (Medina & Ravichandran 2016). Therefore, variations of immune responses and their impacts on myelin regeneration between toxic induced demyelination models need to be considered.

— **Generate local lesion with LPC**

To study remyelination under the LPC-demyelination model, a validation of the changes to the lesion over time was necessary. In our pilot study, I followed a protocol obtained from the literature by injecting 2 µl of LPC or PBS on each side of the corpus callosum. As showed in **Error! Reference source not found.**a, the PBS and LPC injection sides fused and passed the midline because of the large amount of injected liquid. Therefore, in later experiments I adjusted the injection volume to 0.5 µl of LPC or PBS on each side. This resulted in a local white matter lesion restricted to the LPC injection site (section 2.3.1).

— **Astrocytes from SVZ migrate toward lesion within seven days**

Here, I emphasize the changes of the myelin lesion indicated by FM-Green, the reactive astrogliosis indicated by anti-GFAP, and the accumulation of nuclei indicated by Hoechst dye staining (Figure 3.1a). As soon as 6 hrs post LPC injection, the FM-Green signal was absent from the lesion, and the majority of the nuclei were spared. At 1DPI, the edge of the area devoid of FM-Green is cleaner; the majority of nuclei were gone in the lesion, and there was no obvious sign of elevated astrogliosis. At 3 DPI, the FM-Green and Hoechst staining are still absent at the lesion; however, increased $GFAP^+$ cells were detected at the peri-lesion and the SVZ. At 7 DPI, migrating $GFAP^+$ cells reached the lesion site and contributed to $Hoechst^+$ signals in the lesion.

— **Nuclei accumulate at the LPC-induced lesion site**

To better describe the changes at the lesion, sections were imaged with higher magnification (Figure 3.1b). At 10 DPI, there were excessive nuclei accumulation at the area where FM-Green signal is absent, with some of these cells doubled stained with GFAP. At 14 DPI, areas where devoid of FM-Green, covered by $GFAP^+$ cells, and occupied by dense nuclei only partially overlapped. At 21 DPI dense nuclei were observed at the center of $GFAP^+$ area. At 28 DPI, the myelin lesion became harder to identify due to the dense nuclei area that showed comparable levels of FM-Green compare to control. These discrepancies indicate the limitation of using a single marker to identify the lesion/injured area.

— **Proliferative cells in the SVZ and OPCs are present in the naïve brain**

As mentioned, remyelination is carried out by nearby OPCs or proliferative neural progenitor cells that reside within the SVZ. After the lesion, these cells undergo differentiation and maturation. Staining with anti-Ki67 identified a pocket of proliferative cells in the SVZ, a finding consistent with the literature (Figure 3.1c)(Menn et al 2006). Similarly, OPCs were detected by anti-PDGFRα at the corpus callosum (**Error! Reference source not found.**d).

— **Myeloid cells are present at the LPC lesion site**

As mentioned before, other $GFAP^-$ dense nuclei were observed at the lesion at 7 DPI (**Error! Reference source not found.**a). To identify the cell types to which these nuclei belong, I used standard IHC. Of note, the extent of IHC cell labeling is sensitive to tissue fixation conditions. The shorter the brain sections were fixed the more signal could be acquired: in this case, the number of detectable $Olig2^+$ cells decreased with prolonged 4% PFA fixation (**Error! Reference source not found.**b). However, the morphology of the brain tissue was compromised with short fixation (30min). Therefore, one should take caution in quantification when comparing tissue sections prepared under different fixation conditions. At 21DPI, more $Olig2^+$ cells were observed at the LPC injection site compared to PBS (**Error! Reference source not found.**c). However, from our observation $GFAP^+$ and $Olig2^+$ cells do not

add up to the number of nuclei at the lesion site. Since LPC is a potent macrocytic signal, I hypothesized that that myeloid cells are recruited to the lesion. At 21 DPI, I identified a large population of $CD68^+$ cells at the lesion site that varied in size (**Error! Reference source not found.**d). Round and enlarged $CD68^+$ cells are likely to be activated macrophages and small cells are likely microglia. Some large $CD68^+$ cells are dual labeled with anti-Arg-1 (M2 marker), indicating the heterogeneity of the inflammation status at the lesion site.

3.1.2 **LRP1 expression at the myelin lesion**

It has been shown that the expression of *Lrp1* mRNA is elevated in MS lesions (Hendrickx et al 2013). LRP1 is selectively expressed at the rim of an active lesion, a type of lesion that was considered regenerative (Hendrickx et al 2013). To verify the expression of LRP1 in the regenerating lesion following LPC injection, I detected LRP1 protein expression by immunostaining and *Lrp1* mRNA by FISH. At 21 DPI, brain sections from *Lrp1* control ($Lrp1^{flox/flox}$) mice with a LPC lesion were stained with anti-LAMP1 (lysosome marker), anti-PMP70 (peroxisome marker), and anti-LRP1β (Figure 3.3a). I observed that LRP1 protein expression is ubiquitous in the corpus callosum including intact (non-lesioned) tissue. A slight increase of LRP1 signal intensity was observed at the lesion site and was approximately in line with the $PMP70^+$ area. Some $LRP1^+/LAMP1^+$ double labeling or $LRP1^+/LAMP1^+/PMP70^+$ triple labeled cells were observed; however, further optimization of staining and imaging conditions are required to determine cell identity. Parallel sections were probed for *Lrp1* mRNA expression and stained with the Hoechst nuclear dye (Figure 3.3b). The specificity of the FISH antisense probe was controlled with a scrambled probe, under the same hybridization conditions Figure 3.3b, insect A). I observed that the level of *Lrp1* mRNA was elevated at the lesion and is approximately aligned with the area where LRP1 protein expression was elevated (Figure 3.3a). *Lrp1* mRNA is located at the peri-nuclear area of a subset of cells at the lesion (Figure 3.3b, insect B).

To identify if the elevated *Lrp1* mRNA is within cells of the OL-lineage at the lesion, parallel sections were probed for *Lrp1*, stained with anti-Olig2 and Hoechst nuclear dye (Figure 3.4a). I observed that *Lrp1* mRNA is located at the peri-nuclear area of only a subset of $Olig2^+$ cells at the lesion (Figure 3.4**Error! Reference source not found.**a, insect A and B). The distribution of $Olig2^+$ cells and *Lrp1* mRNA showed in Figure 3.4a inset C was centralized at the lesion. To examine if the *Lrp1* mRNA expression was abolished by tamoxifen administration in *Lrp1*$^{flox/flox}$*;CAG-Cre*^{TM} mice, gene ablation was induced in *Lrp1* iKO mice as described in Chapter II (section 2.5.1) and subjected to LPC injection. At 21 DPI, brains were sectioned and probed for *Lrp1* or scramble sequence as control (Figure 3.4b). At the lesion where dense nuclei were observed, little *Lrp1* signals were detected. Suggesting a partial ablation of *Lrp1* in tamoxifen induced knockout, which is consist with biochemical data (a ~50% lost of LRP1 protein level) in Chapter II (section 2.3.1). However, clear signals were detected with both Lrp1 and scramble probes at the needle track (Figure 3.4b insect C). The specificity of these signals at the needle track was examined by cross channel imaging (Figure 3.4b, insect A and B). The red signal seems overlapped with the signal in the green channel (no fluorescent at this channel were used for staining). Suggesting that these signals at the needle track might be auto-fluorescent particles. Together, these results indicated that both LRP1 protein and *Lrp1* mRNA were elevated at the lesion, a subset of $Olig2^+$ cells express high levels of *Lrp1*, but the identity of the rest LRP1 expressing cell are yet to be defined.

3.1.3 LRP1 ablation in myeloid cells affects the size of the LPC induced white matter lesion

In Chapter II, I made use of of *Lrp1*$^{flox/flox}$*;CAG-CreER*^{TM} mice (*Lrp1* iKO) and *Lrp1*$^{flox/flox}$*;Pdgfra-CreER*^{TM} (*Lrp1* iKO^{OL}) showing that LRP1 promotes CNS myelin repair. To determine if LRP1 in phagocytic cells participate in adult white matter repair, I generated *Lrp1*$^{flox/flox}$*;LysM-Cre* (*Lrp1* cKO^{M}) mice that allow gene ablation in a subset of myeloid cells, including neutrophils and macrophages. To confirm the *Lrp1* expression is ablated in myeloid cells, the lymphocyte-enriched fraction was

obtained from blood collected from P56 *Lrp1* control and cKO^{M} mice and subjected to Western Blotting analysis. An approximately 50% decrease of LRP1 in lymphocytes was detected (Figure 3.5a and b). At P56 *Lrp1* cKO^{M} mice were subjected to unilateral injection of LPC into the corpus callosum and PBS on the contralateral side. Littermate control mice were processed in parallel. At 21 DPI, brains were collected and serially sectioned, and the extent of white matter repair was assessed as described in Chapter II (Section 2.3.1). The ratio of lesion repair was similar in *Lrp1* cKO^{M} and control mice. Interestingly however, the extent of white matter lesion demarcated by elevated *Mbp* labeling is less in *Lrp1* cKO^{M} mice compared to controls (Figure 3.5c-e). This demonstrates that Lrp1 in myeloid cells does not impact the rate of myelin recovery. However, LRP1 might participate in confining lesion area such as glia scar formation. Further experiments are required to draw conclusions from this work.

3.1.4 **Identification of the LPC-induced myelin lesion**

— **Charcoal**

To discriminate the technical variation of stereotaxic injection from the heterogeneity of lesion repair itself, I needed to develop proper ways to clearly identify lesion site, even if the repair was complete. I utilized three methods to train blinded observers how to identify the lesion site in the LPC lesion model. To ensure the serial sections captured the entire lesion without having to section the entirety of the brain, I coated the needle with charcoal before LPC or PBS injection. A trace of charcoal is physically intercalated into the injection site, allowing for visualization in the cortex, and importantly this does not impact the progression of lesion repair at the corpus callosum.

— **Cell tracer: CFSE**

Since the size of myelin lesion changes during the remyelination process, to be able to identify the initial injured area is key to reliably quantify the extent of repair. Finding a dye that is not toxic, can stably label the lesion without diffusion, with a long half-life (at least 21 days), and that can survive the debris clearing

process during demyelination was not a trivial task. I came across a cell tracer; Carboxyfluorescein succinimidyl ester (CFSE), a cell permeable fluorescent dye that was developed to trace lymphocyte proliferation that fit our criteria listed above. CFSE forms a covalent bond with intracellular lysine upon entering the cell; therefore, it remains inside the cell and does not diffuse out (Figure 3.6c). CFSE is very stable with little cell toxicity under appropriate concentrations. To determine if CFSE could label the white matter lesion, I mixed CFSE with LPC or PBS at a 1:1 ratio and injected into the corpus callosum sterotaxically (Figure 3.6a, left). When double staining with FM-Red, the intensity of the red signal was higher at the $CFSE^+$ area. This suggested that there was a bleed through from the green channel because our scope filter set was not optimized for CFSE imaging. Of note, there was a slight decrease of nuclei number ($Hoechst^+$ signal) at the $CFSE^+$ site, indicating minor cell toxicity at the given injection volume and concentration. At the CFSE/LPC injection site, $CFSE^+$ area is within the area devoid of FM-Green and FM-Red signals (Figure 3.6a, right). $CFSE^+$ area is approximately aligned with condensed nuclei area ($Hoechst^+$ signal), which is the hallmark of LPC induced myelin lesion. However, the diffusion range of CFSE seems to be narrower than LPC, as the area devoid of FM-Red or FM Green is wider (Figure 3.6b). Alternatively, it might be revealing the difference between the region of insult and the area of demyelination. One OL can myelinate one or several axons depending on the region examined. Demyelination can also happened centrifugally (cell body to sheath), centripetally (sheath to cell body), or focally (Simons et al 2014), suggesting that lesion area depends on the OL myelination geometry and the degenerative signals at the microenvironment. Collectively, lowering the CFSE concentration, imaging with a filter that can separate FM-Red and CFSE signals, and adjusting the injection speed might be able to improve the labeling.

— **Myelin genes**

Since remyelination is a process resembling myelin development, I hypothesized that by detecting the expression of genes that are elevated during OL differentiation I would be able to identify the lesion. I developed an ISH assay to

detect the myelin lesion with *Mag*, *Plp1*, and *Mbp* anti-sense (-) probes (section 2.3.1). To validate the specificity of the ISH condition on the brain tissues, I made use of *Mag* null mice ($Mag^{-/-}$) and in addition generated a *Mag* sense (+) probe as control. As indicated inFigure 3.7, no signals were detected from *Mag* (+) probe on a MAG wt tissue ($Lrp1^{flox/flox}$ in this case) or *Mag* (-) probe on a MAG null tissue ($Mag^{-/-}$) (Figure 3.7a). Under the same conditions, a strong signal was detected on the lesion side of the corpus callosum with the *Mag* (-) probe on the *Lrp1* control and *Lrp1* iKO tissues (Figure 3.7b). Suggesting that this ISH condition is sensitive to separate non-specific binding from the actual signal. Additionally, the elevated *Mag* mRNA signal was specific at the LPC lesion side but not at the PBS injection, supporting the hypothesis that lesion can be identified by OL differentiation genes. However, poor labeling of the nuclei by Hoechst dye staining after ISH assay was observed. For better immune marker co-staining at the lesion site, it might be worth to develop fluorescent-conjugated mRNA probes for wider application in the future.

3.2 LRP1 in axon-glia interaction and regional myelin diversity

In addition to the hypomyelination reported in Chapter II (section 2.3.3), a small portion of axons showed degenerative morphology when *Lrp1* was ablated specifically in OL-lineage (Figure 3.8). P21 optic nerves of *Lrp1* control and cKO^{OL} mice were prepared as described in Chapter II (section 2.5.8), ultrastructural analysis of cross- or longitudinal-sectioned nerves showed a various degree of axon deformation (Figure 3.8a and b). Local myelin sheath detachment, doubled myelination, and the collapse of mitochondria-like organelles were observed (Figure 3.8b). Interestingly, these phenotypes are very similar to $Cnp^{-/-}$, $Mag^{-/-}$, $Plp^{-/-}$, or peroxisomal defective mice (Bottelbergs et al 2010, Lazzarini 2004), in which gene deletion has a minor effect on myelin biogenesis but shows defects in axonal support. Since the *Lrp1* ablation is specific to the OL-lineage, axonal defects might be caused indirectly due to the loss of LRP1 in OLs.

To exclude that the axonal defects are due to retinal ganglia cell (RGC) death, semi-thin sections of plastic embedded retinas were prepared from P10, 21, and 56

of *Lrp1* control and cKO^{OL} mice were stained with Toluidine blue (Figure 3.9). The gross anatomical organization of retinal layers was comparable between *Lrp1* control and cKO^{OL} mice. Importantly, there were no signs of RGC death.

Myelination occurs in sequence, in the brain it happens from caudal to rostral and in spinal cord it happens from rostral to caudal (Baumann & Pham-Dinh 2001). This sequence is under strict regulation, and is highly reproducible. The timing of myelination on certain nerve tracks is also precise; therefore it can serve as a tool to measure human embryo developmental stage (Baumann & Pham-Dinh 2001). To investigate if LRP1 regulates CNS myelination in a region specific manner, myelin protein profiling from distant CNS tissues of P10 and P21 mice was performed (Figure 3.10). LRP1 is ubiquitously expressed across the olfactory bulb, cortex, thalamus, cerebellum, brain stem, spinal cord, and corpus callosum. CNP expression is absent from the olfactory bulb and cortex, and little is found at the corpus callosum. The level of CNP and MBP expression increased in the thalamus, cerebellum, brain stem, and spinal cord from P9 to P21 (Figure 3.10a and b). Interestingly, the pattern of GFAP expression was approximately the opposite of the CNP expression. High GFAP expression was observed in the olfactory bulb, cortex, and thalamus, but low at the tissues that are largely white matter (Figure 3.10b). Collectively, the myelination pattern supports the literature and corresponds to the LRP1 expression pattern, suggesting that LRP1 participates in additional cellular functions in different cell types.

3.3 **Investigate the mechanism of LRP1 in regulating myelin development**

LRP1 is a promiscuous receptor that carries out a broad range of cellular functions as briefly reviewed in Chapter I (section 1.4.3), to pin point the mechanism of LRP1 in regulating myelination is challenging. Here, I summarized several pilot studies and methods I employed to approach this question.

3.3.1 **Dissect LRP1 functional domains: RAP peptides and *Lrp1* N2 mice**

— **Extracellular domain (ECD) antagonist**

It has been shown that more than 40 ligands bind to LRP1 complement-like repeats (CI, CII, CIII, and CIV) at the extracellular domain (ECD). These bindings directly or indirectly regulate signaling pathways by triggering LRP1-mediated endocytosis or phosphorylation. To examine the requirement of the ECD-mediated signaling pathways during myelination, I made use of the potent LRP1 antagonist, RAP, as briefly described in Chapter I (section 1.4.3). Previous studies showed that at a very high dose (75 μM) GST-RAP inhibits oligodendroglial differentiation from neural stem progenitor cells (NSPCs) (Hennen et al 2013). To examine if RAP blocks primary OPC differentiation at a more physiological dose, OPCs were isolated as described in Chapter II (section 2.5.10) and cultured with GST or GST-RAP at 100nM (Figure 3.11a). After 5 days in differentiation medium (DM), OLs were stained with anti-PLP, anti-MBP, and Hoechst dye to assess the extent of OL differentiation. I observed no gross changes in the number of PLP^+ or MBP^+ cells upon RAP inhibition. It has been shown that the binding of RAP to LRP1 is pH sensitive (Prasad et al 2015), and might not be stable enough over the course of OL differentiation. To determine if a more stable version of RAP (stable-RAP) can block OL differentiation, an engineered RAP that is resistant to pH and heat inactivation was applied (Figure 3.11b) (Prasad et al 2015). After 5 days in DM, OLs were stained with anti-MBP and Hoechst dye to assess the extent of OL differentiation. There was no significant change in the number of MBP^+ cells upon wt-RAP or stable-RAP treatment (Figure 3.11c). To ensure that the RAPs I treated were bioactive, COS-7 ligand-receptor binding assay was used to assess the ligand competition effects of RAPs (Figure 3.11d). Previous study has shown that NgR^{OMNI}-Fc, CII-Fc, and CIV-Fc bind to MAG expressing COS-7 cells (Stiles et al 2013). When GST-RAP is added to the system, CII-Fc and CIV-Fc binding to MAG were attenuated but not NgR^{OMNI}-Fc (Stiles et al 2013). Similarly, when I applied tag-free RAP the CII-Fc binding to MAG was attenuated. Together, these experiments suggest that the RAPs I used were bioactive; at least enough to block ligand binding to CII domain, but had no obvious impact on OL differentiation.

— **Intracellular domain (ICD) phospho-dead mutant**

There are two phosphorylation sites at the intracellular domain (ICD) of LRP1, proximal NPxY1 and distal NPxY2 (Figure 3.12a). Previous studies showed that mutation at NPxY1 (N1) is embryonic lethal, but a mutation at NPxY2 (N2) domain is not (Reekmans et al 2009). To examine the requirement of the ICD phosphorylation at the distal NPxY2 in myelination, I made use of N2 mutant mice with NPVYATL peptide sequence mutated to AAVAATL. The N2 allele was identified with the strategy showed in Figure 3.12b and genotyping products as indicated in Figure 3.12c. The LRP1 protein expression was assessed in various tissues of P10 mice with the indicated genotypes. Surprisingly, the level of LRP1 protein was decreased in N2 mutants compared to its heterozygous control in all tissues that were tested (Figure 3.12d and h). To examine if N2 mutant allele was haploid insufficient, brain protein lysates acquired form *Lrp1*$^{n2/+}$, *Lrp1*$^{n2/n2}$, and *Lrp1*$^{+/+}$ mice were subjected to Western blot analysis and probed for LRP1 expression. As shown in Figure 3.12e, there was no obvious difference in LRP1 expression in *Lrp1*$^{n2/+}$ and *Lrp1*$^{+/+}$ mice; however, LRP1 expression in the *Lrp1*$^{n2/n2}$ mice was significantly reduced. To examine if the signaling pathways altered in *Lrp1* cKO^{OL} are similarly regulated in N2 hypomorph brains, lysates were probed with anti-SREBP2, PMP70, PEX2, p-AKT, p-S6, and Actin (Figure 3.12f and g). Preliminary results showed that SREBP2, PMP70, PEX2, p-AKT, and p-S6 are downregulated. A more detailed comparison of myelin protein profile between *Lrp1* control (W) and *Lrp1* cKO^{OL} (O2) or *Lrp1* Het (H) and *Lrp1* N2 (N2) are shown in Figure 3.12i-l at the indicated age (P10-14). Brain lysates were extracted at indicated conditions and subjected to Western blot analysis. Protein levels of Myo1D, PEX5l, PMP70, PLP, and PEX2 were compared (Figure 3.12i and j). Preliminary quantification of protein levels at comparable ages of mice showed that Myo1D and PMP70 are similarly downregulated in N2 mice reminiscent of *Lrp1* cKO^{OL} mice (Figure 3.12k and l).

To assess N2-mediated changes of proteins enriched in peroxisomes, I performed a peroxisome preparation by sucrose gradient isolation. Roman Giger carried out the pilot study (n= 1) and results are shown in Figure 3.13. I observed

that PMP70 and PEX2 are slightly enriched in the light mitochondria fraction, SREBP2 is enriched in the nuclear fraction, and PLP is detected in the myelin fraction. LRP1 is ubiquitously present in all density fractions. I observed that the levels of PMP70 trended to be down regulated in N2 mice. These preliminary results were further verified with lysates from indicated fractions. Fractions were prepared from P10-14 brains of *Lrp1* control (W), *Lrp1* cKO^{OL} (O2), *Lrp1* Het (H), and *Lrp1* N2 (N2) mice (Figure 3.13b-e). I observed a consistent down regulation of PMP70 in N2 and *Lrp1* cKO^{OL} mice in input tissue homogenate, heavy mitochondria, and light mitochondria fractions. However, the age of the mice (P10-P14) and the condition of the input tissue (fresh or freeze-thawed) were not identical. Further experiments need to be performed under strict conditions to get conclusive results.

Similarly, the protein expression profile of N2 mice at later developmental stages was assessed (Figure 3.14). Brain input and light mitochondria fractions were extracted from P19-24 *Lrp1* Het (H) and *Lrp1* N2 (N2) mice. Lysates were subjected to Western blot analysis and probed for LRP1, MAG, CNP, PLP, MBP, PMP70, PEX5l, PEX2 GFAP, GAPDH, Actin, βIIITub, Myo1D, and TSC1 (Figure 3.14a and e). Preliminary quantification showed that LRP1 and Myo1D were significantly down regulated (Figure 3.14b-d and f-h), however, myelin proteins were largely normal, the peroxisomal proteins PMP70 and PEX5l were somewhat reduced (Figure 3.14b-d), and surprisingly, TSC1 appeared to be up-regulated (Figure 3.14h) in N2 mice. At first glance, the protein expression profile appears to be dynamically regulated at different developmental stages. N2 mediated PMP70 changes seem to be most prominent from P10-P20; Myo1D changes were not obvious at P10 but more obvious at P19-24; TSC1 changes seem to be obvious before P21. Since the age of these mice (P19-P24) was not identical and was not properly controlled, further experiments under strictly controlled conditions (age, sex, genetic background) will be required to gain conclusive results.

3.3.2 **LRP1 as a LDL receptor: cholesterol metabolic pathways**

LRP1 is a member of LDL receptor family that functions in cholesterol uptake and homeostasis in peripheral cell types such as endothelial cells hepatocytes and others (van de Sluis et al 2017). To investigate if LPR1 plays a similar role in the OL-lineage, I performed transcriptomic studies using microarray. Specifically, OPCs were isolated from *Lrp1* control and cKO^{OL} pups and subjected to Mouse Gene ST2.1 Affymetrix array analysis. Gene ontology (GO) analysis identified differences in 'Regulation of Cholesterol Biosynthesis Process', 'Cellular Response to Sterol', and 'Regulation of Cholesterol Homeostasis'. Interestingly, 'Cellular Response to Cholesterol', 'Cholesterol Efflux', 'Cholesterol Import', and 'Reverse Cholesterol Transport' were not affected. This suggests that LRP1 in OL-lineage plays a different role than in other non-neural cells, regulating cholesterol synthesis, rather than transport (Figure 3.15).

Genes that were differentially regulated in the GO terms listed in Figure 3.16 were plotted and verified. The mRNA samples used for the microarray studies were of good quality (Figure 3.16a), and relative gene expression fold changes were plotted and grouped base on the GO terms (Figure 3.16b-d). To gauge if there was a compensatory effect upon LRP1 deletion, such as up regulating other LDL family members, the gene expression of the core family members was plotted (Figure 3.16e). Pex genes that are related to Pex2 and significantly regulated were blotted (Figure 3.16f). To validate the array results, the annotation and potential function of each differentially regulated gene was studied. The peroxisomal genes Pex2 and Pex5l were chosen for their potential relevance in regulating myelination. Protein lysates obtained from P56 *Lrp1* control cKO^{OL} mice were subjected to Western blotting analysis (Figure 3.16g). The level of PEX2 but not PEX5l was significantly down regulated in the brain of Lrp1 cKO^{OL} mice (Figure 3.16h and i). Collectively, these studies show that PEX2 is regulated in an *Lrp1* dependent manner, and thus, might be involved in LRP1-mediated regulation of cholesterol homeostasis during OL development.

3.3.3 **LRP1 as a transcriptional regulator: miRNA expression**

Recent studies showed that the LRP1-ICD could translocate to the nucleus to regulate gene expression. In addition, we found that a miRNA was significantly regulated in *Lrp1*$^{-/-}$ OPCs (Figure 3.17). This prompted us to investigate the role of LRP1 as a transcription regulator. All miRNA species that were differentially regulated in *Lrp1*$^{-/-}$ OPCs were plotted in Figure 3.17a and the selected miRNAs with annotation were plotted in Figure 3.17b. Genes of interests that can be transcriptionally regulated by each miRNAs were listed in Figure 3.17c. To validate the changes in miRNA levels, a miRNA qRT-PCR assay was performed (FigureA.17d). Because it has been shown previously that miRNA-155 and miRNA-219 regulate OL development (Dugas et al 2010, Zhao et al 2010), I used them as a positive control to gauge if the changes of miR-16, 19, 20, and 33 were specific to *Lrp1*$^{-/-}$ OPCs. Results showed that a minor strand of miRNA-33, mir33a-3p*, is significantly down regulated (Figure 3.17d). Interestingly, miR-33 is highly expressed in the brain, resides at the intron of *Srebf2* genome, and is down regulated in the liver when mice are fed with high-fat diet (HFD) (Rayner et al 2010). In Affymetrix analysis, miR33 was upregulated in *Lrp1*$^{-/-}$ OPCs but in qRT-PCR assay it was downregulated. This can be explained by the sequences used in each assay for miR33 detection. In Affymetrix, the gene annotation of miR33 is less specific, it might include pri-miRNA, pre-miRNA, and mature miRNA. qRT-PCR on the other hand detects only mature miRNA species. An illustration briefly summarizes the synthesis, maturation, and activation pathways of miRNAs (Figure 3.17e). Since the half-life time of miRNA can be hours to days, this might explain some of the differences between the age of samples.

3.3.4 LRP1 as a novel regulator of organelle trafficking: Myo1D and peroxisome distribution

— **LRP1 regulates Myo1D**

To investigate the role of LRP1 at later OL developmental stages, differentiating OLs ($O4^+$ cells) were prepared from *Lrp1* control and cKO^{OL} pups and subjected to Mouse Gene ST2.1 Affymetrix array analysis (Figure 3.18a). Genes that

were differentially regulated were plotted as relative expression level (Figure 3.18b) and relative fold-change (Figure 3.18c). Genes that were regulated in the same direction as *Lrp1* are highlighted. The annotation and fold-change of each gene are listed in Figure 3.18d. To validate the RNA array results, mRNA was prepared in the same way as the samples submitted for array analysis, and semi-quantitative RT-PCR analysis was performed (Figure 3.18e). Myo1d was significantly downregulated, which is consistent with the array data. To assess if the changes in Myo1d mRNA are also seen at the protein level, OLs and brain lysates were subjected to Western blot analysis (Figure 3.18f and g). Myo1D protein expression was down regulated in both *Lrp1*$^{-/-}$ OPCs and P56 *Lrp1* cKO^{OL} brain tissue. Interestingly, Myo1D expression is dramatically increased during myelination (Yamazaki et al 2014), functionally associated with membrane trafficking *in vivo* (Yamazaki et al 2017), and influences myelination and remyelination when down regulated by siRNA in mice (Yamazaki et al 2018, Yamazaki et al 2016).

Together, these observations suggest that LRP1 regulates *Myo1d* transcriptionally and at the protein level. Further studies are required to answer if this regulation is due to a direct role of *Lrp1* in regulating the *Myo1d* promoter or indirectly through other signaling pathways. For pathway analysis, genes that are differentially regulated were subjected to GO analysis (Figure 3.19). Significant GO terms associated with 'Biological-Process', 'Cellular Component', and 'Molecular Function' were listed in Figure 3.19a. For future data mining, genes that are differentially regulated are listed in Table 3.1. The key words from literature search for the potential link of each gene and myelination/OL development were noted in Figure 3.19b.

— **Study LRP1 and peroxisome subcellular localization**

Because the peroxisome distribution is altered in *Lrp1*$^{-/-}$ OLs as described in Chapter II (section 2.3.7), I further investigated if LRP1 regulates peroxisome subcellular localization through physical contact. A pilot study was performed by immunostaining. I hypothesized that if LRP1 is forming physical contact with

peroxisomes, LRP1 and PMP70 signals should be closely associated. OPCs were isolated from *Lrp1* control pups, cultured in differentiation medium for 5 days, and OLs were then stained with anti-LRP1, anti-LAMP1, anti-PMP70, and Hoechst dye (Figure 3.20a). Preliminary results showed that LRP1 is closely associated with peroxisomes and lysosomes. A Z-stacked image in Figure 3.20b shows that the LRP1 signal (green) always co-localizes with the PMP70 signal (Red) additional controls are needed to confirm this initial observation. Of note, there might be cross-reaction between Alexa488 conjugated anti-LRP1 and rabbit anti-PMP70, as both antibodies were raised in rabbit. Alexa488 conjugation might not completely block the Fc epitope for rabbit anti-Fc secondary antibody.

LRP1 expression decreases during OL differentiation, higher LPR1 levels were detected in OPCs compared to OLs, which is consist with the biochemistry results reported in Chapter II (Figure 2.1). The extent of LRP1 and peroxisome co-localization was analyzed by ImageJ to calculate the Pearson's coefficient. Based on morphology, immature OPCs and mature MBP+ OLs from *Lrp1* control or cKO^{OL} pups were analyzed separately. OPC/OLs were stained with anti-LRP1 and anti-PMP70 in each condition (Figure 3.21a). Pearson's coefficient plot of each representative cells are shown in Figure 3.20b. LRP1 and PMP70 signals were more closely associated in the MBP- stage of OPCs that were prepared from Lrp1 control pups (Figure 3.21b, middle panel). However, this pilot experiment was performed by crude cell categorization based on experience of cell morphology. Therefore, future studies are required in which co-staining with different OL stage markers is used to ensure proper comparison.

Similarly, LRP1 and peroxisome co-localization was observed in astrocytes ($GFAP^+$), fibroblasts, and neurons ($\beta IIITub^+$) (Figure 3.22a). The cells of each category were quantified and the averaged Pearson's r scores were plotted in Figure 3.22b. Since Pearson's r score does not follow a normal distribution ($-1< r <1$), a z-transformation is required before statistical comparison (Figure 3.22c). After the data transformation, the Z score can be compared by a simple Student's t-test. I

observed that the LRP1 and PMP70 signal association is closer in OPCs than in other cell types (Figure 3.22d). This suggests that LRP1 in OPCs has a more intimate role with peroxisomes than in the other cell types. However, as mentioned before, additional controls are required to draw a solid conclusion.

As a principle for single cell analysis, step-wise image processing flow is laid out inFigure 3.23. Raw data of the images under each channel were served as input. However, if the intensity of each non-altered pixel is below the detection limit of our eyes, prepare a histogram-applied image (merged channel in this case) is required in parallel when processing the image (Figure 3.23a). Depending on the noise of the cell staining, a crude area containing a single cell needs to be identified by eye (Figure 3.23b, step1). After clearing the background (Figure 3.23b, step2 and 3), cell silhouette can be determined by threshold setting (Figure 3.23b, step4 and 5), and then the fine cell selection can be applied to the raw data (Figure 3.23b, step 6-9). Depending on the question one asks, the sub-regional analysis can be done (Figure 3.23b, step 10-12).

3.4 **Materials and Methods**

3.4.1 **Mice**

All animal handling and surgical procedures were performed in compliance with local and national animal care guidelines and were approved by the Institutional Animal Care and Use Committee (IACUC). *Lrp1*$^{flox/flox}$ mice were obtained from Steven Gonias (Stiles et al 2013) and crossed with *Olig2-Cre* (Schüller et al 2008), *CAG-CreER*^{TM} (Jackson Laboratories, #004682), *LysM-Cre* (Jackson Laboratories, #004781). *Lrp1*$^{n2/n2}$ mice were kindly provided by Claus Pietrzik (Roebroek et al 2006). *Mag*$^{-/-}$ mice were obtained from Jackson Laboratories (Li et al 1994). Mice were kept on a mixed background of C57BL/6J and 129SV. Throughout the study, male and female littermate animals were used. *Lrp1* 'control' mice harbor at least one functional *Lrp1* allele. Any of the following genotypes *Lrp1*$^{n2/+}$, *Lrp1*$^{+/+}$, *Lrp1*$^{+/flox}$, *Lrp1*$^{flox/flox}$, or *Lrp1*$^{flox/+}$;*Cre*$^{+}$ served as *Lrp1* controls.

3.4.2 **Genotyping**

The methods of tail biopsies to collect genomic DNA (gDNA), PCR condition, and Lrp1 floxed alleles or Cre alleles amplification protocol are described in Chapter II (section 2.5.2). *Lrp1* wt and n2 alleles were amplified with the forward primer [N2F] 5'- GTT CCC TCC ATG CCC TGA CA-3' and [N2R] 5'- GGA GCC TGC CGG AGT GAG A-3'. The wt allele yields a 577 bp product and the n2 allele yields a 487 bp product.

3.4.3 **Quantitative reverse transcription (qRT)-PCR**

For mRNA qRT-PCR, total RNA was isolated from OPCs or OLs of *Lrp1* control and *Lrp1* cKO^{OL} mice using TRIzol (Thermo Fisher, 15596026). cDNA was synthesized by using Olig-dT primers in SuperScript™ III First-Strand Synthesis System (Thermo Fisher, 18080051) following manufacturer's instructions. Relative gene expression was detected by pre-designed primers from qPrimerDepot website and listed as follows:

Forward Primer	Sequence	Reverse Primer	Sequence
A1_Frmd4a_93F	TAGCAGCTCCAGCTTCCTGT	**A2_Frmd4a_93R**	ATGGAAGGGCTCCTATCTCC
B1_Cntn6_104F	CCACGTTCGAAGGTCAAAA	**B2_Cntn6_104R**	AGATCCCGAGACATTTCCCT
C1_Myo1d_91F	CCGATGAATGTGTAGATGCG	**C2_Myo1d_91R**	ACTTCGTGCTGATGGACACC
D3_Fgd4_136F	TCCTCCCATTTATTCCCTGA	**D4_Fgd4_136R**	TGTTCTCCAGCCATTTGTGA
E1_Flrt2_93F	GAAAGTCAGGCCAGTGGAGA	**E2_Flrt2_93R**	TGGATTCGGATGAGCTAAGG
F5_Zfp36l2_101F	GAGGTTTGCCAGGGATTTCT	**F6_Zfp36l2_101R**	TTTCGACCATTACAGGACCC
G3_Lrp1_143F	GTCCAGCAGAGTGACACAGG	**G4_Lrp1_143R**	CCATCAACATCTCCCTCAGC
GAPDH_F	AACTTTGGCATTGTGGAAGG	**GAPDH_R**	GGATGCAGGGATGATGTTCT

For qRT-PCR reaction, SYBR™ Green PCR Master Mix (Thermo Fisher, 4309155) was used and signals were detected by a StepOne Real-Time PCR system (Applied Biosystems).

For miRNA qRT-PCR, miRNA was isolated from OPCs of *Lrp1* control and *Lrp1* cKO^{OL} by using mirVana™ miRNA Isolation Kit (Thermo Fisher, AM1560). miRNA reverse transcription was carried out by using TaqMan™ MicroRNA Reverse Transcription Kit (Thermo Fisher, 4366596) following manufacturer's instructions. Relative miRNA expression was determined by predesigned TaqMan miRAN assays, hsa-miR-33a* (CAA UGU UUC CAC AGU GCA UCA C, 002136), hsa-miR-19b-1* (AGU UUU GCA GGU UUG CAU CCA GC, 002425), mmu-miR-155 (UUA AUG CUA AUU GUG

AUA GGG GU, 002571), hsa-miR-219-2-3p (AGA AUU GUG GCU GGA CAU CUG U, 002390), snoRNA202 (GCT GTA CTG ACT TGA TGA AAG TAC TTT TGA ACC CTT TTC CAT CTG ATG, 001232). For qRT-PCR reaction, TaqMan™ Universal Master Mix II with UNG (Thermo Fisher, 4440038) was used and signals were detected by a StepOne Real-Time PCR system (Applied Biosystems).

3.4.4 **COS-7 cells binding assay**

COS-7 cells were plated in a poly-D-lysine (PDL) coated 24-well plates and transfected by lipofectamine 2000 (Thermo Fisher, 11668027) with plasmid DNA encoding MAG and/or GFP. Ligand-receptor binding assay carried out by following previously established method (Venkatesh et al., 2005)(Stiles 2013). Briefly, AP-conjugated anti-human Fc was pre-incubated with Fc, NgR^{OMNI}-Fc, CII-Fc, or CIV-Fc fusion proteins in a 1:2 ratio. Antibody/protein complex was added to COS-7 cells for 75 min then rinse with opti-MEM to remove unbound complex. Cells were fixed with 1% formaldehyde (1% formaldehyde, 60% acetone, and 20 mM HEPES, pH 7.0), rinsed with HBHA, and heated inactivate at 65°C in HEPES-buffered saline (HBS) for 90 min. Binding was visualized by developing AP reaction with NBT/BCIP substrate. The reaction was terminated by PBS rinsing. For competitive binding experiments, GST, GST-RAP, wt-RAP, or stable-RAP were added into the 75min cell incubation step together with antibody/protein complex.

3.4.5 **Histochemistry**

The methods are as described previously in Chapter II (section 2.5.4).

3.4.6 **In situ hybridization**

General ISH protocol is described previously in Chapter II (section 2.5.5). Method of fluorescent in situ hybridization (FISH) for tissue section is briefly described as follow. The mixture of probes is designed base on the instruction of the Biosearch Technologies Stellaris RNA FISH website. Oligos pellets obtained from the company are dissolved in 200µl TE (10mM Tris-HCl pH8.0, 1mM EDTA) buffer to final concetration of 25µM. Tissue sections mounted on microscope slides were

brought to RT, rinsed 3 times for 5 min each in PBS, and incubated for 10min with 0.2M HCl. Sections were then permeabilized in 1% Triton-x-100/PBS for 2 min. Sections were then rinsed 2 times for 1 min each in PBS, followed by incubation with 2x SSC/10%formamide for 10min. Probes were diluted to 1:100 in preheated (60°C) hybridization buffer (10% Dextran Sulfate, 1mg/mL E. Coli tRNA, 2mM Vanadyl Ribonucleosides, 200ug/mL BSA, 2X SSC, 10% Formamide, and Blocking buffer) then applied to sections, covered with parafilm, and incubated at 37°C overnight in a humidified and sealed container. The next morning slides were rinsed in 2X SSC/10% formamide for 30 min at 37°C, 2X SSC, and incubated in 1% Triton-x-100/PBS. Secondary antibody was prepared in 0.3% triton-x-100/0.1X blocking buffer and incubated for 60min at RT. Sections were then rinsed with 3 times in PBS, 1 time in DEPC, then let dry, mount, and imaging within 2 days. Probes sequences are as follow:

Sequences	Scramble probes	Lrp1 probes
1	GTCAGCACCTTCCATGCACC	CCTGATGGAGCACTAGGG
2	ACCTACTTGGGAGTAAGTGC	ATGGGGGTGCCTTGGTAG
3	ACCTCGGCACCATCTACCCT	CGCCTCTGGCTGCAAAAA
4	TCGTACTTCTGTGGGAATAG	AGGGCGAAGCTCACAGCC
5	TTTACCCGTCGAGACGTCAA	TTCACCCCTGCTTTACTC
6	ACATGTTCGAGACAAGCCCT	CTGCCCCCAAATTCGAAC
7	CTCTTTTCTAGCCGTCAAGT	TGGGAAGGGCCTGCTGAC
8	TCTTGCGCGCGAAAAAGACA	ATGGTACAGTTCCGAGCC
9	TGCACCGTGAATGAGGGTTT	AACCAGGGGCATAGGTGA
10	GCTTCATGTTCCGGGCAAAG	CCTTTCCTTAAGCAAAGC
11	ACCGACTGCACGGTTAAGGA	CCGACTCTTCTATTCTTA
12	CCGAACAGACCACGTACCTT	CCCCTTTATCTTCCTCTC
13	CCTTCCAGCTGCCCATTTTT	CTCTGGTCCTGTTACTTC
14	TTTCTTGCCCAAAAGACCTC	GCCGATGCAAACAGCAGC
15	CTTGAACTGCAGATGCCGCT	CGGGGTCAGCATGGTGTG
16	AAGCGTCTTCCATGCACCAA	CCGGAGACCAGAGCTGAA
17	ACCAACCGGGCCTGGTTCAA	TTGGATGATGGTCTGCCG
18	CGTCAAGTTTCGTCTACCCT	GTGACGACCTGGTACTCA
19	TACCCGTGCAGACCACGTCA	CATCTGTGTCCAACACCT
20	ATCGACATGTTGGGAGTAAG	TTGGCACAGTAGCTCTGG
21	TAGCCCTGAAGACCTCGGCA	AGATGTTGCCTGCAATCC
22	AGCCTTTTTGTGGGAATAGG	GATGGCATCTGACCTAGC
23	TCCGCGCGAGAAAACTACTT	TTGATTGTGTGGTTCCCA
24	TCTACACGCTCTTTTGGTTT	GCGTGAGTTCTGTCACTC
25	GCTTCATCCGGGCAAGAAAA	CCATTGTTACACTGGCGG
26	TGCACCGTGACTACCTTCCA	
27	TTCCACCGAACAGACCACGT	
28	TCGCGACTGCACGGTTACAA	
29	TTGAACTGCAGAGCCCAAAA	
30	GTTGCGCTGCCATTTTTTCT	

3.4.7 **Immunostaining**

Methods were described previously in Chapter II (section 2.5.7). The following primary antibodies were used: rabbit anti-GFAP (Dako, Nr. A 0334, 1:2000), rabbit anti-ki67 (Abcam, ab15580, 1:1000), rat anti-PDGFRα (BD Pharmingen, 558774, 1:500), rabbit anti-Olig2 (Millipore, AB9610, 1:500), rabbit anti-CD68 (Abcam, ab125212, 1:500), goat anti-Arg-1 (Santa Cruz, M-20, sc-18355, 1:250), rabbit anti-PMP70 (Thermo, PA1-650, 1:1000), rat anti-LAMP1 (Abcam, ab25245, 1:500). For myelin staining, sections were incubated in Fluoromyelin-Green or Red (Life technologies, F34651 or F34652, 1:200) reagent for 15 min.

3.4.8 **Transmission electron microscopy (TEM)**

Tissue preparation and image acquisition for semi-thin (0.5 μm) and ultra-thin (75 nm) sections were carried out as described previously in Chapter II (section 2.5.8).

3.4.9 **OPC/OL primary cultures and drug treatment**

OPCs isolation, culture, and drug/peptides treatment were carried out as descried previously in Chapter II (section 2.5.10). GST, RAP, wt-RAP, stable-RAP of indicated concentration were added with differentiation medium to culture every 2 days.

3.4.10 **Western blot analysis**

Protein lysates were analysis as described previously in Chapter II (section 2.5.12). Methods of peroxisome preparation by sucrose gradient are briefly described as follow. Tissue was homogenized in 5ml 0.85M sucrose buffer, overlaid with 5ml 0.25M sucrose buffer, and spawn for 1hr at 25,000rpm SW41. Myelin interphase was removed, and 0.85M sucrose phase was adjusted to 0.25M sucrose with 0.1 mM EDTA and 3mM imidazole-containing water, mixture was spawn for 8 min at 483g, and the nuclear fraction was recovered from the pellet. The supernatant was spawn for 12 min at 12096g, and the heavy mitochondria fraction was recovered from the pellet. The supernatant was spawn for 24 min at 39191g, and the light mitochondria fraction was recovered from the pellet. Primary

antibodies included: rabbit anti-LRP1β 85 kDa (Abcam, ab92544, United Kingdom, 1:2000), mouse anti-βIII tubulin (Promega, G7121, 1:5000), mouse anti-β-actin (Sigma, AC-15 A5441, 1:5000), rat anti-MBP (Millipore, MAB386, 1:1000), rabbit anti-MAG (homemade serum, 1:1000), rabbit anti-PLP (Abcam, ab28486, 1:1000), rat anti-PLP/DM20 (Wendy Macklin AA3 hybridoma, 1:500) rabbit anti-Olig2 (Millipore, AB9610, 1:1000), mouse anti-GFAP (Sigma, G3893, 1:1000), mouse anti-CNPase (Abcam, ab6319, 1:1000), rabbit anti-PXMP3 (PEX2) (One world lab, AP9179c, San Diego, CA, 1:250), and rabbit anti-SREBP2 (One world lab, 7855, 1:500), rabbit anti-pAKT (S473, Cell signaling, 4060S, 1:1000), rabbit anti-p-S6 (Cell signaling, 4856S, 1:500), rabbit anti-Myo1D (Assay biotech ,C16783, 1:500), rabbit anti-TSC1 (Cell signaling, 6935S, 1:1000).

3.4.11 **Microarray and gene ontology analysis**

OPCs and OLs were isolated by immunopanning with anti-PDGFRα and anti-O4 as described previously in Chapter II (section 2.5.10). To compare *Lrp1* control and cKO^{OL} RNA expression profiles, the Mouse Gene ST2.1 Affymetrix array was used. Differentially expressed genes, with a p-value<0.05 set as a cutoff, were subjected to gene ontology (GO) analysis. Go terms were quarried from Mouse Genome Informatics (MGI) GO browser or Gene Ontology Consortium. The fold enrichment was calculated by dividing the number of genes associated with the GO term in our list by the number of genes associated with the GO term in the database.

3.4.12 **Image and statistical analysis**

I apply the same criteria as described in Chapter II (section 2.5.15). For image processing and quantification, ImageJ 1.47 v software was used for threshold setting, annotation, and quantification. For single-cell LRP1 and PMP70 colocalization analysis, an ImageJ plugin named, JACoP, was used (Bolte & Cordelières 2006). The Pearson's r score were transformed to z score following by online calculator: http://onlinestatbook.com/calculators/fisher_z.html before using student's t-test for statistic comparison (Fisher 1915).

3.5 Acknowledgements

I thank Claus Pietrzik for providing *Lrp1*$^{n2/n2}$ mice. I thank Benjamin Segal and David Giles for providing CFSE reagents. I thank Dudley Strickland and Joni Prasad for wt-RAP and stable-RAP peptide. I thank Wei-Chin Ho and Ye Li for bioinformatics and image processing consulting.

3.6 Author contributions

Jing-Ping Lin and Roman Giger designed research. Jing-Ping Lin, Samir Nath, and Roman Giger performed research. Jing-Ping Lin and Samir Nath analyzed data. Ashley Kalinski for FISH protocol and suggestions.

3.7 **Figures**

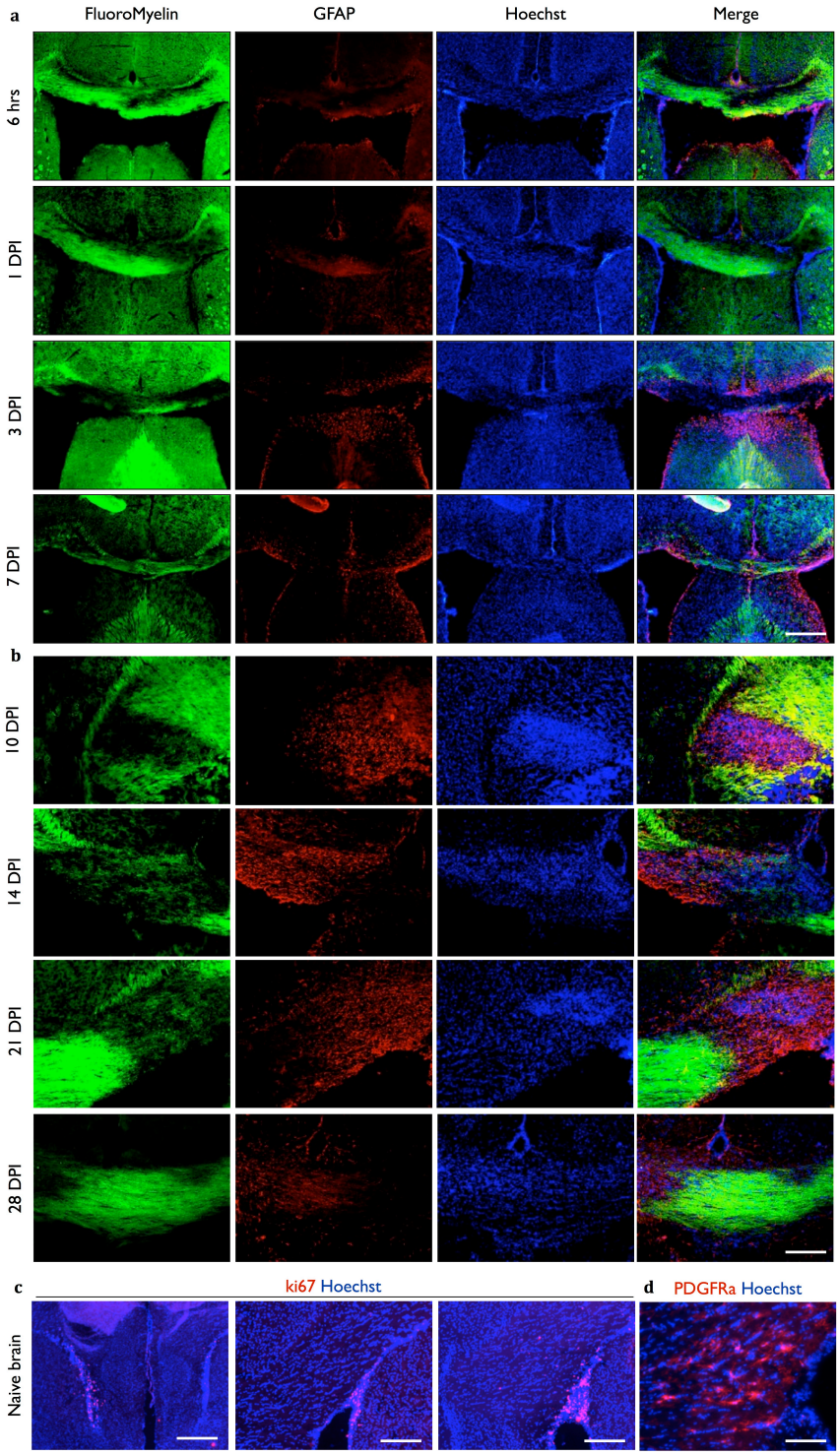
a
FluoroMyelin
GFAP
Hoechst
Merge
6 hrs
1 DPI
3 DPI
7 DPI
b
10 DPI
14 DPI
21 DPI
28 DPI
c
ki67 Hoechst
Naive brain
d
PDGFRa Hoechst

Figure 3.1: LPC induced demyelination, astrogliosis, accumulation of nuclei overtime within the lesion area in the corpus callosum

(a) Coronal forebrain sections of adult WT mice. Mice are subjected to stereotaxic injection of 2µl 1% LPC into the corpus callosum. At the indicated time points post injection of LPC, brains were collected, serially sectioned, and stained with FM Green, anti-GFAP, and Hoechst dye33342. The white matter lesion is identified by the absence of FM-Green labeling, and the $GFAP^+$ cells migrate toward the lesion site. DPI, days post-injection. Scale bar= 500µm. (b) At the indicated time point, brains were collected, serially sectioned, and stained with FM-Green, anti-GFAP and Hoechst dye33342. Dense nuclei and $GFAP^+$ cells accumulated in the LPC injected lesion site at the indicated time point. Differential distribution of $GFAP^+$ area, Hoechst+ accumulated area, and FM-Green devoid area was shown. Scale bar= 200µm. (c) Coronal forebrain sections of adult WT mice stained with anti-Ki67, and Hoechst dye33342. Stained sections are imaged with 4x (left panel), 10x (middle panel), and 20x (right panel) were showed. $Ki67^+$ proliferating cells were identified in the subventricular zone. Scale bar=500 (left), 200 (middle), 100 (right) µm. (d) Coronal forebrain sections of adult naïve mice stained with anti-Pdgfrα and Hoechst dye33342. The pool of $Pdgfr\alpha^+$ OPCs was identified at the corpus callosum. Scale bar= 100µm.

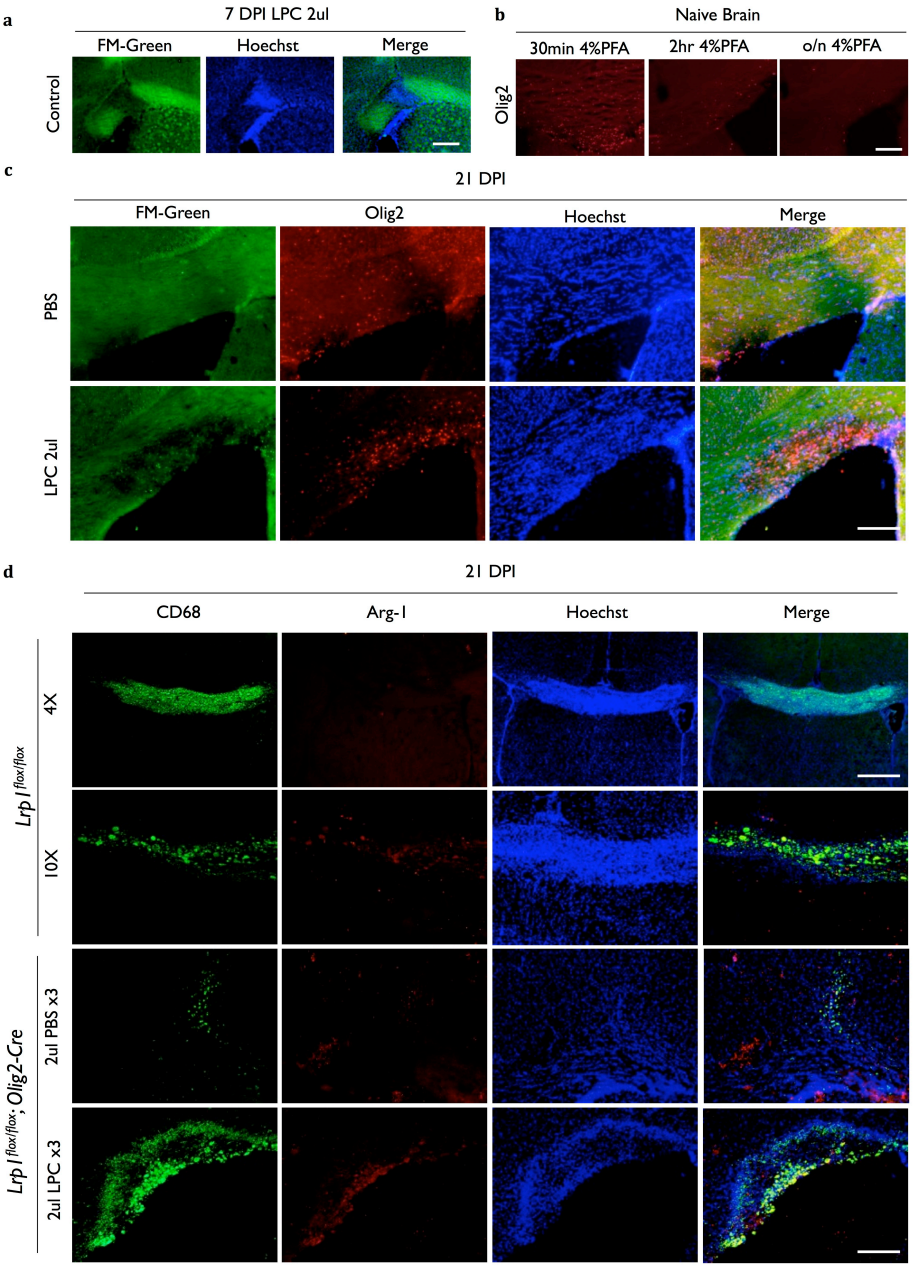
a
7 DPI LPC 2ul
FM-Green
Hoechst
Merge
Control
b
Naive Brain
30min 4%PFA
2hr 4%PFA
o/n 4%PFA
Olig2
c
21 DPI
FM-Green
Olig2
Hoechst
Merge
PBS
LPC 2ul
d
21 DPI
CD68
Arg-1
Hoechst
Merge
Lrp1flox/flox
4X
10X
Lrp1flox/flox; Olig2-Cre
2ul PBS x3
2ul LPC x3

Figure 3.2: LPC induced white matter lesion leads to accumulation of CD68+ myeloid cells and cells in the OL-lineage.
(a) Coronal forebrain sections of adult WT mice. Mice are subjected to stereotaxic injection of 2µl 1% LPC into the corpus callosum. At 7 days post-injection (DPI) of LPC, elevated nuclei staining were observed at the area devoid of FM-Green staining. Scale bar= 200µm. (b) Coronal forebrain sections of adult WT naïve mice with indicated 4% PFA post-fixation duration stained with anti-Olig2 (OL-lineage). Scale bar= 200µm. (c) Coronal forebrain sections of adult WT mice. At 21 DPI of LPC or PBS, brains were collected, serially sectioned, and stained with FM Green, anti-Olig2, and Hoechst dye33342. Elevated Olig2+ cells were observed at the area devoid of FM-Green staining. Scale bar= 200µm. (d) Coronal forebrain sections of adult *Lrp1*$^{flox/flox}$ and *Lrp1*$^{flox/flox}$;*Olig2-Cre* mice. Mice are subjected to stereotaxic injection of 2µl 1% LPC or PBS into the corpus callosum. At 21 DPI of LPC, brains were collected, serially sectioned, and stained with anti-CD68 (myeloid cells), anti-Arg-1 (M2 myeloid cells), and Hoechst dye33342. Elevated CD68^{+} and Arg-1^{+} staining were identified at LPC induced lesion site compare to PBS injection. Scale bar= 500 (upper panel) and 200 (the rest of the panel) µm.

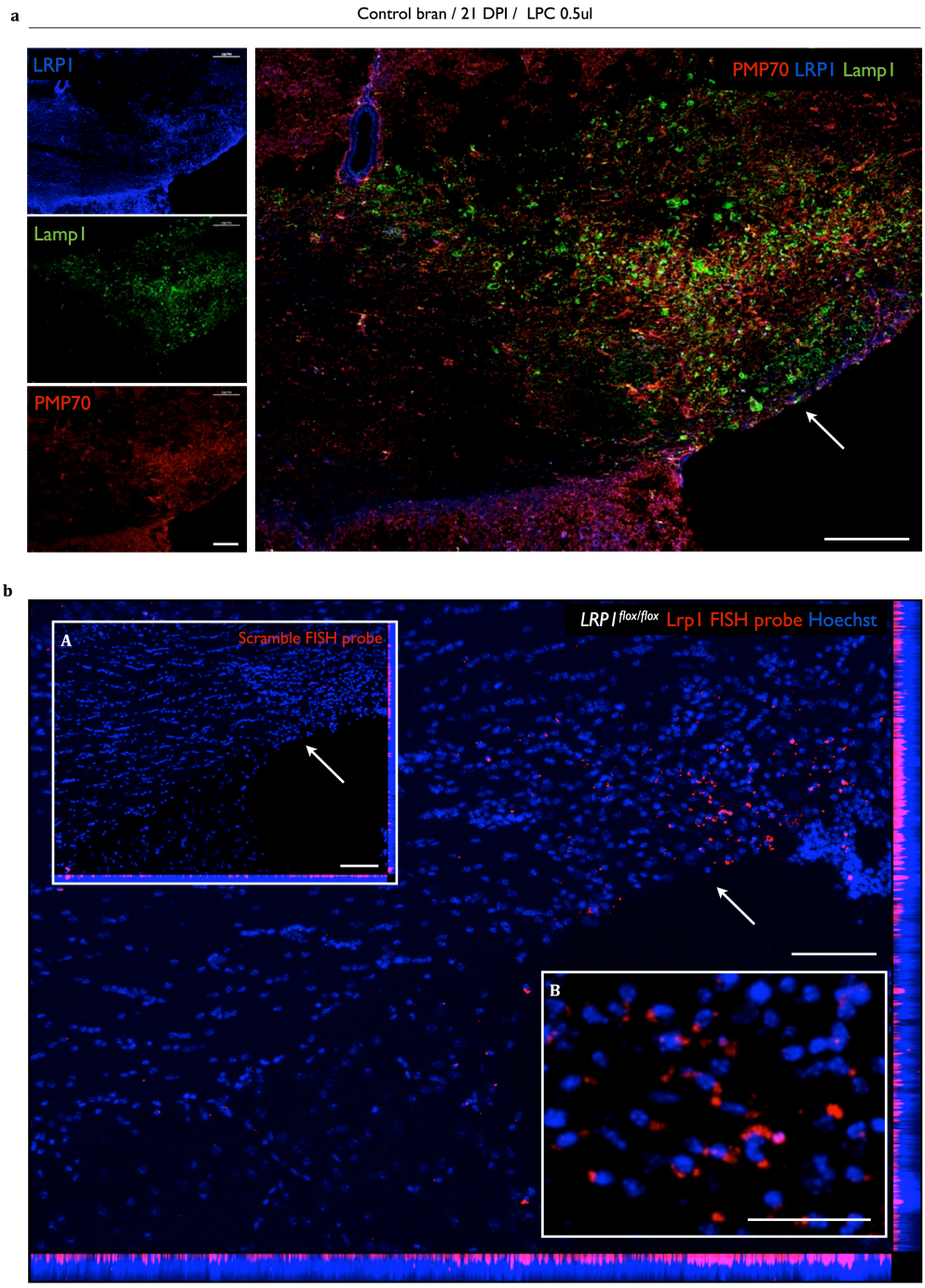
a
Control bran / 21 DPI / LPC 0.5ul
LRP1
Lamp1
PMP70
PMP70 LRP1 Lamp1
b
LRP1 flox/flox Lrp1 FISH probe Hoechst
A
Scramble FISH probe
B

Figure 3.3: Elevated LRP1 protein and mRNA expression are observed in the LPC induced white matter lesion

(a) Coronal forebrain sections of adult control mice. Mice are subjected to stereotaxic injection of 0.5µl 1% LPC into the corpus callosum. At 21 DPI of LPC, brains were collected, serially sectioned, and stained with anti-LRP1, anti-LAMP1 (lysosome), and anti-PMP70 (peroxisome). Elevated LRP1, LAMP1, and PMP70 immunostaining signals were detected at the lesion area. Scale bar= 100µm. (b) Coronal forebrain sections of adult *Lrp1*$^{flox/flox}$ mice. Mice are subjected to stereotaxic injection of 0.5µl 1% LPC into the corpus callosum. At 21 DPI of LPC, brains were collected, serially sectioned, and probed for *Lrp1* by fluorescent *in situ* hybridization (FISH) and stained with Hoechst dye33342. Inset A, the specificity of the FISH signal was controlled by scramble FISH probe generated against random sequences. Scale bar= 100µm. Insect B, enlarged image from the lesion site. Elevated *Lrp1* probe signals were identified at the peri-nucleus. Scale bar= 20µm.

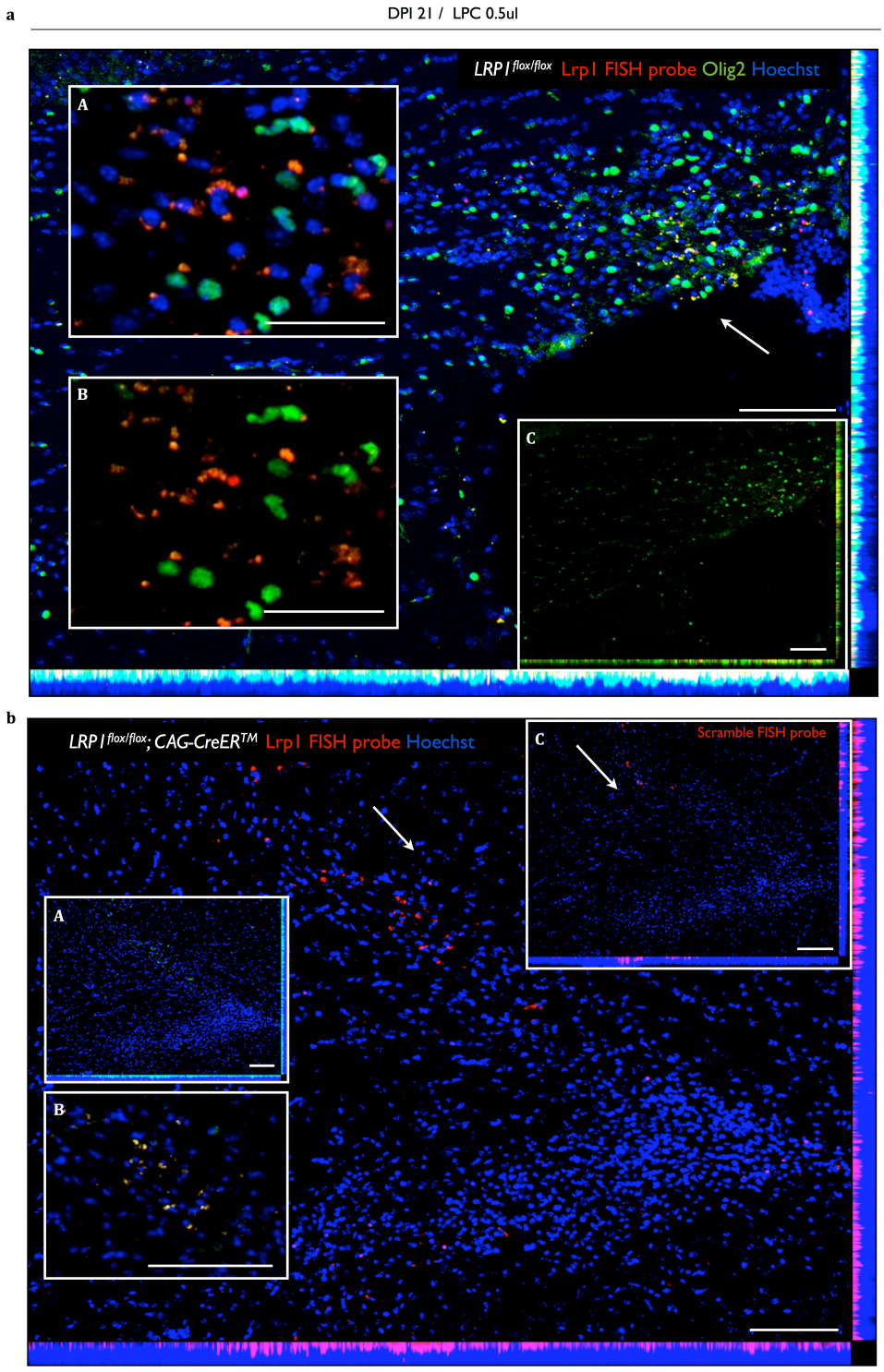
a
DPI 21 / LPC 0.5ul
LRP1 flox/flox Lrp1 FISH probe Olig2 Hoechst
A
B
C
b
LRP1 flox/flox; CAG-CreER™ Lrp1 FISH probe Hoechst
C
Scramble FISH probe
A
B

Figure 3.4: Elevated Lrp1 mRNA is detected in a subset of cells in the OL-lineage.

(a) Coronal forebrain sections of adult *Lrp1*$^{flox/flox}$ mice. Mice are subjected to stereotaxic injection of 0.5µl 1% LPC into the corpus callosum. At 21 DPI of LPC, brains were collected, serially sectioned, and probed for *Lrp1* by FISH and stained with anti-Olig2 and Hoechst dye33342. Scale bar= 100µm. Insect A and B, enlarged image from the lesion site. Elevated *Lrp1* signals were identified at the peri-nucleus of both Olig2^{+} and Olig2^{-} cells. Scale bar= 20µm. Inset C, brains section probed for *Lrp1* by FISH and stained with anti-Olig2. Scale bar= 100µm. (b) Coronal forebrain sections of adult *Lrp1*$^{flox/flox}$*;CAG-CreER*^{TM} mice. *Lrp1* deletion was induced by tamoxifen injection. Mice are subjected to stereotaxic injection of 0.5µl 1% LPC into the corpus callosum. At 21 DPI of LPC, brains were collected, serially sectioned, and probed for *Lrp1* by FISH and stained with Hoechst dye33342. Scale bar= 100µm. Insect A and B, image signal specificity was controlled by imaging on the GFP channel (A) and merged with Cy-5 channel (B) of the lesion site Scale bar= 100µm. Insect C, the specificity of the FISH signal was controlled by scramble FISH probe generated against random sequences. Scale bar= 100µm.

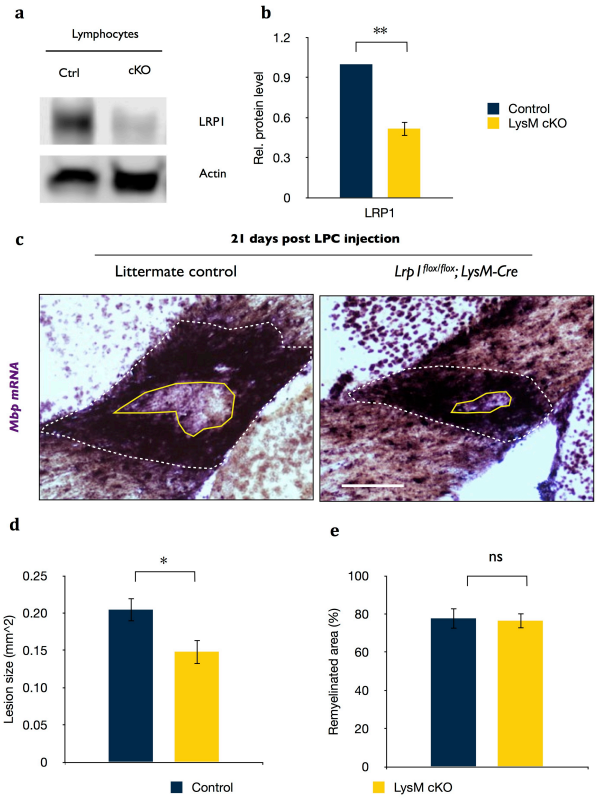
a
Lymphocytes
Ctrl
cKO
LRP1
Actin
b
**
Rel. protein level
1.2
0.9
0.6
0.3
0
LRP1
Control
LysM cKO
c
21 days post LPC injection
Littermate control
Lrp1 flox/flox; LysM-Cre
Mbp mRNA
d
*
Lesion size (mm^2)
0.25
0.20
0.15
0.10
0.05
0
Control
e
ns
Remyelinated area (%)
100
80
60
40
20
0
LysM cKO

Figure 3.5: Ablation of *Lrp1* in myeloid cells does not impact remyelination.
(a) To ensure the LRP1 expression is abolished in the myeloid cells by the Cre-mediated ablation, white blood cells were isolated from blood that are collected from *Lrp1* control and *Lrp1*$^{flox/flox}$*;LysM-Cre* mice. Lymphocytes were lysed and subjected to SDS-PAGE. Representative Western blots probed with anti-LRP1β and anti-β-actin are shown. (b) Quantification of protein levels detected by Western blotting of *Lrp1*$^{flox/flox}$ (n= 3) and *Lrp1*$^{flox/flox}$*;LysM-Cre* (n= 3) lymphocytes lysates. (c) Coronal brain sections through the CC 21 DPI. The outer rim of the lesion area (lesion^{out}) is demarcated by the elevated *Mbp* signal (white dashed line). The non-myelinated area of the lesion is defined by the inner rim of elevated *Mbp* signal (lesion^{in}) and delineated by a solid yellow line. Scale bar= 200μm. (d) Quantification of the initial lesion size (lesion^{out}) in *Lrp1* control (n= 5) and *Lrp1*$^{flox/flox}$*;LysM-Cre* (n= 5) mice. (e) Quantification of white matter repair in *Lrp1* control (n= 5) and *Lrp1*$^{flox/flox}$*;LysM-Cre* (n= 5) mice. The extent of repair was calculated as the percentile of (lesion^{out} - lesion^{int})/(lesion^{out}) x 100. Results are shown as mean ± SEM, *p<0.05, **p<0.01, and ***p<0.001, Student's *t*-test.

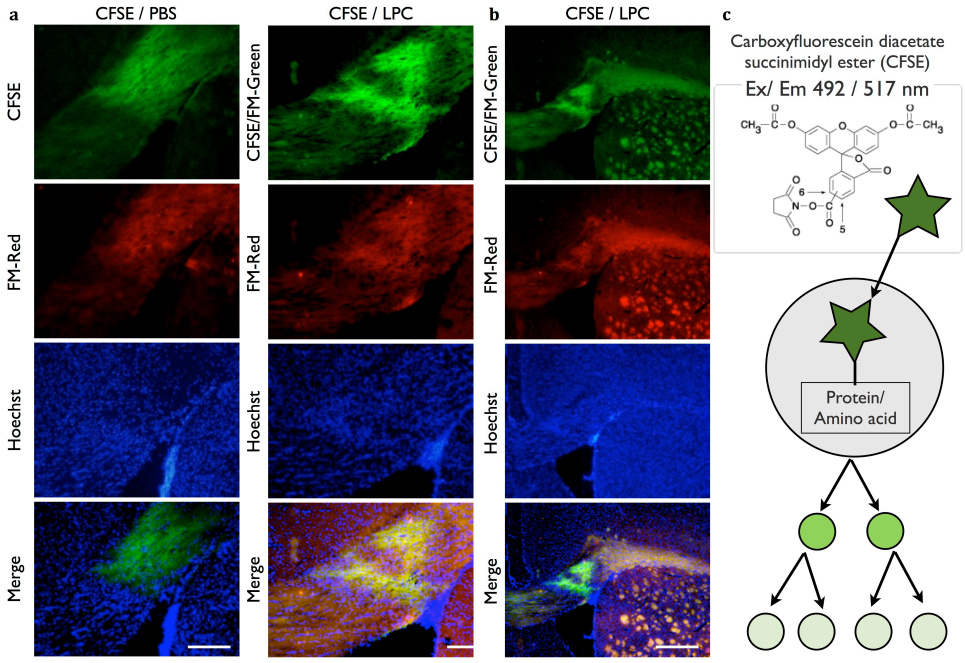
a
CFSE / PBS
CFSE / LPC
b
CFSE / LPC
c
CFSE
FM-Red
Hoechst
Merge
CFSE/FM-Green
FM-Red
Hoechst
Merge
CFSE/FM-Green
FM-Red
Hoechst
Merge
Carboxyfluorescein diacetate
succinimidyl ester (CFSE)
Ex/ Em 492 / 517 nm
Protein/
Amino acid

Figure 3.6: Labeling of the LPC induced white matter lesion with the cell tracker CFSE

(a) Coronal forebrain sections of adult WT mice. Mice are subjected to stereotaxic injection of 0.5µl CFSE/PBS or CFSE/1% LPC mixture into the corpus callosum at each side. At 3 DPI, brains were collected, serially sectioned, and stained with FM-Red and Hoechst dye33342. The injection site is identified by the CFSE labeling under the GFP channel. Scale bar= 200µm. (b) Low magnification of CFSE/1% LPC injected lesion side at 3 DPI. Sections were stained with FM-Green, FM-Red, and Hoechst dye33342. The area that is devoid of FM-Green and FM-Red labeling is wider than $CFSE^+$ area. Scale bar=500µm. (c) The molecule structure of CFSE and the mechanism of action for cell labeling. CFSE is cell permeable, formed a covalent bond with protein and free amino acids. Once the covalent bond is formed, CFSE can pass to another cell unless through cell proliferation. CFSE, carboxyfluorescein diacetate succinimidyl ester.

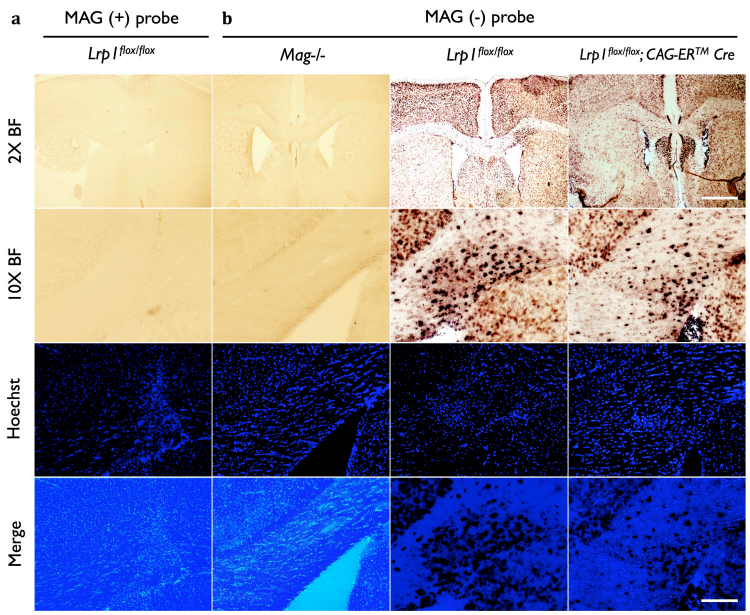
a
MAG (+) probe
b
MAG (-) probe
Lrp1 flox/flox
Mag-/-
Lrp1 flox/flox
Lrp1 flox/flox; CAG-ER™ Cre
2X BF
10X BF
Hoechst
Merge

Figure 3.7: Examination of the specificity of RNA probes used for in situ hybridization

(a) Coronal forebrain sections of adult *Lrp1*$^{flox/flox}$ mice. Naïve brains were collected, serially sectioned, and detected with *Mag* sense (+) probe and stained with Hoechst dye33342. (b) Coronal forebrain sections of adult *Mag*$^{-/-}$, *Lrp1*$^{flox/flox}$, and *Lrp1*$^{flox/flox}$*;Olig2-Cre* mice. Naïve *Mag*$^{-/-}$ brains were collected, serially sectioned, and probed for *Mag* and stained with Hoechst dye33342. *Lrp1*$^{flox/flox}$, and *Lrp1*$^{flox/flox}$*;Olig2-Cre* mice were subjected to stereotaxic injection of PBS or LPC into the corpus callosum at each side. At 21 DPI brains were collected, serially sectioned and probed for *Mag* and stained with Hoechst dye33342. Scale bar= 1mm (2x) and 200µm (10x).

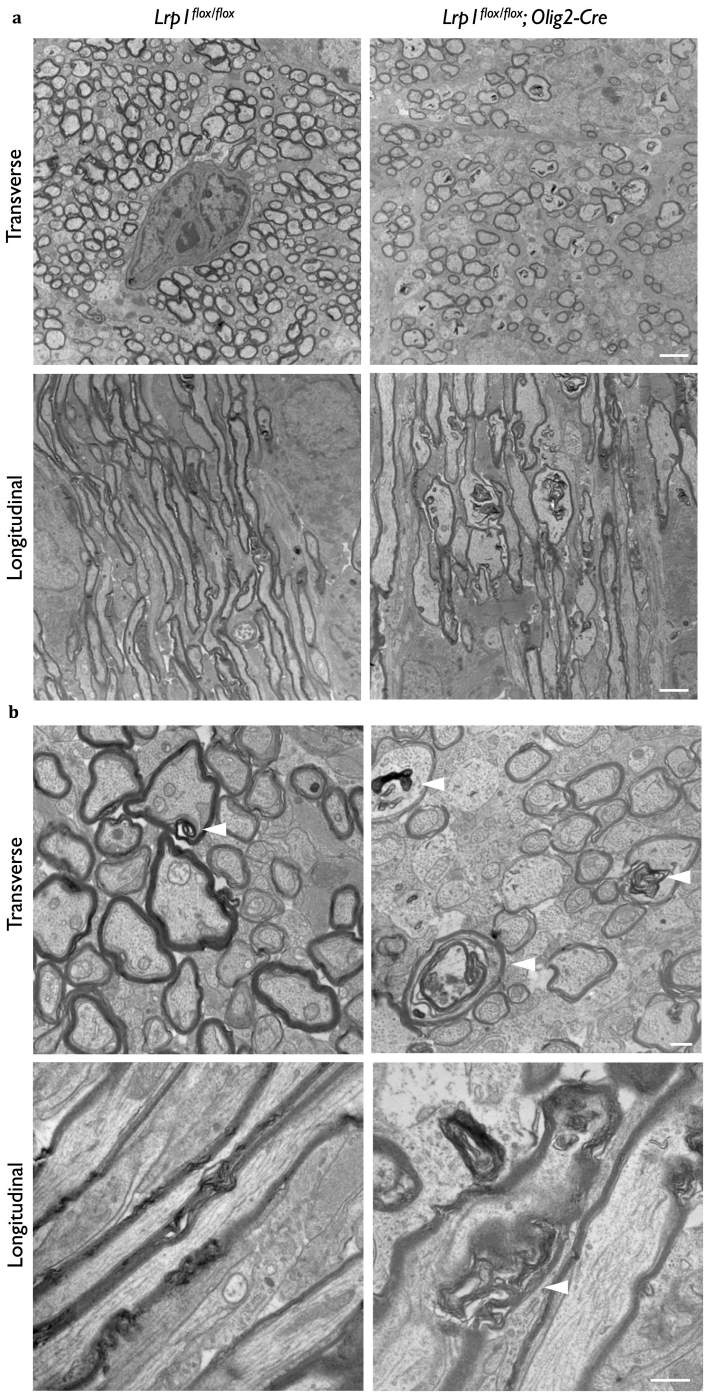
a
Lrp1 flox/flox
Lrp1 flox/flox; Olig2-Cre
Transverse
Longitudinal
b
Transverse
Longitudinal

Figure 3.8: *Lrp1* ablation in the OL-lineage leads to axonal pathology in the optic nerve

(a) Ultrastructural images of optic nerve cross- and longitudinal-sections from P21 control and *Lrp1*$^{flox/flox}$*;Olig2-Cre* conditional knockout mice (*Lrp1* cKO^{OL}). Scale bar= 2μm. (b) High magnification of the ultrastructural image from optic nerve cross- and longitudinal-sections from P21 control and *Lrp1* cKO^{OL}. White arrowheads, the malformed structures, including axon swelling, repeated myelination, myelin out-folding, and myelin uptake particle. Scale bar= 500nm.

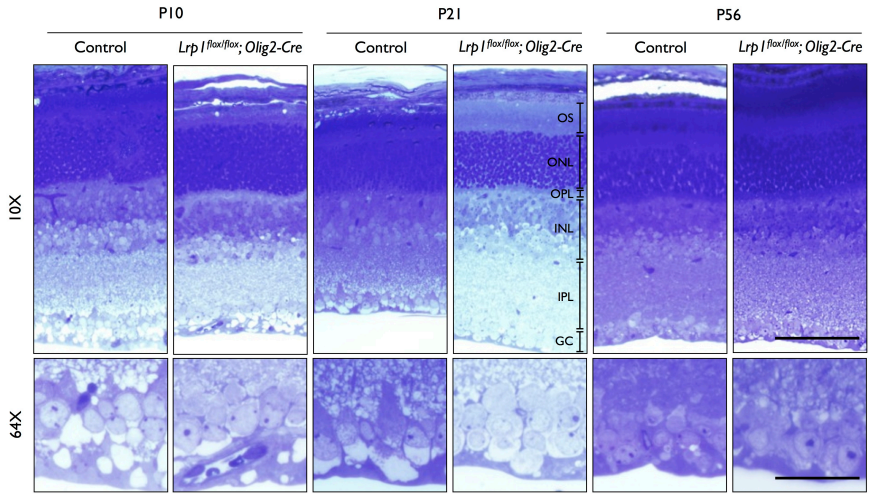
P10
P21
P56
Control
Lrp1 flox/flox; Olig2-Cre
Control
Lrp1 flox/flox; Olig2-Cre
Control
Lrp1 flox/flox; Olig2-Cre
10X
64X
OS
ONL
OPL
INL
IPL
GC

Figure 3.9: *Lrp1* ablation in the OL-lineage does not impact retina ganglion cells (RGC) density or retinal stratification

Retina at P10, P21, and P56 of *Lrp1* control and cKO^{OL} mice were collected, semi-thin sectioned, and stained with toluidine blue (TB). GC, ganglion cell; IPL, inner plexiform layer; INL, inner nuclear layer; OPL, outer plexiform layer; ONL, outer nuclear layer; POS, photoreceptor outer segment; RPE, retinal pigment epithelium. Scale bar= 200μm (10X) and 30μm (64X).

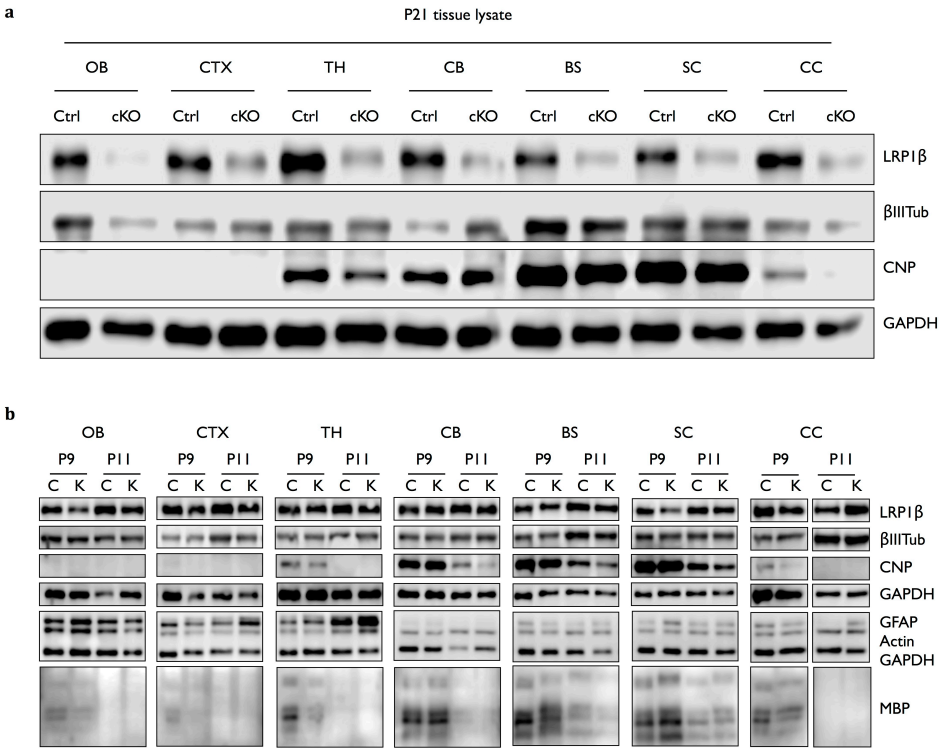
a
P21 tissue lysate
OB
CTX
TH
CB
BS
SC
CC
Ctrl
cKO
LRP1β
βIIITub
CNP
GAPDH
b
P9
P11
C
K
LRP1β
βIIITub
CNP
GAPDH
GFAP
Actin
GAPDH
MBP

Figure 3.10: Brain region specific and developmental stage specific regulation of Myelin proteins in Lrp1 cKO CNS tissue
(a) P21 CNS tissues of *Lrp1* control and *Lrp1* cKO mice were lysed and subjected to SDS-PAGE. Western blots probed with anti-LRP1β, anti- βIIITub, anti-CNP, and anti-GAPDH are shown. (b) P9 and P11 CNS tissues of *Lrp1* control and *Lrp1* cKO mice were lysed and subjected to SDS-PAGE. Western blots probed with anti-LRP1β, anti-βIIITub, anti-CNP, anti-GAPDH, anti-GFAP, anti-Actin, and anti-MBP are shown. OB, olfactory bulb; CTX, cortex; TH, thalamus; CB, cerebellum; BS, brain stem; SC, spinal cord; CC, corpus callosum.

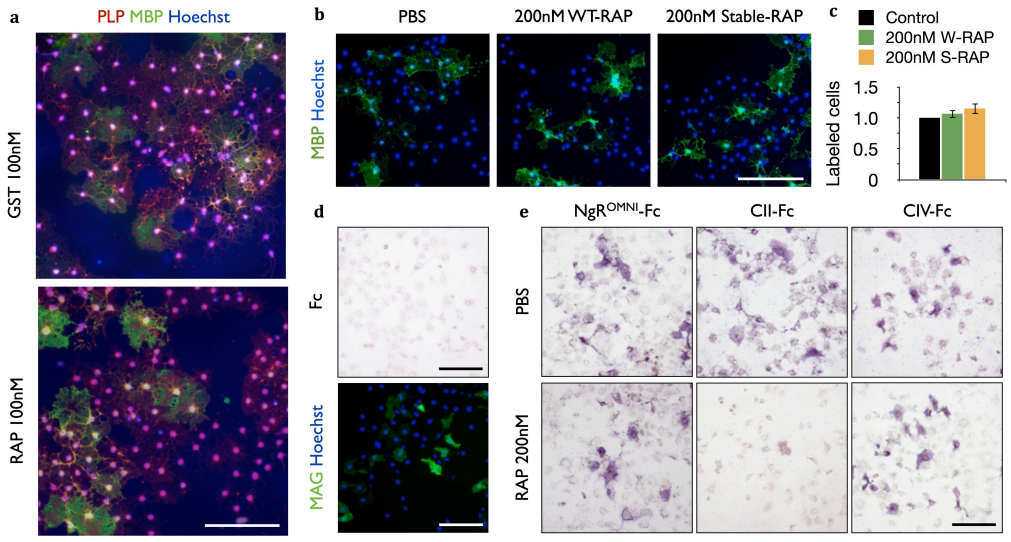
a
PLP MBP Hoechst
GST 100nM
RAP 100nM
b
PBS
200nM WT-RAP
200nM Stable-RAP
MBP Hoechst
c
Control
200nM W-RAP
200nM S-RAP
Labeled cells
1.5
1.0
0.5
0
d
Fc
MAG Hoechst
e
NgR^OMNI-Fc
CII-Fc
CIV-Fc
PBS
RAP 200nM

Figure 3.11: Bath application of the LRP1 antagonist RAP does not inhibit OPC differentiation

(a) OPCs were isolated from P7-9 *Lrp1* control pups by anti-PDGFRα immunopanning. OPC cultured 5 days in differentiation medium (DM) treat with GST or GST-RAP every 2 days. Cultures were stained with anti-MBP, anti-PLP, and Hoechst dye 33342. Scale bar= 100μm. (b) OPCs were isolated from P7-9 *Lrp1* control pups by anti-PDGFRα immunopanning. OPC cultured 5 days in differentiation medium (DM) treat with PBS, WT-RAP, or stable-RAP every 2 days. Cultures were stained with anti-MBP and Hoechst dye 33342. Scale bar= 100μm. (c) Quantification of MBP^+ cells under each of the 3 different conditions (n=4 per condition). (d) COS7 cells co-transfect to express MAG and GFP. Cells were collected, fixed, and stained with Hoechst dye 33342 and anti-Fc. (e) MAG expressing COS7 were treated with Fc, NgR^{omni}-Fc, CII-Fc, and CIV-Fc to bind with MAG. The complex of ligand/ligand binding domain was competed by PBS or RAP. Cells were collected, fixed, and stained with AP-conjugated anti-Fc. Colorimetric BCIP/NBT substrate was used to detect successful binding. RAP, receptor-associated protein; BCIP, 5-Bromo-4-Chloro-3-Indolyl Phosphate; NBT, Nitroblue Tetrazolium. Results are shown as mean values ± SEM, *p<0.05, **p<0.01, and ***p<0.001, 2-way ANOVA, post hoc *t*-test.

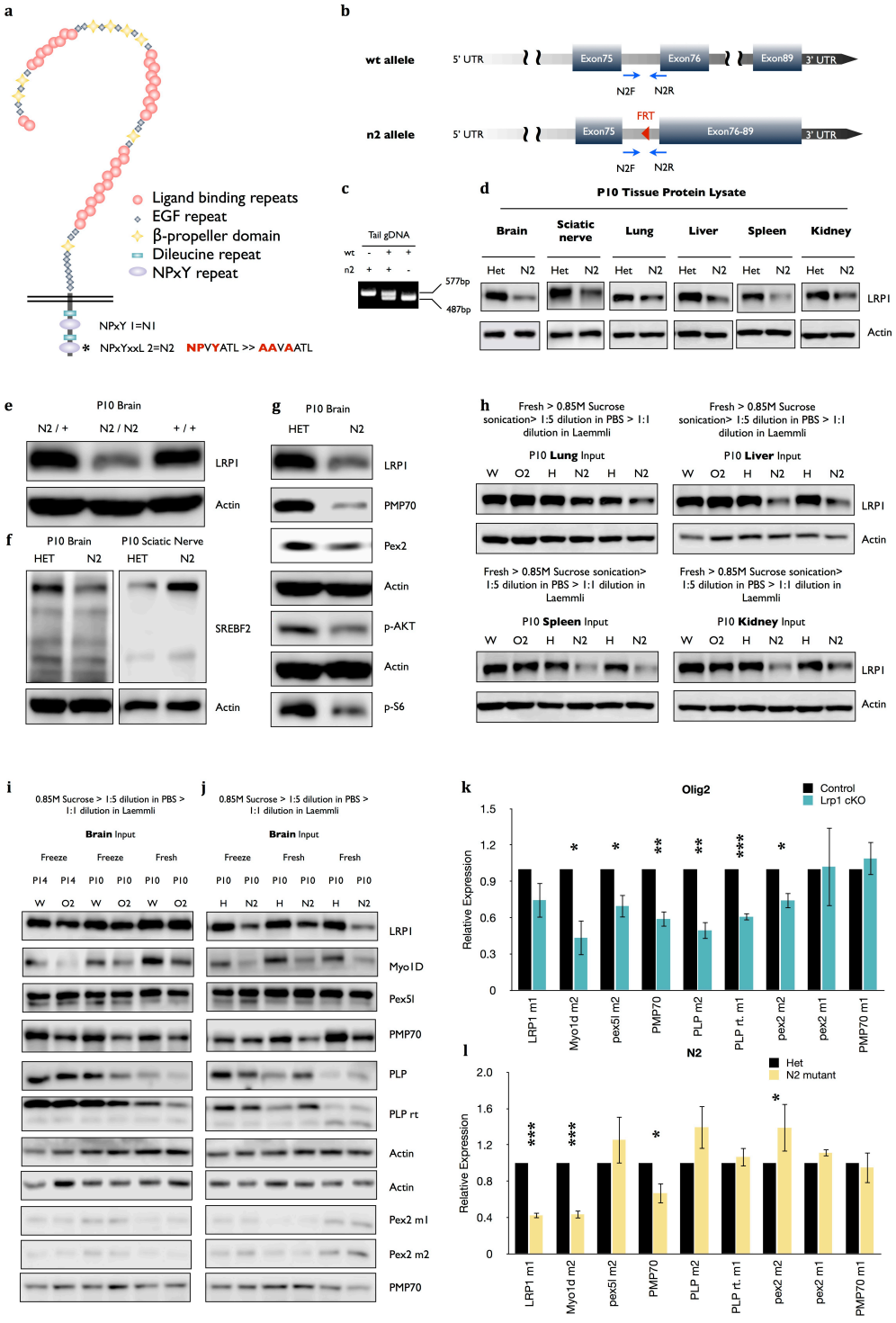
a
Ligand binding repeats
EGF repeat
β-propeller domain
Dileucine repeat
NPxY repeat
NPxY 1=N1
NPxYxxL 2=N2 NPVYATL >> AAVAATL
b
wt allele
5' UTR
Exon75
Exon76
Exon89
3' UTR
N2F
N2R
n2 allele
FRT
Exon76-89
c
Tail gDNA
wt
n2
577bp
487bp
d
P10 Tissue Protein Lysate
Brain
Sciatic nerve
Lung
Liver
Spleen
Kidney
Het
N2
LRP1
Actin
e
P10 Brain
N2 / +
N2 / N2
+ / +
LRP1
Actin
f
P10 Brain
P10 Sciatic Nerve
HET
N2
SREBF2
Actin
g
P10 Brain
HET
N2
LRP1
PMP70
Pex2
Actin
p-AKT
Actin
p-S6
h
Fresh > 0.85M Sucrose sonication> 1:5 dilution in PBS > 1:1 dilution in Laemmli
P10 Lung Input
P10 Liver Input
P10 Spleen Input
P10 Kidney Input
W
O2
H
N2
LRP1
Actin
i
0.85M Sucrose > 1:5 dilution in PBS > 1:1 dilution in Laemmli
Brain Input
Freeze
Fresh
P14
P10
LRP1
Myo1D
Pex5l
PMP70
PLP
PLP rt
Actin
Pex2 m1
Pex2 m2
PMP70
j
0.85M Sucrose > 1:5 dilution in PBS > 1:1 dilution in Laemmli
Brain Input
k
Olig2
Control
Lrp1 cKO
Relative Expression
LRP1 m1
Myo1d m2
pex5l m2
PMP70
PLP m2
PLP rt. m1
pex2 m2
pex2 m1
PMP70 m1
l
N2
Het
N2 mutant
Relative Expression

Figure 3.12: Characterization of *Lrp1*$^{n2/n2}$ mice carrying a mutation in the distal NPxY phosphorylation site of LRP1

(a) The illustration of the LRP1 structure. Distal NPxY mutated to AAxA. (b) The location of PCR primers used for genotyping *Lrp1* wildtype (wt) and *Lrp1* n2 alleles are shown. (c) PCR genotyping of tail genomic DNA. Analysis of PCR products amplified from of *Lrp1*$^{+/+}$, *Lrp1*$^{n2/+}$, and *Lrp1*$^{n2/n2}$. The N2F/N2R primer pair amplifies a 577 bp PCR product from the *Lrp1* n2 allele and a 487 bp PCR product from the *Lrp1* wt allele. (d) Tissues prepared from P10 *Lrp1*$^{n2/+}$ (Het) and *L.rp1*$^{n2/n2}$ (N2) mice were lysed and subjected to SDS-PAGE. Representative Western blots probed with anti-LRP1β and anti-β-actin are shown. (e) Brain lysates prepared from *Lrp1*$^{+/+}$, *Lrp1*$^{n2/+}$, and *Lrp1*$^{n2/n2}$ mice were probed with anti-LRP1β and anti-β-actin. (f) Brain and sciatic nerve lysates prepared from P10 Het and N2 mice were probed with anti-SREBP2 and anti-β-actin. (g) Brain lysates prepared from P10 Het and N2 mice were probed with anti-LRP1β, anti-PMP70, anti-Pex2, anti-β-actin, anti-pAKT, and anti-pS6. (h) Lung, liver, spleen, and kidney lysates prepared from P10 or P14 fresh or freeze *Lrp1* control (W), *Lrp1*$^{flox/flox}$*;Olig2-Cre* (O2), *Lrp1*$^{n2/+}$ (Het), and *Lrp1*$^{n2/n2}$ (N2) mice probed with anti-LRP1β and anti-β-actin are shown. (i and j) Brains were homogenized in 0.85M sucrose, diluted with PBS in a 1:5 ratio, mixed with laemmli in 1:1 ratio, and subjected to SDS-PAGE. Brains from P10 *Lrp1* control (W), *Lrp1*$^{flox/flox}$*;Olig2-Cre* (O2) *Lrp1*$^{n2/+}$ (H), and *Lrp1*$^{n2/n2}$ (N2) mice probed with anti-LRP1β, anti-Myo1D, anti-Pex5l, anti-PMP70, anti-PLP (rabbit), anti-PLP (rat), anti-β-actin, and anti-Pex2 are shown. (k and l) Quantification of protein levels detected by Western blotting under each condition (n=3) is shown. Results are shown as mean values ± SEM, *p<0.05, **p<0.01, and ***p<0.001, 2-way ANOVA, post hoc *t*-test.

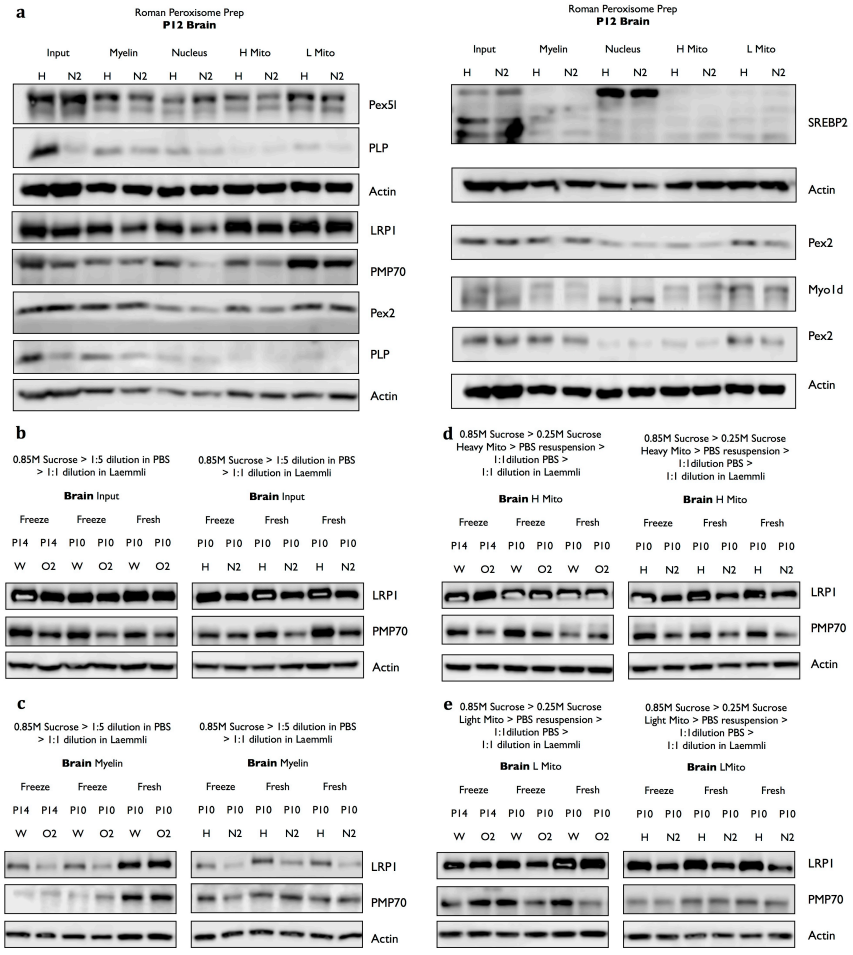
a
Roman Peroxisome Prep
P12 Brain
Input
Myelin
Nucleus
H Mito
L Mito
H
N2
Pex5l
PLP
Actin
LRP1
PMP70
Pex2
PLP
Actin
Roman Peroxisome Prep
P12 Brain
SREBP2
Actin
Pex2
Myo1d
Pex2
Actin
b
0.85M Sucrose > 1:5 dilution in PBS > 1:1 dilution in Laemmli
Brain Input
Freeze
Fresh
P14
P10
W
O2
H
N2
LRP1
PMP70
Actin
c
0.85M Sucrose > 1:5 dilution in PBS > 1:1 dilution in Laemmli
Brain Myelin
LRP1
PMP70
Actin
d
0.85M Sucrose > 0.25M Sucrose Heavy Mito > PBS resuspension > 1:1 dilution PBS > 1:1 dilution in Laemmli
Brain H Mito
LRP1
PMP70
Actin
e
0.85M Sucrose > 0.25M Sucrose Light Mito > PBS resuspension > 1:1 dilution PBS > 1:1 dilution in Laemmli
Brain L Mito
Brain LMito
LRP1
PMP70
Actin

Figure 3.13: Analysis of myelin and peroxisome protein expression in P10-14 *Lrp1*$^{n2/n2}$ and *Lrp1* cKO mouse brain tissue fractionated in a sucrose density gradient

(a) Brains prepared form P12 *Lrp1*$^{n2/+}$ (H) and *Lrp1*$^{n2/n2}$ (N2) mice were subjected to density fractionation to enrich for peroxisomes. Different fractions acquired during peroxisome preparation were subjected to SDS-PAGE. Blots probed with anti-Pex5l, anti-PLP (rabbit), anti-β-actin, anti-LRP1β, anti-PMP70, anti-Pex2, anti-SREBP2, and anti-Myo1D are shown. H Mito, heavy mitochondria; L Mito, light mitochondria. (b-e) Homogenates from each fraction including input (b), myelin enriched (c), H Mito (d), and L Mito (e) were diluted as indicated for each condition and subjected to SDS-PAGE. Fresh or freeze brains were prepared from P10 or 14 *Lrp1* control (W), *Lrp1*$^{flox/flox}$*;Olig2-Cre* (O2) *Lrp1*$^{n2/+}$ (H), and *Lrp1*$^{n2/n2}$ (N2) probed with anti-LRP1β, anti-PMP70, and anti-β-actin are shown.

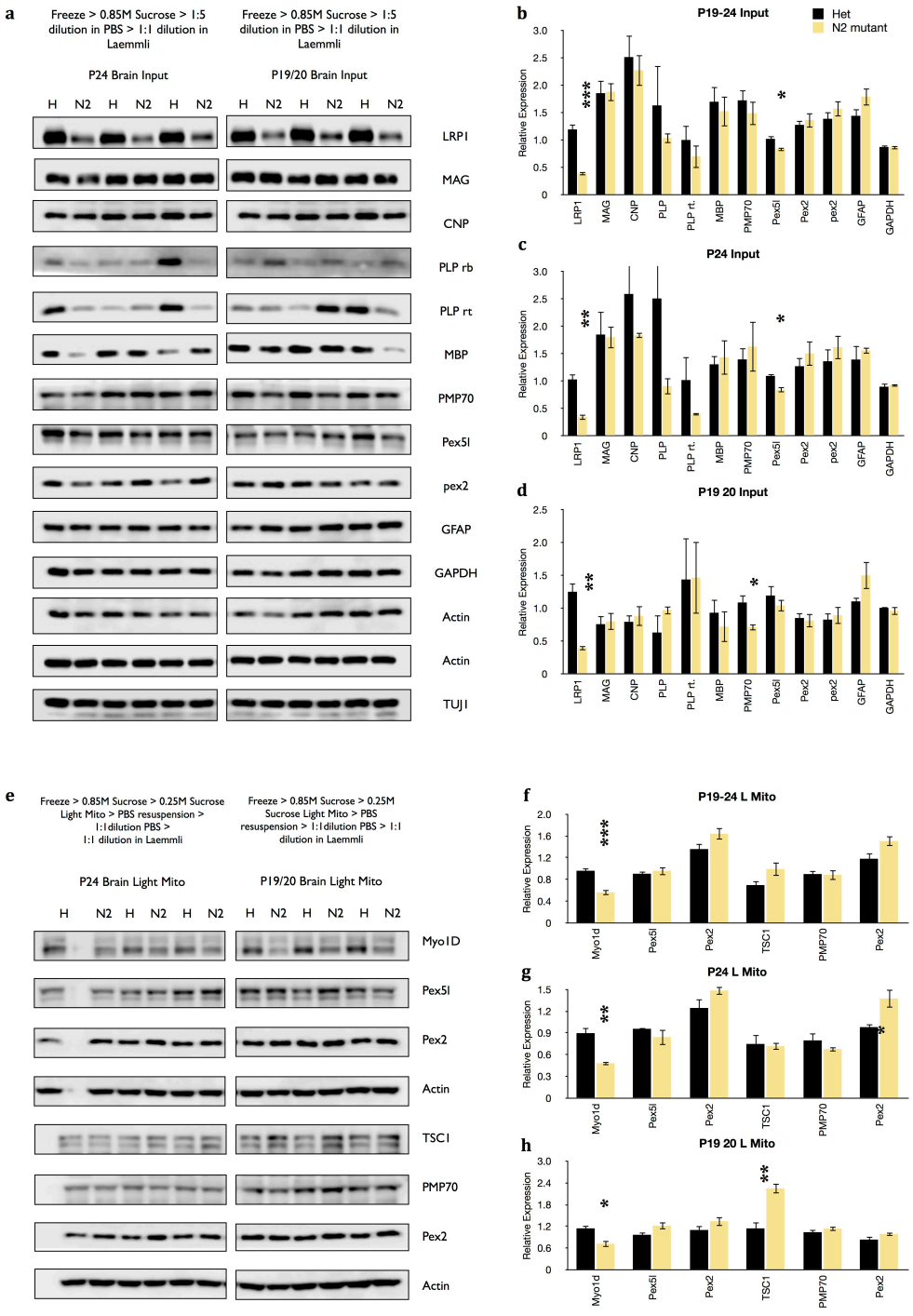
a
Freeze > 0.85M Sucrose > 1:5 dilution in PBS > 1:1 dilution in Laemmli
Freeze > 0.85M Sucrose > 1:5 dilution in PBS > 1:1 dilution in Laemmli
P24 Brain Input
P19/20 Brain Input
H N2 H N2 H N2 H N2 H N2 H N2
LRP1
MAG
CNP
PLP rb
PLP rt
MBP
PMP70
Pex5l
pex2
GFAP
GAPDH
Actin
Actin
TUJ1
b
P19-24 Input
Het
N2 mutant
Relative Expression
LRP1 MAG CNP PLP PLP rt. MBP PMP70 Pex5l Pex2 pex2 GFAP GAPDH
c
P24 Input
d
P19 20 Input
e
Freeze > 0.85M Sucrose > 0.25M Sucrose Light Mito > PBS resuspension > 1:1dilution PBS > 1:1 dilution in Laemmli
Freeze > 0.85M Sucrose > 0.25M Sucrose Light Mito > PBS resuspension > 1:1dilution PBS > 1:1 dilution in Laemmli
P24 Brain Light Mito
P19/20 Brain Light Mito
H N2 H N2 H N2 H N2 H N2 H N2
Myo1D
Pex5l
Pex2
Actin
TSC1
PMP70
Pex2
Actin
f
P19-24 L Mito
Myo1d Pex5l Pex2 TSC1 PMP70 Pex2
g
P24 L Mito
h
P19 20 L Mito

Figure 3.14: Characterization of myelin protein expression in P19-24 brains of *Lrp1*$^{n2/n2}$ mice in fractions enriched for peroxisomes and light mitochondria
(a) Brains form P19-24 *Lrp1*$^{n2/+}$ (H) and *Lrp1*$^{n2/n2}$ (N2) mice were subjected to peroxisome preparation. Homogenate inputs prepared for peroxisome preparation at the indicated condition were subjected to SDS-PAGE. Blots probed with anti-LRP1β, anti-MAG, anti-CNP, anti-PLP (rabbit), anti-PLP (rat), anti-MBP, anti-PMP70, anti-Pex5l, anti-Pex2, anti-GFAP, anti-GAPDH, anti-β-actin, anti-βIIITub are shown. (b) Quantification of protein levels detected by Western blotting in a by combining data points from all mice at P19-24 (n=6) is shown. (c) Quantification of protein levels detected in a by Western blotting from mice at P24 (n=3) is shown. (d) Quantification of protein levels detected in a by Western blotting from mice at P19-20 (n=3) is shown. (e) Brains form P19-24 *Lrp1*$^{n2/+}$ (H) and *Lrp1*$^{n2/n2}$ (N2) mice were subjected to peroxisome preparation. Light mitochondria fractions acquired during peroxisome preparation at the indicated condition were subjected to SDS-PAGE. Blots probed with anti-Myo1D, anti-Pex5l, anti-Pex2, anti-β-actin, anti-TSC1, anti-PMP70 are shown. (b) Quantification of protein levels detected by Western blotting in e by combining data points from all mice at P19-24 (n=6) is shown. (c) Quantification of protein levels detected in e by Western blotting from mice at P24 (n=3) is shown. (d) Quantification of protein levels detected in e by Western blotting from mice at P19-20 (n=3) is shown. Results are shown as mean values ± SEM, *p<0.05, **p<0.01, and ***p<0.001, 2-way ANOVA, post hoc *t*-test.

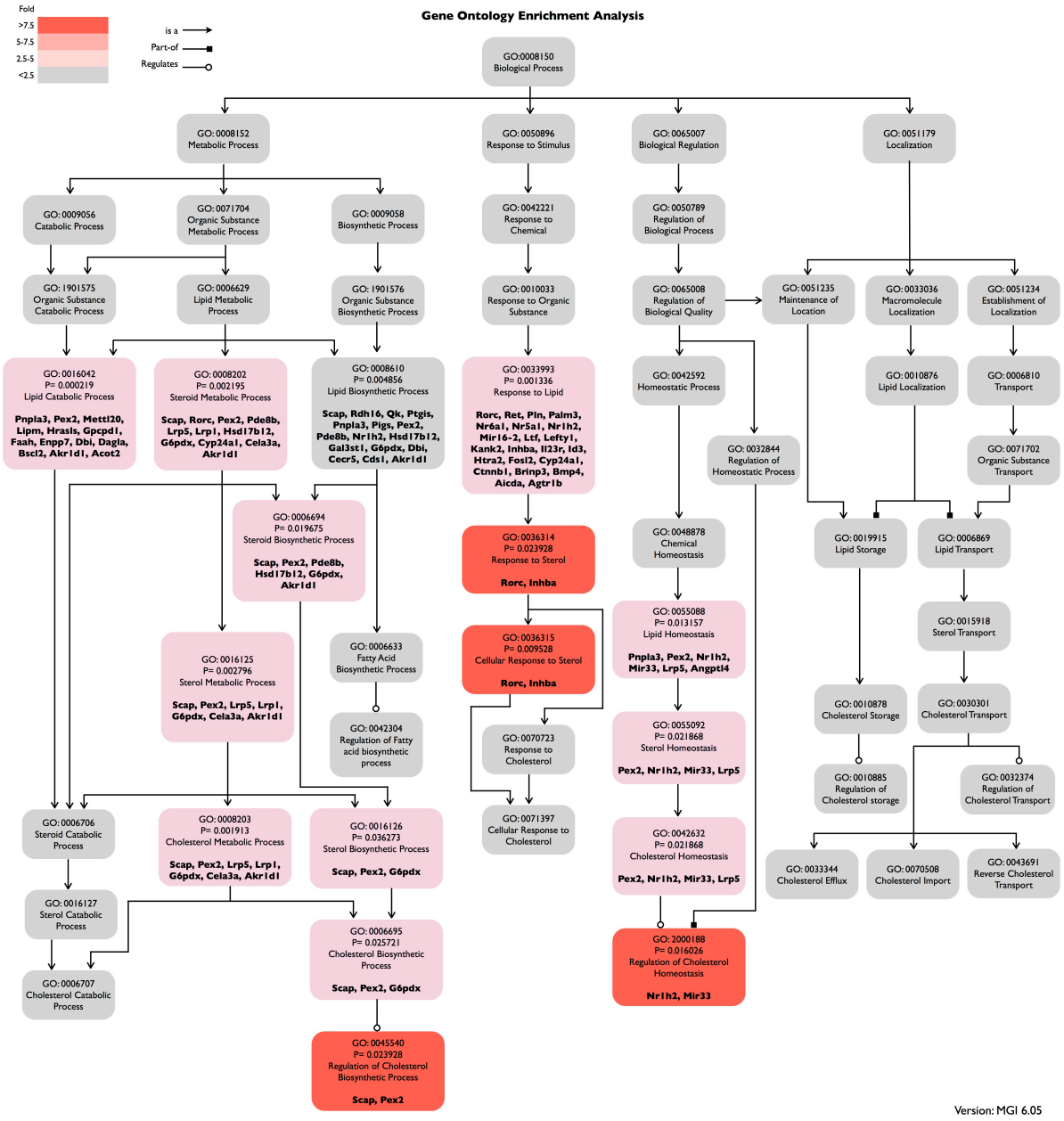
Gene Ontology Enrichment Analysis
Fold
>7.5
5-7.5
2.5-5
<2.5
is a
Part-of
Regulates
GO:0008150
Biological Process
GO:0008152
Metabolic Process
GO:0050896
Response to Stimulus
GO:0065007
Biological Regulation
GO:0051179
Localization
GO:0009056
Catabolic Process
GO:0071704
Organic Substance
Metabolic Process
GO:0009058
Biosynthetic Process
GO:0042221
Response to
Chemical
GO:0050789
Regulation of
Biological Process
GO:1901575
Organic Substance
Catabolic Process
GO:0006629
Lipid Metabolic
Process
GO:1901576
Organic Substance
Biosynthetic Process
GO:0010033
Response to Organic
Substance
GO:0065008
Regulation of
Biological Quality
GO:0051235
Maintenance of
Location
GO:0033036
Macromolecule
Localization
GO:0051234
Establishment of
Localization
GO:0016042
P= 0.000219
Lipid Catabolic Process
Pnpla3, Pex2, Mettl20,
Lipm, Hrasls, Gpcpd1,
Faah, Enpp7, Dbi, Dagla,
Bscl2, Akr1d1, Acot2
GO:0008202
P= 0.002195
Steroid Metabolic Process
Scap, Rorc, Pex2, Pde8b,
Lrp5, Lrp1, Hsd17b12,
G6pdx, Cyp24a1, Cela3a,
Akr1d1
GO:0008610
P= 0.004856
Lipid Biosynthetic Process
Scap, Rdh16, Qk, Ptgis,
Pnpla3, Pigs, Pex2,
Pde8b, Nr1h2, Hsd17b12,
Gal3st1, G6pdx, Dbi,
Cecr5, Cds1, Akr1d1
GO:0033993
P= 0.001336
Response to Lipid
Rorc, Ret, Pin, Palm3,
Nr6a1, Nr5a1, Nr1h2,
Mir16-2, Ltf, Lefty1,
Kank2, Inhba, Il23r, Id3,
Htra2, Fosl2, Cyp24a1,
Ctnnb1, Brinp3, Bmp4,
Aicda, Agtr1b
GO:0042592
Homeostatic Process
GO:0010876
Lipid Localization
GO:0006810
Transport
GO:0032844
Regulation of
Homeostatic Process
GO:0071702
Organic Substance
Transport
GO:0006694
P= 0.019675
Steroid Biosynthetic Process
Scap, Pex2, Pde8b,
Hsd17b12, G6pdx,
Akr1d1
GO:0036314
P= 0.023928
Response to Sterol
Rorc, Inhba
GO:0048878
Chemical
Homeostasis
GO:0019915
Lipid Storage
GO:0006869
Lipid Transport
GO:0016125
P= 0.002796
Sterol Metabolic Process
Scap, Pex2, Lrp5, Lrp1,
G6pdx, Cela3a, Akr1d1
GO:0006633
Fatty Acid
Biosynthetic Process
GO:0036315
P= 0.009528
Cellular Response to Sterol
Rorc, Inhba
GO:0055088
P= 0.013157
Lipid Homeostasis
Pnpla3, Pex2, Nr1h2,
Mir33, Lrp5, Angptl4
GO:0015918
Sterol Transport
GO:0042304
Regulation of Fatty
acid biosynthetic
process
GO:0070723
Response to
Cholesterol
GO:0055092
P= 0.021868
Sterol Homeostasis
Pex2, Nr1h2, Mir33, Lrp5
GO:0010878
Cholesterol Storage
GO:0030301
Cholesterol Transport
GO:0006706
Steroid Catabolic
Process
GO:0008203
P= 0.001913
Cholesterol Metabolic Process
Scap, Pex2, Lrp5, Lrp1,
G6pdx, Cela3a, Akr1d1
GO:0016126
P= 0.036273
Sterol Biosynthetic Process
Scap, Pex2, G6pdx
GO:0071397
Cellular Response to
Cholesterol
GO:0042632
P= 0.021868
Cholesterol Homeostasis
Pex2, Nr1h2, Mir33, Lrp5
GO:0010885
Regulation of
Cholesterol storage
GO:0032374
Regulation of
Cholesterol Transport
GO:0016127
Sterol Catabolic
Process
GO:0006695
P= 0.025721
Cholesterol Biosynthetic
Process
Scap, Pex2, G6pdx
GO:0033344
Cholesterol Efflux
GO:0070508
Cholesterol Import
GO:0043691
Reverse Cholesterol
Transport
GO:0006707
Cholesterol Catabolic
Process
GO:0045540
P= 0.023928
Regulation of Cholesterol
Biosynthetic Process
Scap, Pex2
GO:2000188
P= 0.016026
Regulation of Cholesterol
Homeostasis
Nr1h2, Mir33
Version: MGI 6.05

Figure 3.15: Gene ontology (GO) analysis of *Lrp1* deficient OPCs revealed enrichment of cholesterol biosynthesis and homeostasis genes
Acutely isolated OPCs from *Lrp1* control and *Lrp1*$^{flox/flox}$*;Olig2-Cre* mouse pups were subjected to microarray analysis. GO structure of biological process module related to peroxisome function. Each box shows the GO term ID, *p*-value, GO term, and the genes from the input list associated with the GO term. The color of each box shows the level of enrichment for each GO term. Specific GO terms were queried with the Mouse Genome Informatics (MGI) GO browser. *P*-values were calculated by Fisher's exact test. The fold-enrichment was calculated by dividing the ratio of genes that are associated with each GO term from the input list by the ratio of genes that are expected in the database. mRNA was prepared from acutely isolated OPCs of *Lrp1* controls (n= 4) and cKO^{OL} (n =4) pups and analyzed with the Affymetrix mouse gene 2.1 ST array. Differentially regulated gene products include *G6pdx* (Glucose-6-phosphate 1-dehydrogenase X), *Scap* (Sterol regulatory element-binding protein cleavage-activating protein), *Pex2* (peroxisomal biogenesis factor 2), *Nr1h2* (Nuclear receptor subfamily 1 group H member 2), *Lrp5* (Low-density lipoprotein receptor-related protein 5), *Mir33* (microRNA 33).

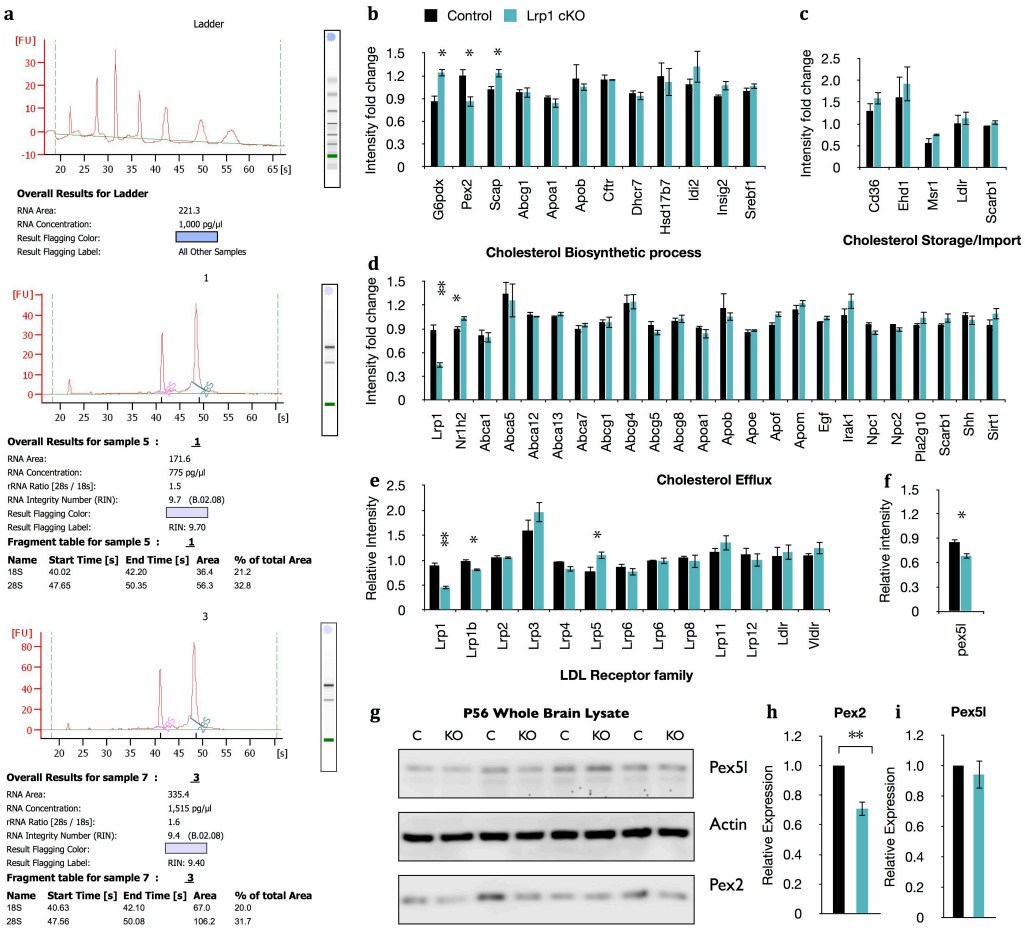
a
Ladder
[FU]
Overall Results for Ladder
RNA Area: 221.3
RNA Concentration: 1,000 pg/µl
Result Flagging Color:
Result Flagging Label: All Other Samples
1
Overall Results for sample 5 : 1
RNA Area: 171.6
RNA Concentration: 775 pg/µl
rRNA Ratio [28s / 18s]: 1.5
RNA Integrity Number (RIN): 9.7 (B.02.08)
Result Flagging Color:
Result Flagging Label: RIN: 9.70
Fragment table for sample 5 : 1
Name Start Time [s] End Time [s] Area % of total Area
18S 40.02 42.20 36.4 21.2
28S 47.65 50.35 56.3 32.8
3
Overall Results for sample 7 : 3
RNA Area: 335.4
RNA Concentration: 1,515 pg/µl
rRNA Ratio [28s / 18s]: 1.6
RNA Integrity Number (RIN): 9.4 (B.02.08)
Result Flagging Color:
Result Flagging Label: RIN: 9.40
Fragment table for sample 7 : 3
Name Start Time [s] End Time [s] Area % of total Area
18S 40.63 42.10 67.0 20.0
28S 47.56 50.08 106.2 31.7
b
Control
Lrp1 cKO
Intensity fold change
G6pdx
Pex2
Scap
Abcg1
Apoa1
Apob
Cftr
Dhcr7
Hsd17b7
Idi2
Insig2
Srebf1
Cholesterol Biosynthetic process
c
Cd36
Ehd1
Msr1
Ldlr
Scarb1
Cholesterol Storage/Import
d
Lrp1
Nr1h2
Abca1
Abca5
Abca12
Abca13
Abca7
Abcg1
Abcg4
Abcg5
Abcg8
Apoa1
Apob
Apoe
Apof
Apom
Egf
Irak1
Npc1
Npc2
Pla2g10
Scarb1
Shh
Sirt1
e
Cholesterol Efflux
Relative Intensity
Lrp1
Lrp1b
Lrp2
Lrp3
Lrp4
Lrp5
Lrp6
Lrp6
Lrp8
Lrp11
Lrp12
Ldlr
Vldlr
LDL Receptor family
f
Relative intensity
pex5l
g
P56 Whole Brain Lysate
C KO C KO C KO C KO
Pex5l
Actin
Pex2
h
Pex2
Relative Expression
i
Pex5l
Relative Expression

Figure 3.16: Validation of genes belonging to the cholesterol metabolism pathway differentially regulated in *Lrp1* control and cKO OPCs

(a) RNA quality control before analyzing with the Affymetrix mouse gene 2.1 ST array. The ratio of 28S/18S in the *Lrp1* control (middle panel) and *Lrp1* cKO (bottom panel) is similar to ladder control (top panel). The quality is sufficient to proceed. (b-f) mRNA was prepared from acutely isolated OPCs of *Lrp1* controls (n= 4) and cKO^{OL} (n= 4) pups and analyzed with the Affymetrix mouse gene 2.1 ST array. Genes that regulate cholesterol biosynthesis process (b), storage/report (c), efflux (d), LDL receptor family (e), and Pex2 related gene (f) are plotted. (g) Immunoblotting of lysates prepared from the P56 brain of *Lrp1* control (C) and *Lrp1$^{flox/flox}$;Olig2-Cre* (KO). Representative blots probed with anti-PEX5L, anti-β-actin, and anti-PEX2. (d) Quantification of Pex2 and Pex5l in *Lrp1* control (n= 4) and KO (n= 4) brain lysate. Results are shown as mean values ±SEM, *p<0.05 and **p<0.01, Student's *t*-test.

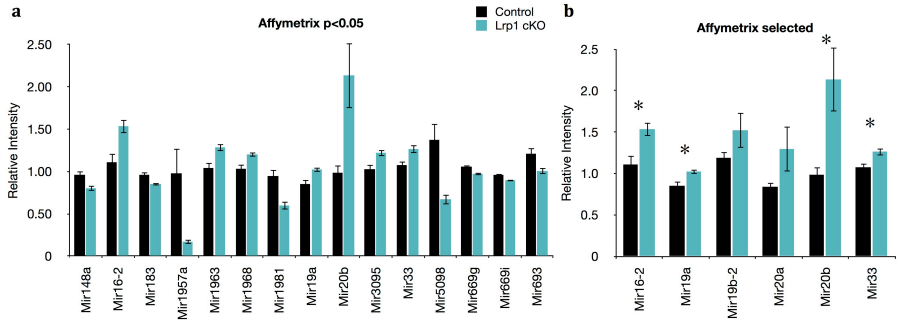

c

miRNA	16-1	16-2	17	19a	19b-1	19b-2	20a	20b	33
Lrp1					v	v	v	v	v
Myo1d	v		v				v	v	v
Pex2	v								v
Pex5l	v	v	v	v	v	v	v	v	
G6pdx	v	v	v	v	v	v		v	v
Scap			v	v				v	
Nr1h2		v							
Srebf1			v		v		v	v	
Srebf2			v	v	v		v	v	v
Mag									
Mbp	v	v	v	v	v	v	v	v	v
Plp1	v	v		v	v	v	v	v	v
Cnp									
Gene no.	6	5	7	6	7	5	7	9	7

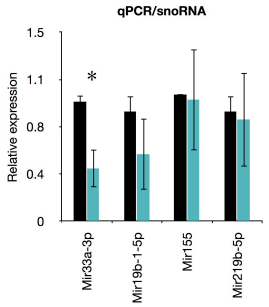

e

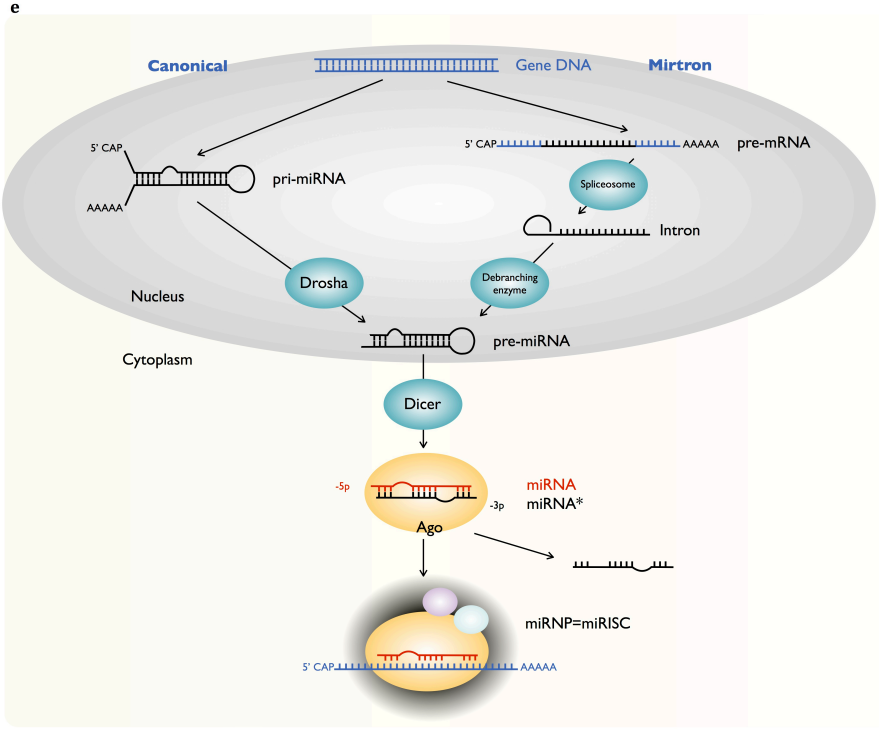

Figure 3.17: Validation of the miRNAs that are differentially regulated in *Lrp1* control and cKO OPCs

(a) RNA was prepared from acutely isolated OPCs of *Lrp1* controls (n= 4) and cKO^{OL} (n= 4) pups and analyzed with the Affymetrix mouse gene 2.1 ST array. miRNAs that are differentially regulated with original $p<0.05$ are plotted. (b) From the Affymetrix results, selective miRNAs with literature annotation and their related isoforms are plotted. (c) Selective miRNAs in b cross-referenced with target gens of interests. Potentially regulated genes for each miRNA are checked. (d) Selective mature miRNAs were validated with miRNA qPCR. The relative expression level of each miRNA was normalized to snoRNA. (e) An illustration showing the pathway of miRNA synthesis, maturation, and activation. The majority of miRNAs are processed through canonical or mirtron pathway. In canonical pathway, pri-miRNA is transcribed from a gene, processed by Drosha to become pre-miRNA, exported to the cytoplasm, further processed by Dicer to become mature miRNA/miRNA* dimer. The name miRNA is given to the dominant strand, and miRNA* is the minor strand. Dominant strand can either be located at the 5' site or 3' site. miRNA is loaded to Ago to carry its function with the half-life from hours to days. The complex constitutes of miRNA, Ago, and other proteins is called miRNP or miRISC. miRNP is the active unit to regulate mRNA transcription or degradation. In mirtron pathway, the intron is spliced out directly from pre-mRNA by the spliceosome, intron than is processed by de-branching enzymes to form pre-miRNA. Results are shown as mean values ±SEM, *$p<0.05$ and **$p<0.01$, Student's *t*-test.

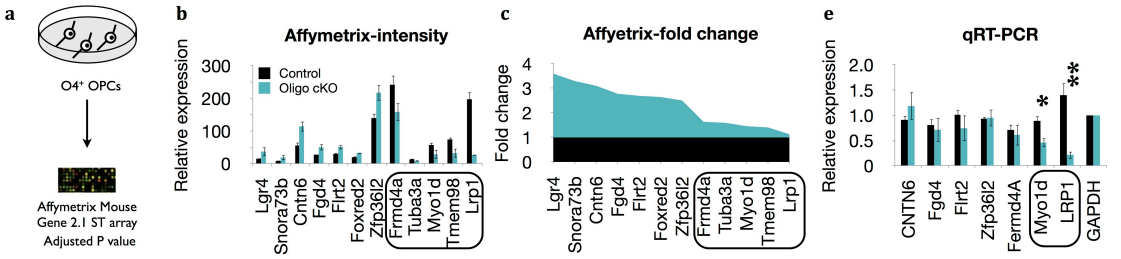

d **Olig2 cKO to control O4+ oligodendrocytes Affymetrix mice gene expression array comparison**

Symbol	Gene ID	Description	Expression level	Fold change	Adjusted p value
Lrp1	16971	low density lipoprotein receptor-related protein 1	7.000	-2.900	0.00000001
Cntn6	53870	contactin 6	5.997	1.076	0.011
Fgd4	224014	FYVE, RhoGEF and PH domain containing 4	5.327	0.833	0.011
Myo1d	338367	myosin ID	4.414	-1.111	0.037
Tmem98	103743	transmembrane protein 98	4.783	-1.287	0.039
Tuba3a	22144	tubulin, alpha 3A	3.392	-0.739	0.039
Frmd4a	209630	FERM domain containing 4A	7.215	-0.646	0.039
Lgr4	107515	leucine-rich repeat-containing G protein-coupled receptor 4	4.289	1.381	0.046
Foxred2	239554	FAD-dependent oxidoreductase domain containing 2	4.539	0.724	0.046
Snora73b	100306945	small nucleolar RNA, H/ACA box 73b	3.426	1.202	0.046
Flrt2	399558	fibronectin leucine rich transmembrane protein 2	5.351	0.765	0.046
Zfp36l2	12193	zinc finger protein 36, C3H type-like 2	7.997	0.593	0.046

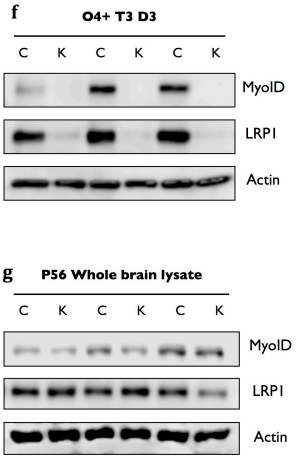

Figure 3.18: Validation of the genes that are differentially regulated in *Lrp1* control and cKO OLs that are O4$^+$

(a) RNA was prepared from acutely isolated OLs of *Lrp1* controls (n= 4) and cKO^{OL} (n= 4) pups by anti-O4 immunopanning and analyzed with the Affymetrix mouse gene 2.1 ST array. (b) The relative expression level of genes that are differentially regulated with adjusted $p<0.05$ are plotted. Genes that are down regulated in *Lrp1* cKO OLs are highlighted. (c) Relative fold change of genes from b are plotted. (e) Selective genes were validated with semi-quantitative qPCR. The relative expression level of each mRNA was normalized to GAPDH mRNA. Genes are highlighted with differential mRNA expression with statistically significant. (d) List of significantly regulated gene symbol, ID, description, expression level, fold change, and adjusted p-value in comparison of *Lrp1* cKO to *Lrp1* control OLs. (f) Validation of the Myo1D expression level with Western blotting. Immunoblotting of lysates prepared from O4$^+$ OLs isolated from *Lrp1* control (C) and *Lrp1$^{flox/flox}$;Olig2-Cre* (K) mice and cultured in T3 containing differentiation medium for 3 days. Representative blots probed with anti-Myo1D, anti-LRP1β, and anti-β-actin. (g) Immunoblotting of lysates prepared from brain lysates of P56 *Lrp1* control (C) and *Lrp1$^{flox/flox}$;Olig2-Cre* (K) mice. Representative blots probed with anti-Myo1D, andti-LRP1β, and anti-β-actin. Results are shown as mean values ±SEM, *p<0.05 and **p<0.01, Student's *t*-test.

a

Gene Ontology Consortium

Biological Process	GO_term	Frequency	Genome frequency	P-value	Corrected P-value	Gene(s)
GO:0019220	regulation of phosphate metabolic process	0.27273	0.02490	0.00219	0.17493	myo1d,lrp1,fgd4,
GO:0051174	regulation of phosphorus metabolic process	0.27273	0.02493	0.00219	0.17552	myo1d,lrp1,fgd4,
GO:0016055	Wnt receptor signaling pathway	0.18182	0.00906	0.00426	0.34078	lrp1,lgr4,
GO:0045860	positive regulation of protein kinase activity	0.18182	0.00938	0.00456	0.36488	lrp1,fgd4,
GO:0031323	regulation of cellular metabolic process	0.45455	0.11417	0.00493	0.39479	myo1d,lrp1,lgr4,fgd4,zfp36l2,
GO:0033674	positive regulation of kinase activity	0.18182	0.01003	0.00519	0.41542	lrp1,fgd4,
GO:0051347	positive regulation of transferase activity	0.18182	0.01038	0.00555	0.44427	lrp1,fgd4,
GO:0044265	cellular macromolecule catabolic process	0.18182	0.01305	0.00865	0.69206	foxred2,zfp36l2,
GO:0050790	regulation of catalytic activity	0.27273	0.04231	0.00966	0.77284	myo1d,lrp1,fgd4,
GO:0019222	regulation of metabolic process	0.45455	0.13337	0.00967	0.77349	myo1d,lrp1,lgr4,fgd4,zfp36l2,
GO:0045859	regulation of protein kinase activity	0.18182	0.01417	0.01013	0.81029	lrp1,fgd4,
GO:0043549	regulation of kinase activity	0.18182	0.01517	0.01154	0.92321	lrp1,fgd4,
GO:0051338	regulation of transferase activity	0.18182	0.01573	0.01237	0.98920	lrp1,fgd4,
GO:0009057	macromolecule catabolic process	0.18182	0.01723	0.01470	1.00000	foxred2,zfp36l2,
GO:0006796	phosphate metabolic process	0.27273	0.04987	0.01511	1.00000	myo1d,lrp1,fgd4,
GO:0006793	phosphorus metabolic process	0.27273	0.04993	0.01516	1.00000	myo1d,lrp1,fgd4,
GO:0065009	regulation of molecular function	0.27273	0.05272	0.01754	1.00000	myo1d,lrp1,fgd4,
GO:0044237	cellular metabolic process	0.54545	0.22384	0.02026	1.00000	foxred2,myo1d,lrp1,lgr4,fgd4,zfp36l2,
GO:0001932	regulation of protein phosphorylation	0.18182	0.02064	0.02068	1.00000	lrp1,fgd4,
GO:0051336	regulation of hydrolase activity	0.18182	0.02143	0.02220	1.00000	myo1d,lrp1,
GO:0044260	cellular macromolecule metabolic process	0.45455	0.16512	0.02358	1.00000	foxred2,lrp1,lgr4,fgd4,zfp36l2,
GO:0043085	positive regulation of catalytic activity	0.18182	0.02217	0.02364	1.00000	lrp1,fgd4,
GO:0042325	regulation of phosphorylation	0.18182	0.02243	0.02417	1.00000	lrp1,fgd4,
GO:0060255	regulation of macromolecule metabolic process	0.36364	0.11073	0.02612	1.00000	lrp1,lgr4,fgd4,zfp36l2,
GO:0009987	cellular process	0.72727	0.39346	0.02633	1.00000	cntn6,foxred2,frmd4a,myo1d,lrp1,lgr4,fgd4,zfp36l2,
GO:0080090	regulation of primary metabolic process	0.36364	0.11152	0.02675	1.00000	lrp1,lgr4,fgd4,zfp36l2,
GO:0031399	regulation of protein modification process	0.18182	0.02487	0.02929	1.00000	lrp1,fgd4,
GO:0050794	regulation of cellular process	0.54545	0.24345	0.03028	1.00000	cntn6,myo1d,lrp1,lgr4,fgd4,zfp36l2,
GO:0044093	positive regulation of molecular function	0.18182	0.02731	0.03481	1.00000	lrp1,fgd4,
GO:0043170	macromolecule metabolic process	0.45455	0.18900	0.04045	1.00000	foxred2,lrp1,lgr4,fgd4,zfp36l2,
GO:0050789	regulation of biological process	0.54545	0.25965	0.04091	1.00000	cntn6,myo1d,lrp1,lgr4,fgd4,zfp36l2,
GO:0008152	metabolic process	0.54545	0.26565	0.04544	1.00000	foxred2,myo1d,lrp1,lgr4,fgd4,zfp36l2,
GO:0032268	regulation of cellular protein metabolic process	0.18182	0.03178	0.04589	1.00000	lrp1,fgd4,

Cellular Component	GO_term	Frequency	Genome frequency	P-value	Corrected P-value	Gene(s)
GO:0005623	cell	1.00000	0.45571	0.00018	0.00509	lrp1,lgr4,fgd4,flrt2,foxred2,tuba3a,tmem98,cntn6,frmd4a,myo1d,zfp36l2,
GO:0044464	cell part	1.00000	0.45571	0.00018	0.00509	lrp1,lgr4,fgd4,flrt2,foxred2,tuba3a,tmem98,cntn6,frmd4a,myo1d,zfp36l2,
GO:0005856	cytoskeleton	0.36364	0.04931	0.00147	0.04263	tuba3a,frmd4a,myo1d,fgd4,
GO:0043229	intracellular organelle	0.72727	0.28364	0.00290	0.08410	tmem98,tuba3a,foxred2,frmd4a,myo1d,lrp1,fgd4,zfp36l2,
GO:0043226	organelle	0.72727	0.28429	0.00295	0.08545	tmem98,tuba3a,foxred2,frmd4a,myo1d,lrp1,fgd4,zfp36l2,
GO:0015629	actin cytoskeleton	0.18182	0.00956	0.00473	0.13716	myo1d,fgd4,
GO:0005737	cytoplasm	0.63636	0.24674	0.00699	0.20268	tmem98,tuba3a,foxred2,frmd4a,lrp1,fgd4,zfp36l2,
GO:0042995	cell projection	0.27273	0.03843	0.00741	0.21489	tuba3a,lrp1,fgd4,
GO:0044424	intracellular part	0.72727	0.32598	0.00758	0.21974	tmem98,tuba3a,foxred2,frmd4a,myo1d,lrp1,fgd4,zfp36l2,
GO:0005622	intracellular	0.72727	0.33316	0.00878	0.25468	tmem98,tuba3a,foxred2,frmd4a,myo1d,lrp1,fgd4,zfp36l2,
GO:0043228	non-membrane-bounded organelle	0.36364	0.08312	0.00976	0.28310	tuba3a,frmd4a,myo1d,fgd4,
GO:0043232	intracellular non-membrane-bounded organelle	0.36364	0.08312	0.00976	0.28310	tuba3a,frmd4a,myo1d,fgd4,
GO:0044425	membrane part	0.54545	0.19938	0.01146	0.33238	flrt2,cntn6,tmem98,frmd4a,lrp1,lgr4,
GO:0005886	plasma membrane	0.36364	0.11270	0.02770	0.80325	cntn6,frmd4a,lrp1,lgr4,
GO:0031224	intrinsic to membrane	0.45455	0.17183	0.02770	0.80330	flrt2,cntn6,tmem98,lrp1,lgr4,
GO:0071944	cell periphery	0.36364	0.11514	0.02974	0.86246	cntn6,frmd4a,lrp1,lgr4,
GO:0016020	membrane	0.54545	0.24277	0.02988	0.86663	flrt2,cntn6,tmem98,frmd4a,lrp1,lgr4,
GO:0005783	endoplasmic reticulum	0.18182	0.03299	0.04909	1.00000	tmem98,foxred2,

Molecular Function	GO_term	Frequency	Genome frequency	P-value	Corrected P-value	Gene(s)
GO:0003779	actin binding	0.18182	0.00941	0.00459	0.04130	myo1d,fgd4,
GO:0008092	cytoskeletal protein binding	0.18182	0.01729	0.01480	0.13320	myo1d,fgd4,
GO:0046872	metal ion binding	0.27273	0.10106	0.09179	0.82614	lrp1,fgd4,zfp36l2,
GO:0043169	cation binding	0.27273	0.10232	0.09454	0.85083	lrp1,fgd4,zfp36l2,
GO:0043167	ion binding	0.27273	0.10267	0.09531	0.85778	lrp1,fgd4,zfp36l2,
GO:0005488	binding	0.54545	0.32157	0.10516	0.94644	foxred2,frmd4a,myo1d,lrp1,fgd4,zfp36l2,
GO:0005515	protein binding	0.36364	0.18291	0.12536	1.00000	frmd4a,myo1d,lrp1,fgd4,
GO:0003824	catalytic activity	0.18182	0.15054	0.50990	1.00000	foxred2,myo1d,

b

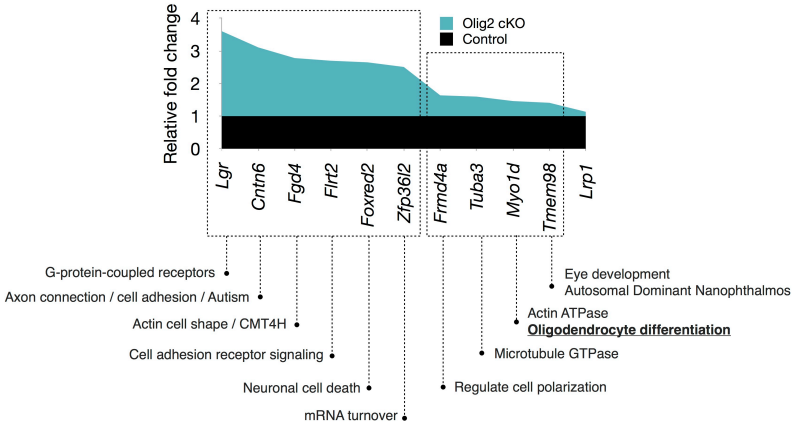

Figure 3.19: Gene ontology (GO) analysis of genes that are differentially regulated in *Lrp1* deficient OLs compares to *Lrp1* control OLs.
(a) Acutely isolated OLs from *Lrp1* control and *Lrp1*$^{flox/flox}$*;Olig2-Cre* mouse pups by anti-O4 immunopanning were subjected to microarray analysis. Differentially expressed genes with adjusted $p<0.05$ are subjected to gene ontology analysis by Gene Ontology Consortium online service. After enrichment analysis, GO terms associated with the 'Biological process', 'cellular component', and 'molecular function' with initial $p<0.05$ is listed. (b) The annotation of potential functions of the genes that are listed.

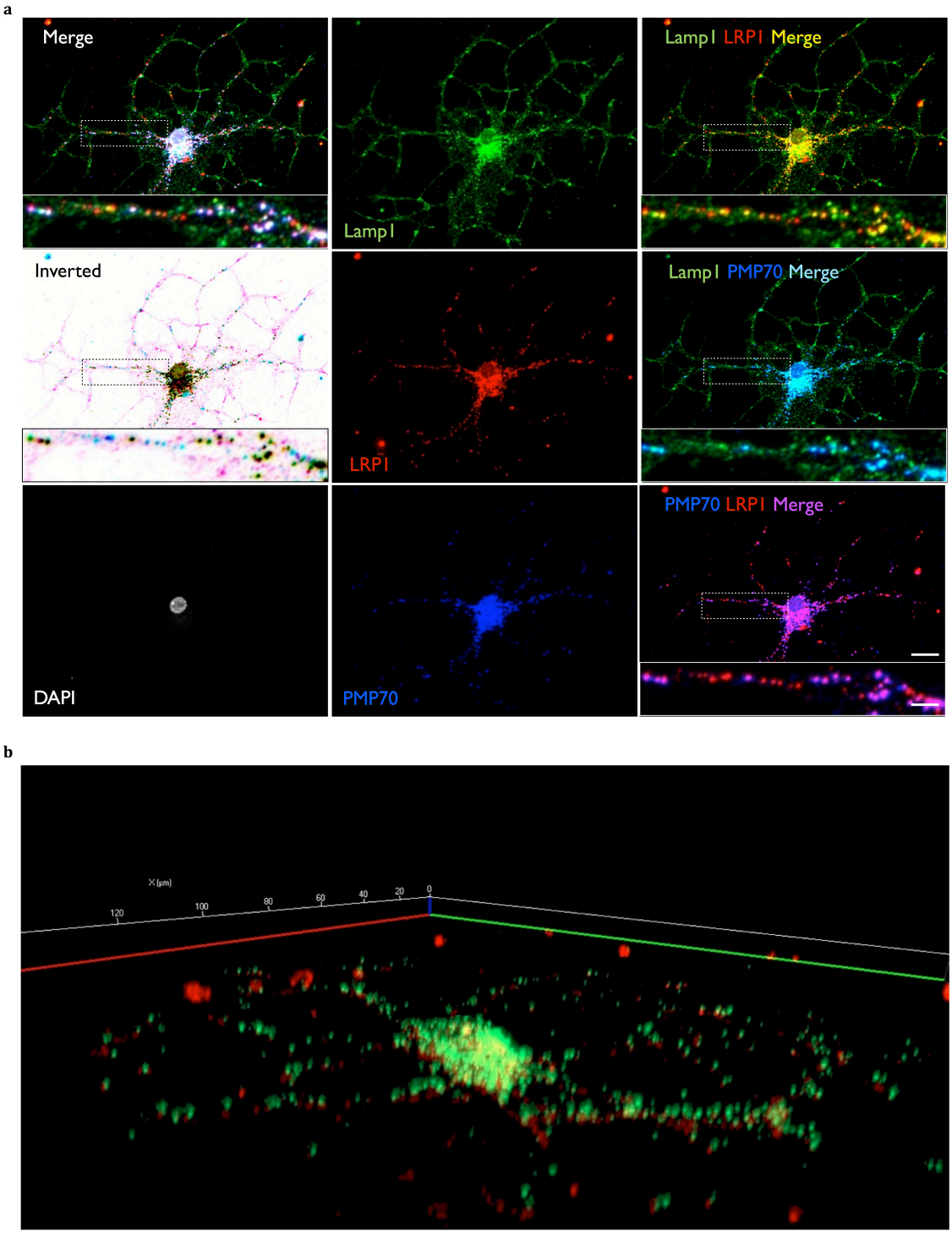
a
Merge
Lamp1
Lamp1 LRP1 Merge
Inverted
LRP1
Lamp1 PMP70 Merge
DAPI
PMP70
PMP70 LRP1 Merge
b
X (µm)
120
100
80
60
40
20
0

Figure 3.20: LRP1 staining in OLs is closely associated with peroxisomes and lysosomes

(a) Primary OLs prepared from *Lrp1* control pups, cultured for 5 days in DM were stained with anti-LRP1β, anti-LAMP1, anti-PMP70, and Hoechst dye 33342. Scale bar= 20μm (main panels) and 5μm (insets). (b) High magnification Z-stacked image of the OL from a. LRP1 (green) and PMP70 (Red).

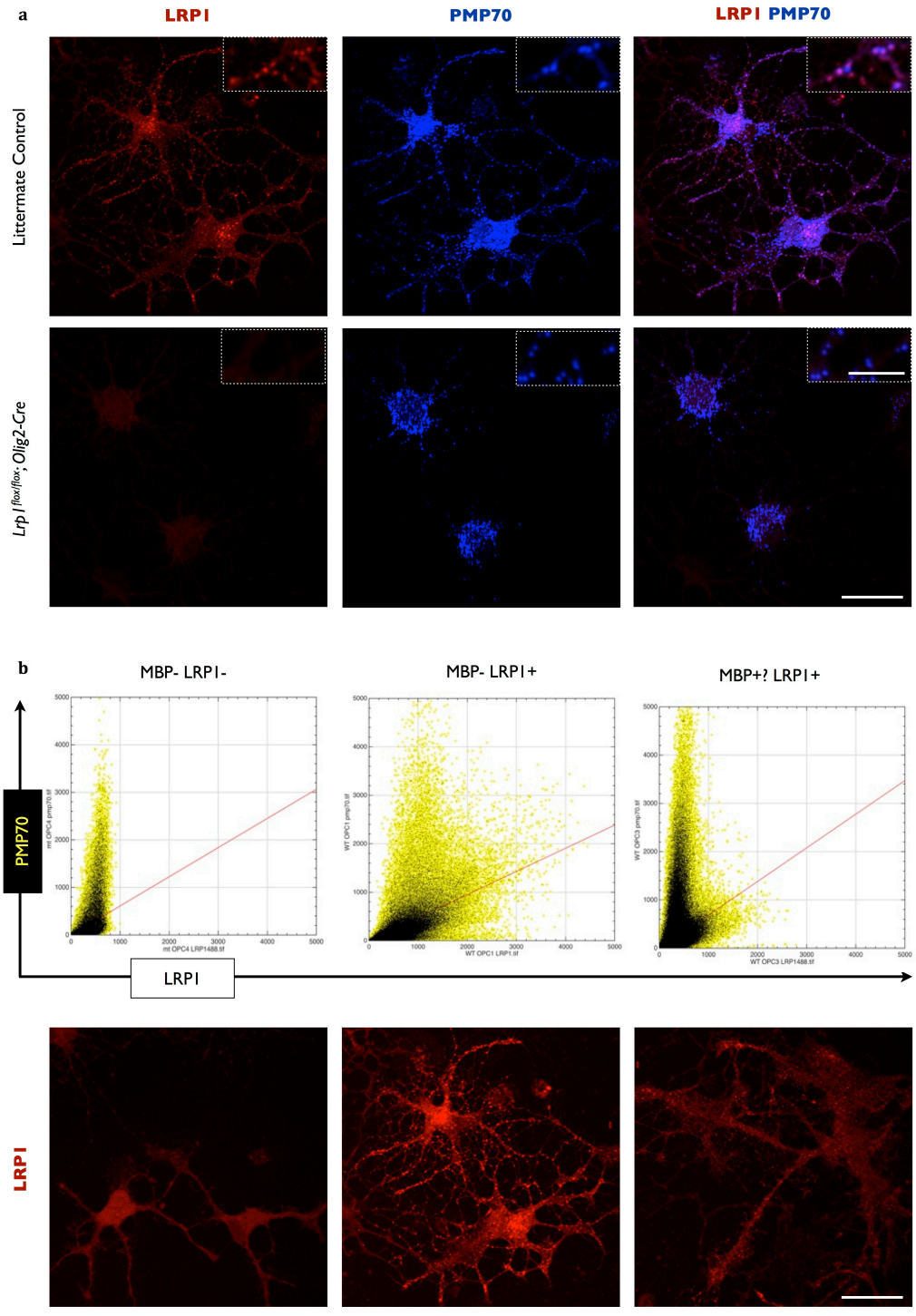
a
LRP1
PMP70
LRP1 PMP70
Littermate Control
Lrp1 flox/flox; Olig2-Cre
b
MBP- LRP1-
MBP- LRP1+
MBP+? LRP1+
PMP70
LRP1
LRP1

Figure 3.21: Co-localization analysis of LRP1 and PMP70 in OPCs and mature OLs.
(a) Primary OLs prepared from *Lrp1* control and cKO^{OL} OL pups, cultured for 5 days in DM were stained with anti-LRP1β and anti-PMP70. Scale bar= 20μm (main panels) and 5μm (insets). (b) Pixel distribution of LRP1 and PMP70 signals for calculating Pearson's correlation. Cells that are $MBP^-/LRP1^-$, $MBP^-/LRP1^+$, and $MBP^+/LRP1^+$ as showed in LRP1 labeling ere analyzed.

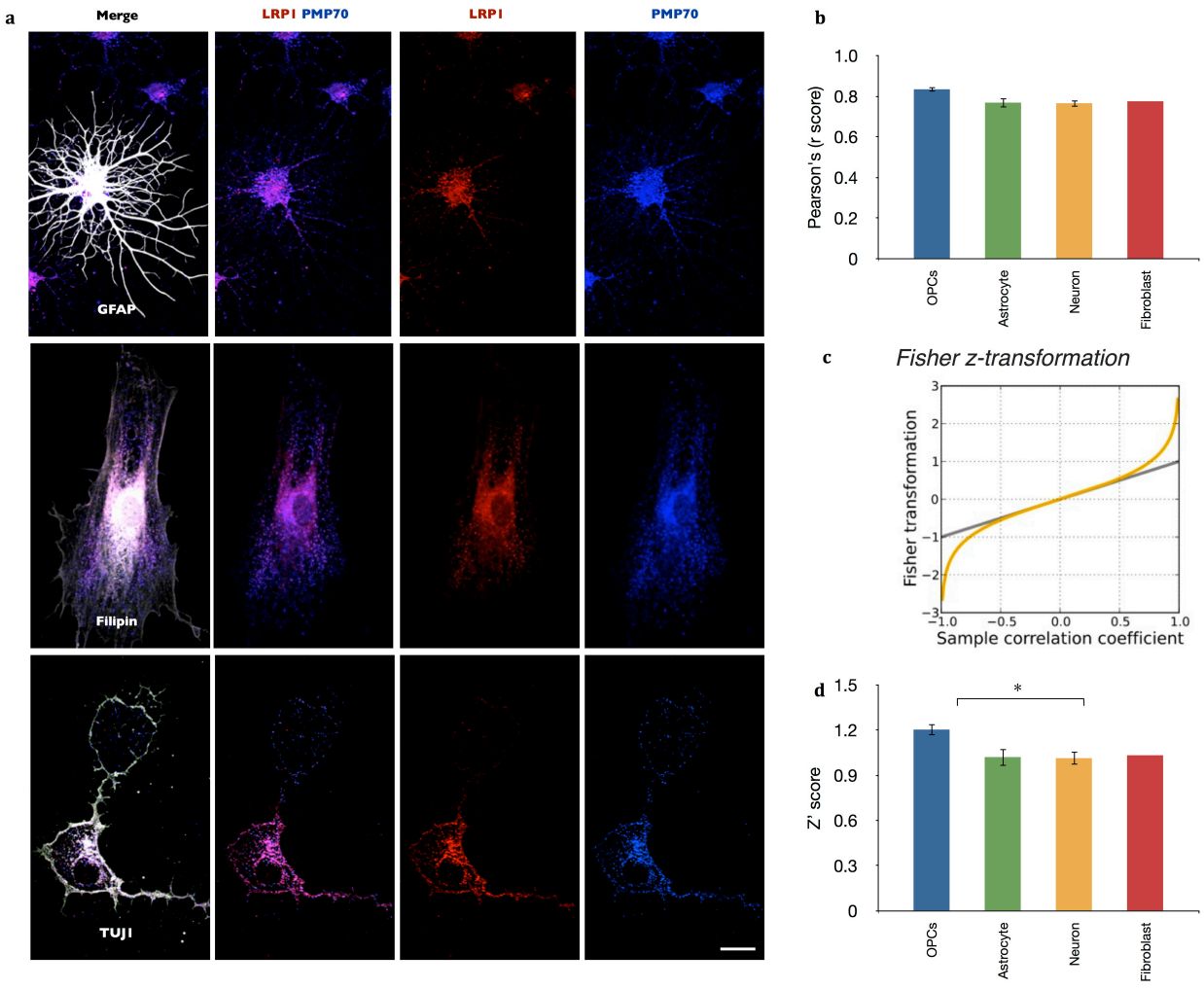
a
Merge
LRP1 PMP70
LRP1
PMP70
GFAP
Filipin
TUJ1
b
Pearson's (r score)
1.0
0.8
0.6
0.4
0.2
0
OPCs
Astrocyte
Neuron
Fibroblast
c
Fisher z-transformation
Fisher transformation
3
2
1
0
−1
−2
−3
−1.0
−0.5
0.0
0.5
1.0
Sample correlation coefficient
d
Z' score
1.5
1.2
0.9
0.6
0.3
0
*
OPCs
Astrocyte
Neuron
Fibroblast

Figure 3.22: Co-localization analysis of LRP1 and PMP70 in OPCs, astrocytes, epithelial cells, and neurons

(a) Each cell type was stained with anti-LRP1β and anti-PMP70. Scale bar= 20μm (b) Quantification of the Pearson's coefficient (n=3 cells) that are average for each cell type. (c) Figure adopted from Fisher z-transformation. Pearson's score does not follow a normal distribution. To perform Student's t-test statistic analysis, Fisher's z-transformation is required. (d) Quantification of the LRP1 and PMP70 co-localization score followed z-transformation to compare between each cell type. Results are shown as mean values ±SEM, *$p<0.05$ and **$p<0.01$, Student's *t*-test.

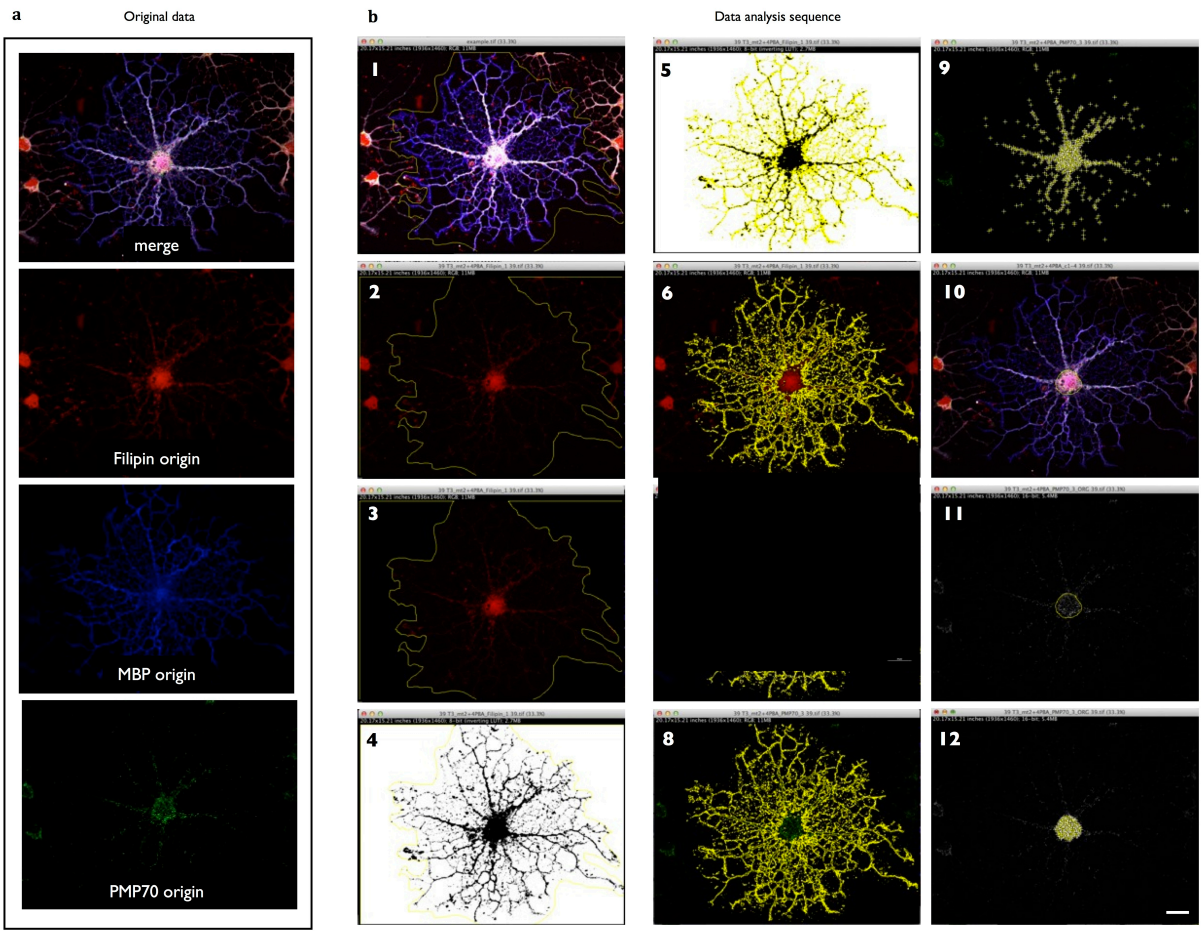
a
Original data
merge
Filipin origin
MBP origin
PMP70 origin
b
Data analysis sequence
1
2
3
4
5
6
8
9
10
11
12

Figure 3.23: Image processing rundown for single cell analysis
(a) Original images of each channel. As an example, OLs were stained with anti-MBP, anit-PMP70, and filipin. (b) Each step of imaging processing: 1, demarcate single isolated cells by hand drawing function in the image J; 2, apply the selection to the membrane staining channel (filipin or MBP) and reverse the selection; 3, delete the signal in the selected area (outside of the selected cell); 4, apply the binary signal threshold of with defined cutoff to the image acquired from 3; 5, create auto-selection along the silhouette of the cell; 6-8, apply the selection to the channel of interest and measure all features that is desired; 9, apply find maxima function to analyze particles to get sub-cellular coordinates; 10-12, information specific in the cell body can be isolated by free hand drawing function and then cell center can be determined.

3.8 **Tables**

Affymetrix mouse gene 2.1 ST array analysis

Symbol	Entrez Gene	Name	Relative Intensity		SEM		*p*-Value
			Control	cKO	Control	cKO	
Aamdc	66273	adipogenesis associated Mth938 domain containing	56.28	45.98	0.51	1.76	**0.001**
Abcf3	27406	ATP-binding cassette, sub-family F (GCN20), member 3	69.50	85.98	6.21	2.37	**0.048**
Abcg8	67470	ATP-binding cassette, sub-family G (WHITE), member 8	7.25	6.09	0.41	0.21	**0.045**
Abhd10	213012	abhydrolase domain containing 10	43.75	68.67	2.95	9.02	**0.039**
Abhd11	68758	abhydrolase domain containing 11	73.77	51.84	5.91	2.85	**0.015**
Abhd3	106861	abhydrolase domain containing 3	141.75	116.20	8.84	5.27	**0.048**
Acat2	110460	acetyl-Coenzyme A acetyltransferase 2	120.20	75.80	11.08	6.30	**0.013**
Acer1	171168	alkaline ceramidase 1	7.08	5.98	0.11	0.12	**0.001**
Acer2	230379	alkaline ceramidase 2	8.87	7.44	0.20	0.17	**0.002**
Acnat1	230161	acyl-coenzyme A amino acid N-acyltransferase 1	6.15	5.18	0.27	0.09	**0.014**
Actl7a	11470	actin-like 7a	9.98	7.24	0.62	0.21	**0.006**
Actn3	11474	actinin alpha 3	11.20	9.87	0.36	0.25	**0.024**
Actrt3	76652	actin related protein T3	7.47	5.88	0.59	0.17	**0.041**
Adam11	11488	a disintegrin and metallopeptidase domain 11	17.28	13.06	0.24	0.89	**0.004**
Adam20	384806	a disintegrin and metallopeptidase domain 20	3.93	4.26	0.12	0.06	**0.043**
Adam6a	238406	a disintegrin and metallopeptidase domain 6A	10.59	9.05	0.43	0.32	**0.03**
Adamts3	330119	a disintegrin-like and metallopeptidase (reprolysin type) with thrombospondin type 1 motif, 3	7.59	5.93	0.35	0.30	**0.012**
Adamts5	23794	a disintegrin-like and metallopeptidase (reprolysin type) with thrombospondin type 1 motif, 5 (aggrecanase-2)	15.81	12.28	1.22	0.60	**0.040**
Adamtsl1	77739	ADAMTS-like 1	7.48	8.93	0.27	0.49	**0.041**
Adat3	100113398	adenosine deaminase, tRNA-specific 3	19.60	14.99	0.83	0.95	**0.011**
Adat3	100113398	adenosine deaminase, tRNA-specific 3	19.60	14.99	0.83	0.95	**0.011**
Adcy2	210044	adenylate cyclase 2	25.46	31.48	1.30	1.36	**0.018**
Adcy4	104110	adenylate cyclase 4	7.88	6.55	0.48	0.19	**0.04**
Adh1	11522	alcohol dehydrogenase 1 (class I)	7.36	6.44	0.18	0.09	**0.004**
Adk	11534	adenosine kinase	57.56	81.94	4.70	8.27	**0.043**
Ado	211488	2-aminoethanethiol (cysteamine) dioxygenase	318.34	233.85	24.17	20.23	**0.036**
Adtrp	109254	androgen dependent TFPI regulating protein	6.19	4.84	0.49	0.25	**0.049**
Agl	77559	amylo-1,6-glucosidase, 4-alpha-glucanotransferase	70.51	87.24	2.93	2.37	**0.004**
Agpat1	55979	1-acylglycerol-3-phosphate O-acyltransferase 1 (lysophosphatidic acid acyltransferase, alpha)	110.30	126.43	4.08	4.75	**0.042**
AI314278	101521	expressed sequence AI314278	16.85	13.30	1.19	0.59	**0.037**
AI646519	99041	expressed sequence AI646519	9.79	8.34	0.10	0.34	**0.007**
Aida	108909	axin interactor, dorsalization associated	51.99	73.03	1.47	7.51	**0.033**
Aifm1	26926	apoptosis-inducing factor, mitochondrion-associated 1	77.57	58.92	4.48	5.31	**0.036**
Aim1l	230806	absent in melanoma 1-like	8.85	7.44	0.28	0.17	**0.005**
Aim2	383619	absent in melanoma 2	13.81	10.67	0.37	0.68	**0.007**
Aimp1	13722	aminoacyl tRNA synthetase complex-interacting multifunctional protein 1	433.74	312.12	37.88	31.50	**0.049**
Akap8l	54194	A kinase (PRKA) anchor protein 8-like	105.04	135.78	4.71	3.04	**0.002**
Akap9	100986	A kinase (PRKA) anchor protein (yotiao) 9	159.81	178.26	4.18	5.25	**0.033**
Akirin2	433693	akirin 2	278.84	249.51	5.15	9.40	**0.034**
Akna	100182	AT-hook transcription factor	17.56	22.10	1.08	1.19	**0.03**
Akr1a1	58810	aldo-keto reductase family 1, member A1 (aldehyde reductase)	652.81	614.13	3.59	11.50	**0.018**
Akr1b10	67861	aldo-keto reductase family 1, member B10 (aldose reductase)	20.15	28.10	2.02	1.93	**0.030**
Akr7a5	110198	aldo-keto reductase family 7, member A5 (aflatoxin aldehyde reductase)	25.87	20.03	0.93	0.28	**0.00**
Alad	17025	aminolevulinate, delta-, dehydratase	136.34	96.33	3.46	5.18	**0.001**
Aldh1a3	56847	aldehyde dehydrogenase family 1, subfamily A3	7.75	6.30	0.22	0.10	**0.001**
Aldh6a1	104776	aldehyde dehydrogenase family 6, subfamily A1	29.97	35.83	0.63	1.99	**0.0**
Alkbh8	67667	alkB, alkylation repair homolog 8 (E. coli)	75.04	104.26	6.07	6.05	**0.014**

Alox5	11689	arachidonate 5-lipoxygenase	58.20	26.36	9.65	3.19	**0.020**
Aloxe3	23801	arachidonate lipoxygenase 3	8.74	6.94	0.66	0.30	**0.047**
Alpi	76768	alkaline phosphatase, intestinal	8.17	7.05	0.19	0.41	**0.048**
Alpk2	225638	alpha-kinase 2	5.82	4.96	0.29	0.18	**0.046**
Ambn	11698	ameloblastin	7.22	6.55	0.12	0.22	**0.036**
Amd1	11702	S-adenosylmethionine decarboxylase 1	2930.47	3338.47	54.32	45.20	**0.001**
Amdhd2	245847	amidohydrolase domain containing 2	31.10	26.53	0.91	1.02	**0.016**
Amh	11705	anti-Mullerian hormone	9.01	7.83	0.46	0.10	**0.046**
Amica1	270152	adhesion molecule, interacts with CXADR antigen 1	7.89	6.89	0.29	0.11	**0.018**
Amigo3	320844	adhesion molecule with Ig like domain 3	23.91	16.89	1.67	0.63	**0.008**
Ammecr1l	225339	AMME chromosomal region gene 1-like	162.91	204.91	5.63	7.40	**0.004**
Amotl1	75723	angiomotin-like 1	24.92	21.40	1.18	0.62	**0.039**
Anapc13	69010	anaphase promoting complex subunit 13	1109.52	969.58	26.42	38.67	**0**
Ankdd1b	271144	ankyrin repeat and death domain containing 1B	9.83	8.04	0.58	0.40	**0.045**
Ankle2	71782	ankyrin repeat and LEM domain containing 2	97.38	112.85	1.74	3.76	**0.010**
Ankmy2	217473	ankyrin repeat and MYND domain containing 2	71.74	99.84	9.40	3.70	**0.032**
Ankrd10	102334	ankyrin repeat domain 10	21.68	26.34	1.05	0.81	**0.013**
Ankrd11	77087	ankyrin repeat domain 11	140.34	167.52	5.78	6.36	**0.020**
Ankrd36	76389	ankyrin repeat domain 36	10.34	9.25	0.26	0.26	**0.024**
Ankrd39	109346	ankyrin repeat domain 39	23.51	17.36	1.82	0.85	**0.022**
Anks1b	77531	ankyrin repeat and sterile alpha motif domain containing 1B	146.64	160.65	4.86	2.99	**0.050**
Ano2	243634	anoctamin 2	11.61	9.39	0.83	0.28	**0.044**
Anxa6	11749	annexin A6	97.88	129.31	8.64	5.77	**0.023**
Ap1m2	11768	adaptor protein complex AP-1, mu 2 subunit	8.57	7.10	0.52	0.18	**0.037**
Ap4m1	11781	adaptor-related protein complex AP-4, mu 1	36.02	41.63	1.87	1.16	**0.043**
Apbb1	11785	amyloid beta (A4) precursor protein-binding, family B, member 1	154.80	99.62	8.59	9.85	**0.006**
Apbb1ip	54519	amyloid beta (A4) precursor protein-binding, family B, member 1 interacting protein	84.62	105.11	6.47	2.83	**0.027**
Apbb2	11787	amyloid beta (A4) precursor protein-binding, family B, member 2	133.00	118.14	4.02	2.43	**0.02**
Apbb3	225372	amyloid beta (A4) precursor protein-binding, family B, member 3	23.54	18.20	1.64	0.92	**0.030**
Apc2	23805	adenomatosis polyposis coli 2	71.65	56.83	3.71	1.87	**0.012**
Apex1	11792	apurinic/apyrimidinic endonuclease 1	121.89	101.86	6.34	3.67	**0.034**
Aplp1	11803	amyloid beta (A4) precursor-like protein 1	407.46	284.13	26.21	26.58	**0.016**
Aplp2	11804	amyloid beta (A4) precursor-like protein 2	594.16	626.01	4.60	9.87	**0.026**
Apoa4	11808	apolipoprotein A-IV	9.72	8.27	0.44	0.37	**0.045**
Apoa5	66113	apolipoprotein A-V	9.39	6.67	0.45	0.19	**0.001**
Apob	238055	apolipoprotein B	7.96	6.59	0.34	0.09	**0.008**
Apobec2	11811	apolipoprotein B mRNA editing enzyme, catalytic polypeptide 2	11.28	9.33	0.15	0.74	**0.042**
Apoc2	11813	apolipoprotein C-II	10.72	8.38	0.72	0.45	**0.033**
App	11820	amyloid beta (A4) precursor protein	733.66	619.83	21.81	37.76	**0.04**
Aqp2	11827	aquaporin 2	10.70	9.46	0.34	0.36	**0.046**
Aqp9	64008	aquaporin 9	9.37	7.76	0.33	0.44	**0.026**
Arc	11838	activity regulated cytoskeletal-associated protein	36.92	28.41	1.73	0.89	**0.005**
Arfip1	99889	ADP-ribosylation factor interacting protein 1	5.11	4.54	0.12	0.12	**0.016**
Arhgap4	171207	Rho GTPase activating protein 4	26.24	17.56	2.08	1.51	**0.015**
Arhgap40	545481	Rho GTPase activating protein 40	11.55	9.26	0.49	0.40	**0.01**
Arhgap6	11856	Rho GTPase activating protein 6	7.69	6.57	0.31	0.17	**0.020**
Arhgef18	102098	rho/rac guanine nucleotide exchange factor (GEF) 18	25.88	19.35	2.03	0.50	**0.02**
Arhgef26	622434	Rho guanine nucleotide exchange factor (GEF) 26	49.15	64.64	5.74	2.54	**0.049**
Arl1	104303	ADP-ribosylation factor-like 1	90.52	96.60	1.25	1.94	**0.039**
Arl14epl	381142	ADP-ribosylation factor-like 14 effector protein-like	11.67	10.31	0.29	0.21	**0.01**
Arl4c	320982	ADP-ribosylation factor-like 4C	51.50	66.48	3.58	2.45	**0.014**
Arl5c	217151	ADP-ribosylation factor-like 5C	10.07	13.66	0.91	0.38	**0.0**
Arl6ip4	65105	ADP-ribosylation factor-like 6 interacting protein 4	111.26	85.77	4.84	6.51	**0.020**
Arl8b	67166	ADP-ribosylation factor-like 8B	466.82	428.75	6.66	10.69	**0.023**
Arpc5	67771	actin related protein 2/3 complex, subunit 5	572.14	487.42	26.19	4.30	**0.019**
Asah1	11886	N-acylsphingosine amidohydrolase 1	233.02	269.93	7.50	11.35	**0.035**
Asb17os	72317	ankyrin repeat and SOCS box-containing 17, opposite strand	7.69	12.00	0.26	1.52	**0.032**
Asb9	69299	ankyrin repeat and SOCS box-containing 9	9.17	7.58	0.54	0.08	**0.026**
Asprv1	67855	aspartic peptidase, retroviral-like 1	10.56	8.09	0.37	0.44	**0.005**
Atad3a	108888	ATPase family, AAA domain containing 3A	50.60	39.15	2.47	1.84	**0.010**

Atad5	237877	ATPase family, AAA domain containing 5	19.54	29.93	0.48	3.75	**0.033**
Atg101	68118	autophagy related 101	44.10	37.85	1.65	1.70	**0.039**
Atg4c	242557	autophagy related 4C, cysteine peptidase	28.55	42.81	2.63	4.91	**0.043**
Atg7	74244	autophagy related 7	87.89	61.68	8.69	4.78	**0.038**
Atg7	74244	autophagy related 7	87.89	61.68	8.69	4.78	**0.038**
Atl1	73991	atlastin GTPase 1	74.45	111.53	6.90	10.71	**0.027**
Atp13a3	224088	ATPase type 13A3	164.98	204.06	7.14	13.41	**0.04**
Atp13a4	224079	ATPase type 13A4	12.92	15.10	0.26	0.80	**0.041**
Atp1a2	98660	ATPase, Na+/K+ transporting, alpha 2 polypeptide	507.45	570.85	4.90	18.13	**0.015**
Atp1b1	11931	ATPase, Na+/K+ transporting, beta 1 polypeptide	114.38	145.71	4.22	9.32	**0.022**
Atp2a1	11937	ATPase, Ca++ transporting, cardiac muscle, fast twitch 1	8.43	7.47	0.23	0.21	**0.02**
Atp2a3	53313	ATPase, Ca++ transporting, ubiquitous	9.51	7.63	0.19	0.48	**0.011**
Atp5o	28080	ATP synthase, H+ transporting, mitochondrial F1 complex, O subunit	14.07	11.19	0.57	0.50	**0.009**
ATP6	17705	ATP synthase F0 subunit 6	2219.60	2476.88	28.13	32.73	**0.001**
Atp6v0a2	21871	ATPase, H+ transporting, lysosomal V0 subunit A2	200.52	160.13	10.10	10.31	**0.031**
Atp6v0a4	140494	ATPase, H+ transporting, lysosomal V0 subunit A4	9.08	6.97	0.51	0.33	**0.01**
ATP8	17706	ATP synthase F0 subunit 8	1509.93	1655.94	42.12	29.13	**0.029**
Atp8a1	11980	ATPase, aminophospholipid transporter (APLT), class I, type 8A, member 1	187.79	218.85	6.09	4.77	**0.007**
Atrx	22589	alpha thalassemia/mental retardation syndrome X-linked homolog (human)	162.23	194.83	1.81	6.62	**0.003**
Atxn1	20238	ataxin 1	33.94	56.45	5.32	6.05	**0.031**
AU015228	99169	expressed sequence AU015228	4.88	4.28	0.12	0.16	**0.03**
AU018091	245128	expressed sequence AU018091	12.49	10.01	0.69	0.56	**0.032**
AU021092	239691	expressed sequence AU021092	23.35	17.24	1.23	1.30	**0.014**
AU022751	102991	expressed sequence AU022751	15.03	12.88	0.57	0.42	**0.023**
Aup1	11993	ancient ubiquitous protein 1	169.89	200.79	4.13	11.83	**0.05**
AV320801	331531	expressed sequence AV320801	6.75	5.61	0.23	0.18	**0.008**
Aven	74268	apoptosis, caspase activation inhibitor	13.57	10.87	0.58	0.66	**0.022**
Avl9	78937	AVL9 homolog (S. cerevisiase)	105.74	131.22	7.37	3.47	**0.020**
Avpr1b	26361	arginine vasopressin receptor 1B	6.95	5.69	0.46	0.14	**0.040**
AW046200	100502619	expressed sequence AW046200	9.92	7.63	0.53	0.42	**0.015**
Awat2	245532	acyl-CoA wax alcohol acyltransferase 2	6.84	6.00	0.15	0.30	**0.046**
Azin1	54375	antizyme inhibitor 1	131.28	163.54	7.11	9.12	**0.03**
B020004J07 Rik	545662	RIKEN cDNA B020004J07 gene	3.91	4.25	0.10	0.08	**0.03**
B020018J22 Rik	100126692	Riken cDNA B020018J22 gene	9.52	7.29	0.40	0.10	**0.002**
B230112J18 Rik	77846	RIKEN cDNA B230112J18 gene	9.55	6.97	0.79	0.29	**0.021**
B230317F23 Rik	320383	RIKEN cDNA B230317F23 gene	27.96	19.67	2.75	0.84	**0.028**
B4galt4	56375	UDP-Gal:betaGlcNAc beta 1,4-galactosyltransferase, polypeptide 4	14.20	17.94	1.21	0.49	**0.029**
B630019A10 Rik	100043541	RIKEN cDNA B630019A10 gene	21.04	14.15	1.08	2.32	**0.036**
B930095G15 Rik	320268	RIKEN cDNA B930095G15 gene	81.40	116.68	8.02	11.26	**0.043**
Bace1	23821	beta-site APP cleaving enzyme 1	284.13	235.59	13.45	14.18	**0.048**
Bag2	213539	BCL2-associated athanogene 2	12.73	8.90	1.42	0.40	**0.040**
Baiap2l2	207495	BAI1-associated protein 2-like 2	16.38	12.62	0.94	0.85	**0.025**
Batf3	381319	basic leucine zipper transcription factor, ATF-like 3	23.32	15.22	1.20	0.54	**0.001**
Bax	12028	BCL2-associated X protein	350.51	290.20	17.49	15.11	**0.040**
Bbs7	71492	Bardet-Biedl syndrome 7 (human)	37.06	45.49	2.05	1.88	**0.023**
BC005512	192885	cDNA sequence BC005512	13.80	18.91	0.46	0.84	**0.002**
BC017643	217370	cDNA sequence BC017643	22.01	14.99	2.22	1.17	**0.031**
BC039771	408057	cDNA sequence BC039771	6.37	5.58	0.07	0.10	**0.001**
BC048602	100126269	cDNA sequence BC048602	7.50	9.37	0.64	0.41	**0.049**
BC049352	408059	cDNA sequence BC049352	6.88	5.94	0.11	0.31	**0.029**
BC051665	218275	cDNA sequence BC051665	6.93	5.68	0.34	0.15	**0.015**

BC100451	58251	cDNA sequence BC100451	11.00	8.07	1.03	0.30	**0.035**
BC107364	329716	cDNA sequence BC107364	11.00	9.19	0.51	0.46	**0.04**
Bcam	57278	basal cell adhesion molecule	9.72	7.68	0.35	0.31	**0.005**
Bcap29	12033	B cell receptor associated protein 29	179.08	228.61	10.08	10.77	**0.015**
Bche	12038	butyrylcholinesterase	121.18	198.19	8.70	29.61	**0.047**
Bckdhb	12040	branched chain ketoacid dehydrogenase E1, beta polypeptide	77.06	57.65	3.12	3.28	**0.005**
Bcl6	12053	B cell leukemia/lymphoma 6	16.97	31.24	2.15	1.46	**0.002**
Bdkrb1	12061	bradykinin receptor, beta 1	7.56	5.51	0.66	0.27	**0.028**
Bend4	666938	BEN domain containing 4	21.13	14.99	1.46	0.59	**0.008**
Bfsp1	12075	beaded filament structural protein 1, in lens-CP94	8.07	7.06	0.26	0.14	**0.015**
Bhlha15	17341	basic helix-loop-helix family, member a15	15.06	12.27	1.06	0.28	**0.043**
Bid	12122	BH3 interacting domain death agonist	20.34	15.59	0.89	0.35	**0.003**
Bik	12124	BCL2-interacting killer	11.85	8.86	0.77	0.73	**0.030**
Blnk	17060	B cell linker	27.06	36.45	1.20	1.87	**0.005**
Bloc1s2	73689	biogenesis of lysosomal organelles complex-1, subunit 2	254.01	211.29	15.59	6.29	**0.044**
Bms1	213895	BMS1 homolog, ribosome assembly protein (yeast)	57.22	67.64	3.16	1.53	**0.025**
Bnip2	12175	BCL2/adenovirus E1B interacting protein 2	185.26	227.25	5.77	8.46	**0.006**
Bpgm	12183	2,3-bisphosphoglycerate mutase	144.96	160.41	4.12	3.21	**0.025**
Bpifa2	19194	BPI fold containing family A, member 2	7.33	6.56	0.20	0.14	**0.020**
Braf	109880	Braf transforming gene	126.06	166.25	5.58	5.30	**0.002**
Brwd1	93871	bromodomain and WD repeat domain containing 1	84.66	71.69	3.15	2.70	**0.020**
Bsx	244813	brain specific homeobox	8.92	7.32	0.32	0.21	**0.006**
Btc	12223	betacellulin, epidermal growth factor family member	7.06	6.40	0.19	0.12	**0.026**
Btf3	218490	basic transcription factor 3	39.31	30.75	1.44	2.08	**0.015**
Btnl9	237754	butyrophilin-like 9	9.95	7.63	0.67	0.32	**0.021**
Btrc	12234	beta-transducin repeat containing protein	93.07	107.30	3.66	4.14	**0.042**
Bysl	53414	bystin-like	49.49	33.93	2.94	1.73	**0.004**
C1ql4	239659	complement component 1, q subcomponent-like 4	6.96	5.72	0.30	0.23	**0.017**
C1qtnf7	109323	C1q and tumor necrosis factor related protein 7	7.33	6.31	0.30	0.27	**0.045**
C1rl	232371	complement component 1, r subcomponent-like	23.93	17.81	1.44	1.39	**0.022**
C5ar2	319430	complement component 5a receptor 2	10.60	9.04	0.38	0.42	**0.033**
C78197	100504352	expressed sequence C78197	7.38	5.82	0.41	0.33	**0.025**
Cables2	252966	CDK5 and Abl enzyme substrate 2	50.07	61.63	3.18	2.98	**0.038**
Cabs1	70977	calcium binding protein, spermatid specific 1	6.15	6.81	0.11	0.16	**0.015**
Cacna1c	12288	calcium channel, voltage-dependent, L type, alpha 1C subunit	41.21	55.47	2.78	3.11	**0.014**
Cacna1f	54652	calcium channel, voltage-dependent, alpha 1F subunit	7.19	5.72	0.32	0.23	**0.010**
Calcb	116903	calcitonin-related polypeptide, beta	9.02	10.89	0.21	0.68	**0.039**
Calhm2	72691	calcium homeostasis modulator 2	12.78	11.12	0.58	0.23	**0.038**
Camkk1	55984	calcium/calmodulin-dependent protein kinase kinase 1, alpha	11.12	13.76	0.42	0.80	**0.026**
Camta2	216874	calmodulin binding transcription activator 2	38.17	44.79	2.03	1.71	**0.047**
Capn7	12339	calpain 7	207.78	244.24	8.21	7.92	**0.019**
Caprin2	232560	caprin family member 2	30.93	35.05	0.82	1.25	**0.032**
Capza1	12340	capping protein (actin filament) muscle Z-line, alpha 1	545.00	623.32	14.25	12.05	**0.006**
Capza2	12343	capping protein (actin filament) muscle Z-line, alpha 2	341.88	366.57	4.11	6.61	**0.019**
Capza2	12343	capping protein (actin filament) muscle Z-line, alpha 2	598.97	694.22	18.95	32.33	**0.044**
Car13	71934	carbonic anhydrase 13	11.21	8.41	0.85	0.59	**0.036**
Car14	23831	carbonic anhydrase 14	77.05	46.80	9.34	7.66	**0.046**
Car15	80733	carbonic anhydrase 15	21.49	14.24	2.21	1.34	**0.031**
Car8	12319	carbonic anhydrase 8	212.20	263.52	10.80	16.66	**0.04**
Card11	108723	caspase recruitment domain family, member 11	8.68	7.54	0.18	0.32	**0.021**
Casr	12374	calcium-sensing receptor	102.66	65.48	3.18	9.96	**0.012**
Casz1	69743	castor zinc finger 1	11.72	10.31	0.23	0.25	**0.006**
Cbln3	56410	cerebellin 3 precursor protein	9.99	7.75	0.61	0.28	**0.015**
Cbr2	12409	carbonyl reductase 2	14.42	20.04	1.49	1.74	**0.049**
Cc2d2b	668310	coiled-coil and C2 domain containing 2B	7.38	5.84	0.30	0.48	**0.035**
Ccar1	67500	cell division cycle and apoptosis regulator 1	302.53	346.67	11.69	9.70	**0.027**
Ccdc114	211535	coiled-coil domain containing 114	9.50	8.27	0.12	0.25	**0.005**
Ccdc122	108811	coiled-coil domain containing 122	13.00	16.74	1.25	0.67	**0.039**
Ccdc137	67291	coiled-coil domain containing 137	38.41	32.71	1.38	1.20	**0.021**
Ccdc158	320696	coiled-coil domain containing 158	6.25	5.21	0.32	0.10	**0.020**

Ccdc167	68597	coiled-coil domain containing 167	99.67	71.85	7.61	3.28	**0.015**
Ccdc172	75645	coiled-coil domain containing 172	5.14	4.77	0.11	0.10	**0.050**
Ccdc178	70950	coiled coil domain containing 178	4.87	4.59	0.08	0.06	**0.031**
Ccdc185	433386	coiled-coil domain containing 185	8.93	7.52	0.22	0.29	**0.008**
Ccdc36	434438	coiled-coil domain containing 36	7.67	9.34	0.36	0.45	**0.027**
Ccdc39	51938	coiled-coil domain containing 39	24.50	36.05	1.46	2.72	**0.010**
Ccdc42	276920	coiled-coil domain containing 42	8.99	7.72	0.41	0.19	**0.032**
Ccdc69	52570	coiled-coil domain containing 69	9.45	7.34	0.56	0.20	**0.01**
Ccdc88a	108686	coiled coil domain containing 88A	442.93	499.38	12.41	18.46	**0.044**
Ccnb1ip1	239083	cyclin B1 interacting protein 1	5.56	4.82	0.25	0.08	**0.032**
Ccny	67974	cyclin Y	240.32	287.74	8.83	17.12	**0.049**
Ccser2	72972	coiled-coil serine rich 2	660.84	783.02	23.18	27.41	**0.014**
Cct2	12461	chaperonin containing Tcp1, subunit 2 (beta)	1032.51	900.80	21.21	31.36	**0.013**
Cct2	12461	chaperonin containing Tcp1, subunit 2 (beta)	763.14	705.62	16.61	15.04	**0.042**
Cd101	630146	CD101 antigen	11.96	9.69	0.50	0.65	**0.033**
Cd163l1	244233	CD163 molecule-like 1	11.86	10.32	0.54	0.31	**0.050**
Cd164	53599	CD164 antigen	759.21	878.59	25.33	21.57	**0.012**
Cd200r4	239849	CD200 receptor 4	6.51	5.31	0.33	0.21	**0.023**
Cd209g	70192	CD209g antigen	6.01	7.04	0.38	0.07	**0.037**
Cd38	12494	CD38 antigen	18.63	26.47	0.75	2.18	**0.01**
Cd3d	12500	CD3 antigen, delta polypeptide	8.21	6.81	0.41	0.18	**0.020**
Cd3e	12501	CD3 antigen, epsilon polypeptide	6.80	5.73	0.25	0.16	**0.01**
Cd4	12504	CD4 antigen	7.07	6.08	0.20	0.23	**0.017**
Cd8b1	12526	CD8 antigen, beta chain 1	6.91	5.36	0.59	0.22	**0.050**
Cdh16	12556	cadherin 16	10.42	8.53	0.41	0.33	**0.01**
Cdh22	104010	cadherin 22	24.16	17.10	1.79	0.76	**0.011**
Cdh23	22295	cadherin 23 (otocadherin)	5.91	5.33	0.12	0.12	**0.017**
Cdh24	239096	cadherin-like 24	16.27	11.67	1.08	0.89	**0.016**
Cdhr1	170677	cadherin-related family member 1	11.75	8.73	0.98	0.21	**0.024**
Cdhr4	69398	cadherin-related family member 4	9.04	7.34	0.27	0.54	**0.03**
Cdk15	271697	cyclin-dependent kinase 15	7.19	5.91	0.24	0.42	**0.038**
Cdkal1	68916	CDK5 regulatory subunit associated protein 1-like 1	24.26	31.99	0.25	2.30	**0.02**
Cdkn3	72391	cyclin-dependent kinase inhibitor 3	34.72	55.61	6.43	3.14	**0.027**
Cdnf	227526	cerebral dopamine neurotrophic factor	5.91	5.09	0.23	0.23	**0.045**
Cdpf1	72355	cysteine rich, DPF motif domain containing 1	23.31	20.80	0.44	0.53	**0.011**
Cdrt4	66338	CMT1A duplicated region transcript 4	9.19	7.70	0.53	0.24	**0.041**
Cdsn	386463	corneodesmosin	15.59	11.43	1.20	0.76	**0.026**
Cdx2	12591	caudal type homeobox 2	7.63	5.99	0.43	0.12	**0.010**
Cdyl	12593	chromodomain protein, Y chromosome-like	31.30	25.64	0.92	0.60	**0.002**
Ceacam13	69785	carcinoembryonic antigen-related cell adhesion molecule 13	3.97	4.42	0.04	0.04	**0.000**
Ceacam14	67084	carcinoembryonic antigen-related cell adhesion molecule 14	5.76	7.49	0.07	0.22	**0.000**
Ceacam18	72431	carcinoembryonic antigen-related cell adhesion molecule 18	7.25	5.16	0.42	0.26	**0.005**
Cela1	109901	chymotrypsin-like elastase family, member 1	11.55	8.77	0.17	0.17	**2E-05**
Celf5	319586	CUGBP, Elav-like family member 5	27.39	23.91	0.34	1.13	**0.026**
Celf6	76183	CUGBP, Elav-like family member 6	13.16	10.11	0.61	0.32	**0.004**
Cep19	66994	centrosomal protein 19	49.39	62.99	3.50	2.60	**0.021**
Cep44	382010	centrosomal protein 44	25.14	32.78	0.87	1.68	**0.007**
Cep57l1	103268	centrosomal protein 57-like 1	32.04	24.20	2.15	1.31	**0.021**
Cers5	71949	ceramide synthase 5	91.50	126.15	5.89	10.11	**0.03**
Ces1g	12623	carboxylesterase 1G	7.98	6.33	0.45	0.24	**0.018**
Ces2c	234671	carboxylesterase 2C	5.01	3.78	0.18	0.11	**0.001**
Ces2f	71903	carboxylesterase 2F	4.92	5.63	0.10	0.07	**0.001**
Cfap20	14894	cilia and flagella associated protein 20	120.17	182.56	10.09	18.74	**0.026**
Chaf1b	110749	chromatin assembly factor 1, subunit B (p60)	8.78	10.57	0.62	0.18	**0.032**
Chchd7	66433	coiled-coil-helix-coiled-coil-helix domain containing 7	27.40	21.98	1.91	0.94	**0.0**
Chl1	12661	cell adhesion molecule with homology to L1CAM	104.93	124.45	6.34	2.48	**0.028**
Chn2	69993	chimerin 2	309.66	253.88	17.07	11.26	**0.034**
Chrdl1	83453	chordin-like 1	68.32	107.40	6.20	5.12	**0.003**
Chrna2	110902	cholinergic receptor, nicotinic, alpha polypeptide 2 (neuronal)	13.91	9.41	0.60	0.64	**0.002**
Chrna9	231252	cholinergic receptor, nicotinic, alpha polypeptide 9	9.99	8.31	0.08	0.50	**0.016**
Chrnb3	108043	cholinergic receptor, nicotinic, beta polypeptide 3	6.12	5.54	0.05	0.11	**0.003**

Cisd1	52637	CDGSH iron sulfur domain 1	153.74	131.51	5.75	4.89	**0.026**
Clca2	80797	chloride channel calcium activated 2	6.24	8.64	0.76	0.55	**0.043**
Clca3	23844	chloride channel calcium activated 3	5.88	5.38	0.19	0.06	**0.045**
Cldn1	12737	claudin 1	9.46	7.99	0.31	0.37	**0.023**
Cldn24	100039801	claudin 24	5.91	4.90	0.37	0.09	**0.038**
Cldn26	74720	claudin 26	10.71	9.72	0.16	0.29	**0.025**
Cldn5	12741	claudin 5	10.33	7.61	0.36	0.44	**0.003**
Clec2d	93694	C-type lectin domain family 2, member d	6.56	7.77	0.15	0.35	**0.018**
Clec4f	51811	C-type lectin domain family 4, member f	15.44	12.80	0.62	0.30	**0.009**
Clic1	114584	chloride intracellular channel 1	108.24	147.39	5.83	4.54	**0.002**
Clic5	224796	chloride intracellular channel 5	12.92	9.92	0.83	0.80	**0.040**
Clic6	209195	chloride intracellular channel 6	6.71	5.42	0.49	0.18	**0.048**
Clpx	270166	caseinolytic mitochondrial matrix peptidase chaperone subunit	87.43	110.05	5.86	4.54	**0.022**
Clrn2	624224	clarin 2	9.15	7.48	0.37	0.50	**0.036**
Clta	12757	clathrin, light polypeptide (Lca)	510.79	457.57	10.29	6.59	**0.005**
Cltc	67300	clathrin, heavy polypeptide (Hc)	332.02	377.09	11.86	11.29	**0.033**
Cmtm2b	75502	CKLF-like MARVEL transmembrane domain containing 2B	5.36	6.05	0.20	0.08	**0.021**
Cmtm7	102545	CKLF-like MARVEL transmembrane domain containing 7	56.58	42.44	4.34	3.63	**0.047**
Cnep1r1	382030	CTD nuclear envelope phosphatase 1 regulatory subunit 1	50.34	76.33	2.85	8.52	**0.028**
Cnga4	233649	cyclic nucleotide gated channel alpha 4	7.95	6.96	0.26	0.21	**0.024**
Cngb1	333329	cyclic nucleotide gated channel beta 1	19.56	16.87	0.55	0.60	**0.016**
Cnn3	71994	calponin 3, acidic	270.23	305.93	11.36	6.86	**0.04**
Cnot2	72068	CCR4-NOT transcription complex, subunit 2	155.62	179.37	4.61	7.14	**0.031**
Cntn6	53870	contactin 6	56.48	115.63	4.64	7.95	**0.001**
Col13a1	12817	collagen, type XIII, alpha 1	9.76	8.01	0.62	0.20	**0.035**
Col18a1	12822	collagen, type XVIII, alpha 1	10.92	8.27	0.84	0.08	**0.020**
Col1a1	12842	collagen, type I, alpha 1	203.31	165.67	9.33	6.64	**0.017**
Col2a1	12824	collagen, type II, alpha 1	18.75	23.38	0.63	1.78	**0.050**
Col4a4	12829	collagen, type IV, alpha 4	10.88	9.81	0.27	0.10	**0.010**
Col4a5	12830	collagen, type IV, alpha 5	10.92	9.45	0.26	0.12	**0.002**
Col6a4	68553	collagen, type VI, alpha 4	7.96	7.34	0.08	0.12	**0.006**
Col8a2	329941	collagen, type VIII, alpha 2	9.70	7.21	0.71	0.08	**0.013**
Col9a2	12840	collagen, type IX, alpha 2	30.65	22.06	1.78	1.37	**0.009**
Colec11	71693	collectin sub-family member 11	14.55	10.20	1.48	0.67	**0.0**
Commd4	66199	COMM domain containing 4	214.90	188.09	9.22	5.70	**0.048**
Copa	12847	coatomer protein complex subunit alpha	714.62	818.21	25.47	27.68	**0.033**
Cops4	26891	COP9 (constitutive photomorphogenic) homolog, subunit 4 (Arabidopsis thaliana)	167.97	202.97	5.80	11.91	**0.038**
Coq2	71883	coenzyme Q2 homolog, prenyltransferase (yeast)	28.19	36.77	1.78	2.15	**0.022**
COX1	17708	cytochrome c oxidase subunit I	1958.80	2203.15	40.15	81.63	**0.036**
COX1	17708	cytochrome c oxidase subunit I	1974.29	2201.90	16.77	86.25	**0.041**
Cox19	68033	cytochrome c oxidase assembly protein 19	46.81	53.95	0.69	2.53	**0.035**
COX3	17710	cytochrome c oxidase subunit III	2010.78	2191.49	50.85	48.12	**0.042**
Cox4i1	12857	cytochrome c oxidase subunit IV isoform 1	1101.53	912.27	27.63	25.93	**0.002**
Cox5b	12859	cytochrome c oxidase subunit Vb	223.98	168.08	13.03	8.13	**0.011**
Cox6b2	333182	cytochrome c oxidase subunit VIb polypeptide 2	162.82	114.59	9.38	3.68	**0.003**
Cps1	227231	carbamoyl-phosphate synthetase 1	8.22	7.27	0.27	0.24	**0.038**
Cracr2a	381812	calcium release activated channel regulator 2A	13.50	10.73	0.82	0.77	**0.050**
Cradd	12905	CASP2 and RIPK1 domain containing adaptor with death domain	17.01	13.19	1.34	0.58	**0.04**
Cramp1l	57354	Crm, cramped-like (Drosophila)	38.65	51.80	1.61	4.67	**0.037**
Crb2	241324	crumbs homolog 2 (Drosophila)	7.91	6.22	0.57	0.22	**0.033**
Crct1	74175	cysteine-rich C-terminal 1	5.96	5.24	0.21	0.18	**0.044**
Crhr2	12922	corticotropin releasing hormone receptor 2	11.25	9.11	0.31	0.27	**0.002**
Crim1	50766	cysteine rich transmembrane BMP regulator 1 (chordin like)	22.99	33.28	2.11	1.84	**0.010**
Crls1	66586	cardiolipin synthase 1	108.79	138.84	7.47	5.75	**0.019**
Crxos	546024	cone-rod homeobox, opposite strand	5.31	6.05	0.26	0.06	**0.033**
Crybb2	12961	crystallin, beta B2	28.26	21.65	1.19	0.79	**0.004**
Csad	246277	cysteine sulfinic acid decarboxylase	62.97	46.64	3.92	1.04	**0.007**
Csf2rb2	12984	colony stimulating factor 2 receptor, beta 2, low-affinity (granulocyte-macrophage)	22.54	18.43	0.40	1.29	**0.023**

Csmd1	94109	CUB and Sushi multiple domains 1	38.43	46.92	1.28	1.64	**0.007**
Csmd3	239420	CUB and Sushi multiple domains 3	80.42	101.20	5.93	5.21	**0.039**
Csn1s2b	12992	casein alpha s2-like B	6.05	6.82	0.12	0.28	**0.043**
Csnk2a2	13000	casein kinase 2, alpha prime polypeptide	172.04	195.32	5.77	5.32	**0.03**
Cstb	13014	cystatin B	404.90	351.06	7.73	16.30	**0.024**
Ctnna2	12386	catenin (cadherin associated protein), alpha 2	104.89	112.59	0.75	2.58	**0.029**
Ctns	83429	cystinosis, nephropathic	58.95	84.04	3.47	3.51	**0.002**
Cts8	56094	cathepsin 8	4.70	6.10	0.34	0.29	**0.021**
Ctsd	13033	cathepsin D	740.18	788.89	7.31	9.87	**0.007**
Cttnbp2nl	80281	CTTNBP2 N-terminal like	144.19	183.32	7.61	8.92	**0.016**
Ctu2	66965	cytosolic thiouridylase subunit 2 homolog (S. pombe)	36.63	29.87	1.14	0.58	**0.00**
Cuta	67675	cutA divalent cation tolerance homolog (E. coli)	656.31	514.97	41.01	21.41	**0.02**
Cx3cr1	13051	chemokine (C-X3-C motif) receptor 1	261.28	353.99	3.16	14.17	**0.001**
Cxcl13	55985	chemokine (C-X-C motif) ligand 13	13.38	9.01	0.75	0.37	**0.00**
Cxcr2	12765	chemokine (C-X-C motif) receptor 2	11.35	9.43	0.41	0.38	**0.014**
Cyb5a	109672	cytochrome b5 type A (microsomal)	218.52	181.00	3.32	11.05	**0.017**
Cyb5r2	320635	cytochrome b5 reductase 2	7.00	6.26	0.17	0.22	**0.04**
Cyp1b1	13078	cytochrome P450, family 1, subfamily b, polypeptide 1	6.34	5.37	0.04	0.34	**0.029**
Cyp26b1	232174	cytochrome P450, family 26, subfamily b, polypeptide 1	16.67	13.05	0.89	0.36	**0.009**
Cyp2d11	545123	cytochrome P450, family 2, subfamily d, polypeptide 11	4.06	3.69	0.06	0.11	**0.021**
Cyp2f2	13107	cytochrome P450, family 2, subfamily f, polypeptide 2	7.34	6.75	0.11	0.18	**0.028**
Cyp2j5	13109	cytochrome P450, family 2, subfamily j, polypeptide 5	5.42	5.03	0.11	0.11	**0.047**
Cyp2w1	545817	cytochrome P450, family 2, subfamily w, polypeptide 1	9.23	7.46	0.49	0.52	**0.049**
Cyp3a59	100041449	cytochrome P450, family 3, subfamily a, polypeptide 59	6.46	4.65	0.61	0.20	**0.03**
Cyp4a31	666168	cytochrome P450, family 4, subfamily a, polypeptide 31	5.05	6.76	0.45	0.38	**0.027**
Cysrt1	67859	cysteine rich tail 1	20.08	14.04	1.45	0.40	**0.007**
CYTB	17711	cytochrome b	2366.10	2623.74	52.30	61.24	**0.019**
D5Ertd683e	100504556	DNA segment, Chr 5, ERATO Doi 683, expressed	6.44	7.36	0.26	0.08	**0.014**
D6Ertd474e	52285	DNA segment, Chr 6, ERATO Doi 474, expressed	7.48	6.32	0.29	0.27	**0.026**
Dab1	13131	disabled 1	113.87	96.49	4.61	1.23	**0.011**
Dact3	629378	dapper homolog 3, antagonist of beta-catenin (xenopus)	11.80	14.51	0.18	1.06	**0.046**
Dagla	269060	diacylglycerol lipase, alpha	42.54	52.81	1.04	3.44	**0.029**
Dapk2	13143	death-associated protein kinase 2	17.62	13.37	1.31	0.84	**0.034**
Dbndd1	72185	dysbindin (dystrobrevin binding protein 1) domain containing 1	14.87	12.66	0.40	0.64	**0.026**
Dbx2	223843	developing brain homeobox 2	29.66	23.80	2.24	0.79	**0.048**
Dcdc2a	195208	doublecortin domain containing 2a	11.55	9.75	0.32	0.48	**0.021**
Dcdc2b	100504491	doublecortin domain containing 2b	9.71	7.50	0.53	0.24	**0.009**
Dclk1	13175	doublecortin-like kinase 1	105.06	127.62	6.42	4.70	**0.030**
Dcps	69305	decapping enzyme, scavenger	91.73	75.20	4.61	4.14	**0.037**
Dcst1	77772	DC-STAMP domain containing 1	10.30	8.36	0.25	0.44	**0.009**
Dcst2	329702	DC-STAMP domain containing 2	8.97	7.63	0.20	0.17	**0.002**
Dda1	66498	DET1 and DDB1 associated 1	28.90	24.12	1.57	1.14	**0.049**
Ddah2	51793	dimethylarginine dimethylaminohydrolase 2	113.30	93.52	5.09	1.07	**0.01**
Ddrgk1	77006	DDRGK domain containing 1	162.94	130.33	7.80	8.11	**0.03**
Ddx26b	236790	DEAD/H (Asp-Glu-Ala-Asp/His) box polypeptide 26B	98.84	121.39	5.73	2.92	**0.013**
Ddx39	68278	DEAD (Asp-Glu-Ala-Asp) box polypeptide 39	48.06	37.91	2.28	1.03	**0.007**
Ddx39b	53817	DEAD (Asp-Glu-Ala-Asp) box polypeptide 39B	266.63	232.27	3.94	11.33	**0.029**
Ddx50	94213	DEAD (Asp-Glu-Ala-Asp) box polypeptide 50	144.57	164.72	6.37	4.87	**0.046**
Defa-ps12	654452	defensin, alpha, pseudogene 12	4.25	4.68	0.03	0.10	**0.005**
Defa-rs1	13218	defensin, alpha, related sequence 1	14.90	12.67	0.65	0.62	**0.047**
Defa-rs12	13221	defensin, alpha, related sequence 12	22.08	25.56	0.45	0.71	**0.006**
Defa-rs2	13222	defensin, alpha, related sequence 2	6.95	6.09	0.24	0.17	**0.027**
Defa-rs4	13223	defensin, alpha,, related sequence 4	8.13	7.17	0.29	0.18	**0.03**
Defb33	654453	defensin beta 33	12.79	10.28	0.58	0.44	**0.014**
Defb35	246084	defensin beta 35	10.53	7.81	0.88	0.37	**0.029**
Defb44-ps	654454	defensin beta 44, pseudogene	4.85	4.53	0.08	0.05	**0.016**
Defb8	244334	defensin beta 8	5.38	4.34	0.39	0.16	**0.049**
Dennd5a	19347	DENN/MADD domain containing 5A	265.89	334.74	13.70	17.20	**0.02**

Dennd5b	320560	DENN/MADD domain containing 5B	25.85	38.60	1.51	4.77	**0.04**
Denr	68184	density-regulated protein	298.28	237.33	8.94	8.54	**0.003**
Depdc1a	76131	DEP domain containing 1a	24.56	41.88	2.95	5.72	**0.036**
Desi2	78825	desumoylating isopeptidase 2	14.07	22.06	0.73	2.17	**0.013**
Dgka	13139	diacylglycerol kinase, alpha	27.35	49.36	3.06	6.37	**0.021**
Dgke	56077	diacylglycerol kinase, epsilon	19.09	24.53	1.47	1.43	**0.038**
Dgkg	110197	diacylglycerol kinase, gamma	11.15	9.04	0.59	0.37	**0.023**
Dgki	320127	diacylglycerol kinase, iota	10.21	13.42	0.57	0.96	**0.0**
Dhcr24	74754	24-dehydrocholesterol reductase	666.85	494.15	28.40	34.29	**0.008**
Dhrs7b	216820	dehydrogenase/reductase (SDR family) member 7B	74.22	50.42	5.24	3.20	**0.008**
Dhrsx	236082	dehydrogenase/reductase (SDR family) X chromosome	25.48	21.89	0.91	1.10	**0.046**
Dhx30	72831	DEAH (Asp-Glu-Ala-His) box polypeptide 30	38.72	35.92	0.70	0.50	**0.017**
Dhx36	72162	DEAH (Asp-Glu-Ala-His) box polypeptide 36	156.61	176.60	2.79	6.56	**0.031**
Dhx57	106794	DEAH (Asp-Glu-Ala-Asp/His) box polypeptide 57	48.67	64.49	1.76	4.56	**0.0**
Diap2	54004	diaphanous homolog 2 (Drosophila)	14.21	19.21	0.83	1.52	**0.03**
Dirc2	224132	disrupted in renal carcinoma 2 (human)	87.49	121.70	9.47	6.84	**0.026**
Dkk1	13380	dickkopf homolog 1 (Xenopus laevis)	11.63	10.02	0.55	0.22	**0.035**
Dkk2	56811	dickkopf homolog 2 (Xenopus laevis)	10.35	9.07	0.22	0.22	**0.006**
Dlg4	13385	discs, large homolog 4 (Drosophila)	27.47	33.65	1.94	1.23	**0.036**
Dlk1	13386	delta-like 1 homolog (Drosophila)	10.89	8.16	0.77	0.54	**0.027**
Dll4	54485	delta-like 4 (Drosophila)	5.78	4.85	0.06	0.16	**0.002**
Dll4	54485	delta-like 4 (Drosophila)	5.96	4.62	0.33	0.24	**0.017**
Dlx3	13393	distal-less homeobox 3	12.66	9.83	0.70	0.46	**0.015**
Dlx4	13394	distal-less homeobox 4	8.84	8.20	0.08	0.10	**0.00**
Dmrt2	226049	doublesex and mab-3 related transcription factor 2	10.11	9.50	0.19	0.13	**0.039**
Dmrtb1	56296	DMRT-like family B with proline-rich C-terminal, 1	30.48	23.47	1.80	2.16	**0.047**
Dmtn	13829	dematin actin binding protein	11.85	10.56	0.40	0.26	**0.035**
Dmwd	13401	dystrophia myotonica-containing WD repeat motif	42.91	34.30	3.31	1.00	**0.047**
Dmxl2	235380	Dmx-like 2	91.16	115.49	3.31	4.16	**0.004**
Dnaaf1	68270	dynein, axonemal assembly factor 1	14.25	10.49	1.07	0.66	**0.025**
Dnah3	381917	dynein, axonemal, heavy chain 3	6.02	5.34	0.05	0.17	**0.009**
Dnah6	330355	dynein, axonemal, heavy chain 6	7.17	6.62	0.16	0.08	**0.021**
Dnah9	237806	dynein, axonemal, heavy chain 9	8.27	7.66	0.23	0.09	**0.044**
Dnaic2	432611	dynein, axonemal, intermediate chain 2	15.11	10.90	0.55	0.91	**0.007**
Dnajb11	67838	DnaJ (Hsp40) homolog, subfamily B, member 11	402.08	356.22	9.41	14.53	**0.038**
Dnajc15	66148	DnaJ (Hsp40) homolog, subfamily C, member 15	105.17	172.50	13.23	18.48	**0.025**
Dnajc16	214063	DnaJ (Hsp40) homolog, subfamily C, member 16	54.71	44.94	2.65	0.47	**0.011**
Dnajc2	22791	DnaJ (Hsp40) homolog, subfamily C, member 2	177.44	146.15	8.38	8.31	**0.038**
Dnajc22	72778	DnaJ (Hsp40) homolog, subfamily C, member 22	11.22	9.05	0.37	0.38	**0.007**
Dnajc30	66114	DnaJ (Hsp40) homolog, subfamily C, member 30	71.14	54.96	2.39	2.10	**0.002**
Dnd1	213236	dead end homolog 1 (zebrafish)	13.61	10.18	1.02	0.43	**0.021**
Dnmbp	71972	dynamin binding protein	24.13	37.00	1.93	2.06	**0.004**
Dock1	330662	dedicator of cytokinesis 1	96.93	138.47	4.30	8.11	**0.004**
Dock2	94176	dedicator of cyto-kinesis 2	13.87	18.93	0.78	1.42	**0.021**
Dock7	67299	dedicator of cytokinesis 7	72.24	104.33	7.71	6.32	**0.018**
Dopey1	320615	dopey family member 1	77.40	94.20	2.83	3.66	**0.011**
Dpcr1	268949	diffuse panbronchiolitis critical region 1 (human)	8.44	6.93	0.23	0.34	**0.010**
Dppa4	73693	developmental pluripotency associated 4	6.38	5.38	0.33	0.21	**0.042**
Dpy19l2	320752	dpy-19-like 2 (C. elegans)	5.66	5.20	0.17	0.08	**0.047**
Dpyd	99586	dihydropyrimidine dehydrogenase	19.86	26.29	1.74	1.92	**0.048**
Drap1	66556	Dr1 associated protein 1 (negative cofactor 2 alpha)	197.75	169.66	9.61	6.14	**0.05**
Dtl	76843	denticleless homolog (Drosophila)	15.59	22.61	1.88	1.61	**0.030**
Dtna	13527	dystrobrevin alpha	78.72	103.85	6.07	8.23	**0.049**
Dtwd2	68857	DTW domain containing 2	11.18	14.09	0.54	0.79	**0.022**
Dusp7	235584	dual specificity phosphatase 7	105.13	93.71	1.30	1.18	**0.001**
Dynll2	68097	dynein light chain LC8-type 2	151.45	122.91	6.30	2.79	**0.006**
Eaf2	106389	ELL associated factor 2	7.10	6.06	0.22	0.17	**0.010**
Ear10	93725	eosinophil-associated, ribonuclease A family, member 10	3.50	4.35	0.09	0.30	**0.03**
Ebag9	55960	estrogen receptor-binding fragment-associated gene 9	177.56	218.99	10.58	9.68	**0.028**
Ecsit	26940	ECSIT homolog (Drosophila)	72.39	57.03	4.16	4.12	**0.039**
Edn2	13615	endothelin 2	8.74	7.16	0.16	0.34	**0.006**

Efcab12	212516	EF-hand calcium binding domain 12	6.95	5.49	0.50	0.22	**0.037**
Efcc1	58229	EF hand and coiled-coil domain containing 1	13.33	11.48	0.56	0.49	**0.05**
Efhb	211482	EF hand domain family, member B	7.27	6.08	0.21	0.19	**0.005**
Egr4	13656	early growth response 4	13.24	11.09	0.67	0.51	**0.043**
Ehd1	13660	EH-domain containing 1	51.84	34.76	2.19	2.55	**0.002**
Ehd1	13660	EH-domain containing 1	544.77	388.38	24.69	40.99	**0.02**
Eif1ax	66235	eukaryotic translation initiation factor 1A, X-linked	757.12	646.53	29.76	31.97	**0.045**
Eif2b1	209354	eukaryotic translation initiation factor 2B, subunit 1 (alpha)	35.05	45.73	1.76	2.71	**0.016**
Eif4a2	13682	eukaryotic translation initiation factor 4A2	1207.98	1579.63	72.03	26.70	**0.00**
Eif4a2	13682	eukaryotic translation initiation factor 4A2	159.51	234.12	26.67	12.89	**0.045**
Elf3	13710	E74-like factor 3	5.42	5.10	0.06	0.09	**0.027**
Elf5	13711	E74-like factor 5	4.99	4.26	0.25	0.12	**0.040**
Elovl3	12686	elongation of very long chain fatty acids (FEN1/Elo2, SUR4/Elo3, yeast)-like 3	5.40	4.59	0.20	0.12	**0.013**
Elp2	58523	elongator acetyltransferase complex subunit 2	81.37	98.63	3.60	5.72	**0.043**
Elp3	74195	elongator acetyltransferase complex subunit 3	31.02	39.72	1.15	2.28	**0.01**
Eme1	268465	essential meiotic endonuclease 1 homolog 1 (S. pombe)	8.30	7.39	0.09	0.20	**0.006**
Eml3	225898	echinoderm microtubule associated protein like 3	16.43	13.48	0.98	0.42	**0.033**
Engase	217364	endo-beta-N-acetylglucosaminidase	16.14	12.97	0.90	0.69	**0.031**
Enho	69638	energy homeostasis associated	45.59	37.51	2.70	0.58	**0.026**
Enox1	239188	ecto-NOX disulfide-thiol exchanger 1	20.83	27.82	1.76	1.18	**0.016**
Enpep	13809	glutamyl aminopeptidase	6.23	5.60	0.10	0.17	**0.020**
Eomes	13813	eomesodermin homolog (Xenopus laevis)	7.24	5.97	0.18	0.33	**0.015**
Epb4.1l3	13823	erythrocyte protein band 4.1-like 3	178.55	145.07	12.45	5.64	**0.050**
Epb4.1l5	226352	erythrocyte protein band 4.1-like 5	51.18	75.33	2.62	2.77	**0.001**
Epha10	230735	Eph receptor A10	20.63	17.35	0.44	0.88	**0.016**
Ephb4	13846	Eph receptor B4	9.83	7.80	0.64	0.49	**0.044**
Epm2a	13853	epilepsy, progressive myoclonic epilepsy, type 2 gene alpha	14.24	20.54	1.21	1.60	**0.02**
Epn2	13855	epsin 2	220.31	257.29	4.40	6.03	**0.003**
Epo	13856	erythropoietin	7.20	5.99	0.37	0.23	**0.032**
Eprs	107508	glutamyl-prolyl-tRNA synthetase	301.05	286.77	3.29	3.69	**0.028**
Eps8l2	98845	EPS8-like 2	9.36	7.75	0.23	0.32	**0.007**
Epx	13861	eosinophil peroxidase	7.15	6.19	0.29	0.21	**0.037**
Eral1	57837	Era (G-protein)-like 1 (E. coli)	36.78	45.11	2.11	1.59	**0.020**
Erap1	80898	endoplasmic reticulum aminopeptidase 1	25.62	40.74	1.00	3.95	**0.010**
Erbb4	13869	v-erb-a erythroblastic leukemia viral oncogene homolog 4 (avian)	208.47	258.62	8.56	13.53	**0.020**
Erc2	238988	ELKS/RAB6-interacting/CAST family member 2	34.76	43.98	1.98	2.40	**0.025**
Ercc6l	236930	excision repair cross-complementing rodent repair deficiency complementation group 6 like	11.03	16.30	1.11	0.98	**0.012**
Eri1	67276	exoribonuclease 1	66.85	82.80	3.54	4.99	**0.040**
Erlin2	244373	ER lipid raft associated 2	65.52	95.04	5.35	9.30	**0.033**
Ero1l	50527	ERO1-like (S. cerevisiae)	108.43	155.05	8.88	12.31	**0.022**
Esp24	1001267 76	exocrine gland secreted peptide 24	3.53	3.85	0.10	0.07	**0.037**
Espnl	227357	espin-like	11.86	9.62	0.59	0.40	**0.020**
Esr1	13982	estrogen receptor 1 (alpha)	8.13	7.59	0.18	0.03	**0.023**
Esr2	13983	estrogen receptor 2 (beta)	9.03	7.71	0.37	0.35	**0.040**
Esrrg	26381	estrogen-related receptor gamma	13.74	11.16	0.46	0.32	**0.004**
Etfb	110826	electron transferring flavoprotein, beta polypeptide	222.58	184.46	12.28	6.02	**0.032**
Etl4	208618	enhancer trap locus 4	10.50	8.98	0.45	0.22	**0.023**
Etnk2	214253	ethanolamine kinase 2	9.48	10.54	0.23	0.25	**0.020**
Etohi1	626848	ethanol induced 1	16.94	33.91	1.13	6.81	**0.049**
Etos1	114660	ectopic ossification 1	11.04	8.40	0.58	0.56	**0.017**
Etv2	14008	ets variant 2	7.43	6.39	0.23	0.31	**0.034**
Etv5	104156	ets variant 5	253.95	374.39	27.59	14.23	**0.008**
Eva1a	232146	eva-1 homolog A (C. elegans)	8.27	6.81	0.50	0.17	**0.033**
Evpl	14027	envoplakin	11.53	10.06	0.53	0.27	**0.047**
Exoc3l	277978	exocyst complex component 3-like	9.99	8.29	0.62	0.20	**0.039**
Exoc3l4	74190	exocyst complex component 3-like 4	10.66	7.96	0.28	0.47	**0.003**
Exoc5	105504	exocyst complex component 5	208.45	244.81	1.24	4.61	**0.000**
Eya1	14048	eyes absent 1 homolog (Drosophila)	142.30	218.53	4.34	10.96	**0.001**

F3	14066	coagulation factor III	37.09	50.75	0.59	4.75	**0.03**
F8	14069	coagulation factor VIII	10.48	8.49	0.48	0.20	**0.009**
F8a	14070	factor 8-associated gene A	12.72	15.21	0.42	0.66	**0.018**
Faah	14073	fatty acid amide hydrolase	26.12	37.21	1.16	4.16	**0.042**
Fancm	104806	Fanconi anemia, complementation group M	28.64	37.01	0.99	3.00	**0.038**
Fank1	66930	fibronectin type 3 and ankyrin repeat domains 1	7.40	6.68	0.07	0.25	**0.032**
Fau	14109	Finkel-Biskis-Reilly murine sarcoma virus (FBR-MuSV) ubiquitously expressed (fox derived)	1770.89	1602.26	19.02	20.41	**0.001**
Fbn1	14118	fibrillin 1	14.53	20.59	0.40	1.46	**0.007**
Fbxl17	50758	F-box and leucine-rich repeat protein 17	52.91	73.51	4.66	5.33	**0.027**
Fbxl20	72194	F-box and leucine-rich repeat protein 20	47.59	66.66	3.62	3.44	**0.009**
Fbxo2	230904	F-box protein 2	31.48	21.89	1.77	1.18	**0.004**
Fbxo21	231670	F-box protein 21	85.23	106.84	2.98	2.48	**0.001**
Fbxo25	66822	F-box protein 25	38.16	50.41	4.09	2.38	**0.041**
Fbxw16	320083	F-box and WD-40 domain protein 16	9.26	13.66	0.62	1.64	**0.046**
Fcrl5	329693	Fc receptor-like 5	8.97	8.04	0.11	0.22	**0.008**
Fcrl6	677296	Fc receptor-like 6	10.90	8.89	0.36	0.36	**0.01**
Fdps	110196	farnesyl diphosphate synthetase	504.86	376.11	40.24	32.95	**0.048**
Fer1l4	74562	fer-1-like 4 (C. elegans)	7.72	6.67	0.34	0.23	**0.04**
Fgd1	14163	FYVE, RhoGEF and PH domain containing 1	41.88	33.43	2.35	2.48	**0.048**
Fgd4	224014	FYVE, RhoGEF and PH domain containing 4	28.09	51.59	1.43	4.86	**0.004**
Fgf16	80903	fibroblast growth factor 16	5.13	5.85	0.19	0.12	**0.018**
Fgf17	14171	fibroblast growth factor 17	10.97	8.55	0.39	0.18	**0.001**
Fgf21	56636	fibroblast growth factor 21	9.08	7.69	0.17	0.32	**0.009**
Fgf6	14177	fibroblast growth factor 6	6.31	5.38	0.17	0.23	**0.018**
Fignl2	668225	fidgetin-like 2	16.11	12.84	0.65	0.83	**0.021**
Fitm1	68680	fat storage-inducing transmembrane protein 1	7.44	6.31	0.20	0.10	**0.002**
Fjx1	14221	four jointed box 1 (Drosophila)	152.30	117.48	10.92	7.35	**0.038**
Fkbp10	14230	FK506 binding protein 10	17.51	15.33	0.36	0.61	**0.021**
Fkbp8	14232	FK506 binding protein 8	71.22	63.95	0.45	1.82	**0.008**
Flrt2	399558	fibronectin leucine rich transmembrane protein 2	30.69	51.94	2.91	3.56	**0.004**
Fmo9	240894	flavin containing monooxygenase 9	6.68	5.78	0.25	0.26	**0.047**
Fndc3a	319448	fibronectin type III domain containing 3A	106.44	129.01	4.25	7.90	**0.046**
Folr4	64931	folate receptor 4 (delta)	17.85	16.11	0.27	0.27	**0.004**
Fopnl	66086	Fgfr1op N-terminal like	5.86	5.25	0.12	0.15	**0.020**
Foxa1	15375	forkhead box A1	7.73	6.32	0.15	0.20	**0.001**
Foxe1	110805	forkhead box E1	11.21	12.90	0.35	0.18	**0.005**
Foxh1	14106	forkhead box H1	6.87	5.42	0.42	0.19	**0.020**
Foxi2	270004	forkhead box I2	16.26	12.91	0.81	0.52	**0.013**
Foxi3	232077	forkhead box I3	8.30	7.16	0.41	0.21	**0.047**
Foxl2	26927	forkhead box L2	8.71	6.48	0.66	0.44	**0.031**
Foxr1	382074	forkhead box R1	11.65	10.04	0.29	0.30	**0.009**
Foxred2	239554	FAD-dependent oxidoreductase domain containing 2	20.36	33.69	1.87	1.46	**0.001**
Fpgs	14287	folylpolyglutamyl synthetase	11.09	8.67	0.78	0.60	**0.050**
Fras1	231470	Fraser syndrome 1 homolog (human)	7.35	8.55	0.18	0.17	**0.003**
Frmd4a	209630	FERM domain containing 4A	242.90	160.25	14.54	13.66	**0.006**
Frmd6	319710	FERM domain containing 6	12.42	14.61	0.40	0.71	**0.036**
Frmd7	385354	FERM domain containing 7	13.49	12.42	0.30	0.17	**0.020**
Frs3os	100126242	fibroblast growth factor receptor substrate 3, opposite strand	7.07	9.44	0.09	0.64	**0.010**
Fscn2	238021	fascin homolog 2, actin-bundling protein, retinal (Strongylocentrotus purpuratus)	8.08	5.75	0.72	0.10	**0.02**
Fstl4	320027	follistatin-like 4	7.57	6.37	0.28	0.26	**0.021**
Gaa	14387	glucosidase, alpha, acid	72.76	57.98	3.22	4.98	**0.05**
Gab3	210710	growth factor receptor bound protein 2-associated protein 3	29.10	42.83	1.49	3.10	**0.007**
Gabbr2	242425	gamma-aminobutyric acid (GABA) B receptor, 2	81.85	93.51	1.67	4.11	**0.039**
Gabrr2	14409	gamma-aminobutyric acid (GABA) C receptor, subunit rho 2	9.56	8.04	0.49	0.20	**0.029**
Galnt2	108148	UDP-N-acetyl-alpha-D-galactosamine:polypeptide N-acetylgalactosaminyltransferase 2	23.39	29.97	0.79	2.56	**0.049**
Galnt9	231605	UDP-N-acetyl-alpha-D-galactosamine:polypeptide N-acetylgalactosaminyltransferase 9	12.26	10.05	0.41	0.15	**0.002**

Gapt	238875	Grb2-binding adaptor, transmembrane	6.62	6.12	0.12	0.05	**0.010**
Garem1	242915	GRB2 associated, regulator of MAPK1-like	30.13	18.23	2.64	1.83	**0.010**
Gart	14450	phosphoribosylglycinamide formyltransferase	41.32	49.48	1.80	1.96	**0.022**
Gas7	14457	growth arrest specific 7	67.22	47.43	6.48	4.43	**0.045**
Gas8	104346	growth arrest specific 8	54.92	39.51	2.74	2.57	**0.006**
Gatsl2	80909	GATS protein-like 2	25.05	35.14	0.97	0.91	**0.000**
Gbx2	14472	gastrulation brain homeobox 2	7.02	5.72	0.45	0.27	**0.048**
Gcgr	14527	glucagon receptor	14.82	11.41	0.90	0.27	**0.011**
Gck	103988	glucokinase	11.95	9.16	0.31	0.50	**0.003**
Gcsh	68133	glycine cleavage system protein H (aminomethyl carrier)	65.76	52.59	0.56	2.09	**0.001**
Gdpd3	68616	glycerophosphodiester phosphodiesterase domain containing 3	8.79	7.21	0.47	0.37	**0.038**
Gem	14579	GTP binding protein (gene overexpressed in skeletal muscle)	19.40	15.60	0.95	0.68	**0.018**
Gfpt1	14583	glutamine fructose-6-phosphate transaminase 1	136.91	165.88	5.73	7.20	**0.020**
Gfy	100039953	golgi-associated olfactory signaling regulator	26.54	21.30	1.02	1.27	**0.018**
Ggt5	23887	gamma-glutamyltransferase 5	8.76	10.47	0.36	0.58	**0.048**
Ghsr	208188	growth hormone secretagogue receptor	10.21	7.46	0.98	0.13	**0.031**
Gid4	66771	GID complex subunit 4, VID24 homolog (S. cerevisiae)	72.95	95.61	8.38	2.98	**0.04**
Gid8	76425	GID complex subunit 8 homolog (S. cerevisiae)	36.91	53.41	3.57	4.14	**0.024**
Gimap3	83408	GTPase, IMAP family member 3	9.47	10.50	0.26	0.32	**0.045**
Gipr	381853	gastric inhibitory polypeptide receptor	12.66	10.39	0.73	0.24	**0.026**
Gjb2	14619	gap junction protein, beta 2	29.53	20.88	2.48	1.22	**0.020**
Gjb4	14621	gap junction protein, beta 4	8.18	6.71	0.46	0.30	**0.037**
Glp1r	14652	glucagon-like peptide 1 receptor	6.76	5.86	0.11	0.24	**0.015**
Gm13238	236069	carnitine deficiency-associated gene expressed in ventricle 3 pseudogene	10.27	6.75	1.10	0.79	**0.040**
Gm13369	100502743	heterogeneous nuclear ribonucleoprotein A3-like	12.76	17.29	0.39	0.62	**0.001**
Gm41	245502	melanoma antigen, family B, 4 pseudogene	15.21	19.43	0.96	1.32	**0.041**
Gm4910	236844	predicted pseudogene 4910	9.88	8.69	0.29	0.15	**0.010**
Gm4926	237749	T-cell immunoglobulin and mucin domain containing 2 pseudogene	6.72	5.84	0.23	0.25	**0.039**
Gm6194	620966	transmembrane protein 189 pseudogene	17.09	14.00	0.78	0.61	**0.020**
Gm6238	621542	predicted pseudogene 6238	34.24	39.69	1.57	1.47	**0.044**
Gm6981	629557	glyceraldehyde-3-phosphate dehydrogenase pseudogene	58.77	83.72	2.35	4.72	**0.003**
Gm8801	667766	protein phosphatase 1, regulatory subunit 10 pseudogene	20.88	17.49	0.68	0.88	**0.022**
Gnas	14683	GNAS (guanine nucleotide binding protein, alpha stimulating) complex locus	13.57	12.97	0.16	0.06	**0.014**
Gnat1	14685	guanine nucleotide binding protein, alpha transducing 1	14.49	9.22	1.47	0.71	**0.018**
Gnat2	14686	guanine nucleotide binding protein, alpha transducing 2	4.91	4.47	0.15	0.05	**0.029**
Gnat3	242851	guanine nucleotide binding protein, alpha transducing 3	6.77	5.86	0.32	0.07	**0.03**
Gng11	66066	guanine nucleotide binding protein (G protein), gamma 11	68.30	55.89	4.33	1.69	**0.037**
Gng4	14706	guanine nucleotide binding protein (G protein), gamma 4	81.63	109.25	5.20	9.49	**0.043**
Gngt2	14710	guanine nucleotide binding protein (G protein), gamma transducing activity polypeptide 2	31.94	22.81	2.95	1.58	**0.034**
Golt1a	68338	golgi transport 1 homolog A (S. cerevisiae)	14.32	9.75	1.53	0.53	**0.030**
Golt1b	66964	golgi transport 1 homolog B (S. cerevisiae)	229.86	276.09	15.27	10.76	**0.048**
Gpatch2	67769	G patch domain containing 2	24.66	32.03	1.29	2.16	**0.026**
Gpbp1	73274	GC-rich promoter binding protein 1	327.72	367.33	5.13	7.67	**0.005**
Gpc3	14734	glypican 3	86.63	64.00	4.22	5.25	**0.015**
Gpm6b	14758	glycoprotein m6b	644.24	815.50	17.52	18.90	**0.001**
Gpr141	353346	G protein-coupled receptor 141	5.17	4.75	0.15	0.04	**0.037**
Gpr142	217302	G protein-coupled receptor 142	11.89	10.10	0.56	0.21	**0.025**
Gpr182	11536	G protein-coupled receptor 182	9.69	11.95	0.04	0.86	**0.039**
Gpr45	93690	G protein-coupled receptor 45	6.63	8.07	0.11	0.39	**0.012**
Gpr55	227326	G protein-coupled receptor 55	12.12	8.35	1.03	0.27	**0.012**
Gpr62	436090	G protein-coupled receptor 62	43.44	30.30	4.25	2.48	**0.037**
Gpr82	319200	G protein-coupled receptor 82	6.82	10.71	0.27	0.86	**0.005**
Gpr83	14608	G protein-coupled receptor 83	7.91	10.77	0.50	0.77	**0.0**
Gpr97	54672	G protein-coupled receptor 97	10.79	8.02	0.82	0.56	**0.032**
Gpx1	14775	glutathione peroxidase 1	982.06	900.80	16.76	25.70	**0.038**
Gpx2	14776	glutathione peroxidase 2	3.97	5.14	0.09	0.38	**0.023**

Gramd1a	52857	GRAM domain containing 1A	139.27	104.16	7.88	5.19	**0.010**
Gramd3	107022	GRAM domain containing 3	274.63	208.54	13.90	21.44	**0.041**
Greb1l	381157	growth regulation by estrogen in breast cancer-like	14.13	11.56	0.64	0.82	**0.047**
Grem2	23893	gremlin 2 homolog, cysteine knot superfamily (Xenopus laevis)	8.25	6.93	0.38	0.15	**0.017**
Gria2	14800	glutamate receptor, ionotropic, AMPA2 (alpha 2)	453.10	539.59	12.81	20.32	**0.011**
Grik2	14806	glutamate receptor, ionotropic, kainate 2 (beta 2)	102.91	127.51	4.59	8.44	**0.043**
Grin1	14810	glutamate receptor, ionotropic, NMDA1 (zeta 1)	46.28	29.67	2.96	2.59	**0.006**
Grin3b	170483	glutamate receptor, ionotropic, NMDA3B	12.78	10.89	0.62	0.23	**0.028**
Grm1	14816	glutamate receptor, metabotropic 1	12.96	10.66	0.37	0.53	**0.012**
Grrp1	72690	glycine/arginine rich protein 1	12.92	11.51	0.29	0.40	**0.029**
Gspt2	14853	G1 to S phase transition 2	29.98	41.24	3.48	1.95	**0.030**
Gstt2	14872	glutathione S-transferase, theta 2	7.05	5.33	0.29	0.15	**0.002**
Gtf2a1	83602	general transcription factor II A, 1	234.59	251.24	5.40	2.58	**0.032**
Gtf2f1	98053	general transcription factor IIF, polypeptide 1	144.44	110.18	11.48	6.53	**0.04**
Gtsf1	74174	gametocyte specific factor 1	5.66	5.05	0.23	0.08	**0.043**
Gucy2c	14917	guanylate cyclase 2c	12.82	11.31	0.41	0.13	**0.01**
Guk1	14923	guanylate kinase 1	122.75	100.72	6.17	1.80	**0.014**
Gulo	268756	gulonolactone (L-) oxidase	10.93	7.95	0.59	0.17	**0.003**
Gyltl1b	228366	glycosyltransferase-like 1B	7.35	6.33	0.31	0.03	**0.017**
H2afb1	68231	H2A histone family, member B1	15.38	11.46	0.93	0.27	**0.007**
H2bfm	69389	H2B histone family, member M	8.25	9.36	0.13	0.39	**0.035**
Hck	15162	hemopoietic cell kinase	18.96	14.62	0.76	0.72	**0.006**
Hdac11	232232	histone deacetylase 11	14.71	13.41	0.34	0.27	**0.024**
Hdx	245596	highly divergent homeobox	15.72	21.44	1.15	1.03	**0.010**
Heg1	77446	HEG homolog 1 (zebrafish)	54.29	35.92	4.18	3.71	**0.02**
Hemt1	15202	hematopoietic cell transcript 1	7.62	6.45	0.37	0.19	**0.03**
Henmt1	66715	HEN1 methyltransferase homolog 1 (Arabidopsis)	10.41	8.63	0.64	0.16	**0.036**
Heph	15203	hephaestin	10.88	8.89	0.46	0.49	**0.026**
Herc1	235439	hect (homologous to the E6-AP (UBE3A) carboxyl terminus) domain and RCC1 (CHC1)-like domain (RLD) 1	84.85	100.23	2.47	3.77	**0.014**
Hhatl	74770	hedgehog acyltransferase-like	14.10	10.86	0.65	0.09	**0.003**
Hhex	15242	hematopoietically expressed homeobox	20.69	15.97	1.44	1.01	**0.036**
Hhipl1	214305	hedgehog interacting protein-like 1	7.23	7.86	0.18	0.13	**0.032**
Hist1h2bh	319182	histone cluster 1, H2bh	4.86	6.49	0.40	0.31	**0.018**
Hist2h2ab	621893	histone cluster 2, H2ab	127.65	183.25	6.79	16.40	**0.020**
Hivep2	15273	human immunodeficiency virus type I enhancer binding protein 2	32.13	45.85	1.30	2.56	**0.0**
Hmg20a	66867	high mobility group 20A	134.19	170.95	7.54	8.42	**0.017**
Hmgcll1	208982	3-hydroxymethyl-3-methylglutaryl-Coenzyme A lyase-like 1	14.41	20.64	1.17	2.12	**0.042**
Hmgn5	50887	high-mobility group nucleosome binding domain 5	65.29	81.26	0.78	6.04	**0.04**
Hnf1b	21410	HNF1 homeobox B	6.56	6.03	0.07	0.10	**0.005**
Hnmt	140483	histamine N-methyltransferase	19.14	28.77	1.69	2.75	**0.025**
Hnrnpab	15384	heterogeneous nuclear ribonucleoprotein A/B	946.11	835.50	10.83	17.47	**0.002**
Hnrnpk	15387	heterogeneous nuclear ribonucleoprotein K	205.49	227.00	2.52	7.52	**0.04**
Hnrnpm	76936	heterogeneous nuclear ribonucleoprotein M	727.83	663.70	15.49	19.13	**0.040**
Homer3	26558	homer homolog 3 (Drosophila)	15.12	13.06	0.47	0.50	**0.024**
Hottip	791364	Hoxa distal transcript antisense RNA	8.89	6.74	0.84	0.26	**0.050**
Hoxa13	15398	homeobox A13	8.83	7.31	0.11	0.10	**6E-05**
Hoxa5	15402	homeobox A5	8.10	6.70	0.48	0.14	**0.030**
Hoxaas3	72628	Hoxa cluster antisense RNA 3	10.32	8.96	0.28	0.31	**0.017**
Hoxb6	15414	homeobox B6	7.32	5.93	0.39	0.23	**0.021**
Hoxc13	15422	homeobox C13	6.71	5.79	0.19	0.06	**0.004**
Hoxd8	15437	homeobox D8	16.70	11.20	2.08	0.39	**0.040**
Hrh1	15465	histamine receptor H1	11.64	10.41	0.34	0.26	**0.028**
Hrh3	99296	histamine receptor H3	12.94	10.58	0.84	0.38	**0.043**
Hs3st3b1	54710	heparan sulfate (glucosamine) 3-O-sulfotransferase 3B1	11.89	9.38	0.56	0.58	**0.021**
Hs3st4	628779	heparan sulfate (glucosamine) 3-O-sulfotransferase 4	11.28	9.98	0.15	0.41	**0.024**
Hsd11b2	15484	hydroxysteroid 11-beta dehydrogenase 2	19.14	14.34	0.84	0.46	**0.002**
Hsd17b13	243168	hydroxysteroid (17-beta) dehydrogenase 13	6.93	5.73	0.39	0.12	**0.026**
Hsf2	15500	heat shock factor 2	109.63	135.83	3.30	8.49	**0.028**
Hsf3	245525	heat shock transcription factor 3	4.58	4.27	0.06	0.10	**0.035**
Htr3b	57014	5-hydroxytryptamine (serotonin) receptor 3B	10.07	8.09	0.45	0.30	**0.010**

Hydin	244653	HYDIN, axonemal central pair apparatus protein	7.22	6.63	0.16	0.16	**0.040**
Ido2	209176	indoleamine 2,3-dioxygenase 2	11.68	9.82	0.53	0.38	**0.029**
Iffo1	320678	intermediate filament family orphan 1	68.78	51.62	3.04	1.00	**0.002**
Ifit1	15957	interferon-induced protein with tetratricopeptide repeats 1	17.53	14.69	0.50	0.96	**0.040**
Ifna5	15968	interferon alpha 5	31.20	23.84	2.40	1.78	**0.049**
Ifna9	15972	interferon alpha 9	8.20	5.97	0.85	0.25	**0.045**
Ifngr2	15980	interferon gamma receptor 2	61.33	79.30	2.92	2.37	**0.003**
Igf2	16002	insulin-like growth factor 2	29.81	22.51	2.28	1.72	**0.043**
Igf2bp2	319765	insulin-like growth factor 2 mRNA binding protein 2	35.79	47.09	3.09	1.57	**0.017**
Igfals	16005	insulin-like growth factor binding protein, acid labile subunit	8.66	7.44	0.34	0.35	**0.048**
Igfbp6	16012	insulin-like growth factor binding protein 6	13.17	9.00	0.82	0.54	**0.005**
Ighmbp2	20589	immunoglobulin mu binding protein 2	17.32	13.32	1.27	0.84	**0.039**
Ihh	16147	Indian hedgehog	23.31	20.14	0.88	0.82	**0.039**
Il1f10	215274	interleukin 1 family, member 10	11.02	9.62	0.27	0.31	**0.014**
Il1r1	16177	interleukin 1 receptor, type I	8.17	6.72	0.28	0.48	**0.040**
Il1rapl2	60367	interleukin 1 receptor accessory protein-like 2	5.99	4.76	0.09	0.12	**0.000**
Il1rl1	17082	interleukin 1 receptor-like 1	6.48	5.35	0.40	0.17	**0.040**
Il1rl2	107527	interleukin 1 receptor-like 2	7.17	6.61	0.07	0.08	**0.002**
Il27ra	50931	interleukin 27 receptor, alpha	16.08	13.89	0.58	0.32	**0.016**
Il31	76399	interleukin 31	9.06	7.55	0.30	0.26	**0.009**
Il7	16196	interleukin 7	6.16	6.85	0.22	0.17	**0.046**
Il9	16198	interleukin 9	10.20	8.41	0.31	0.20	**0.003**
Il9r	16199	interleukin 9 receptor	11.99	9.77	0.47	0.66	**0.034**
Ing5	66262	inhibitor of growth family, member 5	25.71	20.20	1.68	0.49	**0.020**
Inpp1	16329	inositol polyphosphate-1-phosphatase	24.60	32.51	1.79	1.19	**0.010**
Inpp5j	170835	inositol polyphosphate 5-phosphatase J	11.64	10.13	0.26	0.32	**0.010**
Ints6	18130	integrator complex subunit 6	83.07	94.89	0.56	2.23	**0.002**
Ints8	72656	integrator complex subunit 8	75.83	93.71	2.19	6.12	**0.033**
Intu	380614	inturned planar cell polarity effector homolog (Drosophila)	11.49	9.57	0.47	0.44	**0.024**
Ipo13	230673	importin 13	234.23	178.64	10.26	6.44	**0.004**
Ipo4	75751	importin 4	78.57	59.90	6.89	2.90	**0.047**
Iqca	74918	IQ motif containing with AAA domain	6.32	5.46	0.30	0.15	**0.042**
Iqcf1	74267	IQ motif containing F1	5.68	7.13	0.45	0.34	**0.044**
Iqck	434232	IQ motif containing K	7.77	6.52	0.47	0.15	**0.047**
Irak2	108960	interleukin-1 receptor-associated kinase 2	19.57	15.26	0.61	0.95	**0.009**
Irak3	73914	interleukin-1 receptor-associated kinase 3	8.66	6.27	0.69	0.38	**0.02**
Ireb2	64602	iron responsive element binding protein 2	95.81	113.51	3.57	1.64	**0.004**
Irf2bp1	272359	interferon regulatory factor 2 binding protein 1	67.93	48.21	5.43	3.23	**0.02**
Irf6	54139	interferon regulatory factor 6	8.17	6.62	0.38	0.30	**0.018**
Irs3	16369	insulin receptor substrate 3	9.50	7.49	0.51	0.53	**0.033**
Irx4	50916	Iroquois related homeobox 4 (Drosophila)	9.07	7.84	0.20	0.35	**0.023**
Isca2	74316	iron-sulfur cluster assembly 2 homolog (S. cerevisiae)	192.19	167.78	6.38	4.30	**0.019**
Isl1	16392	ISL1 transcription factor, LIM/homeodomain	7.56	6.25	0.46	0.11	**0.033**
Itih5l-ps	634882	inter-alpha (globulin) inhibitor H5-like, pseudogene	6.06	5.39	0.19	0.19	**0.048**
Itsn1	16443	intersectin 1 (SH3 domain protein 1A)	33.45	39.59	2.17	0.74	**0.037**
Jam3	83964	junction adhesion molecule 3	312.23	271.38	4.27	15.61	**0.045**
Jmjd1c	108829	jumonji domain containing 1C	354.86	397.57	8.11	13.48	**0.035**
Jtb	23922	jumping translocation breakpoint	138.53	110.53	2.68	3.28	**0.001**
Kansl1l	68691	KAT8 regulatory NSL complex subunit 1-like	22.95	29.34	1.91	1.39	**0.035**
Kat2a	14534	K(lysine) acetyltransferase 2A	81.43	73.18	1.25	3.06	**0.047**
Katnb1	74187	katanin p80 (WD40-containing) subunit B 1	64.49	51.42	2.64	1.58	**0.01**
Kcna5	16493	potassium voltage-gated channel, shaker-related subfamily, member 5	8.35	6.76	0.33	0.26	**0.009**
Kcnd1	16506	potassium voltage-gated channel, Shal-related family, member 1	23.87	18.89	1.38	1.13	**0.031**
Kcne1	16509	potassium voltage-gated channel, Isk-related subfamily, member 1	7.97	6.75	0.24	0.07	**0.003**
Kcng3	225030	potassium voltage-gated channel, subfamily G, member 3	9.71	7.10	0.74	0.29	**0.017**
Kcnh6	192775	potassium voltage-gated channel, subfamily H (eag-related), member 6	7.56	6.53	0.29	0.16	**0.022**
Kcnj9	16524	potassium inwardly-rectifying channel, subfamily J, member 9	11.72	9.72	0.76	0.12	**0.041**
Kcnk12	210741	potassium channel, subfamily K, member 12	11.98	9.21	0.49	0.75	**0.021**
Kcnk4	16528	potassium channel, subfamily K, member 4	18.87	14.27	0.75	0.74	**0.005**
Kcnmb2	72413	potassium large conductance calcium-activated channel, subfamily M,	17.06	11.27	2.02	0.89	**0.039**

		beta member 2					
Kcnmb3	100502876	potassium large conductance calcium-activated channel, subfamily M, beta member 3	10.96	8.46	0.69	0.46	**0.024**
Kcnn1	84036	potassium intermediate/small conductance calcium-activated channel, subfamily N, member 1	20.51	14.29	1.13	1.12	**0.008**
Kcnn4	16534	potassium intermediate/small conductance calcium-activated channel, subfamily N, member 4	10.28	8.71	0.54	0.23	**0.037**
Kcnq2	16536	potassium voltage-gated channel, subfamily Q, member 2	19.91	21.94	0.48	0.67	**0.050**
Kcnq4	60613	potassium voltage-gated channel, subfamily Q, member 4	16.21	12.72	0.81	0.41	**0.008**
Kcns1	16538	K+ voltage-gated channel, subfamily S, 1	8.70	7.10	0.32	0.49	**0.03**
Kcns2	16539	K+ voltage-gated channel, subfamily S, 2	10.42	8.67	0.29	0.52	**0.026**
Kctd13	233877	potassium channel tetramerisation domain containing 13	71.01	56.48	2.60	4.45	**0.030**
Kctd7	212919	potassium channel tetramerisation domain containing 7	13.39	12.11	0.33	0.24	**0.020**
Kdelc1	72050	KDEL (Lys-Asp-Glu-Leu) containing 1	57.06	71.11	2.92	3.08	**0.016**
Kdelr1	68137	KDEL (Lys-Asp-Glu-Leu) endoplasmic reticulum protein retention receptor 1	80.11	97.15	5.43	3.90	**0.043**
Kdelr2	66913	KDEL (Lys-Asp-Glu-Leu) endoplasmic reticulum protein retention receptor 2	1099.88	1226.12	40.48	27.46	**0.042**
Kdm1b	218214	lysine (K)-specific demethylase 1B	29.98	42.66	2.82	3.66	**0.034**
Keg1	64697	kidney expressed gene 1	9.47	7.80	0.47	0.13	**0.014**
Kif12	16552	kinesin family member 12	8.84	7.09	0.39	0.36	**0.017**
Kif17	16559	kinesin family member 17	12.09	10.51	0.30	0.32	**0.011**
Kif4	16571	kinesin family member 4	28.52	39.62	3.69	2.08	**0.040**
Kif5a	16572	kinesin family member 5A	35.50	46.23	1.31	2.33	**0.007**
Klc1	16593	kinesin light chain 1	226.05	189.84	8.40	2.96	**0.007**
Klc3	232943	kinesin light chain 3	17.11	15.26	0.29	0.24	**0.00**
Klf14	619665	Kruppel-like factor 14	15.50	12.10	0.93	0.73	**0.028**
Klhl15	236904	kelch-like 15	23.65	19.15	1.09	1.17	**0.031**
Klhl25	207952	kelch-like 25	22.56	26.85	0.61	0.92	**0.008**
Klhl26	234378	kelch-like 26	33.42	25.48	0.13	1.70	**0.003**
Klhl30	70788	kelch-like 30	12.54	10.11	0.70	0.23	**0.016**
Klk1b24	16617	kallikrein 1-related peptidase b24	9.11	6.18	0.91	0.31	**0.023**
Kmt2a	214162	lysine (K)-specific methyltransferase 2A	105.27	142.10	6.85	10.28	**0.025**
Kncn	654462	kinocilin	12.73	10.21	0.64	0.41	**0.016**
Kpna6	16650	karyopherin (importin) alpha 6	60.32	76.49	5.05	3.57	**0.040**
Kremen2	73016	kringle containing transmembrane protein 2	12.15	10.32	0.19	0.19	**0.000**
Krt12	268482	keratin 12	13.38	10.67	0.52	0.51	**0.010**
Krt13	16663	keratin 13	10.38	8.88	0.26	0.35	**0.014**
Krt15	16665	keratin 15	5.94	7.29	0.21	0.33	**0.014**
Krt17	16667	keratin 17	5.08	4.53	0.19	0.06	**0.032**
Krt35	53617	keratin 35	9.38	8.21	0.26	0.26	**0.019**
Krt6b	16688	keratin 6B	7.30	5.66	0.12	0.30	**0.002**
Krt78	332131	keratin 78	14.40	12.33	0.69	0.38	**0.039**
Krt79	223917	keratin 79	10.62	8.74	0.50	0.24	**0.015**
Krt81	64818	keratin 81	29.00	20.44	1.52	1.35	**0.01**
Krt85	53622	keratin 85	10.45	8.76	0.10	0.28	**0.001**
Krt9	107656	keratin 9	7.91	6.54	0.31	0.22	**0.011**
Krtap19-1	170657	keratin associated protein 19-1	5.45	4.64	0.22	0.23	**0.046**
Krtap19-4	170654	keratin associated protein 19-4	51.71	41.59	2.48	3.13	**0.044**
Krtap28-13	71386	keratin associated protein 28-13	4.10	4.77	0.06	0.14	**0.005**
Krtap31-1	70831	keratin associated protein 31-1	7.50	9.80	0.25	0.80	**0.034**
Krtap5-1	50774	keratin associated protein 5-1	48.38	36.69	2.44	3.19	**0.027**
Krtap5-1	50774	keratin associated protein 5-1	49.78	40.11	1.47	3.62	**0.048**
Krtap5-3	77215	keratin associated protein 5-3	7.37	6.49	0.20	0.09	**0.007**
Krtap7-1	71363	keratin associated protein 7-1	8.00	5.48	0.88	0.13	**0.030**
Krtap9-5	435286	keratin associated protein 9-5	4.90	5.24	0.09	0.09	**0.032**
Lamtor4	66096	late endosomal/lysosomal adaptor, MAPK and MTOR activator 4	240.06	213.29	8.50	5.58	**0.039**
Lce1m	66203	late cornified envelope 1M	16.84	12.14	0.98	1.41	**0.034**
Lce3c	94060	late cornified envelope 3C	112.06	84.68	5.52	6.42	**0.02**
Lcmt1	30949	leucine carboxyl methyltransferase 1	139.05	193.25	15.21	13.56	**0.038**
Lcn4	16821	lipocalin 4	5.09	4.54	0.06	0.18	**0.025**

Lct	226413	lactase	8.24	6.90	0.49	0.17	**0.042**
Lctl	235435	lactase-like	10.62	9.43	0.48	0.07	**0.050**
Ldb3	24131	LIM domain binding 3	8.83	7.19	0.37	0.33	**0.016**
Lfng	16848	LFNG O-fucosylpeptide 3-beta-N-acetylglucosaminyltransferase	38.33	28.17	1.14	1.98	**0.004**
Lgals12	56072	lectin, galactose binding, soluble 12	6.46	5.43	0.32	0.05	**0.019**
Lgals3	16854	lectin, galactose binding, soluble 3	19.40	15.38	1.02	0.18	**0.008**
Lgr4	107515	leucine-rich repeat-containing G protein-coupled receptor 4	15.50	39.53	0.87	7.01	**0.014**
Lhx1	16869	LIM homeobox protein 1	9.31	8.20	0.29	0.26	**0.030**
Lhx5	16873	LIM homeobox protein 5	6.06	4.92	0.35	0.11	**0.021**
Lhx9	16876	LIM homeobox protein 9	6.42	5.87	0.06	0.09	**0.002**
Lim2	233187	lens intrinsic membrane protein 2	10.40	9.35	0.37	0.17	**0.041**
Lkaaear1	277496	LKAAEAR motif containing 1 (IKAAEAR murine motif)	6.27	5.42	0.16	0.09	**0.003**
Llph	66225	LLP homolog, long-term synaptic facilitation (Aplysia)	521.73	377.36	26.14	13.63	**0.003**
Llph	66225	LLP homolog, long-term synaptic facilitation (Aplysia)	25.70	15.33	3.31	0.79	**0.023**
Loxhd1	240411	lipoxygenase homology domains 1	7.37	6.47	0.14	0.18	**0.01**
Lpar1	14745	lysophosphatidic acid receptor 1	49.46	56.07	0.83	1.67	**0.012**
Lpar2	53978	lysophosphatidic acid receptor 2	9.67	7.69	0.50	0.48	**0.029**
Lpo	76113	lactoperoxidase	10.28	8.44	0.46	0.25	**0.012**
Lrfn2	70530	leucine rich repeat and fibronectin type III domain containing 2	14.22	12.38	0.32	0.61	**0.038**
Lrguk	74354	leucine-rich repeats and guanylate kinase domain containing	6.24	5.65	0.09	0.04	**0.001**
Lrmp	16970	lymphoid-restricted membrane protein	9.09	7.74	0.31	0.32	**0.022**
Lrp1	16971	low density lipoprotein receptor-related protein 1	198.48	27.08	11.83	1.04	**7E-06**
Lrp2	14725	low density lipoprotein receptor-related protein 2	8.39	7.23	0.17	0.18	**0.004**
Lrrc1	214345	leucine rich repeat containing 1	10.68	17.10	0.53	0.80	**0.001**
Lrrc3	237387	leucine rich repeat containing 3	19.05	15.92	0.62	0.65	**0.013**
Lrrc31	320352	leucine rich repeat containing 31	7.22	5.98	0.28	0.30	**0.024**
Lrrc42	77809	leucine rich repeat containing 42	156.74	109.25	7.34	8.45	**0.005**
Lrrc73	224813	leucine rich repeat containing 73	78.28	53.90	3.20	4.40	**0.004**
Lrrtm4	243499	leucine rich repeat transmembrane neuronal 4	98.24	122.47	6.80	3.85	**0.021**
Lrsam1	227738	leucine rich repeat and sterile alpha motif containing 1	18.43	15.34	0.70	0.69	**0.020**
Lsg1	224092	large subunit GTPase 1 homolog (S. cerevisiae)	130.21	105.87	6.86	3.31	**0.019**
Lsm7	66094	LSM7 homolog, U6 small nuclear RNA associated (S. cerevisiae)	856.96	701.58	19.21	8.20	**0.000**
Lsm7	66094	LSM7 homolog, U6 small nuclear RNA associated (S. cerevisiae)	731.75	626.94	24.17	21.25	**0.017**
Lsmem1	380755	leucine-rich single-pass membrane protein 1	12.39	10.76	0.45	0.38	**0.032**
Lta4h	16993	leukotriene A4 hydrolase	44.70	63.90	3.41	4.84	**0.018**
Ltbp2	16997	latent transforming growth factor beta binding protein 2	9.96	8.36	0.38	0.36	**0.022**
Lypd8	70163	LY6/PLAUR domain containing 8	9.45	7.25	0.11	0.39	**0.002**
Lysmd1	217779	LysM, putative peptidoglycan-binding, domain containing 1	24.11	44.00	2.05	6.00	**0.020**
Lyz1	17110	lysozyme 1	5.94	7.77	0.25	0.69	**0.046**
Macrod1	107227	MACRO domain containing 1	54.67	41.38	2.79	3.25	**0.021**
Magea1	17137	melanoma antigen, family A, 1	7.44	5.57	0.45	0.13	**0.007**
Magea10	236852	melanoma antigen family A, 10	6.52	5.37	0.30	0.21	**0.021**
Magea2	17138	melanoma antigen, family A, 2	10.92	8.34	0.57	0.28	**0.007**
Magea3	17139	melanoma antigen, family A, 3	10.01	7.72	0.42	0.59	**0.020**
Magi2	50791	membrane associated guanylate kinase, WW and PDZ domain containing 2	14.62	20.63	1.27	1.30	**0.016**
Malt1	240354	mucosa associated lymphoid tissue lymphoma translocation gene 1	15.25	23.10	1.12	1.96	**0.013**
Maml2	270118	mastermind like 2 (Drosophila)	178.82	214.09	5.12	13.34	**0.049**
Man2a2	140481	mannosidase 2, alpha 2	71.18	93.68	5.01	3.45	**0.010**
Man2c1	73744	mannosidase, alpha, class 2C, member 1	19.55	16.04	1.23	0.71	**0.0**
Map3k12	26404	mitogen-activated protein kinase kinase kinase 12	21.64	15.12	1.45	1.59	**0.023**
Map3k6	53608	mitogen-activated protein kinase kinase kinase 6	10.79	9.13	0.36	0.22	**0.007**
Map6	17760	microtubule-associated protein 6	8.03	11.34	0.30	1.15	**0.032**
Map7d1	245877	MAP7 domain containing 1	124.79	100.62	7.07	3.27	**0.021**
Mapk8	26419	mitogen-activated protein kinase 8	138.24	180.02	8.89	4.88	**0.006**
Mapkbp1	26390	mitogen-activated protein kinase binding protein 1	14.64	17.37	0.43	0.93	**0.038**
March4	381270	membrane-associated ring finger (C3HC4) 4	10.02	8.33	0.37	0.27	**0.011**
Matr3	17184	matrin 3	528.69	629.76	22.78	34.32	**0.050**
Mb	17189	myoglobin	9.21	7.43	0.27	0.35	**0.007**
Mbd4	17193	methyl-CpG binding domain protein 4	14.58	23.12	0.95	2.65	**0.023**
Mbnl1	56758	muscleblind-like 1 (Drosophila)	257.93	325.32	13.02	10.33	**0.007**

Mbtd1	103537	mbt domain containing 1	79.63	88.60	0.91	2.45	**0.014**
Mbtps1	56453	membrane-bound transcription factor peptidase, site 1	79.17	97.54	4.25	2.98	**0.012**
Mc1r	17199	melanocortin 1 receptor	8.76	6.91	0.50	0.27	**0.017**
Mc2r	17200	melanocortin 2 receptor	5.76	6.63	0.19	0.19	**0.018**
Mchr1	207911	melanin-concentrating hormone receptor 1	13.32	11.79	0.20	0.56	**0.042**
Mcm3	17215	minichromosome maintenance deficient 3 (S. cerevisiae)	34.93	46.40	1.50	3.19	**0.017**
Mcmbp	210711	MCM (minichromosome maintenance deficient) binding protein	105.10	134.25	4.17	10.07	**0.037**
Mcts1	68995	malignant T cell amplified sequence 1	41.55	54.89	2.16	4.51	**0.04**
Mdh1b	76668	malate dehydrogenase 1B, NAD (soluble)	4.98	4.40	0.20	0.13	**0.048**
Med10	28077	mediator complex subunit 10	14.10	11.19	0.41	0.68	**0.011**
Med11	66172	mediator complex subunit 11	27.49	21.31	1.07	0.87	**0.004**
Med14	26896	mediator complex subunit 14	81.98	101.42	6.65	3.23	**0.039**
Mep1a	17287	meprin 1 alpha	7.47	6.33	0.26	0.08	**0.006**
Mest	17294	mesoderm specific transcript	30.37	43.29	1.61	2.13	**0.003**
Mfn1	67414	mitofusin 1	168.50	215.24	9.80	5.39	**0.006**
Mfsd2b	432628	major facilitator superfamily domain containing 2B	13.15	11.53	0.40	0.25	**0.013**
Mgat1	17308	mannoside acetylglucosaminyltransferase 1	18.31	12.57	0.90	0.95	**0.005**
Mgat3	17309	mannoside acetylglucosaminyltransferase 3	152.90	114.31	3.84	6.38	**0.002**
Mgat4e	71001	MGAT4 family, member E	8.90	7.44	0.39	0.18	**0.015**
Mgp	17313	matrix Gla protein	312.09	97.58	80.90	21.64	**0.043**
Mir101b	724062	microRNA 101b	4.26	4.68	0.09	0.10	**0.02**
Mir137	387155	microRNA 137	3.80	4.51	0.06	0.17	**0.007**
Mir142	387160	microRNA 142	13.83	19.03	0.78	1.56	**0.02**
Mir149	387167	microRNA 149	59.82	42.63	2.32	3.29	**0.005**
Mir150	387168	microRNA 150	6.04	8.34	0.29	0.32	**0.002**
Mir184	387179	microRNA 184	7.31	9.62	0.40	0.48	**0.010**
Mir190b	100124481	microRNA 190b	3.47	3.80	0.04	0.08	**0.011**
Mir1946a	100316697	microRNA 1946a	40.49	27.66	4.63	1.94	**0.043**
Mir1946a	100316697	microRNA 1946a	47.92	32.70	4.65	3.90	**0.046**
Mir1953	100316704	microRNA 1953	5.40	4.16	0.13	0.16	**0.001**
Mir1961	100316841	microRNA 1961	3.58	3.76	0.04	0.06	**0.046**
Mir199b	387239	microRNA 199b	4.73	4.37	0.14	0.05	**0.049**
Mir1a-2	723959	microRNA 1a-2	4.96	8.13	0.48	1.07	**0.035**
Mir210	387206	microRNA 210	84.51	112.99	8.21	8.02	**0.048**
Mir211	387207	microRNA 211	6.10	4.82	0.45	0.20	**0.039**
Mir2137	100316779	microRNA 2137	172.69	108.39	10.87	7.44	**0.003**
Mir2137	100316779	microRNA 2137	140.41	101.58	9.00	12.80	**0.048**
Mir224	723894	microRNA 224	6.07	7.90	0.32	0.49	**0.021**
Mir290a	100049710	microRNA 290a	4.32	3.92	0.12	0.03	**0.022**
Mir301b	791069	microRNA 301b	19.34	27.35	1.57	2.65	**0.040**
Mir3091	100526556	microRNA 3091	51.93	30.52	4.84	4.83	**0.020**
Mir30a	387225	microRNA 30a	4.40	3.97	0.16	0.07	**0.044**
Mir3102	100526508	microRNA 3102	8.02	5.66	0.81	0.19	**0.029**
Mir3473d	100628592	microRNA 3473d	45.06	35.85	2.21	2.76	**0.04**
Mir382	723912	microRNA 382	6.07	4.80	0.37	0.17	**0.021**
Mir3961	100628621	microRNA 3961	9.25	13.20	0.68	1.35	**0.04**
Mir411	723936	microRNA 411	3.41	3.67	0.04	0.05	**0.0**
Mir431	723866	microRNA 431	14.71	11.52	0.78	0.96	**0.04**
Mir450-2	723938	microRNA 450-2	6.13	8.94	0.22	0.67	**0.007**

Mir450b	751532	microRNA 450b	3.36	3.50	0.04	0.03	**0.047**
Mir465	723888	microRNA 465	4.03	4.89	0.19	0.18	**0.017**
Mir466h	100124446	microRNA 466h	22.09	41.90	2.88	5.75	**0.022**
Mir466n	10052652 4	microRNA 466n	4.42	5.29	0.10	0.30	**0.034**
Mir467f	10031674 9	microRNA 467f	10.12	33.79	3.33	9.04	**0.049**
Mir468	723871	microRNA 468	12.86	10.63	0.73	0.17	**0.025**
Mir483	723874	microRNA 483	65.74	33.42	3.06	3.21	**0.000**
Mir483	723874	microRNA 483	65.74	33.42	3.06	3.21	**0.000**
Mir487b	723940	microRNA 487b	6.21	7.09	0.12	0.24	**0.017**
Mir494	723878	microRNA 494	53.12	41.77	2.74	1.90	**0.014**
Mir5118	10062858 9	microRNA 5118	9.66	7.29	0.39	0.44	**0.007**
Mir5135	10062860 4	microRNA 5135	60.28	42.94	3.28	2.42	**0.005**
Mir574	100124451	microRNA 574	44.40	26.39	2.48	1.12	**0.001**
Mir669e	10031680 6	microRNA 669e	5.17	5.99	0.07	0.18	**0.006**
Mir669j	10031677 0	microRNA 669j	7.32	10.89	0.64	0.72	**0.010**
Mir669m-1	10031670 1	microRNA 669m-1	50.66	71.18	7.28	2.79	**0.039**
Mir676	751534	microRNA 676	6.34	5.72	0.11	0.14	**0.012**
Mir681	751538	microRNA 681	5.92	4.68	0.41	0.22	**0.037**
Mir98	723947	microRNA 98	4.75	5.83	0.09	0.29	**0.012**
Mir99b	387230	microRNA 99b	29.43	20.63	3.09	1.04	**0.036**
Mirlet7a-1	387244	microRNA let7a-1	19.85	12.62	1.94	0.61	**0.012**
Misp	78906	mitotic spindle positioning	9.97	11.99	0.38	0.65	**0.036**
Mixl1	27217	Mix1 homeobox-like 1 (Xenopus laevis)	8.33	6.65	0.33	0.24	**0.006**
Mks1	380718	Meckel syndrome, type 1	21.80	16.02	1.54	1.05	**0.021**
Mlkl	74568	mixed lineage kinase domain-like	10.72	9.01	0.48	0.32	**0.025**
Mllt4	17356	myeloid/lymphoid or mixed-lineage leukemia (trithorax homolog, Drosophila); translocated to, 4	37.66	43.98	1.32	1.62	**0.023**
Mms22l	212377	MMS22-like, DNA repair protein	21.57	28.15	1.38	1.08	**0.010**
Mob1b	68473	MOB kinase activator 1B	138.44	152.08	1.64	4.90	**0.039**
Mon2	67074	MON2 homolog (yeast)	173.99	195.89	4.35	2.64	**0.005**
Morc2a	74522	microrchidia 2A	76.29	86.99	1.80	3.65	**0.039**
Mospd3	68929	motile sperm domain containing 3	71.78	62.72	1.23	2.33	**0.014**
Mpp6	56524	membrane protein, palmitoylated 6 (MAGUK p55 subfamily member 6)	270.07	307.11	8.45	10.60	**0.034**
Mrgpra1	233221	MAS-related GPR, member A1	14.13	10.38	0.90	0.67	**0.016**
Mrgprb8	404240	MAS-related GPR, member B8	4.86	5.58	0.25	0.11	**0.038**
Mroh2a	100040766	maestro heat-like repeat family member 2A	7.31	6.17	0.33	0.12	**0.019**
Mroh5	268816	maestro heat-like repeat family member 5	19.38	16.19	0.86	0.74	**0.031**
Mrpl13	68537	mitochondrial ribosomal protein L13	207.08	225.64	5.32	3.19	**0.024**
Mrpl14	68463	mitochondrial ribosomal protein L14	57.85	38.38	6.49	1.59	**0.027**
Mrpl18	67681	mitochondrial ribosomal protein L18	195.94	154.00	8.37	10.37	**0.02**
Mrpl40	18100	mitochondrial ribosomal protein L40	31.83	24.69	1.80	2.10	**0.042**
Mrvi1	17540	MRV integration site 1	17.30	13.77	0.87	0.26	**0.008**
Ms4a15	545279	membrane-spanning 4-domains, subfamily A, member 15	18.51	16.42	0.36	0.73	**0.042**
Ms4a18	76002	membrane-spanning 4-domains, subfamily A, member 18	6.60	5.73	0.22	0.07	**0.009**
Ms4a5	269063	membrane-spanning 4-domains, subfamily A, member 5	7.26	6.41	0.21	0.21	**0.03**
Msh5	17687	mutS homolog 5 (E. coli)	12.19	10.72	0.33	0.37	**0.026**
Msl2	77853	male-specific lethal 2 homolog (Drosophila)	356.64	297.83	11.08	16.43	**0.025**
Mslnl	328783	mesothelin-like	11.93	9.59	0.48	0.32	**0.007**
Mst1r	19882	macrophage stimulating 1 receptor (c-met-related tyrosine kinase)	9.73	8.18	0.35	0.24	**0.011**
Msx1os	93895	msh homeobox 1 opposite strand	14.37	11.55	0.73	0.52	**0.020**

Msx1os	93895	msh homeobox 1 opposite strand	9.71	7.11	0.80	0.36	**0.025**
Mtg1	212508	mitochondrial GTPase 1 homolog (S. cerevisiae)	54.65	65.79	3.12	3.00	**0.042**
Mtg2	52856	mitochondrial ribosome associated GTPase 2	31.47	19.94	3.64	2.64	**0.043**
Mtl5	17771	metallothionein-like 5, testis-specific (tesmin)	10.39	8.80	0.38	0.41	**0.030**
Mtmr4	170749	myotubularin related protein 4	46.54	56.78	1.71	1.56	**0.004**
Mtus2	77521	microtubule associated tumor suppressor candidate 2	17.54	12.63	0.97	1.26	**0.021**
Mtx1	17827	metaxin 1	70.60	57.69	4.32	1.83	**0.033**
Mtx3	382793	metaxin 3	33.48	48.86	1.79	5.75	**0.043**
Muc1	17829	mucin 1, transmembrane	8.06	6.81	0.45	0.19	**0.042**
Muc13	17063	mucin 13, epithelial transmembrane	7.65	6.09	0.41	0.17	**0.012**
Mustn1	66175	musculoskeletal, embryonic nuclear protein 1	26.23	21.89	1.37	0.88	**0.038**
Mut	17850	methylmalonyl-Coenzyme A mutase	105.22	84.86	2.45	7.60	**0.044**
Mvk	17855	mevalonate kinase	88.25	64.92	3.60	8.49	**0.045**
Mybbp1a	18432	MYB binding protein (P160) 1a	99.73	86.28	4.07	2.98	**0.037**
Mybph	53311	myosin binding protein H	16.39	18.06	0.29	0.58	**0.043**
Myf6	17878	myogenic factor 6	5.28	6.61	0.24	0.35	**0.021**
Myh11	17880	myosin, heavy polypeptide 11, smooth muscle	12.76	10.61	0.39	0.33	**0.006**
Myh13	544791	myosin, heavy polypeptide 13, skeletal muscle	6.59	5.52	0.33	0.15	**0.025**
Myl12a	67268	myosin, light chain 12A, regulatory, non-sarcomeric	351.35	263.44	24.24	19.35	**0.030**
Myl6b	216459	myosin, light polypeptide 6B	15.54	10.34	1.86	0.78	**0.042**
Mylk3	213435	myosin light chain kinase 3	8.58	7.65	0.37	0.09	**0.050**
Myo15b	217328	myosin XVB	10.26	9.00	0.27	0.31	**0.022**
Myo1d	338367	myosin ID	58.06	30.80	4.11	6.75	**0.014**
Myo9a	270163	myosin IXa	120.45	148.61	9.27	6.62	**0.048**
Naa38	78304	N(alpha)-acetyltransferase 38, NatC auxiliary subunit	150.36	131.58	2.28	6.65	**0.037**
Naa40	70999	N(alpha)-acetyltransferase 40, NatD catalytic subunit, homolog (S. cerevisiae)	21.62	29.53	1.78	2.20	**0.031**
Nacad	192950	NAC alpha domain containing	158.52	123.61	4.24	4.36	**0.001**
Naif1	71254	nuclear apoptosis inducing factor 1	9.85	8.49	0.21	0.31	**0.012**
Nbeal1	269198	neurobeachin like 1	35.27	45.69	3.37	1.35	**0.028**
Ncapd3	78658	non-SMC condensin II complex, subunit D3	37.50	52.01	3.93	3.88	**0.039**
Nckap1	50884	NCK-associated protein 1	724.63	806.25	14.67	25.37	**0.032**
Ncoa6	56406	nuclear receptor coactivator 6	72.47	85.44	4.24	2.42	**0.038**
Ncr1	17086	natural cytotoxicity triggering receptor 1	8.37	7.28	0.20	0.36	**0.038**
ND2	17717	NADH dehydrogenase subunit 2	1984.30	2365.40	48.36	74.93	**0.005**
ND2	17717	NADH dehydrogenase subunit 2	2039.40	2386.83	50.88	87.99	**0.01**
ND3	17718	NADH dehydrogenase subunit 3	2693.91	2921.86	35.17	53.95	**0.012**
ND3	17718	NADH dehydrogenase subunit 3	1568.64	1729.05	30.21	40.90	**0.020**
ND4L	17720	NADH dehydrogenase subunit 4L	1646.40	1880.52	49.13	57.68	**0.021**
ND4L	17720	NADH dehydrogenase subunit 4L	1425.15	1657.49	47.30	79.31	**0.046**
Ndufa7	66416	NADH dehydrogenase (ubiquinone) 1 alpha subcomplex, 7 (B14.5a)	278.93	249.48	6.16	6.53	**0.02**
Ndufa8	68375	NADH dehydrogenase (ubiquinone) 1 alpha subcomplex, 8	207.40	174.85	10.47	6.12	**0.04**
Ndufb3	66495	NADH dehydrogenase (ubiquinone) 1 beta subcomplex 3	432.33	373.46	16.70	9.77	**0.02**
Ndufb7	66916	NADH dehydrogenase (ubiquinone) 1 beta subcomplex, 7	395.23	312.97	10.46	14.54	**0.004**
Ndufb8	67264	NADH dehydrogenase (ubiquinone) 1 beta subcomplex 8	213.26	189.08	2.08	8.65	**0.035**
Ndufs2	226646	NADH dehydrogenase (ubiquinone) Fe-S protein 2	302.34	261.13	10.13	6.69	**0.01**
Necap2	66147	NECAP endocytosis associated 2	179.51	218.04	2.59	9.59	**0.008**
Necap2	66147	NECAP endocytosis associated 2	182.16	217.94	3.19	9.68	**0.013**
Nedd8	18002	neural precursor cell expressed, developmentally down-regulated gene 8	968.19	819.76	13.73	27.52	**0.00**
Nedd8	18002	neural precursor cell expressed, developmentally down-regulated gene 8	1233.44	1091.56	33.67	29.35	**0.019**
Nedd8	18002	neural precursor cell expressed, developmentally down-regulated gene 8	1233.44	1091.56	33.67	29.35	**0.019**
Nefm	18040	neurofilament, medium polypeptide	13.55	17.45	0.40	1.21	**0.022**
Neurl1b	240055	neuralized homolog 1b (Drosophila)	12.44	10.32	0.65	0.57	**0.049**
Neurod6	11922	neurogenic differentiation 6	11.43	6.67	1.18	0.09	**0.007**
Neurog3	11925	neurogenin 3	11.19	10.14	0.21	0.29	**0.027**
Nfatc4	73181	nuclear factor of activated T cells, cytoplasmic, calcineurin dependent 4	15.03	11.66	0.68	0.36	**0.005**
Nfe2l1	18023	nuclear factor, erythroid derived 2,-like 1	68.03	77.12	3.25	1.31	**0.041**

Ngb	64242	neuroglobin	20.34	15.11	1.35	0.60	**0.012**
Ngfrap1	12070	nerve growth factor receptor (TNFRSF16) associated protein 1	1431.12	1187.78	45.90	33.18	**0.005**
Ngly1	59007	N-glycanase 1	39.26	56.65	4.33	3.96	**0.025**
Nhlh1	18071	nescient helix loop helix 1	12.72	8.09	1.58	0.59	**0.034**
Nhlrc4	621239	NHL repeat containing 4	9.34	7.32	0.21	0.21	**0.000**
Nifk	67949	nucleolar protein interacting with the FHA domain of MKI67	85.05	112.14	5.28	7.05	**0.022**
Nkpd1	69547	NTPase, KAP family P-loop domain containing 1	8.26	6.44	0.51	0.23	**0.017**
Nkx2-5	18091	NK2 homeobox 5	11.78	9.56	0.48	0.55	**0.023**
Nkx3-2	12020	NK3 homeobox 2	9.49	8.40	0.15	0.35	**0.031**
Nle1	217011	notchless homolog 1 (Drosophila)	20.92	14.74	2.23	1.13	**0.05**
Nmrk1	225994	nicotinamide riboside kinase 1	6.77	8.32	0.50	0.33	**0.041**
Nmrk2	69564	nicotinamide riboside kinase 2	9.27	6.95	0.22	0.40	**0.002**
Nnat	18111	neuronatin	1313.19	1515.96	73.01	20.09	**0.037**
Noa1	56412	nitric oxide associated 1	154.50	131.34	4.82	4.38	**0.012**
Nod1	107607	nucleotide-binding oligomerization domain containing 1	25.95	21.97	0.79	1.32	**0.041**
Nodal	18119	nodal	10.32	7.91	0.69	0.45	**0.027**
Nol4l	329540	nucleolar protein 4-like	22.88	28.36	0.83	1.77	**0.031**
Nop14	75416	NOP14 nucleolar protein	58.15	62.78	0.95	1.39	**0.034**
Npas3	27386	neuronal PAS domain protein 3	118.04	166.27	7.55	6.59	**0.00**
Npc1l1	237636	NPC1-like 1	17.93	14.44	0.59	0.42	**0.003**
Npffr1	237362	neuropeptide FF receptor 1	12.65	11.47	0.34	0.27	**0.035**
Npm2	328440	nucleophosmin/nucleoplasmin 2	16.70	13.87	0.80	0.84	**0.050**
Npy4r	19065	neuropeptide Y receptor Y4	7.22	6.38	0.20	0.10	**0.009**
Npy6r	18169	neuropeptide Y receptor Y6	4.06	4.40	0.11	0.07	**0.047**
Nr1d2	353187	nuclear receptor subfamily 1, group D, member 2	45.43	69.83	6.24	7.67	**0.049**
Nr1i3	12355	nuclear receptor subfamily 1, group I, member 3	8.99	7.69	0.43	0.27	**0.043**
Nr5a1	26423	nuclear receptor subfamily 5, group A, member 1	6.29	5.89	0.06	0.14	**0.041**
Nrap	18175	nebulin-related anchoring protein	10.72	9.16	0.29	0.50	**0.035**
Nrd1	230598	nardilysin, N-arginine dibasic convertase, NRD convertase 1	549.64	501.18	16.81	10.09	**0.048**
Nrde2	217827	nrde-2 necessary for RNA interference, domain containing	26.79	21.90	1.03	1.09	**0.017**
Nrg1	211323	neuregulin 1	41.83	55.44	2.78	1.96	**0.007**
Nrgn	64011	neurogranin	10.41	9.15	0.41	0.19	**0.030**
Nrl	18185	neural retina leucine zipper gene	7.38	6.69	0.12	0.20	**0.026**
Nsd1	18193	nuclear receptor-binding SET-domain protein 1	329.82	376.42	7.24	10.63	**0.011**
Ntsr1	18216	neurotensin receptor 1	14.58	10.61	0.58	0.34	**0.001**
Nucb1	18220	nucleobindin 1	44.07	53.95	2.33	2.65	**0.031**
Nuggc	100503545	nuclear GTPase, germinal center associated	10.21	9.16	0.28	0.19	**0.021**
Nxf2	83454	nuclear RNA export factor 2	4.75	4.98	0.06	0.04	**0.025**
Nxf3	245610	nuclear RNA export factor 3	5.39	5.79	0.12	0.10	**0.045**
Oas1h	246729	2'-5' oligoadenylate synthetase 1H	4.95	5.69	0.08	0.10	**0.001**
Oat	18242	ornithine aminotransferase	67.72	91.82	2.68	6.30	**0.013**
Oaz1	18245	ornithine decarboxylase antizyme 1	533.69	641.28	28.13	9.15	**0.011**
Obox1	71468	oocyte specific homeobox 1	4.81	4.11	0.14	0.11	**0.007**
Ocrl	320634	oculocerebrorenal syndrome of Lowe	31.78	43.15	1.44	2.28	**0.006**
Ocstamp	74614	osteoclast stimulatory transmembrane protein	13.45	9.11	1.56	0.37	**0.036**
Odf2	18286	outer dense fiber of sperm tails 2	62.25	100.61	7.96	12.42	**0.041**
Ogfod2	66627	2-oxoglutarate and iron-dependent oxygenase domain containing 2	22.26	17.77	1.28	1.01	**0.033**
Ogn	18295	osteoglycin	6.66	8.59	0.33	0.37	**0.008**
Oip5	70645	Opa interacting protein 5	9.16	12.65	0.59	1.29	**0.049**
Olfr1012	258561	olfactory receptor 1012	6.31	5.33	0.21	0.21	**0.016**
Olfr1015	258564	olfactory receptor 1015	5.42	7.21	0.30	0.51	**0.024**
Olfr1022	258582	olfactory receptor 1022	4.95	4.21	0.20	0.14	**0.023**
Olfr1036	258245	olfactory receptor 1036	4.81	3.98	0.28	0.09	**0.032**
Olfr1042	257941	olfactory receptor 1042	4.28	4.94	0.15	0.14	**0.017**
Olfr1052	259012	olfactory receptor 1052	4.21	4.76	0.10	0.19	**0.040**
Olfr1061	259022	olfactory receptor 1061	3.96	4.99	0.26	0.24	**0.028**
Olfr1066	257880	olfactory receptor 1066	5.08	6.23	0.12	0.35	**0.020**
Olfr1085	258583	olfactory receptor 1085	22.18	15.60	2.07	1.17	**0.033**
Olfr11	218066	olfactory receptor 11	6.20	5.26	0.37	0.09	**0.047**
Olfr1105	258085	olfactory receptor 1105	5.44	4.13	0.31	0.07	**0.007**

Olfr1132	258833	olfactory receptor 1132	4.24	5.48	0.31	0.20	**0.015**
Olfr1155	258636	olfactory receptor 1155	4.58	5.23	0.13	0.20	**0.033**
Olfr1170	258525	olfactory receptor 1170	6.10	4.75	0.39	0.15	**0.019**
Olfr1188	258921	olfactory receptor 1188	5.20	4.23	0.12	0.08	**0.000**
Olfr120	258624	olfactory receptor 120	4.27	5.05	0.24	0.13	**0.030**
Olfr1209	258453	olfactory receptor 1209	5.50	4.64	0.25	0.13	**0.024**
Olfr1217	258903	olfactory receptor 1217	3.69	3.92	0.05	0.07	**0.037**
Olfr1225	258893	olfactory receptor 1225	5.03	5.49	0.13	0.12	**0.038**
Olfr124	259064	olfactory receptor 124	4.14	3.70	0.09	0.11	**0.020**
Olfr1249	257984	olfactory receptor 1249	3.91	4.81	0.06	0.26	**0.014**
Olfr1258	258980	olfactory receptor 1258	3.90	4.25	0.12	0.06	**0.047**
Olfr1262	258976	olfactory receptor 1262	5.18	6.03	0.23	0.14	**0.020**
Olfr127	258374	olfactory receptor 127	6.28	7.80	0.28	0.55	**0.048**
Olfr1274-ps	258330	olfactory receptor 1274, pseudogene	3.31	3.69	0.09	0.12	**0.049**
Olfr1275	257980	olfactory receptor 1275	3.70	4.15	0.12	0.06	**0.013**
Olfr1316	258737	olfactory receptor 1316	5.77	4.77	0.28	0.22	**0.031**
Olfr1346	258918	olfactory receptor 1346	7.66	6.22	0.35	0.30	**0.021**
Olfr1348	258915	olfactory receptor 1348	8.06	7.19	0.33	0.13	**0.050**
Olfr1349	269862	olfactory receptor 1349	7.39	6.05	0.26	0.23	**0.008**
Olfr1360	258536	olfactory receptor 1360	24.94	15.04	2.69	0.99	**0.014**
Olfr1361	258534	olfactory receptor 1361	8.56	9.64	0.23	0.18	**0.011**
Olfr1366	258280	olfactory receptor 1366	4.29	4.82	0.14	0.05	**0.011**
Olfr1370	258528	olfactory receptor 1370	8.78	7.46	0.15	0.36	**0.015**
Olfr141	257913	olfactory receptor 141	4.98	6.26	0.11	0.37	**0.017**
Olfr1414	259041	olfactory receptor 1414	7.05	5.33	0.63	0.11	**0.036**
Olfr1417	258938	olfactory receptor 1417	13.91	9.88	0.66	0.45	**0.002**
Olfr1426	258805	olfactory receptor 1426	4.88	5.91	0.21	0.33	**0.037**
Olfr1443	258693	olfactory receptor 1443	4.29	4.78	0.12	0.16	**0.043**
Olfr1447	258698	olfactory receptor 1447	4.61	4.11	0.05	0.07	**0.001**
Olfr1459	258684	olfactory receptor 1459	4.26	4.05	0.06	0.04	**0.027**
Olfr1484	258288	olfactory receptor 1484	7.18	5.80	0.26	0.21	**0.006**
Olfr157	100040268	olfactory receptor 157	8.44	6.91	0.50	0.31	**0.040**
Olfr170	258959	olfactory receptor 170	3.71	4.59	0.15	0.28	**0.031**
Olfr186	258318	olfactory receptor 186	5.05	5.66	0.20	0.08	**0.028**
Olfr204	258994	olfactory receptor 204	4.23	4.71	0.11	0.16	**0.046**
Olfr211	258914	olfactory receptor 211	17.33	12.29	1.25	1.15	**0.025**
Olfr218	258880	olfactory receptor 218	6.69	8.70	0.74	0.33	**0.049**
Olfr220	546747	olfactory receptor 220	6.02	5.24	0.21	0.18	**0.0**
Olfr237-ps1	258648	olfactory receptor 237, pseudogene 1	4.62	5.10	0.11	0.05	**0.008**
Olfr259	258766	olfactory receptor 259	14.19	24.23	1.16	1.57	**0.002**
Olfr283	259038	olfactory receptor 283	7.89	9.05	0.27	0.36	**0.042**
Olfr3	18328	olfactory receptor 3	9.53	8.06	0.51	0.25	**0.040**
Olfr315	258531	olfactory receptor 315	11.62	8.43	0.67	0.31	**0.005**
Olfr356	258617	olfactory receptor 356	9.04	10.19	0.13	0.41	**0.037**
Olfr371	258858	olfactory receptor 371	14.15	12.09	0.71	0.40	**0.044**
Olfr402	258703	olfactory receptor 402	5.76	4.76	0.39	0.10	**0.048**
Olfr46	18345	olfactory receptor 46	5.31	5.80	0.10	0.03	**0**
Olfr477	258928	olfactory receptor 477	3.67	4.08	0.06	0.08	**0.007**
Olfr484	258492	olfactory receptor 484	18.32	23.41	1.17	1.29	**0.027**
Olfr5	18349	olfactory receptor 5	5.40	4.75	0.18	0.14	**0.029**
Olfr502	258734	olfactory receptor 502	3.75	4.55	0.06	0.20	**0.01**
Olfr523	258511	olfactory receptor 523	15.25	10.89	0.68	0.43	**0.002**
Olfr527	257939	olfactory receptor 527	21.84	18.34	0.39	0.49	**0.001**
Olfr535	258956	olfactory receptor 535	9.85	7.54	0.55	0.24	**0.009**
Olfr543	257947	olfactory receptor 543	9.76	6.57	0.72	0.46	**0.010**
Olfr549	259105	olfactory receptor 549	30.83	25.74	1.08	0.35	**0.004**
Olfr550	259108	olfactory receptor 550	5.24	4.42	0.16	0.23	**0.027**
Olfr559	259116	olfactory receptor 559	17.94	23.97	2.32	0.71	**0.047**
Olfr569	259092	olfactory receptor 569	6.03	4.98	0.34	0.16	**0.030**
Olfr572	259093	olfactory receptor 572	4.04	4.60	0.03	0.20	**0.036**

Olfr612	545985	olfactory receptor 612	16.08	12.09	0.52	0.73	**0.004**
Olfr624	258189	olfactory receptor 624	4.94	4.75	0.03	0.07	**0.038**
Olfr655	258817	olfactory receptor 655	7.29	6.69	0.10	0.16	**0.018**
Olfr676	259099	olfactory receptor 676	5.61	6.62	0.13	0.36	**0.038**
Olfr685	258160	olfactory receptor 685	11.34	9.68	0.42	0.34	**0.022**
Olfr686	259072	olfactory receptor 686	9.12	7.47	0.43	0.31	**0.021**
Olfr687	668035	olfactory receptor 687	5.26	6.80	0.13	0.22	**0.001**
Olfr691	259063	olfactory receptor 691	10.89	7.88	0.70	0.25	**0.007**
Olfr720	258387	olfactory receptor 720	5.18	5.75	0.08	0.21	**0.041**
Olfr725	258314	olfactory receptor 725	4.11	4.43	0.05	0.07	**0.01**
Olfr739	258663	olfactory receptor 739	9.19	7.04	0.67	0.47	**0.040**
Olfr782	257985	olfactory receptor 782	4.82	6.12	0.15	0.24	**0.004**
Olfr820	258670	olfactory receptor 820	9.03	13.59	0.64	1.15	**0.013**
Olfr821	258772	olfactory receptor 821	5.79	4.51	0.22	0.11	**0.002**
Olfr885	257885	olfactory receptor 885	4.50	5.24	0.13	0.18	**0.015**
Olfr910	258807	olfactory receptor 910	4.46	3.95	0.14	0.12	**0.032**
Olfr914	258782	olfactory receptor 914	14.50	11.24	0.89	0.62	**0.02**
Olfr922	258777	olfactory receptor 922	5.41	4.51	0.32	0.03	**0.032**
Olfr97	258505	olfactory receptor 97	5.23	4.67	0.13	0.18	**0.045**
Olfr979	259112	olfactory receptor 979	4.43	3.80	0.20	0.12	**0.034**
Omp	18378	olfactory marker protein	9.26	7.79	0.16	0.34	**0.008**
Onecut1	15379	one cut domain, family member 1	8.45	7.47	0.31	0.18	**0.034**
Oog2	381570	oogenesin 2	8.08	7.24	0.25	0.12	**0.024**
Oosp3	225923	oocyte secreted protein 3	6.63	5.87	0.26	0.07	**0.032**
Orc4	26428	origin recognition complex, subunit 4	95.74	127.26	5.23	8.13	**0.017**
Os9	216440	amplified in osteosarcoma	216.06	191.34	4.98	8.16	**0.041**
Osbpl6	99031	oxysterol binding protein-like 6	33.43	44.94	2.08	3.83	**0.038**
Oscp1	230751	organic solute carrier partner 1	23.45	25.82	0.73	0.53	**0.040**
Ost4	67695	oligosaccharyltransferase 4 homolog (S. cerevisiae)	1174.65	1358.85	36.65	35.99	**0.012**
Ost4	67695	oligosaccharyltransferase 4 homolog (S. cerevisiae)	480.81	534.77	15.99	3.15	**0.016**
Ost4	67695	oligosaccharyltransferase 4 homolog (S. cerevisiae)	662.15	742.52	25.67	19.30	**0.05**
Otog	18419	otogelin	10.60	8.73	0.36	0.21	**0.004**
Otop1	21906	otopetrin 1	9.12	7.28	0.18	0.27	**0.001**
Otud1	71198	OTU domain containing 1	41.65	56.99	1.92	3.08	**0.01**
P2rx6	18440	purinergic receptor P2X, ligand-gated ion channel, 6	11.03	8.56	0.37	0.29	**0.002**
P4htm	74443	prolyl 4-hydroxylase, transmembrane (endoplasmic reticulum)	38.47	29.72	2.67	2.10	**0.042**
Pabpc1	18458	poly(A) binding protein, cytoplasmic 1	59.35	67.09	1.34	1.55	**0.009**
Palld	72333	palladin, cytoskeletal associated protein	15.11	20.34	0.85	1.72	**0.03**
Palm	18483	paralemmin	43.90	32.88	2.63	0.93	**0.008**
Palmd	114301	palmdelphin	15.00	20.69	0.63	1.73	**0.021**
Pam	18484	peptidylglycine alpha-amidating monooxygenase	49.21	59.18	2.97	1.65	**0.026**
Pan3	72587	PAN3 polyA specific ribonuclease subunit homolog (S. cerevisiae)	147.87	197.88	10.53	10.75	**0.016**
Papln	170721	papilin, proteoglycan-like sulfated glycoprotein	9.80	8.20	0.34	0.29	**0.012**
Parn	74108	poly(A)-specific ribonuclease (deadenylation nuclease)	91.05	118.89	6.51	5.49	**0.017**
Pask	269224	PAS domain containing serine/threonine kinase	12.42	13.85	0.33	0.40	**0.034**
Pax6	18508	paired box 6	18.71	16.42	0.62	0.69	**0.049**
Pbrm1	66923	polybromo 1	167.41	200.07	6.97	7.06	**0.017**
Pcdh11x	245578	protocadherin 11 X-linked	195.44	244.10	9.50	15.88	**0.039**
Pcdh12	53601	protocadherin 12	7.03	5.81	0.25	0.24	**0.01**
Pcdhb17	93888	protocadherin beta 17	33.15	50.03	3.22	5.93	**0.05**
Pcid2	234069	PCI domain containing 2	27.99	23.03	1.25	1.35	**0.036**
Pclo	26875	piccolo (presynaptic cytomatrix protein)	27.24	34.17	1.45	2.01	**0.031**
Pcmtd2	245867	protein-L-isoaspartate (D-aspartate) O-methyltransferase domain containing 2	80.38	118.70	2.60	14.74	**0.04**
Pcp4l1	66425	Purkinje cell protein 4-like 1	20.67	16.75	0.92	0.47	**0.009**
Pdcd1lg2	58205	programmed cell death 1 ligand 2	8.05	6.45	0.27	0.12	**0.002**
Pde11a	241489	phosphodiesterase 11A	9.35	7.09	0.32	0.26	**0.001**
Pde3a	54611	phosphodiesterase 3A, cGMP inhibited	21.47	26.38	1.52	0.19	**0.02**
Pdlim5	56376	PDZ and LIM domain 5	143.81	178.14	6.90	4.24	**0.005**
Pdzd7	100503041	PDZ domain containing 7	10.66	9.12	0.10	0.43	**0.013**

Pdzd9	67983	PDZ domain containing 9	6.88	7.94	0.14	0.24	**0.009**
Peak1	244895	pseudopodium-enriched atypical kinase 1	80.61	131.21	9.53	13.19	**0.021**
Pex14	56273	peroxisomal biogenesis factor 14	25.94	21.75	1.20	1.17	**0.047**
Pex6	224824	peroxisomal biogenesis factor 6	45.40	32.82	2.59	2.23	**0.01**
Pgam1	18648	phosphoglycerate mutase 1	276.26	231.59	5.94	9.14	**0.006**
Pgap3	320655	post-GPI attachment to proteins 3	8.78	7.57	0.34	0.25	**0.029**
Pgc	109820	progastricsin (pepsinogen C)	8.89	7.16	0.65	0.17	**0.042**
Pgls	66171	6-phosphogluconolactonase	131.03	108.84	4.90	4.00	**0.013**
Pglyrp1	21946	peptidoglycan recognition protein 1	25.98	14.09	1.51	1.58	**0.002**
Pglyrp4	384997	peptidoglycan recognition protein 4	7.09	5.99	0.28	0.27	**0.030**
Phf11a	219131	PHD finger protein 11A	29.88	23.89	1.58	1.76	**0.04**
Phxr4	18689	per-hexamer repeat gene 4	51.90	116.33	7.47	8.02	**0.001**
Pias2	17344	protein inhibitor of activated STAT 2	87.36	124.26	8.52	11.09	**0.039**
Pias4	59004	protein inhibitor of activated STAT 4	59.42	40.17	5.75	1.96	**0.019**
Picalm	233489	phosphatidylinositol binding clathrin assembly protein	635.17	706.62	23.41	11.24	**0.033**
Piezo2	667742	piezo-type mechanosensitive ion channel component 2	13.25	19.01	1.16	2.01	**0.048**
Pik3ca	18706	phosphatidylinositol 3-kinase, catalytic, alpha polypeptide	73.59	102.64	7.01	7.77	**0.032**
Pikfyve	18711	phosphoinositide kinase, FYVE finger containing	74.89	102.98	4.01	3.68	**0.002**
Pim1	18712	proviral integration site 1	9.04	11.66	0.10	1.05	**0.048**
Pink1	68943	PTEN induced putative kinase 1	43.04	49.89	1.54	1.66	**0.023**
Pirt	193003	phosphoinositide-interacting regulator of transient receptor potential channels	11.31	9.10	0.63	0.42	**0.027**
Pkd2l1	329064	polycystic kidney disease 2-like 1	8.00	6.57	0.47	0.13	**0.027**
Pkhd1l1	192190	polycystic kidney and hepatic disease 1-like 1	6.33	5.81	0.15	0.08	**0.023**
Pla2g1b	18778	phospholipase A2, group IB, pancreas	5.36	5.76	0.10	0.11	**0.04**
Pla2g2c	18781	phospholipase A2, group IIC	14.01	11.53	0.73	0.54	**0.035**
Plcd3	72469	phospholipase C, delta 3	10.79	9.50	0.21	0.33	**0.016**
Plekha4	69217	pleckstrin homology domain containing, family A (phosphoinositide binding specific) member 4	11.50	10.17	0.48	0.14	**0.037**
Plekhg2	101497	pleckstrin homology domain containing, family G (with RhoGef domain) member 2	11.10	13.21	0.51	0.61	**0.038**
Plin4	57435	perilipin 4	12.69	8.55	1.46	0.50	**0.04**
Plod2	26432	procollagen lysine, 2-oxoglutarate 5-dioxygenase 2	87.66	147.36	10.23	18.29	**0.029**
Plxnb1	235611	plexin B1	41.34	51.78	1.10	3.07	**0.018**
Pnmt	18948	phenylethanolamine-N-methyltransferase	7.09	5.19	0.64	0.22	**0.031**
Pnpla1	433091	patatin-like phospholipase domain containing 1	7.20	6.20	0.38	0.14	**0.05**
Pnpla7	241274	patatin-like phospholipase domain containing 7	12.68	10.07	0.89	0.12	**0.027**
Podnl1	244550	podocan-like 1	6.97	5.90	0.34	0.18	**0.033**
Pold4	69745	polymerase (DNA-directed), delta 4	59.67	44.78	2.91	2.85	**0.01**
Pold4	69745	polymerase (DNA-directed), delta 4	98.79	81.47	5.13	3.58	**0.032**
Pole2	18974	polymerase (DNA directed), epsilon 2 (p59 subunit)	11.20	18.14	1.46	1.78	**0.024**
Pom121l2	195236	POM121 membrane glycoprotein-like 2 (rat)	9.58	8.33	0.42	0.29	**0.050**
Pop5	117109	processing of precursor 5, ribonuclease P/MRP family (S. cerevisiae)	127.17	102.39	4.43	6.50	**0.020**
Pou4f2	18997	POU domain, class 4, transcription factor 2	8.71	7.25	0.42	0.19	**0.019**
Ppapdc3	227721	phosphatidic acid phosphatase type 2 domain containing 3	24.73	18.41	1.81	1.65	**0.042**
Ppie	56031	peptidylprolyl isomerase E (cyclophilin E)	23.05	19.50	0.66	0.75	**0.012**
Ppm1b	19043	protein phosphatase 1B, magnesium dependent, beta isoform	95.07	111.27	2.67	3.02	**0.007**
Ppp1r13l	333654	protein phosphatase 1, regulatory (inhibitor) subunit 13 like	9.49	7.07	0.66	0.31	**0.02**
Ppp1r18	76448	protein phosphatase 1, regulatory subunit 18	33.90	29.24	0.96	1.19	**0.023**
Ppp2r2b	72930	protein phosphatase 2, regulatory subunit B, beta	112.44	133.10	4.20	5.56	**0.025**
Ppp4c	56420	protein phosphatase 4, catalytic subunit	138.61	116.84	5.24	6.62	**0.042**
Ppp6r2	71474	protein phosphatase 6, regulatory subunit 2	171.12	209.74	13.07	6.19	**0.037**
Pqlc1	66943	PQ loop repeat containing 1	7.65	6.96	0.13	0.21	**0.033**
Pramef6	195555	PRAME family member 6	6.65	5.10	0.33	0.38	**0.022**
Pramel1	83491	preferentially expressed antigen in melanoma-like 1	9.98	9.27	0.19	0.17	**0.033**
Prcp	72461	prolylcarboxypeptidase (angiotensinase C)	81.97	65.46	3.04	2.73	**0.01**
Prdx4	53381	peroxiredoxin 4	103.25	139.41	9.31	6.09	**0.017**
Prh1	19131	proline rich protein HaeIII subfamily 1	12.66	8.72	0.57	0.84	**0.008**
Prkar1a	19084	protein kinase, cAMP dependent regulatory, type I, alpha	82.96	73.18	3.41	1.43	**0.038**
Prkcdbp	109042	protein kinase C, delta binding protein	38.22	43.68	1.04	1.70	**0.033**
Prkd1	18760	protein kinase D1	19.34	27.20	1.49	1.91	**0.018**

Prkrir	72981	protein-kinase, interferon-inducible double stranded RNA dependent inhibitor, repressor of (P58 repressor)	421.47	500.30	24.65	19.76	**0.047**
Prl	19109	prolactin	6.00	6.62	0.07	0.24	**0.045**
Prl7a1	19113	prolactin family 7, subfamily a, member 1	4.79	4.20	0.22	0.08	**0.044**
Prorsd1	67939	prolyl-tRNA synthetase domain containing 1	40.91	28.32	4.94	0.49	**0.044**
Proser2	227545	proline and serine rich 2	12.31	10.43	0.43	0.15	**0.006**
Prox1	19130	prospero homeobox 1	47.63	70.23	5.65	6.68	**0.042**
Prph2	19133	peripherin 2	15.47	11.57	0.60	0.35	**0.001**
Prr15l	217138	proline rich 15-like	10.57	8.33	0.70	0.19	**0.021**
Prr23a	623166	proline rich 23A	7.43	6.82	0.18	0.10	**0.024**
Prr27	73779	proline rich 27	17.27	12.31	1.12	1.16	**0.022**
Prrx1	18933	paired related homeobox 1	35.26	41.41	1.53	1.14	**0.018**
Prss12	19142	protease, serine 12 neurotrypsin (motopsin)	10.04	10.98	0.21	0.26	**0.030**
Prss28	114661	protease, serine 28	8.94	10.28	0.30	0.39	**0.034**
Prss32	69814	protease, serine 32	16.30	12.54	1.30	0.49	**0.036**
Prss41	71003	protease, serine 41	13.60	11.75	0.29	0.35	**0.007**
Prss44	73336	protease, serine 44	4.90	4.38	0.10	0.09	**0.008**
Prss58	232717	protease, serine 58	5.04	4.51	0.17	0.06	**0.026**
Psg-ps1	232919	pregnancy specific glycoprotein pseudogene 1	10.02	8.27	0.51	0.26	**0.023**
Psmb10	19171	proteasome (prosome, macropain) subunit, beta type 10	119.35	79.69	4.68	7.00	**0.003**
Psmb3	26446	proteasome (prosome, macropain) subunit, beta type 3	24.54	15.47	2.51	2.22	**0.035**
Psmd1	70247	proteasome (prosome, macropain) 26S subunit, non-ATPase, 1	341.08	290.14	16.83	5.84	**0.029**
Psmd4	19185	proteasome (prosome, macropain) 26S subunit, non-ATPase, 4	264.25	243.37	3.78	6.45	**0.031**
Psme4	103554	proteasome (prosome, macropain) activator subunit 4	136.76	155.86	1.96	5.12	**0.013**
Psors1c2	57390	psoriasis susceptibility 1 candidate 2 (human)	16.60	13.70	0.50	0.60	**0.010**
Ptbp3	230257	polypyrimidine tract binding protein 3	235.53	292.75	6.12	21.27	**0.041**
Pten	19211	phosphatase and tensin homolog	283.42	335.93	12.45	12.25	**0.024**
Ptf1a	19213	pancreas specific transcription factor, 1a	6.29	5.53	0.17	0.08	**0.007**
Ptgdr	19214	prostaglandin D receptor	5.18	4.76	0.04	0.16	**0.0**
Ptgir	19222	prostaglandin I receptor (IP)	9.30	7.75	0.15	0.13	**0.000**
Ptgs1	19224	prostaglandin-endoperoxide synthase 1	29.74	39.14	0.84	1.30	**0.001**
Ptgs2os2	102639566	prostaglandin-endoperoxide synthase 2, opposite strand 2	5.91	6.51	0.15	0.18	**0.043**
Pth1r	19228	parathyroid hormone 1 receptor	30.15	23.73	1.86	0.66	**0.018**
Ptk6	20459	PTK6 protein tyrosine kinase 6	6.19	5.30	0.20	0.09	**0.01**
Ptpn12	19248	protein tyrosine phosphatase, non-receptor type 12	178.41	209.63	7.39	9.54	**0.041**
Ptpn13	19249	protein tyrosine phosphatase, non-receptor type 13	18.05	26.47	0.61	1.72	**0.004**
Ptpn22	19260	protein tyrosine phosphatase, non-receptor type 22 (lymphoid)	8.18	7.04	0.37	0.11	**0.025**
Ptpn4	19258	protein tyrosine phosphatase, non-receptor type 4	143.36	184.85	5.61	11.59	**0.018**
Ptpn9	56294	protein tyrosine phosphatase, non-receptor type 9	71.93	99.38	7.98	5.38	**0.029**
Ptprz1	19283	protein tyrosine phosphatase, receptor type Z, polypeptide 1	1465.39	1669.48	26.55	38.73	**0.005**
Pum1	80912	pumilio RNA-binding family member 1	118.29	125.64	1.79	2.20	**0.041**
Pum2	80913	pumilio RNA-binding family member 2	134.15	152.39	3.57	2.07	**0.004**
Pus1	56361	pseudouridine synthase 1	20.78	23.67	0.42	0.59	**0.007**
Pvalb	19293	parvalbumin	13.91	10.13	0.56	0.64	**0.004**
Pwp2	110816	PWP2 periodic tryptophan protein homolog (yeast)	13.97	11.87	0.64	0.40	**0.032**
Pycrl	66194	pyrroline-5-carboxylate reductase-like	54.28	41.06	3.37	2.99	**0.026**
Pyy	217212	peptide YY	9.75	8.14	0.32	0.40	**0.020**
Rab11fip4	268451	RAB11 family interacting protein 4 (class II)	13.28	10.27	1.10	0.26	**0.038**
Rab11fip4os2	72218	RAB11 family interacting protein 4 (class II), opposite strand 2	5.39	6.06	0.15	0.21	**0.039**
Rab22a	19334	RAB22A, member RAS oncogene family	31.92	43.31	2.70	2.32	**0.019**
Rab39b	67790	RAB39B, member RAS oncogene family	140.86	113.01	2.78	3.77	**0.001**
Rab4b	19342	RAB4B, member RAS oncogene family	72.05	48.45	3.65	3.19	**0.00**
Rab9b	319642	RAB9B, member RAS oncogene family	36.27	27.72	2.89	0.94	**0.031**
Rabgap1l	29809	RAB GTPase activating protein 1-like	62.02	75.45	2.71	2.60	**0.012**
Ralgapa1	56784	Ral GTPase activating protein, alpha subunit 1	141.67	167.65	5.75	6.44	**0.024**
Ran	19384	RAN, member RAS oncogene family	526.85	472.38	11.41	13.95	**0.023**
Rassf10	78748	Ras association (RalGDS/AF-6) domain family (N-terminal) member 10	50.09	32.25	5.23	4.19	**0.037**
Rb1cc1	12421	RB1-inducible coiled-coil 1	105.02	132.08	3.03	3.62	**0.00**

Rbbp8	225182	retinoblastoma binding protein 8	37.46	51.65	2.50	3.36	**0.015**
Rbm15b	109095	RNA binding motif protein 15B	75.12	101.87	7.89	5.99	**0.04**
Rbm3os	70226	RNA binding motif protein 3, opposite strand	7.78	11.78	0.64	1.11	**0.021**
Rbpj	19664	recombination signal binding protein for immunoglobulin kappa J region	101.72	124.76	3.31	7.76	**0.034**
Rcor1	217864	REST corepressor 1	30.99	40.45	2.30	2.82	**0.041**
Rcsd1	226594	RCSD domain containing 1	26.77	21.12	1.54	1.24	**0.029**
Rec114	73673	REC114 meiotic recombination protein	14.82	19.53	1.22	0.77	**0.017**
Rec8	56739	REC8 meiotic recombination protein	6.06	5.65	0.08	0.14	**0.043**
Reep5	13476	receptor accessory protein 5	916.39	728.51	13.34	48.71	**0.010**
Relb	19698	avian reticuloendotheliosis viral (v-rel) oncogene related B	11.17	9.14	0.19	0.33	**0.002**
Rem1	19700	rad and gem related GTP binding protein 1	7.82	6.25	0.47	0.17	**0.019**
Repin1	58887	replication initiator 1	41.49	36.45	1.69	0.73	**0.034**
Ret	19713	ret proto-oncogene	14.82	12.16	0.59	0.91	**0.049**
Rev3l	19714	REV3-like, catalytic subunit of DNA polymerase zeta RAD54 like (S. cerevisiae)	387.91	492.66	21.33	19.51	**0.011**
Rex2	100043034	reduced expression 2	5.80	9.29	0.20	0.71	**0.003**
Rexo2	104444	REX2, RNA exonuclease 2 homolog (S. cerevisiae)	440.15	341.06	32.29	22.80	**0.046**
Rfx2	19725	regulatory factor X, 2 (influences HLA class II expression)	9.20	7.21	0.32	0.45	**0.011**
Rfx3	19726	regulatory factor X, 3 (influences HLA class II expression)	64.51	84.27	2.68	1.70	**0.001**
Rfx4	71137	regulatory factor X, 4 (influences HLA class II expression)	67.71	101.12	4.73	11.74	**0.039**
Rgmb	68799	repulsive guidance molecule family member B	41.96	57.67	1.58	4.58	**0.018**
Rgs6	50779	regulator of G-protein signaling 6	9.16	8.27	0.16	0.31	**0.044**
Rgs9	19739	regulator of G-protein signaling 9	47.61	40.01	1.71	0.48	**0.005**
Rhbdd3	279766	rhomboid domain containing 3	31.07	39.44	2.36	2.24	**0.042**
Rhoj	80837	ras homolog gene family, member J	18.87	23.12	1.22	0.45	**0.017**
Rhov	228543	ras homolog gene family, member V	10.23	8.25	0.62	0.40	**0.036**
Rhox2d	434760	reproductive homeobox 2D	5.38	6.44	0.15	0.35	**0.033**
Rhox2f	434764	reproductive homeobox 2F	5.12	4.29	0.17	0.26	**0.035**
Rhox2g	434766	reproductive homeobox 2G	5.16	4.10	0.31	0.11	**0.017**
Rhox4f	636177	reproductive homeobox 4F	4.81	6.69	0.20	0.38	**0.005**
Rhox5	18617	reproductive homeobox 5	5.68	6.84	0.21	0.36	**0.031**
Rian	75745	RNA imprinted and accumulated in nucleus	15.20	25.92	1.82	1.66	**0.005**
Rian	75745	RNA imprinted and accumulated in nucleus	34.17	46.61	1.58	3.03	**0.011**
Rimkla	194237	ribosomal modification protein rimK-like family member A	28.67	33.17	0.85	1.62	**0.049**
Rin3	217835	Ras and Rab interactor 3	30.45	26.92	1.16	0.74	**0.043**
Ring1	19763	ring finger protein 1	69.18	47.91	1.14	2.17	**0.000**
Ring1	19763	ring finger protein 1	35.85	28.67	2.13	1.25	**0.027**
Ripk4	72388	receptor-interacting serine-threonine kinase 4	7.28	5.81	0.53	0.21	**0.041**
Rmdn3	67809	regulator of microtubule dynamics 3	32.29	27.22	0.76	0.85	**0.004**
Rmnd5a	68477	required for meiotic nuclear division 5 homolog A (S. cerevisiae)	56.02	68.90	2.80	2.52	**0.014**
Rn7sk	19817	RNA, 7SK, nuclear	2920.23	3429.36	39.96	74.42	**0.001**
Rnf121	75212	ring finger protein 121	57.46	83.85	1.15	5.28	**0.003**
Rnf148	71300	ring finger protein 148	6.70	5.73	0.28	0.25	**0.041**
Rnf151	67504	ring finger protein 151	7.69	6.64	0.07	0.32	**0.018**
Rnf166	68718	ring finger protein 166	38.54	25.94	4.49	1.84	**0.041**
Rnf2	19821	ring finger protein 2	152.47	197.76	12.33	7.81	**0.021**
Rnf212	671564	ring finger protein 212	10.38	11.55	0.33	0.19	**0.022**
Rnf220	66743	ring finger protein 220	46.66	36.75	2.17	1.63	**0.011**
Rnf38	73469	ring finger protein 38	185.40	206.10	5.38	6.17	**0.045**
Rnpep	215615	arginyl aminopeptidase (aminopeptidase B)	10.23	8.53	0.44	0.37	**0.025**
Rnpep	215615	arginyl aminopeptidase (aminopeptidase B)	65.63	57.80	2.66	0.74	**0.030**
Ropn1	76378	ropporin, rhophilin associated protein 1	6.41	6.92	0.09	0.11	**0.014**
Ros1	19886	Ros1 proto-oncogene	7.15	6.46	0.16	0.14	**0.017**
Rp9	55934	retinitis pigmentosa 9 (human)	87.43	103.77	2.73	4.05	**0.015**
Rpl19	19921	ribosomal protein L19	14.31	12.71	0.11	0.23	**0.001**
Rpl19	19921	ribosomal protein L19	2112.40	1958.20	22.45	42.81	**0.019**
Rpl27	19942	ribosomal protein L27	1848.80	1730.63	25.39	13.01	**0.006**
Rpl3	27367	ribosomal protein L3	70.28	45.91	4.35	3.92	**0.006**
Rpl39	67248	ribosomal protein L39	2234.72	2445.54	49.54	23.72	**0.009**

Rpl3l	66211	ribosomal protein L3-like	7.10	6.22	0.19	0.16	**0.012**
Rpl4	67891	ribosomal protein L4	2044.06	2148.22	22.87	27.84	**0.028**
Rpl41	67945	ribosomal protein L41	184.10	112.23	14.27	14.04	**0.012**
Rpl7a	27176	ribosomal protein L7A	1912.56	1786.17	41.70	24.77	**0.040**
Rprml	104582	reprimo-like	16.88	13.08	1.28	0.74	**0.042**
Rps27	57294	ribosomal protein S27	24.82	14.72	3.32	1.67	**0.035**
Rptn	20129	repetin	4.64	5.00	0.08	0.06	**0.010**
Rrp1	18114	ribosomal RNA processing 1 homolog (S. cerevisiae)	221.12	181.30	10.47	3.07	**0.011**
Rrp7a	74778	ribosomal RNA processing 7 homolog A (S. cerevisiae)	42.69	70.62	2.00	7.08	**0.009**
Rsbn1l	242860	round spermatid basic protein 1-like	39.12	49.44	2.33	2.00	**0.02**
Rsf1	233532	remodeling and spacing factor 1	206.32	184.04	4.67	7.28	**0.042**
Rsg1	76166	REM2 and RAB-like small GTPase 1	7.46	8.43	0.20	0.31	**0.04**
Rtn1	104001	reticulon 1	183.91	168.62	3.53	3.40	**0.02**
Rtn4rl2	269295	reticulon 4 receptor-like 2	19.56	15.40	1.13	1.00	**0.033**
Ryk	20187	receptor-like tyrosine kinase	151.05	198.53	8.51	14.45	**0.03**
Ryr3	20192	ryanodine receptor 3	11.07	12.34	0.35	0.23	**0.02**
S100a3	20197	S100 calcium binding protein A3	78.16	52.51	6.09	5.70	**0.022**
S100a4	20198	S100 calcium binding protein A4	326.21	224.79	24.31	14.77	**0.012**
S100a6	20200	S100 calcium binding protein A6 (calcyclin)	2278.25	1957.97	38.78	49.84	**0.002**
S100pbp	74648	S100P binding protein	60.96	85.97	3.60	5.57	**0.009**
S1pr5	94226	sphingosine-1-phosphate receptor 5	52.39	27.73	5.85	3.64	**0.012**
Sacm1l	83493	SAC1 (suppressor of actin mutations 1, homolog)-like (S. cerevisiae)	93.55	132.70	3.99	9.45	**0.009**
Sall3	20689	sal-like 3 (Drosophila)	39.04	46.49	1.42	2.32	**0.034**
Sbk1	104175	SH3-binding kinase 1	30.51	36.91	1.64	1.78	**0.038**
Scgb1b20	545948	secretoglobin, family 1B, member 20	15.67	11.20	0.88	0.57	**0.005**
Scin	20259	scinderin	6.39	6.78	0.06	0.08	**0.006**
Scly	50880	selenocysteine lyase	29.29	19.81	3.27	0.71	**0.030**
Scn3b	235281	sodium channel, voltage-gated, type III, beta	64.15	84.39	3.12	7.15	**0.04**
Scnn1b	20277	sodium channel, nonvoltage-gated 1 beta	6.24	5.38	0.13	0.18	**0.008**
Scnn1g	20278	sodium channel, nonvoltage-gated 1 gamma	18.57	14.86	1.33	0.62	**0.044**
Scoc	56367	short coiled-coil protein	17.21	14.11	0.80	0.52	**0.017**
Scpep1	74617	serine carboxypeptidase 1	83.29	103.61	3.31	6.83	**0.04**
Sdc2	15529	syndecan 2	109.55	135.41	4.83	8.64	**0.040**
Sdcbp2	228765	syndecan binding protein (syntenin) 2	14.55	11.39	1.17	0.42	**0.043**
Sdsl	257635	serine dehydratase-like	10.90	8.75	0.70	0.30	**0.031**
Sec14l3	380683	SEC14-like 3 (S. cerevisiae)	11.39	9.41	0.46	0.33	**0.013**
Selm	114679	selenoprotein M	210.49	184.40	7.25	6.91	**0.040**
Sept7	235072	septin 7	1363.45	1438.87	28.45	11.03	**0.048**
Serinc1	56442	serine incorporator 1	534.07	630.68	24.65	27.24	**0.039**
Serpina3a	74069	serine (or cysteine) peptidase inhibitor, clade A, member 3A	6.65	5.31	0.38	0.26	**0.027**
Serpina6	12401	serine (or cysteine) peptidase inhibitor, clade A, member 6	5.61	4.89	0.18	0.12	**0.017**
Serpinb5	20724	serine (or cysteine) peptidase inhibitor, clade B, member 5	4.49	5.13	0.08	0.21	**0.030**
Serpinb6d	238568	serine (or cysteine) peptidase inhibitor, clade B, member 6d	6.36	5.29	0.33	0.04	**0.018**
Serping1	12258	serine (or cysteine) peptidase inhibitor, clade G, member 1	10.80	7.91	0.78	0.61	**0.027**
Sesn1	140742	sestrin 1	62.35	83.65	7.35	3.87	**0.043**
Sesn3	75747	sestrin 3	233.48	292.79	8.41	10.20	**0.004**
Setd8	67956	SET domain containing (lysine methyltransferase) 8	179.53	145.66	5.90	5.39	**0.005**
Sfta2	433102	surfactant associated 2	9.37	8.48	0.21	0.21	**0.023**
Sgce	20392	sarcoglycan, epsilon	99.13	114.35	3.28	5.17	**0.047**
Sgpl1	20397	sphingosine phosphate lyase 1	100.47	127.72	8.29	4.75	**0.029**
Sgpp1	81535	sphingosine-1-phosphate phosphatase 1	108.85	134.58	8.18	5.89	**0.043**
Sh2b2	23921	SH2B adaptor protein 2	20.10	17.06	0.55	1.11	**0.050**
Sh3rf2	269016	SH3 domain containing ring finger 2	10.86	9.09	0.37	0.16	**0.005**
Sh3tc1	231147	SH3 domain and tetratricopeptide repeats 1	11.64	14.27	0.83	0.65	**0.047**
Shisa6	380702	shisa homolog 6 (Xenopus laevis)	114.12	170.10	9.71	6.02	**0.003**
Siah2	20439	seven in absentia 2	21.13	18.05	0.91	0.73	**0.039**
Siglec5	233186	sialic acid binding Ig-like lectin 5	7.89	9.10	0.20	0.33	**0.0**
Sil1	81500	endoplasmic reticulum chaperone SIL1 homolog (S. cerevisiae)	102.11	76.86	4.51	7.07	**0.024**
Sin3b	20467	transcriptional regulator, SIN3B (yeast)	36.85	32.24	0.83	1.02	**0.013**
Sipa1l3	74206	signal-induced proliferation-associated 1 like 3	28.51	36.68	2.26	1.13	**0.018**
Sis	69983	sucrase isomaltase (alpha-glucosidase)	5.44	6.84	0.29	0.32	**0.018**

Six1	20471	sine oculis-related homeobox 1	12.96	11.14	0.31	0.45	**0.016**
Slamf7	75345	SLAM family member 7	7.13	6.20	0.14	0.13	**0.003**
Slamf8	74748	SLAM family member 8	9.09	7.63	0.19	0.51	**0.037**
Slamf9	98365	SLAM family member 9	14.05	18.31	0.95	1.23	**0.033**
Slc12a5	57138	solute carrier family 12, member 5	13.08	10.68	0.82	0.29	**0.033**
Slc16a10	72472	solute carrier family 16 (monocarboxylic acid transporters), member 10	12.28	17.23	1.87	0.52	**0.0**
Slc16a3	80879	solute carrier family 16 (monocarboxylic acid transporters), member 3	16.05	13.25	0.58	0.72	**0.023**
Slc16a8	57274	solute carrier family 16 (monocarboxylic acid transporters), member 8	10.64	7.63	0.85	0.38	**0.018**
Slc17a4	319848	solute carrier family 17 (sodium phosphate), member 4	7.74	6.42	0.44	0.26	**0.040**
Slc17a5	235504	solute carrier family 17 (anion/sugar transporter), member 5	26.78	37.17	0.51	4.20	**0.049**
Slc18b1	76306	solute carrier family 18, subfamily B, member 1	32.21	37.55	1.74	1.21	**0.045**
Slc22a3	20519	solute carrier family 22 (organic cation transporter), member 3	45.22	63.46	4.08	3.26	**0.01**
Slc23a3	22626	solute carrier family 23 (nucleobase transporters), member 3	13.22	11.67	0.43	0.22	**0.019**
Slc25a12	78830	solute carrier family 25 (mitochondrial carrier, Aralar), member 12	68.88	80.02	2.00	3.97	**0.05**
Slc25a19	67283	solute carrier family 25 (mitochondrial thiamine pyrophosphate carrier), member 19	24.80	19.18	0.66	1.01	**0.003**
Slc25a25	227731	solute carrier family 25 (mitochondrial carrier, phosphate carrier), member 25	14.87	12.25	0.80	0.57	**0.037**
Slc25a3	18674	solute carrier family 25 (mitochondrial carrier, phosphate carrier), member 3	158.30	147.32	0.74	3.84	**0.031**
Slc30a3	22784	solute carrier family 30 (zinc transporter), member 3	9.97	8.85	0.21	0.30	**0.022**
Slc30a6	210148	solute carrier family 30 (zinc transporter), member 6	30.28	43.13	2.46	4.25	**0.040**
Slc31a1	20529	solute carrier family 31, member 1	122.20	169.51	8.03	16.56	**0.042**
Slc31a2	20530	solute carrier family 31, member 2	50.33	42.62	2.22	1.81	**0.036**
Slc32a1	22348	solute carrier family 32 (GABA vesicular transporter), member 1	8.51	7.57	0.20	0.19	**0.014**
Slc35e4	103710	solute carrier family 35, member E4	34.56	25.75	2.60	1.12	**0.021**
Slc37a1	224674	solute carrier family 37 (glycerol-3-phosphate transporter), member 1	12.20	9.31	0.63	0.26	**0.01**
Slc38a11	320106	solute carrier family 38, member 11	6.39	5.31	0.25	0.20	**0.015**
Slc38a3	76257	solute carrier family 38, member 3	118.11	156.35	5.63	10.63	**0.019**
Slc38a7	234595	solute carrier family 38, member 7	36.04	30.24	1.58	0.93	**0.020**
Slc39a3	106947	solute carrier family 39 (zinc transporter), member 3	20.70	18.32	0.56	0.45	**0.016**
Slc39a7	14977	solute carrier family 39 (zinc transporter), member 7	159.54	128.18	4.90	3.93	**0.002**
Slc47a1	67473	solute carrier family 47, member 1	9.28	8.35	0.30	0.06	**0.023**
Slc47a2	380701	solute carrier family 47, member 2	9.71	8.18	0.53	0.23	**0.04**
Slc4a5	232156	solute carrier family 4, sodium bicarbonate cotransporter, member 5	7.19	6.23	0.35	0.07	**0.037**
Slc4a7	218756	solute carrier family 4, sodium bicarbonate cotransporter, member 7	80.17	102.80	5.30	4.89	**0.020**
Slc52a3	69698	solute carrier protein family 52, member 3	10.03	8.43	0.28	0.13	**0.002**
Slc5a4b	64454	solute carrier family 5 (neutral amino acid transporters, system A), member 4b	13.88	11.50	0.63	0.27	**0.013**
Slc5a8	216225	solute carrier family 5 (iodide transporter), member 8	10.75	9.71	0.39	0.05	**0.037**
Slc6a12	14411	solute carrier family 6 (neurotransmitter transporter, betaine/GABA), member 12	8.41	6.99	0.08	0.29	**0.003**
Slc6a17	229706	solute carrier family 6 (neurotransmitter transporter), member 17	10.27	7.17	1.12	0.20	**0.034**
Slc6a5	104245	solute carrier family 6 (neurotransmitter transporter, glycine), member 5	9.14	7.57	0.47	0.25	**0.026**
Slco2a1	24059	solute carrier organic anion transporter family, member 2a1	17.35	13.32	0.75	1.29	**0.035**
Slfn8	276950	schlafen 8	16.50	11.55	0.47	0.82	**0.002**
Slit3	20564	slit homolog 3 (Drosophila)	15.99	12.60	0.89	0.76	**0.03**
Sln	66402	sarcolipin	4.51	4.06	0.08	0.02	**0.002**
Smad7	17131	SMAD family member 7	125.08	79.71	10.68	5.13	**0.009**
Smarcd2	83796	SWI/SNF related, matrix associated, actin dependent regulator of chromatin, subfamily d, member 2	21.04	17.28	0.87	0.66	**0.014**
Smyd1	12180	SET and MYND domain containing 1	10.40	8.76	0.27	0.23	**0.004**
Smyd3	69726	SET and MYND domain containing 3	28.14	33.12	1.20	1.43	**0.037**
Snhg5	72655	small nucleolar RNA host gene 5	268.65	212.25	18.18	13.15	**0.05**
Snhg6	73824	small nucleolar RNA host gene 6	1425.40	1318.51	10.61	35.63	**0.028**
Snhg7os	329369	small nucleolar RNA host gene 7, opposite strand	14.92	12.65	0.83	0.25	**0.040**
Snora73b	1003069	small nucleolar RNA, H/ACA box 73b	8.82	20.58	0.88	4.16	**0.03**

	45						
Snph	241727	syntaphilin	24.87	20.56	1.18	0.52	**0.015**
Snrk	20623	SNF related kinase	33.03	43.88	1.02	1.28	**0.001**
Snrnp40	66585	small nuclear ribonucleoprotein 40 (U5)	107.16	87.42	1.64	5.18	**0.011**
Snrpg	68011	small nuclear ribonucleoprotein polypeptide G	596.85	506.60	14.10	23.32	**0.016**
Sntb1	20649	syntrophin, basic 1	8.93	7.17	0.35	0.26	**0.007**
Sntb2	20650	syntrophin, basic 2	16.37	13.57	0.64	0.81	**0.035**
Snx10	71982	sorting nexin 10	43.33	55.65	2.45	3.95	**0.038**
Snx16	74718	sorting nexin 16	37.31	55.20	3.83	5.82	**0.04**
Snx20	71607	sorting nexin 20	13.88	10.96	0.94	0.41	**0.029**
Socs2	216233	suppressor of cytokine signaling 2	8.25	7.51	0.23	0.19	**0.049**
Soga1	320706	suppressor of glucose, autophagy associated 1	126.89	106.04	4.87	4.06	**0.017**
Soga3	67412	SOGA family member 3	78.56	65.57	3.42	1.31	**0.012**
Sorbs2os	319940	sorbin and SH3 domain containing 2, opposite strand	6.55	7.50	0.14	0.22	**0.011**
Sord	20322	sorbitol dehydrogenase	40.62	58.01	1.91	3.36	**0.004**
Sowahb	78088	sosondowah ankyrin repeat domain family member B	7.94	6.57	0.50	0.19	**0.043**
Sox14	20669	SRY (sex determining region Y)-box 14	15.02	12.25	0.57	0.25	**0.004**
Sox9	20682	SRY (sex determining region Y)-box 9	78.93	104.01	7.47	6.71	**0.047**
Sp5	64406	trans-acting transcription factor 5	12.42	9.72	0.74	0.45	**0.020**
Spaca5	278203	sperm acrosome associated 5	4.88	6.60	0.27	0.53	**0.03**
Spag4	245865	sperm associated antigen 4	11.92	10.21	0.49	0.40	**0.035**
Spata13	219140	spermatogenesis associated 13	24.53	28.35	0.79	1.26	**0.042**
Spata31d1c	238683	spermatogenesis associated 31 subfamily D, member 1C	8.35	6.93	0.51	0.18	**0.039**
Spata45	75558	spermatogenesis associated 45	8.95	6.93	0.69	0.37	**0.042**
Spatc1l	76573	spermatogenesis and centriole associated 1 like	11.16	9.19	0.57	0.42	**0.032**
Spdya	70891	speedy homolog A (Xenopus laevis)	13.40	16.67	0.73	1.11	**0.049**
Speer3	71026	spermatogenesis associated glutamate (E)-rich protein 3	4.41	5.21	0.17	0.28	**0.050**
Speer4c	1005029 67	spermatogenesis associated glutamate (E)-rich protein 4c	14.17	20.72	1.47	2.06	**0.04**
Sphkap	77629	SPHK1 interactor, AKAP domain containing	8.76	7.74	0.32	0.24	**0.045**
Spin1	20729	spindlin 1	230.42	289.59	9.19	14.13	**0.013**
Spin1	20729	spindlin 1	165.60	204.24	12.17	7.43	**0.035**
Spns3	77577	spinster homolog 3	15.23	13.33	0.62	0.35	**0.037**
Spocd1	622480	SPOC domain containing 1	15.23	11.64	1.06	0.19	**0.016**
Sprr1a	20753	small proline-rich protein 1A	11.23	8.39	0.71	0.33	**0.011**
Spry4	24066	sprouty homolog 4 (Drosophila)	82.77	122.49	12.40	9.21	**0.042**
Spsb4	211949	splA/ryanodine receptor domain and SOCS box containing 4	11.48	9.22	0.86	0.11	**0.040**
Sptbn1	20742	spectrin beta, non-erythrocytic 1	281.44	255.64	4.83	4.80	**0.009**
Srcin1	56013	SRC kinase signaling inhibitor 1	18.33	12.85	2.00	0.62	**0.039**
Srebf1	20787	sterol regulatory element binding transcription factor 1	28.84	23.76	0.21	1.80	**0.03**
Srsf2	20382	serine/arginine-rich splicing factor 2	587.71	520.02	24.76	9.28	**0.043**
Ssbp2	66970	single-stranded DNA binding protein 2	32.99	61.44	4.89	4.41	**0.005**
Ssna1	68475	Sjogren's syndrome nuclear autoantigen 1	75.74	55.35	3.69	3.18	**0.006**
Sspo	243369	SCO-spondin	8.92	7.91	0.31	0.14	**0.024**
Sstr3	20607	somatostatin receptor 3	20.14	15.02	0.94	0.75	**0.01**
Sstr5	20609	somatostatin receptor 5	10.93	8.95	0.74	0.10	**0.038**
Ssu2	243612	ssu-2 homolog (C. elegans)	9.23	7.41	0.48	0.37	**0.025**
Stab2	192188	stabilin 2	8.52	7.16	0.30	0.04	**0.00**
Stac2	217154	SH3 and cysteine rich domain 2	7.43	5.60	0.46	0.30	**0.016**
Stambpl1	76630	STAM binding protein like 1	81.80	63.47	2.58	6.47	**0.039**
Stat6	20852	signal transducer and activator of transcription 6	13.91	18.91	1.09	0.96	**0.014**
Stc2	20856	stanniocalcin 2	16.44	11.92	0.42	0.61	**0.001**
Stfa3	20863	stefin A3	4.43	5.45	0.23	0.32	**0.042**
Stk17b	98267	serine/threonine kinase 17b (apoptosis-inducing)	53.07	85.07	6.45	5.47	**0.009**
Stk3	56274	serine/threonine kinase 3	74.21	116.04	8.31	6.34	**0.007**
Stk32c	57740	serine/threonine kinase 32C	16.44	11.31	0.45	0.98	**0.003**
Stmn4	56471	stathmin-like 4	1437.50	1141.75	41.65	59.81	**0.007**
Stoml1	69106	stomatin-like 1	23.93	18.64	1.15	0.74	**0.008**
Ston1	77057	stonin 1	8.47	11.80	0.43	0.38	**0.001**
Strn4	97387	striatin, calmodulin binding protein 4	41.96	50.86	1.27	1.25	**0.002**
Stxbp2	20911	syntaxin binding protein 2	68.73	46.35	4.56	5.03	**0.016**

Sub1	20024	SUB1 homolog (S. cerevisiae)	471.15	442.70	8.13	5.34	**0.026**
Sult2a1	20859	sulfotransferase family 2A, dehydroepiandrosterone (DHEA)-preferring, member 1	4.83	5.63	0.21	0.25	**0.048**
Sult2a3	629203	sulfotransferase family 2A, dehydroepiandrosterone (DHEA)-preferring, member 3	6.06	5.28	0.17	0.26	**0.042**
Sult2b1	54200	sulfotransferase family, cytosolic, 2B, member 1	7.81	6.94	0.25	0.18	**0.03**
Susd2	71733	sushi domain containing 2	9.95	8.82	0.28	0.19	**0.016**
Suz12	52615	suppressor of zeste 12 homolog (Drosophila)	163.80	213.56	4.68	11.93	**0.008**
Swap70	20947	SWA-70 protein	26.37	36.76	1.32	3.01	**0.019**
Syap1	67043	synapse associated protein 1	88.19	99.70	2.37	3.05	**0.025**
Syf2	68592	SYF2 homolog, RNA splicing factor (S. cerevisiae)	313.09	271.96	8.80	10.75	**0.025**
Syf2	68592	SYF2 homolog, RNA splicing factor (S. cerevisiae)	365.44	303.40	13.49	16.84	**0.028**
Syf2	68592	SYF2 homolog, RNA splicing factor (S. cerevisiae)	363.13	306.04	15.02	17.65	**0.049**
Syk	20963	spleen tyrosine kinase	8.67	9.91	0.26	0.37	**0.035**
Sympk	68188	symplekin	155.94	127.33	6.80	6.25	**0.021**
Syn2	20965	synapsin II	63.92	89.83	7.36	6.20	**0.036**
Synb	239167	syncytin b	18.31	14.93	0.84	0.73	**0.023**
Syndig1l	627191	synapse differentiation inducing 1 like	10.99	8.55	0.71	0.24	**0.017**
Synj1	104015	synaptojanin 1	93.85	116.13	4.56	2.81	**0.006**
Synpo	104027	synaptopodin	10.43	9.29	0.37	0.23	**0.040**
Synpo2	118449	synaptopodin 2	7.62	6.61	0.34	0.14	**0.034**
Syt15	319508	synaptotagmin XV	14.54	10.68	1.47	0.45	**0.046**
Taar4	209513	trace amine-associated receptor 4	8.41	7.09	0.40	0.28	**0.036**
Tab1	66513	TGF-beta activated kinase 1/MAP3K7 binding protein 1	23.80	30.71	1.66	2.15	**0.044**
Taf1	270627	TAF1 RNA polymerase II, TATA box binding protein (TBP)-associated factor	120.10	139.80	1.69	1.64	**0.000**
Taf1d	75316	TATA box binding protein (Tbp)-associated factor, RNA polymerase I, D	103.50	159.54	8.29	17.35	**0.027**
Taf5l	102162	TAF5-like RNA polymerase II, p300/CBP-associated factor (PCAF)-associated factor	28.64	33.20	1.57	0.93	**0.047**
Taok1	216965	TAO kinase 1	238.28	279.02	6.41	9.04	**0.010**
Taok1	216965	TAO kinase 1	320.78	410.14	30.12	16.65	**0.041**
Tapbpl	213233	TAP binding protein-like	21.66	16.34	1.35	0.33	**0.009**
Tarbp2	21357	TAR (HIV) RNA binding protein 2	24.87	20.83	1.10	0.50	**0.015**
Tas2r105	57252	taste receptor, type 2, member 105	5.41	4.73	0.20	0.11	**0.025**
Tas2r107	387342	taste receptor, type 2, member 107	3.58	4.15	0.03	0.12	**0.00**
Tas2r119	57254	taste receptor, type 2, member 119	10.65	8.38	0.66	0.22	**0.017**
Tbc1d23	67581	TBC1 domain family, member 23	114.21	148.50	8.59	7.98	**0.027**
Tbc1d8	54610	TBC1 domain family, member 8	36.49	42.29	0.95	1.77	**0.028**
Tbcel	272589	tubulin folding cofactor E-like	42.46	52.07	2.14	1.35	**0.009**
Tbx19	83993	T-box 19	10.50	8.63	0.36	0.57	**0.033**
Tcam1	75870	testicular cell adhesion molecule 1	9.27	7.36	0.68	0.32	**0.043**
Tceb2	67673	transcription elongation factor B (SIII), polypeptide 2	1293.10	1104.23	36.63	33.84	**0.009**
Tcf3	21423	transcription factor 3	60.57	76.10	4.86	3.08	**0.036**
Tcl1	21432	T cell lymphoma breakpoint 1	7.50	6.21	0.49	0.11	**0.042**
Tcn2	21452	transcobalamin 2	42.96	59.50	1.94	3.10	**0.004**
Tcp11l2	216198	t-complex 11 (mouse) like 2	81.68	113.15	8.19	3.39	**0.012**
Tex12	66654	testis expressed gene 12	5.49	6.21	0.24	0.17	**0.049**
Tex18	83559	testis expressed gene 18	4.99	4.35	0.21	0.15	**0.049**
Tfam	21780	transcription factor A, mitochondrial	21.84	30.05	1.87	2.42	**0.04**
Tfap2a	21418	transcription factor AP-2, alpha	8.03	6.85	0.39	0.23	**0.042**
Tfeb	21425	transcription factor EB	14.05	11.19	0.40	0.99	**0.036**
Tgfb2	21808	transforming growth factor, beta 2	30.74	49.66	4.28	4.91	**0.027**
Tgfbr2	21813	transforming growth factor, beta receptor II	20.40	17.08	0.50	0.63	**0.006**
Tgfbr3	21814	transforming growth factor, beta receptor III	9.95	8.90	0.25	0.19	**0.02**
Tgm6	241636	transglutaminase 6	10.39	7.87	0.39	0.47	**0.006**
Tgm7	640543	transglutaminase 7	10.24	8.33	0.23	0.34	**0.004**
Thap6	381650	THAP domain containing 6	25.59	35.85	2.13	2.30	**0.02**
Thpo	21832	thrombopoietin	9.27	7.87	0.35	0.14	**0.010**
Thumpd3	14911	THUMP domain containing 3	60.99	54.65	1.67	1.46	**0.029**
Timm10b	14356	translocase of inner mitochondrial membrane 10B	21.41	16.93	1.67	0.59	**0.045**

Timm13	30055	translocase of inner mitochondrial membrane 13	228.88	181.44	14.69	3.48	**0.020**
Timm8a1	30058	translocase of inner mitochondrial membrane 8A1	16.65	13.62	0.97	0.69	**0.044**
Timm8b	30057	translocase of inner mitochondrial membrane 8B	930.93	874.70	16.23	10.29	**0.026**
Timp3	21859	tissue inhibitor of metalloproteinase 3	177.26	241.40	8.72	21.66	**0.033**
Tktl1	83553	transketolase-like 1	7.56	6.35	0.33	0.19	**0.020**
Tlr4	21898	toll-like receptor 4	13.80	18.82	0.90	1.44	**0.025**
Tlx2	21909	T cell leukemia, homeobox 2	8.78	7.87	0.18	0.13	**0.007**
Tmbim1	69660	transmembrane BAX inhibitor motif containing 1	218.31	163.82	14.30	12.38	**0.028**
Tmc8	217356	transmembrane channel-like gene family 8	11.05	8.18	0.13	0.23	**4E-05**
Tmem104	320534	transmembrane protein 104	43.09	60.39	5.34	1.93	**0.02**
Tmem108	81907	transmembrane protein 108	500.50	252.51	39.27	25.49	**0.00**
Tmem108	81907	transmembrane protein 108	414.88	242.11	51.60	33.08	**0.03**
Tmem11	216821	transmembrane protein 11	29.20	24.06	1.00	1.65	**0.037**
Tmem110	69179	transmembrane protein 110	20.73	32.41	0.91	4.63	**0.048**
Tmem117	320709	transmembrane protein 117	37.70	54.13	4.07	3.98	**0.028**
Tmem119	231633	transmembrane protein 119	26.56	20.75	1.48	1.44	**0.030**
Tmem121	69195	transmembrane protein 121	44.67	49.61	0.96	1.75	**0.049**
Tmem150c	231503	transmembrane protein 150C	27.11	21.85	0.51	1.11	**0.005**
Tmem160	69094	transmembrane protein 160	61.53	47.99	4.41	2.29	**0.034**
Tmem161a	234371	transmembrane protein 161A	22.44	27.34	0.72	0.62	**0.002**
Tmem164	209497	transmembrane protein 164	15.36	18.52	1.00	0.76	**0.046**
Tmem167	66074	transmembrane protein 167	8.48	7.14	0.33	0.29	**0.023**
Tmem189	407243	transmembrane protein 189	60.70	43.58	1.77	2.41	**0.001**
Tmem201	230917	transmembrane protein 201	55.22	64.51	1.40	3.47	**0.048**
Tmem208	66320	transmembrane protein 208	205.28	174.25	11.35	5.44	**0.049**
Tmem229a	319832	transmembrane protein 229A	42.80	55.85	3.55	3.65	**0.043**
Tmem234	76799	transmembrane protein 234	713.12	538.96	11.49	13.31	**6E-05**
Tmem234	76799	transmembrane protein 234	887.72	734.64	16.75	23.91	**0.002**
Tmem234	76799	transmembrane protein 234	148.84	135.89	3.87	2.37	**0.029**
Tmem236	625286	transmembrane protein 236	7.58	6.69	0.19	0.09	**0.005**
Tmem238	664968	transmembrane protein 238	19.43	15.91	1.07	0.69	**0.033**
Tmem253	619301	transmembrane protein 253	8.67	7.13	0.34	0.25	**0.011**
Tmem256	69186	transmembrane protein 256	150.10	128.63	1.34	6.47	**0.017**
Tmem261	66928	transmembrane protein 261	168.17	111.80	13.84	6.94	**0.011**
Tmem30b	238257	transmembrane protein 30B	7.57	6.16	0.26	0.31	**0.013**
Tmem37	170706	transmembrane protein 37	15.47	11.32	0.98	0.84	**0.018**
Tmem5	216395	transmembrane protein 5	105.29	81.24	3.52	4.10	**0.004**
Tmem63a	208795	transmembrane protein 63a	163.73	106.99	7.33	19.91	**0.037**
Tmem87b	72477	transmembrane protein 87B	41.39	61.49	1.50	3.11	**0.001**
Tmem89	69384	transmembrane protein 89	30.01	24.80	1.39	0.76	**0.017**
Tmem98	103743	transmembrane protein 98	74.72	34.52	3.30	6.86	**0.002**
Tmprss11f	243083	transmembrane protease, serine 11f	5.02	4.69	0.02	0.08	**0.005**
Tmprss2	50528	transmembrane protease, serine 2	7.07	6.25	0.32	0.04	**0.044**
Tmprss6	71753	transmembrane serine protease 6	10.65	8.09	0.69	0.22	**0.012**
Tnfrsf11a	21934	tumor necrosis factor receptor superfamily, member 11a, NFKB activator	16.64	12.82	0.90	0.54	**0.011**
Tnfrsf13c	72049	tumor necrosis factor receptor superfamily, member 13c	20.80	16.59	0.66	0.71	**0.00**
Tnfrsf22	79202	tumor necrosis factor receptor superfamily, member 22	29.27	22.28	1.59	2.01	**0.034**
Tnfsf11	21943	tumor necrosis factor (ligand) superfamily, member 11	10.54	8.35	0.42	0.40	**0.009**
Tnn	329278	tenascin N	10.24	8.60	0.44	0.29	**0.020**
Tnni1	21952	troponin I, skeletal, slow 1	61.12	38.67	8.31	2.42	**0.041**
Tnrc6c	217351	trinucleotide repeat containing 6C	38.34	55.39	1.58	4.17	**0.009**
Tnxb	81877	tenascin XB	12.46	10.86	0.42	0.27	**0.02**
Toporsl	68274	topoisomerase I binding, arginine/serine-rich like	4.25	4.72	0.14	0.13	**0.049**
Tor1aip1	208263	torsin A interacting protein 1	59.84	75.82	2.65	4.06	**0.017**
Tox	252838	thymocyte selection-associated high mobility group box	75.71	96.14	6.10	4.64	**0.037**
Tpd52l2	66314	tumor protein D52-like 2	12.59	30.13	1.71	4.04	**0.007**
Tppp	72948	tubulin polymerization promoting protein	496.17	360.81	36.10	36.17	**0.038**
Tprn	97031	taperin	57.85	41.93	1.58	2.62	**0.002**
Tpte	234129	transmembrane phosphatase with tensin homology	5.85	7.10	0.25	0.39	**0.035**
Trabd2b	666048	TraB domain containing 2B	6.67	5.40	0.46	0.07	**0.034**

Tradd	71609	TNFRSF1A-associated via death domain	29.34	21.34	2.46	2.01	**0.045**
Traf1	22029	TNF receptor-associated factor 1	8.01	7.02	0.23	0.13	**0.010**
Traf3ip2	103213	TRAF3 interacting protein 2	16.49	24.50	1.40	0.39	**0.001**
Traf5	22033	TNF receptor-associated factor 5	9.83	8.88	0.19	0.25	**0.024**
Traip	22036	TRAF-interacting protein	20.57	16.31	1.28	0.71	**0.027**
Trappc5	66682	trafficking protein particle complex 5	50.37	43.48	0.76	1.43	**0.005**
Trem1	58217	triggering receptor expressed on myeloid cells 1	11.35	9.25	0.53	0.17	**0.01**
Treml1	71326	triggering receptor expressed on myeloid cells-like 1	15.20	11.96	0.86	0.44	**0.016**
Treml4	224840	triggering receptor expressed on myeloid cells-like 4	12.87	11.05	0.37	0.11	**0.003**
Trhr2	170732	thyrotropin releasing hormone receptor 2	13.90	11.59	0.83	0.26	**0.04**
Trim24	21848	tripartite motif-containing 24	136.23	151.27	3.87	4.47	**0.044**
Trim54	58522	tripartite motif-containing 54	9.56	8.38	0.29	0.21	**0.016**
Trim63	433766	tripartite motif-containing 63	12.44	10.94	0.39	0.39	**0.036**
Trim7	94089	tripartite motif-containing 7	7.92	9.01	0.27	0.35	**0.049**
Triml1	244448	tripartite motif family-like 1	8.52	7.63	0.22	0.25	**0.035**
Trip6	22051	thyroid hormone receptor interactor 6	16.90	12.35	1.41	0.38	**0.020**
Trmt10b	69934	tRNA methyltransferase 10B	40.49	57.48	3.33	3.85	**0.016**
Trmt12	68260	tRNA methyltranferase 12	12.83	9.03	1.20	0.27	**0.02**
Trmt61a	328162	tRNA methyltransferase 61A	15.86	13.31	0.45	0.56	**0.012**
Trpm3	226025	transient receptor potential cation channel, subfamily M, member 3	11.92	15.42	0.33	0.65	**0.003**
Try4	22074	trypsin 4	13.82	12.71	0.34	0.30	**0.049**
Tshr	22095	thyroid stimulating hormone receptor	7.35	9.09	0.53	0.15	**0.020**
Tshz1	110796	teashirt zinc finger family member 1	72.40	94.68	1.59	4.31	**0.00**
Tsr3	68327	TSR3 20S rRNA accumulation	29.99	26.57	0.44	1.28	**0.0**
Tssc1	380752	tumor suppressing subtransferable candidate 1	64.02	49.48	1.47	3.42	**0.008**
Tsx	22127	testis specific X-linked gene	30.01	21.90	1.49	1.13	**0.005**
Ttc13	234875	tetratricopeptide repeat domain 13	39.08	57.92	2.39	6.77	**0.039**
Ttc14	67120	tetratricopeptide repeat domain 14	58.95	52.52	1.45	2.10	**0.05**
Ttc24	214191	tetratricopeptide repeat domain 24	7.52	5.97	0.59	0.06	**0.039**
Ttc36	192653	tetratricopeptide repeat domain 36	7.59	5.99	0.45	0.22	**0.019**
Tubgcp5	233276	tubulin, gamma complex associated protein 5	51.91	80.29	6.92	8.83	**0.045**
Tubgcp5	233276	tubulin, gamma complex associated protein 5	51.91	80.29	6.92	8.83	**0.045**
Tulp2	56734	tubby-like protein 2	9.34	7.63	0.18	0.31	**0.003**
Txndc5	105245	thioredoxin domain containing 5	37.05	50.42	2.20	2.12	**0.005**
Tyr	22173	tyrosinase	6.02	4.98	0.20	0.11	**0.004**
Ube4bos3	74310	ubiquitination factor E4B, opposite strand 3	10.27	8.70	0.52	0.21	**0.032**
Ubqlnl	244179	ubiquilin-like	6.54	5.39	0.22	0.16	**0.005**
Ubtd2	327900	ubiquitin domain containing 2	83.04	104.62	3.01	6.56	**0.024**
Ubxn10	212190	UBX domain protein 10	5.68	5.11	0.10	0.06	**0.002**
Ulk2	29869	unc-51 like kinase 2	230.03	287.97	11.81	10.17	**0.010**
Unc5c	22253	unc-5 homolog C (C. elegans)	153.96	184.26	4.39	11.06	**0.044**
Unc5d	210801	unc-5 homolog D (C. elegans)	9.86	9.00	0.20	0.29	**0.049**
Upb1	103149	ureidopropionase, beta	7.71	6.19	0.52	0.30	**0.044**
Urad	231903	ureidoimidazoline (2-oxo-4-hydroxy-4-carboxy-5) decarboxylase	10.88	9.23	0.42	0.42	**0.032**
Urb1	207932	URB1 ribosome biogenesis 1 homolog (S. cerevisiae)	16.19	14.03	0.72	0.32	**0.033**
Usb1	101985	U6 snRNA biogenesis 1	19.79	16.82	0.35	0.69	**0.009**
Use1	67023	unconventional SNARE in the ER 1 homolog (S. cerevisiae)	288.70	234.82	9.95	7.53	**0.005**
Usp12	22217	ubiquitin specific peptidase 12	12.81	17.09	0.80	1.16	**0.023**
Usp17le	625530	ubiquitin specific peptidase 17-like E	12.59	8.80	1.33	0.50	**0.037**
Usp24	329908	ubiquitin specific peptidase 24	211.04	252.95	4.44	10.84	**0.012**
Usp29	57775	ubiquitin specific peptidase 29	9.60	11.40	0.42	0.37	**0.019**
Usp3	235441	ubiquitin specific peptidase 3	81.75	97.56	1.70	4.96	**0.023**
Usp33	170822	ubiquitin specific peptidase 33	159.95	198.54	7.76	8.01	**0.013**
Usp35	244144	ubiquitin specific peptidase 35	11.17	9.09	0.45	0.70	**0.047**
Usp36	72344	ubiquitin specific peptidase 36	40.59	34.46	1.01	1.74	**0.023**
Usp44	327799	ubiquitin specific peptidase 44	6.19	5.32	0.27	0.09	**0.023**
Usp45	77593	ubiquitin specific petidase 45	36.63	50.34	4.96	1.99	**0.043**
Usp8	84092	ubiquitin specific peptidase 8	177.43	200.07	7.20	4.17	**0.035**
Utrn	22288	utrophin	14.80	17.45	0.47	0.36	**0.004**
Uts2	24111	urotensin 2	8.20	6.59	0.38	0.17	**0.008**
Uts2b	224065	urotensin 2B	4.96	4.52	0.13	0.05	**0.022**

Uts2r	217369	urotensin 2 receptor	9.18	7.82	0.21	0.24	**0.005**
Vav3	57257	vav 3 oncogene	10.41	11.65	0.32	0.19	**0.015**
Vcam1	22329	vascular cell adhesion molecule 1	52.87	81.70	3.05	10.40	**0.038**
Vegfb	22340	vascular endothelial growth factor B	143.25	110.97	10.42	4.57	**0.030**
Vezf1	22344	vascular endothelial zinc finger 1	483.46	551.55	9.82	23.76	**0.038**
Vgll3	73569	vestigial like 3 (Drosophila)	7.78	6.55	0.41	0.22	**0.038**
Vil1	22349	villin 1	8.24	6.97	0.28	0.11	**0.006**
Vipr1	22354	vasoactive intestinal peptide receptor 1	13.89	11.27	0.59	0.73	**0.03**
Vit	74199	vitrin	34.39	61.90	2.95	8.71	**0.024**
Vkorc1	27973	vitamin K epoxide reductase complex, subunit 1	271.20	226.55	8.82	6.98	**0.007**
Vmn1r115	667273	vomeronasal 1 receptor 115	4.35	4.86	0.12	0.13	**0.026**
Vmn1r116	667268	vomeronasal 1 receptor 116	8.61	6.65	0.25	0.68	**0.035**
Vmn1r122	435951	vomeronasal 1 receptor 122	3.84	4.34	0.10	0.17	**0.045**
Vmn1r123	384695	vomeronasal 1 receptor 123	4.32	3.88	0.13	0.09	**0.031**
Vmn1r128	667199	vomeronasal 1 receptor 128	5.28	4.26	0.32	0.19	**0.034**
Vmn1r24	171191	vomeronasal 1 receptor 24	5.33	7.13	0.27	0.27	**0.003**
Vmn1r34	546901	vomeronasal 1 receptor 34	13.39	11.81	0.48	0.40	**0.046**
Vmn1r94	620537	vomeronasal 1 receptor 94	14.58	9.26	1.75	0.47	**0.026**
Vmn2r107	22312	vomeronasal 2, receptor 107	4.57	3.88	0.15	0.07	**0.006**
Vmn2r16	384220	vomeronasal 2, receptor 16	5.75	4.82	0.21	0.20	**0.019**
Vmn2r17	384221	vomeronasal 2, receptor 17	4.88	6.02	0.23	0.28	**0.020**
Vmn2r32	22311	vomeronasal 2, receptor 32	5.83	5.23	0.04	0.21	**0.031**
Vmn2r71	233445	vomeronasal 2, receptor 71	3.70	4.82	0.06	0.37	**0.023**
Vmn2r74	546980	vomeronasal 2, receptor 74	4.19	4.83	0.14	0.21	**0.043**
Vmn2r99	665376	vomeronasal 2, receptor 99	3.81	4.49	0.18	0.17	**0.03**
Vpreb2	22363	pre-B lymphocyte gene 2	18.33	15.15	0.85	0.68	**0.03**
Vps13c	320528	vacuolar protein sorting 13C (yeast)	37.99	49.77	2.33	2.10	**0.009**
Vps36	70160	vacuolar protein sorting 36 (yeast)	334.06	269.13	9.74	7.89	**0.002**
Vsx2	12677	visual system homeobox 2	12.83	9.93	1.02	0.31	**0.035**
Vti1a	53611	vesicle transport through interaction with t-SNAREs 1A	16.38	19.79	0.80	0.39	**0.009**
Vwa3a	233813	von Willebrand factor A domain containing 3A	11.57	8.69	0.67	0.70	**0.025**
Vwc2	319922	von Willebrand factor C domain containing 2	19.96	13.87	0.88	0.81	**0.002**
Wbp1l	226178	WW domain binding protein 1 like	74.81	61.80	4.54	2.36	**0.044**
Wbp5	22381	WW domain binding protein 5	362.51	497.07	17.27	12.91	**0.001**
Wdfy2	268752	WD repeat and FYVE domain containing 2	14.64	11.16	1.03	0.51	**0.02**
Wdr16	71860	WD repeat domain 16	9.80	8.17	0.56	0.32	**0.045**
Wdr25	212198	WD repeat domain 25	22.38	18.89	0.27	0.94	**0.011**
Wdr27	71682	WD repeat domain 27	7.26	6.11	0.32	0.11	**0.015**
Wdr47	99512	WD repeat domain 47	17.76	26.76	1.27	1.81	**0.007**
Wdr77	70465	WD repeat domain 77	59.24	80.54	7.23	4.40	**0.05**
Wdr93	626359	WD repeat domain 93	8.45	6.79	0.49	0.32	**0.03**
Wfdc13	408190	WAP four-disulfide core domain 13	13.85	11.85	0.42	0.53	**0.025**
Wfdc9	629754	WAP four-disulfide core domain 9	10.04	8.11	0.64	0.33	**0.036**
Wif1	24117	Wnt inhibitory factor 1	12.19	9.92	0.91	0.14	**0.049**
Wipi1	52639	WD repeat domain, phosphoinositide interacting 1	48.00	58.43	3.32	1.16	**0.025**
Wnt1	22408	wingless-type MMTV integration site family, member 1	7.81	6.19	0.40	0.32	**0.018**
Wnt16	93735	wingless-type MMTV integration site family, member 16	6.98	5.83	0.27	0.22	**0.016**
Wnt2	22413	wingless-type MMTV integration site family, member 2	10.07	8.45	0.35	0.14	**0.005**
Wnt4	22417	wingless-type MMTV integration site family, member 4	13.00	10.57	0.14	0.60	**0.008**
Wnt6	22420	wingless-type MMTV integration site family, member 6	9.51	7.61	0.68	0.26	**0.041**
Wsb2	59043	WD repeat and SOCS box-containing 2	76.45	55.95	6.76	4.42	**0.044**
Wscd1	216881	WSC domain containing 1	143.90	125.25	2.56	5.00	**0.016**
Wwc1	211652	WW, C2 and coiled-coil domain containing 1	12.53	15.30	1.07	0.31	**0.048**
Xab2	67439	XPA binding protein 2	83.42	67.15	4.03	4.07	**0.030**
Xirp1	22437	xin actin-binding repeat containing 1	9.44	8.24	0.37	0.26	**0.037**
Xkr5	319581	X Kell blood group precursor-related family, member 5	14.92	13.79	0.30	0.13	**0.013**
Xlr3a	22445	X-linked lymphocyte-regulated 3A	15.17	11.22	1.39	0.69	**0.043**
Xpo4	57258	exportin 4	75.12	88.81	2.51	4.84	**0.046**
Xrcc1	22594	X-ray repair complementing defective repair in Chinese hamster cells 1	54.20	40.66	2.52	2.19	**0.007**
Yap1	22601	yes-associated protein 1	15.52	18.98	0.65	0.77	**0.014**

Yif1a	68090	Yip1 interacting factor homolog A (S. cerevisiae)	143.86	109.02	12.64	5.09	**0.043**
Ywhae	22627	tyrosine 3-monooxygenase/tryptophan 5-monooxygenase activation protein, epsilon polypeptide	1214.09	1309.46	23.10	18.35	**0.018**
Zan	22635	zonadhesin	8.13	7.27	0.26	0.10	**0.023**
Zbed3	72114	zinc finger, BED domain containing 3	36.53	46.01	1.29	2.17	**0.009**
Zbed5	71970	zinc finger, BED-type containing 5	15.05	10.14	1.76	0.70	**0.041**
Zbtb21	114565	zinc finger and BTB domain containing 21	29.30	20.63	2.77	1.75	**0.04**
Zbtb33	56805	zinc finger and BTB domain containing 33	69.81	86.74	3.68	5.50	**0.04**
Zbtb40	230848	zinc finger and BTB domain containing 40	31.69	22.23	3.21	0.54	**0.027**
Zbtb7c	207259	zinc finger and BTB domain containing 7C	8.92	7.26	0.34	0.50	**0.033**
Zc3h12b	547176	zinc finger CCCH-type containing 12B	13.75	22.87	1.21	2.99	**0.030**
Zdbf2	73884	zinc finger, DBF-type containing 2	12.14	9.98	0.77	0.40	**0.048**
Zdhhc18	503610	zinc finger, DHHC domain containing 18	54.69	42.47	3.74	1.91	**0.027**
Zdhhc2	70546	zinc finger, DHHC domain containing 2	641.68	770.78	19.60	47.66	**0.046**
Zdhhc21	68268	zinc finger, DHHC domain containing 21	45.34	55.24	3.45	1.98	**0.047**
Zdhhc24	70605	zinc finger, DHHC domain containing 24	31.53	24.47	1.87	0.61	**0.011**
Zfand3	21769	zinc finger, AN1-type domain 3	146.74	186.73	3.16	6.88	**0.00**
Zfhx4	80892	zinc finger homeodomain 4	11.44	8.34	1.13	0.54	**0.047**
Zfp108	54678	zinc finger protein 108	22.49	12.26	3.42	1.13	**0.030**
Zfp109	56869	zinc finger protein 109	10.19	8.12	0.48	0.29	**0.01**
Zfp13	22654	zinc finger protein 13	28.08	19.40	1.44	0.99	**0.003**
Zfp157	72154	zinc finger protein 157	82.79	105.04	2.83	8.41	**0.046**
Zfp26	22688	zinc finger protein 26	108.75	135.79	2.50	8.57	**0.023**
Zfp28	22690	zinc finger protein 28	12.54	18.86	0.97	2.29	**0.044**
Zfp296	63872	zinc finger protein 296	11.84	9.23	0.41	0.23	**0.001**
Zfp346	26919	zinc finger protein 346	47.13	55.28	2.67	1.74	**0.043**
Zfp36l1	12192	zinc finger protein 36, C3H type-like 1	310.95	460.24	36.42	8.31	**0.007**
Zfp36l2	12193	zinc finger protein 36, C3H type-like 2	140.35	218.59	6.96	12.43	**0.002**
Zfp410	52708	zinc finger protein 410	60.22	86.03	1.40	4.50	**0.002**
Zfp442	668923	zinc finger protein 442	22.52	49.49	2.52	5.58	**0.005**
Zfp445	235682	zinc finger protein 445	119.53	146.45	10.07	4.20	**0.049**
Zfp462	242466	zinc finger protein 462	253.09	303.32	15.14	6.43	**0.022**
Zfp474	66758	zinc finger protein 474	7.76	6.95	0.32	0.06	**0.047**
Zfp521	225207	zinc finger protein 521	92.06	135.17	6.68	12.77	**0.024**
Zfp524	66056	zinc finger protein 524	82.31	52.80	4.17	3.92	**0.002**
Zfp541	666528	zinc finger protein 541	11.75	9.76	0.47	0.10	**0.006**
Zfp553	233887	zinc finger protein 553	27.99	21.17	2.20	1.45	**0.041**
Zfp563	240068	zinc finger protein 563	19.82	27.40	0.15	2.26	**0.02**
Zfp606	67370	zinc finger protein 606	20.67	26.75	0.82	0.94	**0.003**
Zfp609	214812	zinc finger protein 609	53.25	74.08	2.86	7.60	**0.043**
Zfp618	72701	zinc finger protein 618	12.86	15.61	0.58	0.59	**0.016**
Zfp653	319601	zinc finger protein 653	18.94	14.48	0.57	0.61	**0.002**
Zfp677	210503	zinc finger protein 677	5.39	8.61	0.43	1.16	**0.040**
Zfp775	243372	zinc finger protein 775	15.04	11.07	1.37	0.60	**0.038**
Zfp81	224694	zinc finger protein 81	125.27	172.39	9.74	16.50	**0.049**
Zfp821	75871	zinc finger protein 821	54.23	66.73	1.50	4.50	**0.039**
Zfp839	72805	zinc finger protein 839	29.02	24.94	0.36	0.79	**0.003**
Zfp943	74670	zinc finger prtoein 943	7.88	9.71	0.27	0.43	**0.011**
Zfp943	74670	zinc finger prtoein 943	31.39	46.33	3.96	3.87	**0.036**
Zfp948	381066	zinc finger protein 948	53.85	79.46	5.29	7.60	**0.033**
Zfp954	232853	zinc finger protein 954	9.84	13.65	0.44	1.28	**0.030**
Zfp958	233987	zinc finger protein 958	59.56	40.10	5.11	5.41	**0.040**
Znrf4	20834	zinc and ring finger 4	11.59	9.49	0.43	0.62	**0.032**
Zscan4b	665780	zinc finger and SCAN domain containing 4B	4.67	5.85	0.38	0.22	**0.036**
Zswim4	212168	zinc finger SWIM-type containing 4	12.68	10.78	0.41	0.33	**0.012**
Zzef1	195018	zinc finger, ZZ-type with EF hand domain 1	61.85	74.67	3.95	3.26	**0.046**

Table 3.1: List of differentially regulated genes in O4$^+$ OL*s* upon *Lrp1* ablation

3.9 **Bibliography**

Baumann N, Pham-Dinh D. 2001. Biology of oligodendrocyte and myelin in the mammalian central nervous system. In *Physiological Reviews*, pp. 871-927

Blakemore WF, Franklin RJM. 2008. Remyelination in experimental models of toxin-induced demyelination. In *Curr. Top. Microbiol. Immunol.*, pp. 193-212

Bolte S, Cordelières FP. 2006. A guided tour into subcellular colocalization analysis in light microscopy. In *J Microsc*, pp. 213-32

Bottelbergs A, Verheijden S, Hulshagen L, Gutmann DH, Goebbels S, et al. 2010. Axonal integrity in the absence of functional peroxisomes from projection neurons and astrocytes. In *Glia*, pp. 1532-43

Dugas JC, Cuellar TL, Scholze A, Ason B, Ibrahim A, et al. 2010. Dicer1 and miR-219 Are required for normal oligodendrocyte differentiation and myelination. In *Neuron*, pp. 597-611

Fisher RA. 1915. Frequency Distribution of the Values of the Correlation Coefficient in Samples from an Indefinitely Large Population. In *Biometrika*, pp. 507-21: [Oxford University Press, Biometrika Trust]

Hall SM. 1972. The effect of injections of lysophosphatidyl choline into white matter of the adult mouse spinal cord. In *Journal of Cell Science*, pp. 535-46

Hendrickx DAE, Koning N, Schuurman KG, van Strien ME, van Eden CG, et al. 2013. Selective upregulation of scavenger receptors in and around demyelinating areas in multiple sclerosis. In *J. Neuropathol. Exp. Neurol.*, pp. 106-18

Hennen E, Safina D, Haussmann U, Wörsdörfer P, Edenhofer F, et al. 2013. A LewisX Glycoprotein Screen Identifies the Low Density Lipoprotein Receptor-related Protein 1 (LRP1) as a Modulator of Oligodendrogenesis in Mice. In *Journal of Biological Chemistry*, pp. 16538-45

Lauber K, Bohn E, Kröber SM, Xiao Y-j, Blumenthal SG, et al. 2003. Apoptotic cells induce migration of phagocytes via caspase-3-mediated release of a lipid attraction signal. In *Cell*, pp. 717-30

Lazzarini RA. 2004. Myelin Biology and Disorders. Academic Press

Li C, Tropak MB, Gerlai R, Clapoff S, Abramow-Newerly W, et al. 1994. Myelination in the absence of myelin-associated glycoprotein. In *Nature*, pp. 747-50

Medina CB, Ravichandran KS. 2016. Do not let death dous part: ‘find-me’ signals in communication between dying cells and the phagocytes. pp. 979-89: Nature Publishing Group

Menn B, Garcia-Verdugo JM, Yaschine C, Gonzalez-Perez O, Rowitch D, Alvarez-Buylla A. 2006. Origin of Oligodendrocytes in the Subventricular Zone of the Adult Brain. In *J. Neurosci.*, pp. 7907-18

Peter C, Waibel M, Keppeler H, Lehmann R, Xu G, et al. 2012. Release of lysophospholipid 'find-me' signals during apoptosis requires the ATP-binding cassette transporter A1. In *Autoimmunity*, pp. 568-73

Prasad JM, Migliorini M, Galisteo R, Strickland DK. 2015. Generation of a Potent Low Density Lipoprotein Receptor-related Protein 1 (LRP1) Antagonist by Engineering a Stable Form of the Receptor-associated Protein (RAP) D3 Domain. In *Journal of Biological Chemistry*, pp. 17262-68

Rayner KJ, Suárez Y, Dávalos A, Parathath S, Fitzgerald ML, et al. 2010. MiR-33 contributes to the regulation of cholesterol homeostasis. In *Science*, pp. 1570-73

Reekmans SM, Pflanzner T, Gordts PLSM, Isbert S, Zimmermann P, et al. 2009. Inactivation of the proximal NPXY motif impairs early steps in LRP1 biosynthesis. In *Cell. Mol. Life Sci.*, pp. 135-45

Roebroek AJM, Reekmans S, Lauwers A, Feyaerts N, Smeijers L, Hartmann D. 2006. Mutant Lrp1 knock-in mice generated by recombinase-mediated cassette exchange reveal differential importance of the NPXY motifs in the intracellular domain of LRP1 for normal fetal development. In *Mol. Cell. Biol.*, pp. 605-16

Schüller U, Heine VM, Mao J, Kho AT, Dillon AK, et al. 2008. Acquisition of Granule Neuron Precursor Identity Is a Critical Determinant of Progenitor Cell Competence to Form Shh-Induced Medulloblastoma. In *Cancer Cell*, pp. 123-34

Shields SA, Gilson JM, Blakemore WF, Franklin RJ. 1999. Remyelination occurs as extensively but more slowly in old rats compared to young rats following gliotoxin-induced CNS demyelination. In *Glia*, pp. 77-83

Simons M, Misgeld T, Kerschensteiner M. 2014. A unified cell biological perspective on axon-myelin injury. In *The Journal of Cell Biology*, pp. 335-45

Stiles TL, Dickendesher TL, Gaultier A, Fernandez-Castaneda A, Mantuano E, et al. 2013. LDL receptor-related protein-1 is a sialic-acid-independent receptor for myelin-associated glycoprotein that functions in neurite outgrowth inhibition by MAG and CNS myelin. In *Journal of Cell Science*, pp. 209-20

Thiam AR, Farese RV, Walther TC. 2013. The biophysics and cell biology of lipid droplets. In *Nat. Rev. Mol. Cell Biol.*, pp. 775-86: Nature Publishing Group

van de Sluis B, Wijers M, Herz J. 2017. News on the molecular regulation and function of hepatic low-density lipoprotein receptor and LDLR-related protein 1. In *Current Opinion in Lipidology*, pp. 241-47

Yamazaki R, Baba H, Yamaguchi Y. 2018. Unconventional Myosin ID is Involved in Remyelination After Cuprizone-Induced Demyelination. In *Neurochem Res*, pp. 195-204

Yamazaki R, Ishibashi T, Baba H, Yamaguchi Y. 2014. Unconventional myosin ID is expressed in myelinating oligodendrocytes. In *J. Neurosci. Res.*, pp. 1286-94

Yamazaki R, Ishibashi T, Baba H, Yamaguchi Y. 2016. Knockdown of Unconventional Myosin ID Expression Induced Morphological Change in Oligodendrocytes. In *ASN NEURO*

Yamazaki R, Ishibashi T, Baba H, Yamaguchi Y. 2017. Expression of Unconventional Myosin VI in Oligodendrocytes. In *Neurochem Res*, pp. 3372-81

Zhao X, Pan Z, Wu J, Zhou G, Zeng Y. 2010. Automatic identification and morphometry of optic nerve fibers in electron microscopy images. In *Comput Med Imaging Graph*, pp. 179-84

CHAPTER IV

General Discussion and Future Direction

4.1 Abstract

Low-density lipoprotein receptor-related protein 1 (LRP1) is one of the most promiscuous cell surface receptors. As of February 2018, thousands of research articles concerning LRP1's function in cellular debris phagocytosis, cytoskeletal remodeling, intra- and inter-cellular vesicle trafficking, energy homeostasis, lipid metabolism, transcriptional and post-transcriptional regulation, and more have been published. Given the broad spectrum of cellular functions LRP1 can influence, it is tempting to speculate that LRP1 coordinates many different signaling events in any given cell type, and likely operates in a context dependent manner. Even though LRP1 is such a well-studied "old" receptor, recent research has uncovered new and surprising functions. In Chapter II, I described my work that revealed new roles for LRP1 in facilitating CNS myelin repair and development through promoting oligodendrocytes (OLs) differentiation by regulating cholesterol homeostasis and peroxisome biogenesis. In Chapter III, I have described the potential non-cell autonomous roles of LRP1 in regulating CNS myelin repair. Additionally, I have speculated that LRP1 might participate in regulating axon-glia interaction, miRNA expression, and organelle trafficking during myelin development. Collectively, based on these new observations, I discuss several aspects of LRP1 and myelin biology in the context of glia-glia or axon-glia interaction and provide an outlook where research of LRP1 may be heading.

4.2 General Discussion

In Chapter II, several key conclusions have been discussed regarding how LRP1 influences CNS myelination. I will expand on these conclusions and discuss

some interesting findings described in Chapter II and III. I then will briefly summarize and interpret major findings, review how they support or disagree with the literature, and develop new hypotheses for future research.

4.2.1 How can non-cell-autonomous roles of LRP1 impact CNS remyelination?

Effective CNS remyelination requires numerous cellular events to occur in an ordered time and space specific manner; such as controlled demyelination, macrophage-like immune cell mediated myelin debris removal, OPC recruitment, and myelin regeneration. LRP1 is a potent multifunctional scavenger receptor that is ubiquitously expressed in all CNS cell types. In Chapter II, I have investigated the cell-autonomous role of LRP1 in the OL-lineage during remyelination (section 2.3.2); however, given its broad expression and functions, additional, non-cell-autonomous roles for LRP1 are conceivable.

— **Controlled inflammation and demyelination**

It was shown that LRP1 expression is increased at MS lesions in both human postmortem brain tissue and mouse EAE CNS tissue (Chuang et al 2016, Hendrickx et al 2013). Elevated LRP1 expression at the MS lesion was found in astrocytes and microglia. LRP1 is protective during CNS autoimmunity. The ablation of LRP1 in microglia (*Cx3cr1* promoter) but not peripheral macrophages (*LysM* promoter) activated pro-inflammatory signals and worsened the EAE severity score in mice (Chuang et al 2016). Similarly, I found LRP1 protein and *Lrp1* mRNA expression were elevated at the LPC-induced white matter lesion (Figure 3.3 and Figure 3.4). Nuclei of cells not belonging to the OL or astrocyte lineage were found and accumulated at the myelin lesion site, though the identity of each cell type and how they may contribute or inhibit remyelination has yet to be defined (Figure 3.1 and Figure 3.2). Interestingly, $CD68^{+}$ (pro-inflammatory macrophages and microglia) and $Arg\text{-}1^{+}$ (M2 macrophage marker) cells were observed at the LPC-induced white matter lesion (Figure 3.2). LRP1 is a key regulator that promotes the switch of M1 (pro-inflammatory) macrophages toward M2 (anti-inflammatory) macrophages (May et al 2013). It has been shown that the M1 to M2 switch in the microglia and

macrophages is important for OPC differentiation during CNS remyelination after LPC injection (Miron et al 2013).

In the LPC-mediated CNS demyelination model, $GFAP^+$ cells (astrocytes) migrate toward and occupy the lesion within seven days (Figure 3.1). Controversial reports exist, debating whether astrogliosis is pro- or anti-demyelination or pro- or anti-remyelination (Nair et al 2008). Hyperactive astrocytes are the major component of the glial scar. Scarring tissue generates a barrier between normal and inflamed tissue to restrain the region of degeneration (Nair et al 2008). It has been considered that the dense astrocyte matrix is inhibitory during remyelination by preventing OPCs from accessing the impacted region (Fok-Seang et al 1995, Groves et al 1993). However, it has been shown that OPCs failed to remyelinate in the absence of astrocytes in the adult rat (Talbott et al 2005). In the mouse EAE model and individuals with multiple sclerosis, hyaluronan (HA) is highly expressed at the white matter lesion site. HA is a glycosaminoglycan component of the ECM that plays important roles in CNS morphogenesis, stability, and remodeling (Asher et al 1991, Bignami & Asher 1992, Eggli et al 1992). HA binds to CD44 and activates migration of astrocytes (Bourguignon et al 2007). CD44 is expressed by astrocytes in normal white matter (Girgrah et al 1991, Quackenbush et al 1985), its level is elevated upon CNS injury (Jones et al 2000). It has been reported that LRP1 binds and internalizes CD44 to adjust adhesive properties in tumor cells (Perrot et al 2012); therefore, a role for astroglial LRP1 in ECM remolding through HA/CD44 signal during remyelination appears likely.

— **Myelin debris removal**

As soon as CNS myelin is damaged, an inflammatory response is observed, characterized by macrophage-like cells near the lesion site, that help remove myelin debris (Miron et al 2013, Skripuletz et al 2012). In cuprizone-induced demyelination, astrogliosis is followed by microgliosis. Deletion of astrocytes lead to failure of microglia-mediated myelin debris removal, and consecutive remyelination was delayed (Skripuletz et al 2012). The expression of multiple scavenger receptors

is elevated at the rim of an active MS lesion, such as CD68, CXCL16, Class A macrophage SR, LOX-1, FcFRIII, and LRP1. LRP1-expressing MEFs and glial cells uptake myelin vesicles containing MBP *in vitro* (Gaultier et al 2008). MBP is a major component of myelin debris, suggesting that LRP1 participates in myelin debris clearing. In our pilot experiments, LRP1 ablation in myeloid cells (*LysM-Cre*) does not impact the remyelination rate. However, the initial demyelination area is smaller (Figure 3.5). Whether or not this LPR1-mediated debris clean up or lesion confinement contributes to CNS remyelination needs further study.

— **The heterogeneity of remyelination**

As mentioned in Chapter II (section 1.3.3.2), the difference between multiple demyelination models should be considered when interpreting the relevance of our findings. LPC or EtBr focal injection creates a lesion, in which distinct phase of demyelination and remyelination are observed. However, compromised BBB and axonal damage from the injection might introduce confounding effects to alter the microenvironment of the lesion and consequentially alter remyelination (Dousset et al 1995, Waxman et al 1979). On the other hand, cuprizone-induced white matter lesion recruits OPCs and undergoes debris removal at the same time, causes overlapping demyelination and remyelination (Irvine & Blakemore 2006). Cuprizone is a copper chelator, which is reported to target copper-dependent mitochondrial functions (Pasquini et al 2007). The impairment in energy productions might be a confounding effect of axonal degeneration and failure in myelin repair. Whether chemically induced white matter damage or mouse EAE models can mimic the inflammatory responses caused by MS or other CNS diseases, and how knowledge gained from studies in the mouse can be applied to human white matter disorders needs further investigation.

4.2.2 How can OL-derived LRP1 impact axon diameter, function, and stability

— **Uncoupled compact myelin formation and OL-axon interaction**

In addition to facilitating rapid conduction of electric signals along the axon, myelination provides trophic support to axons. It has been speculated that

formation of myelin sheaths are required for the apical growth of axons. While the compact myelin remains unaffected, reduced axon caliber, nodal structural abnormality, redundant hypermyelination, myelin detachment, and late onset of axonal degeneration were observed in mice lacking PNS MAG (Yin et al 1998). Of note, axon caliber is associated with the inter-neurofilament spacing, which is regulated by the phosphorylation of neurofilament (Hsieh et al 1994, Nixon et al 1994). The distance between each nearby neurofilament in myelinated fibers of the *Mag*$^{-/-}$ sciatic nerve is significantly shorter compared to wildtype controls, starting from P35 and persisting to P90 (the longest time point assessed). Interestingly, this shortened distance is comparable to the one observed in non-myelinated nerves of wildtype control and *Mag*$^{-/-}$ mice (Yin et al 1998). Similarly, it has been shown that in the CNS, OLs impact axon caliber in a compact myelin-independent manner (Sánchez et al 1996) as exemplified in Shiverer (Chernoff 1981), Jimpy (Meier & MacPike 1970), and Quaking mice (Sidman et al 1964). These mutants show defects in compact myelin formation but their OL maturation and wrapping is normal. As non-myelinated axons are smaller in caliber than myelinated axons, the inter-neurofilament distance and axon caliber is comparable in the ensheathed axon and myelinated axon (Sánchez et al 1996). In line with the literature, nodal defects, neuronal atrophy, myelin detachment, and redundant hypermyelination (Figure 3.8) were also observed in the optic nerve following inducible *Lrp1* ablation. Suggesting that LRP1 might be involved in OL-axon interaction.

— **Selective myelination and hypomyelination**

To interpret the morphological changes in the nervous system, it is important to bear in mind that there is regional heterogeneity in axon caliber and the degree of myelination. In particular, optic nerve myelination is initiated from the chiasm and progresses toward the eye (Colello et al 1994). The inter-neurofilament spacing is reduced at the nodes of Ranvier (Hsieh et al 1994), and axons typically reduce 10-15% of their size at the paranodal region, possibly due to the tight junction. Near the optic nerve head, the progression of optic nerve myelination is blocked by a dense layer of astrocytes—called lamina cribrosa, located about 150μm away from the

retinal excavation (Sánchez et al 1996). At the optic nerve head, axons with smaller caliber are found, of which 90% are myelinated and expand in axon diameter at more distal regions (Sánchez et al 1996, Waxman & Swadlow 1976). Three major populations of axons with different calibers (~0.5, ~0.8, and ~1.5μm) were reported in the adult monkey optic nerve (Sanchez et al 1986). In the rat optic nerve, the major population of axon diameter shifts from 0.3-0.5μm (P4) to 0.7-0.9 μm (P28) during postnatal development (Colello et al 1994).

In sync with the references, three major axon populations (~0.3, ~0.6, and ~1.3μm) with different calibers were reported in the P21 mouse optic nerve. The major population of axon diameter shift from 0.2-0.4μm (P10) to 0.5-0.7μm (P21 and P56) during postnatal development. Interestingly, a larger fraction of axons with a diameter of 0.2-0.4μm, and smaller fraction of axons with a diameter of 0.5-0.7 μm was observed in *Lrp1* mutant optic nerves compared to controls (Figure 2.5h, k, and n). Independently of genotype, the majority of axons larger than 1μm in diameter are myelinated, and axons smaller than 0.2μm are not myelinated. Intermediate-sized axons, 0.3-0.9μm in diameter, are significantly less frequently myelinated in *Lrp1* deficient mice (Figure 2.5f, i, and l). While axon density is comparable between genotypes (Figure 2.5r), large diameter axons (>1μm) were more frequently observed in *Lrp1* cKO^{OL} mice compared to controls (Figure 2.5s). I found nodes (sodium channel staining) formed significantly more frequently on large (>1μm) caliber axons in *Lrp1* cKO^{OL} mice compared to controls (Figure 2.4i). Moreover, these morphological features concerning axon caliber and myelination status were correlated with optic nerve CAP recording (Figure 2.7).

In the PNS, the extent of myelination strictly correlates with axon diameter. Larger axons express more Nrg1-III, which binds to ErbB receptors on the Schwann cells to initiate myelination (Taveggia et al 2005). In the CNS, a less strict correlation was reported; however, OLs seem to selectively ensheath polystyrene fibers that are >400nm in diameter in the absence of dynamic signals. On the contrary, the signal, level, and isotype of Nrg1s appear to correlate with neuronal signals. ErbB receptor

ablation in OLs leads to hypomyelination that phenocopied defects observed in social isolation (Makinodan et al 2012). Social isolation leads to Nrg1-III down-regulation and hypomyelination (Makinodan et al 2012). The expression level of Nrg1 subtype correlates with neuronal firing (Liu et al 2011). Overexpressing Nrg1-I drives myelination of small caliber axons that are not myelinated in normal condition (Brinkmann et al 2008). Suggesting that the physical difficulty of myelin wrapping along small axons might be overcome by increasing the yet-to-be-defined axonal signals. Moreover, similar to what I found, selective hypomyelination of small caliber axons was observed in the optic nerves of *Fyn*$^{-/-}$ or *Fyn*$^{-/-}$*, Mag*$^{-/-}$ mice while large axons were unaffected (Biffiger et al 2000). An explanation for this finding is that a lower ratio of cytoplasm volume to each myelin sheath was speculated for small axons. As one OL myelinates ~50 small axons but a few or only one large axon (Hildebrand et al 1993), in the latter case the OL cell body might be directly associated with an axon to provide energy support more effectively (Biffiger et al 2000).

— **Search for OL-axon regulator by studying the caliber of axons in vivo**

Collectively, these results suggest that LRP1 participates in normal axon-glia interaction. It will be interesting to compare the previously described axonal features when each myelin protein is manipulated. While the ultrastructural EM studies provide a wealth of detail, the high technical threshold in preparing artifact-free sample, in getting enough representative pictures under a small field of imaging, and the quantification process is labor-intensive make it hard to draw conclusion correctly. We learned the localization dependent heterogeneity of the axons by study with the monkey optic nerves (Sanchez et al 1986). It was showed that the density, size, and myelination status of axons vary significantly in different regions of the nerve. Four poles of superior, inferior, nasal, and temporal were defined, central and peripheral were separated, and 16 portions of a nerve were denoted and subject to quantification. Large fibers were found more frequently in the peripheral superior nerve. The highest density of all fibers was located centrally in the infero-temporal quadrant. Although how each axonal population correlates to

nerve function is still unclear, correct characterization is important for accessing pathologic changes in the optic system (Sanchez et al 1986). Developing higher throughput imaging and processing methods are required to advance this field (Comin et al 2014).

4.2.3 How can cholesterol impact myelination and remyelination

From Chapter I to III (section 1.3.2.1 and 2.3.6) we have learned that cholesterol is a key component in the CNS myelin health and disease, the regulation of intercellular cholesterol metabolism is tightly controlled, and LRP1 is involved in cholesterol homeostasis. *Lrp1* germ line null is embryonic lethal (Herz et al 1992). Interestingly, defects in OPC maturation in primary culture are more prominent than *in vivo* when *Lrp1* is specifically deleted in the OL-lineage. It is tempting to speculate that $Lrp1^{-/-}$ OPCs are able to acquire metabolites (such as cholesterol) from neighboring $Lrp1^{+/+}$ cells *in vivo*; thereby, masking a more severe defect in CNS myelin development. This "masking effect" is incomplete however, as *Lrp1* conditional KO mice still exhibit a hypomyelination phenotype. *In vitro*, OPCs that are deficient for *Lrp1* are isolated from cells that may provide cholesterol inter-cellularly, and thus, the differentiation phenotype is more pronounced. Here, LRP1's involvement in cholesterol homeostasis and topological distribution during myelin development or repair under the context of cell-cell interaction is discussed.

— **As a signaling regulator**

Regulation of cholesterol homeostasis including uptake, biosynthesis, catabolism, and lateral exchange between CNS cells has been extensively reviewed (Björkhem & Meaney 2004, Courtney & Landreth 2016, Orth & Bellosta 2012, Saher et al 2005, Saher & Stumpf 2015, Tall & Yvan-Charvet 2015, Vitali et al 2014). Multiple genes involved in cholesterol metabolism were altered in $Lrp1^{-/-}$ OPCs, gene ontology analysis identified differences in 'Regulation of Cholesterol Biosynthesis Process, 'Cellular Response to Sterol', and 'Regulation of Cholesterol Homeostasis' (Figure 3.15). Gene products associated with each GO term including glucose-6-phosphate dehydrogenase x-linked/G6PDH (*G6pdx*), Liver X Receptor-Beta/LXRβ

(*Nr1h2*), SREBP Cleavage-Activating Protein/SCAP (*Scap*), Peroxin2 (*Pex2*), LRP1 (*Lrp1*), LRP5 (*Lrp5*), Retinoid-Related Orphan Receptor Gamma/RZRG (*Rorc*), Follicle-Stimulating Hormone-Releasing Protein/FRP (*Inhba*) and miRNA33 (*Mir33*). In *Lrp1*$^{-/-}$ cells the cholesterol sensing apparatus seems to be intact, as bath applied cholesterol leads to a decrease in SREBP2. Accumulating evidence shows that these molecular pathways are either directly linked to or cross talk with pathways that are important for myelin biogenesis. In line with the view of RCT, *Scap* ablation in astrocytes leads to hypomyelination and this can be reversed by high-fat diet (Camargo et al 2017). Other than SREBP2, LXRs are the master regulators of cholesterol homeostasis and inflammation in the brain. LXRβ is expressed dominantly in the liver and the brain, and LXR signals were found to be disrupted in many neurodegenerative diseases (Courtney & Landreth 2016). In response to cholesterol, LXRs form heterodimers with RXR, LXR-RXR binds to LXRE (LXR response elements) in the nucleus and activates or represses gene transcription. Ligand-bound LXR can be SUMOylated and repress iNOS (M1 pro-inflammation gene) expression to suppress a pro-inflammatory response. Furthermore, LXR controls cholesterol efflux in cholesterol-loaded cells, cholesterol-laden cells (foam cells) activate TLR signaling, TLR aggravates inflammation by feed-forward signaling, reducing cholesterol efflux (Tall & Yvan-Charvet 2015). The lingering of myelin-derived cholesterol limits CNS remyelination, treating with an LXR agonist (GW3965) improves lesion recovery (Cantuti-Castelvetri et al 2018). Cholesterol-lowering drugs (e.g. statins) are anti-inflammatory by inhibiting TLR-mediated cytokine or chemokine production (Angelovich et al 2015, Lin et al 2011), and promote remyelination in animal models of MS (Chrast et al 2011, Paintlia et al 2005, Paintlia et al 2008, Stanislaus et al 2002, Youssef et al 2002). However, cholesterol is the rate-limiting factor for myelin growth in the normal brain (Saher et al 2005, Saher & Stumpf 2015), indicating the exquisite balance at the cellular level of cholesterol is pivotal.

— **As a structural lipid of the membrane**

Cholesterol is the key molecule in the lipid raft, where the membrane is more "rigid", different in size, and varies in molecular composition. A lipid raft is considered a platform for carrying out protein sorting, signaling, and caveolae-mediated (clathrin-independent) endocytosis (Gielen et al 2006). Lipid raft is an operational definition; the name was given to the partition of membrane that resists cold Triton X-100 extraction, called detergent-resistant membrane (DRM), recovered by gradient flotation (Brown & London 2000, Brown & Rose 1992, Simons & Ikonen 1997). Compositional study of DRMs revealed a list of potential raft-associated lipids and proteins (Foster et al 2003); however, the constituents varied from one extraction to another due to the detergents used or different technical practices (Banerjee et al 1995, Chamberlain 2004, Schuck et al 2003).

It was postulated that myelin, lipid, and protein sorting, at least to some degree, are coupled with lipid rafts. This is indeed the case for PLP, which was endocytosed through a cholesterol-dependent pathway to the late endosomes/lysosomes (LE/Lys) compartment, and trafficed through cell cytosol myelinic channels to the myelin leading edge. On the other hand, MAG and MOG are sorted through a clathrin-dependent pathway and targeted to LE/Lys and recycling endosomes (RE), respectively (White & Krämer-Albers 2014). Defects in PLP sorting may lead to diseases that feature hypomyelination (Kramer-Albers et al 2006). Signals that are important for myelination or OL development are integrated at lipid rafts through Fyn activation, such as myelin protein synthesis, cytoskeleton recruitment, and morphological differentiation (White & Krämer-Albers 2014). LRP1 is enriched in lipid rafts, and Fyn binds to LRP1 phosphorylation sites (Guttman et al 2009), suggesting it might be a direct downstream signaling target of LRP1 for regulating myelination.

4.2.4 How can peroxisome impacts myelin biology

In Chapter II (section 2.3.7), I have identified a novel role for LRP1 in regulating peroxisome biogenesis and subcellular distribution. The role of the

PPARγ signaling pathway and how it regulates CNS myelin and OL differentiation is discussed (section 2.4). Here I consider peroxisomes as a functional unit and how myelin-associated peroxisomes impact myelin formation and axonal integrity.

— **Consider peroxisome as an all-purposed logistic vehicle**

Peroxisomes are single membrane-bounded organelles that are versatile in function. Peroxisomes execute multiple functions including reactive oxygen species (ROS) elimination, the pre-squalene sequence of cholesterol biosynthesis, lipid oxidation, ATP production, and serve as anti-viral innate immune platform. Of note, the TSC1/2 complex resides on peroxisomes, speculating far-reaching signaling regulatory functions of peroxisomes (Cohen et al 2000, Desvergne & Wahli 1999, Dixit et al 2010, Faust & Kovacs 2014, Titorenko & Rachubinski 2004). Peroxisomes orchestrate many critical metabolic pathways through collaborating with their environment by forming membrane contacts with other organelles such as lysosomes and mitochondria (Fransen et al 2017, Shai et al 2016). Recent work indicated that newly synthesized peroxisomes are a hybrid product of mitochondria and ER (Sugiura et al 2017), which is different from fission-derived peroxisomes. Stressing the diversity of peroxisome origin, their function, localization, and composition. The heterogeneity of peroxisomes in size, localization, interior protein/RNA components, and membrane contacts emphasize their ability to respond promptly to metabolic changes (Chung et al 2013, Thoms 2015).

From previous work it was thought that peroxisome merely functions in segregating unique enzymatic reactions. Not until recently was it suggested that peroxisomes may also be utilized as an intracellular mRNA shuttle (Haimovich et al 2016). Local mRNA translation is essential for highly specialized cells, such as neurons and OLs, to meet the metabolic demands for making timely responses (Gumy et al 2010). However, how mRNA is shuttled and if peroxisome is involved are still remain largely unknown. In the CNS, myelinated axons rarely harbor their own peroxisomes; however, OL-derived peroxisomes were found to accumulate at the paranodal myelin lamina (Kassmann 2014), where intense axon-glia metabolite

exchange happens. This orientation suggests that axons rely on adjacent glia cells for providing peroxisomal support to cover their metabolic needs. This idea was proposed in a similar phrase in 1973 (Holtzman et al 1973); however, direct evidence for and the underlying mechanisms of peroxisome-mediated intercellular support are still elusive. *Pex2*, *Pex5*, and *Pex13* germline null mice have been generated to study ZS, a spectrum of syndromes characterized by peroxisome biogenesis disorder, neuronal cell death, and hypomyelination (Berger et al 2016). However, due to the embryonic, hypertonic, and neonatal death, this limits the window to study peroxisomal function in later developmental stages (Baes & Van Veldhoven 2012). Interestingly, severe neuronal defects in the whole brain *Pex5* KO were found; however, the cell type specific KOs including neuron, astrocyte, or OLs showed no deficits (Baes & Van Veldhoven 2012). This discrepancy suggests that peroxisomes are involved in a lateral shuttling pathway—a "masking effect", and also reveals the drawbacks of using the single *loxP-Cre* system *in vivo*.

— **A hierarchical role for peroxisomes in cholesterol metabolism?**

There are many studies concerning each PEX protein function in peroxisome biogenesis, PPARs signaling in lipid homeostasis and inflammation, and the structure of peroxisome proliferators (PPs) in stimulating peroxisome production in the liver. However, the gap between how PPs regulate PEX and through which PPAR signaling pathway they promote peroxisome biogenesis remains understudied. Given the sparsity of knowledge, little tools are available regarding peroxisome manipulation as a whole. Interestingly, disruption of any of the PEX genes seems to cause dysfunctional peroxisomes, as characterized in patients with spontaneous mutations in PEX genes. In our studies, extra cholesterol did not seem to promote OPC differentiation, however, the transition from OPCs to MBP^{+} OLs was significantly accelerated when treated with pioglitazone in $Lrp^{+/+}$ OPCs. The number of peroxisomes seems to stay constant once an OL is mature, and pioglitazone treatment does not increase the peroxisome number nor alter distribution. In the $Lrp1^{-/-}$ deficient OPCs however, pioglitazone treatment moderately increases the localization of peroxisomes into cellular processes. When $Lrp1^{-/-}$ deficient OPCs are

treated with pioglitazone combined with cholesterol, the peroxisome number, distribution, and cell size were restored to normal. Suggesting that in *Lrp1*$^{-/-}$ deficient OPCs, both peroxisomal functions and cholesterol homeostasis are disrupted. Combine with the observations in *Lrp*$^{+/+}$ OPCs, a possible explanation for this combined treatment to restore OL differentiation in *Lrp1*$^{-/-}$ deficient cells is formed. I speculated that only when peroxisomal functions are increased in *Lrp*$^{-/-}$ OPCs, free cholesterol can promote myelin-like membrane growth. In another words, I the intact peroxisomes are the pre-requisite for normal cholesterol-mediated function under the control of LRP1. The actual casual effect remains to be validated.

4.2.5 Speculations on how LRP1 impacts myelin biology

— **LRP1 regulates Myo1d: motor protein trafficking on cytoskeleton**

Myo1d mRNA expression was strongly reduced in *Lrp1* deficient O4^{+} OLs (Figure 3.18e), the protein expression of MYO1D is below the detection limit in mature OLs in the absence of LRP1 (Figure 3.18f and g). Myo1d is a non-conventional myosin expressed exclusively in mature OLs (Yamazaki et al 2014), as was found in myelin proteomic studies (Roth et al 2006, Werner et al 2007). MYO1D co-localized with PLP in OL processes and with actin at the leading edge (Yamazaki et al 2014, Yamazaki et al 2017), equivalent to myelinic channels I have discussed (section 1.3.1). Knocking down *Myo1d* in immature OLs by siRNA results in PLP accumulation at the peri-nucleus, attenuated OL differentiation, and disrupted myelin processes (Yamazaki et al 2016). The morphology of OLs lacking MYO1D phenocopies OLs that are deficient in LRP1 (Figure 2.10d and Figure 2.11e) or treated with statin (Smolders et al 2010). Moreover, PLP trafficking is cholesterol-dependent at lipid rafts where LRP1 is enriched. Interestingly, knocking down *Myo1d* in mature MBP^{+} OLs leads to the collapse/degeneration of myelin-like membranes (Yamazaki et al 2016). Currently there is no available mouse model to study MYO1D in vivo; however, *Myo1d* KO rats are deficient in planar cell polarity (Hegan et al 2015). Knocking down Myo1d by siRNA at the corpus callosum impairs

remyelination following cuprizone treatment (Yamazaki et al 2018). Of note, Myosin2p in yeast transports peroxisomes along actin to the budding daughter cell ((Hoepfner et al 2001), and peroxisomes form contacts with lysosomes to exchange cholesterol (Chu et al 2015). It is tempting to speculate that LRP1 transcriptionally regulates MYO1D, which directs the movement of peroxisomes to shuttle cholesterol, therefore myelin membrane extension positively feeds back to generate more myelin proteins. It is of interest to investigate if peroxisome distribution, biogenesis, and cholesterol homeostasis are also altered; if pioglitazone and cholesterol treatment can restore the hypomyelination phenotype; and if myelin dynamic trafficking is disrupted in *Myo1d* deficient OLs. With the observations I made in *Lrp1* deficient cells, we are one step closer to understanding how these signaling pathways orchestrate CNS myelin in health and disease.

4.3 Future Direction

Following the arguments presented in the previous section, I will discuss future directions of my work on Lrp1 in the OL lineage and potential experiments to address questions listed below.

— **The role of Lrp1 in different cell types and its contribution to myelin repair**

To examine if LRP1 is required in astrocytes, microglia, or peripheral immune cells during CNS myelin repair, *Lrp1* tissue-specific knockout (KO) can be employed. *Lrp1*$^{flox/flox}$ need to be crossed with constitutive (*Cre*) or inducible (*CreER*^{TM}) mouse lines, where *Cre* expression is under the promoter of the *Gfap* (astrocyte), *Cx3cr1* (microglia), *LysM* (myeloid cell), *CD4* (T_H cell), *CD8* (T_C cell), or *CD19* (B cell) promoter to generate mice that lack Lrp1 is specific cell types. Following chemically induced axon demyelination, remyelination will be assayed as described in Chapter II (section 2.5.3 and 2.5.6). When combined with EM studies, this will allow us to assess the extent of myelin repair and provide insights into the importance of Lrp1 in specific cell types. At different post-injury time points, the level of debris phagocytosis and the progress of OPC differentiation will need to be

examined. Once the cellular events that contribute to remyelination are revealed, *in vitro* studies will follow to search for potential non-cell autonomous mechanisms. Applying fluorescent-labeled myelin to cultured cells can test the ability of LRP1-mediated myelin debris uptake. *Lrp1* deficient astrocytes, microglia, or immune cells co-cultured with OPCs in a contact-dependent or independent manner can be used to analyze if LRP1-mediated signaling cues provided by specific cell types are needed for OPC differentiation and myelin sheet formation.

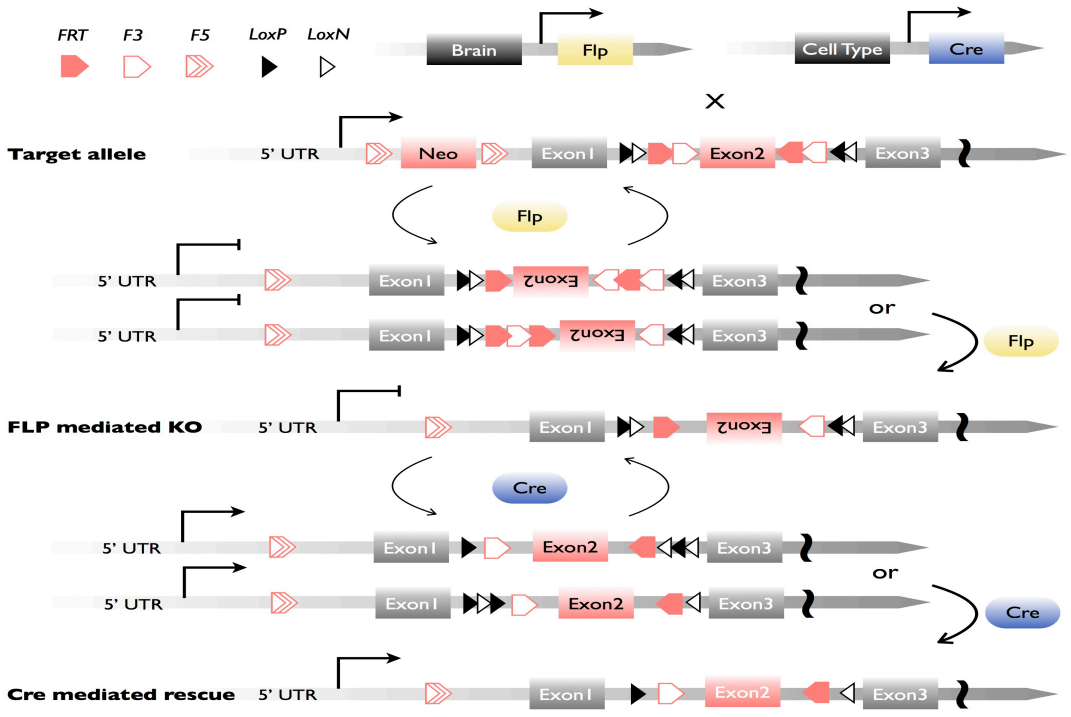

Figure 4.1: Genetic manipulation strategies to study masking effect
Flipase (Flp) or Cre recombinase expression is driven by tissue-specific promoters that are pre-established can be used to perform conditional knockout or tissue-specific rescue. FRT, F3, and F5 are flippase recognition sequence. LoxP and LoxN are cre recognition sequence. This is figure was created by Jing-Ping Lin.

To study potential masking effects, including the inter-cellular shuttling of metabolites or organelles (mitochondria, exosomes, or peroxisomes) during myelination, new mouse genetic tools will need to be developed (Figure 4.1). Take advantage of the site-specific recombinase (SSR) system (Branda & Dymecki 2004) by flanking specific alleles with *LoxP* and *FRT* site-specific sequences and then cross these with well-established tissue-specific flipase (Flp) and Cre mouse driver lines. This approach will allow us to address potential "masking effects" *in vivo*. New

genetic tools will allows us to interrogate the presence of pathways, and cell types involved in rescuing (or masking) defects in OPC differentiation. For example, by using forebrain specific Cre promoter (*Nestin*) to delete LRP1 and rescues it with tissue specific Flp, I can examine the requirement of LRP1 in each CNS cell type in an LRP1 null environment. Similarly, transplantation of each cell type into a brain with the specific gene ablated can be performed in parallel.

— **Identification of LRP1-PPARγ regulated genes important for CNS myelination**

To search for the LRP1-regulated genes that are transcribed by PPARγ activation during OPC development, RNA sequencing can be employed. By comparing the expression profile between *Lrp1* control OPCs, *Lrp1*$^{-/-}$ OPCs, *Lrp1* control OPCs treated with pioglitazone, and *Lrp1*$^{-/-}$ OPCs treated with pioglitazone, I will be able to discover differentially regulated genes under each condition. Because *Lrp1*$^{-/-}$ OPCs do not differentiate in the presence of pioglitazone, this will allow us to rule out many genes that are not sufficient to drive OPC differentiation. Gene products that are differentially regulated between *Lrp1* control OPCs and *Lrp1*$^{-/-}$ OPCs treated with pioglitazone are candidates for OPC maturation. Novel candidates can then be overexpressed or knocked down in *Lrp1*$^{-/-}$ OPCs to examine whether they can rescue the differentiation defects. Also, OPCs isolated from the Lrp1-N2 mice, treated with or without pioglitazone, can be added to the comparison to examine the requirement of the distal NPxY phosphorylation site of LRP1 in regulation of gene transcription. The correlation of genetic function at a transcriptional and translational level should be considered, as miRNAs or long-noncoding RNAs were found to dynamically regulate RNA stability and/or coordinate expression of groups of genes. By RNA sequencing, I will be able to generate a wealth of data under each condition for coding and non-coding RNAs that will be mined using bioinformatics tools similar to the ones described in chapter II. This work may shed light on how different aspects of LRP1 signaling contribute to specific cellular needs during OL lineage maturation and CNS myelination.

— **The role of LRP1 in regulating organelle trafficking**

To assess if LRP1 is required for peroxisome trafficking and subcellular organelle distribution, regular live imaging and super-resolution microscopy (STORM for example) may be needed. OPCs isolated from mice with a peroxisomal protein fused to GFP or equivalents will be cultured. Following stimulation of each signaling pathway or gene manipulation, the speed, localization, and morphology of peroxisomes will be recorded. The local transcriptome associated with peroxisomes at the myelinic channels can be analyzed by merFISH (Moffitt et al 2016). By comparing the RNA profiles in OPC/OLs contacted by neurons versus non-contacted cells in KO-KO, KO-control, and control-control groups, I will be able to identify new pathways that are regulated within cells. Sub-cellular domains can be defined, identified, and analyzed differentially as well. This platform can be used to identify the peroxisomal regulation through neuron-glia interaction and stimulation-mediated dynamic changes in the future as well.

To study how LRP1 may be involved in peroxisome trafficking, an in depth experimental approach, similar to Figure 3.20-Figure 3.23 may need to be developed. An interesting hypothesis has developed based on the RNA profiling studies of Lrp1 control and *Lrp1*$^{-/-}$ OPCs. I found that Myosin ID (*Myo1d*) expression is significantly reduced in *Lrp1*$^{-/-}$ OPCs (Figure 3.18). Myo1d is an unconventional myosin comprised of an ATP- and actin-binding head, two IQ domain-containing necks for calmodulin binding, and a lipid-binding tail (Benesh et al 2010, Yamazaki et al 2014). Very recently it was reported that Myo1d is important for myelin repair. Questions such as if the LRP1-ICD binds to *Myo1d* or regulates *Myo1d* mRNA expression transcriptionally (promoter region) and/or post-transcriptionally (miRNA or equivalent); and if Myo1D co-localizes with peroxisomes and/or is important for subcellular distribution and trafficking or peroxisomes will be interesting to pursue. For example, it will be important to test if *Myo1d* overexpression rescues the *Lrp1*$^{-/-}$ OPC/OL phenotype; the dynamic and heterogeneity of peroxisome size, localization, interior protein/RNA components, and membrane contacts direct their ability to respond in a timely manner to meet

local metabolic demands between neuronal cells. Peroxisomes in the brain are called “microperoxisomes” (McKenna et al 1976), compared to those found in other tissues (~1 um in liver cells) they are smaller in size (30-200 nm). Therefore, studying microperoxisomes is challenging, because their size is below the deflection limit of conventional light microscopy (Kassmann et al 2011). Newer tools, such as super-resolution microscopy, will be essential to track their morphology and distribution in detail.

4.4 **Concluding Remarks**

Over the past few decades our knowledge of myelin biology has expanded enormously. Scientists have moved from basic single myelin gene characterization to ‘omics’ studies. The model of myelination has been refined to incorporate activity dependent internode plasticity. Regulatory pathways between different neuronal cells have been integrated to build hypothesis. Building on these previous findings and attempting to envision the bigger picture under the context of a network is most likely the future of myelin biology. As the advance of RNA sequencing techniques, getting the transcriptome from a single neuronal cell is not impossible anymore. However, due to the nature of these cells, they are large and highly polarized, sequencing reads from an isolated cell cannot reveal the changes in subcellular localization or 3D orientation. Both aspects are important to consider for revealing consecutive local responses. In addition, the heterogeneity of expression profiles in different cell types varies topologically and temporally in the brain, which posts a major challenge in interpreting information from isolated cells to match morphology and function. *In situ* profiling is a foreseeable future to overcome these current limits in single cell sequencing. As the techniques regarding multiplex FISH developing, we will be able to acquire single cell transcriptome with spatial resolution. This advance will give us more information to interpret the complex regulatory mechanism of the CNS myelination in health and disease. Although the throughput to acquire multiplex FISH data is still low and the analytic methods is conceptually lagging, it is certainly exciting to see how it can lead us to another level of comprehension. We are only in the beginning of understanding the logic of

metabolic coupling between neuronal cells, and still have a long way to go before applying this knowledge clinically. However, as long as we keep trying, the answer can only be closer.

4.5 **Bibliography**

Angelovich TA, Hearps AC, Jaworowski A. 2015. Inflammation-induced foam cell formation in chronic inflammatory disease. pp. 683-93: Nature Publishing Group

Asher R, Perides G, Vanderhaeghen JJ, Bignami A. 1991. Extracellular matrix of central nervous system white matter: Demonstration of an hyaluronate-protein complex. In *J. Neurosci. Res.*, pp. 410-21: Wiley Subscription Services, Inc., A Wiley Company

Baes M, Van Veldhoven PP. 2012. Mouse models for peroxisome biogenesis defects and β-oxidation enzyme deficiencies. In *Biochim. Biophys. Acta*, pp. 1489-500

Banerjee P, Joo JB, Buse JT, Dawson G. 1995. Differential solubilization of lipids along with membrane proteins by different classes of detergents. In *Chem. Phys. Lipids*, pp. 65-78

Benesh AE, Nambiar R, McConnell RE, Mao S, Tabb DL, Tyska MJ. 2010. Differential localization and dynamics of class I myosins in the enterocyte microvillus. In *Mol. Biol. Cell*, pp. 970-78

Berger J, Dorninger F, Forss-Petter S, Kunze M. 2016. Peroxisomes in brain development and function. In *BBA - Molecular Cell Research*, pp. 934-55: The Authors

Biffiger K, Bartsch S, Montag D, Aguzzi A, Schachner M, Bartsch U. 2000. Severe hypomyelination of the murine CNS in the absence of myelin-associated glycoprotein and fyn tyrosine kinase. In *J. Neurosci.*, pp. 7430-37

Bignami A, Asher R. 1992. Some observations on the localization of hyaluronic acid in adult, newborn and embryonal rat brain. In *Int. J. Dev. Neurosci.*, pp. 45-57

Björkhem I, Meaney S. 2004. Brain cholesterol: long secret life behind a barrier. In *Arterioscler. Thromb. Vasc. Biol.*, pp. 806-15

Bourguignon LYW, Gilad E, Peyrollier K, Brightman A, Swanson RA. 2007. Hyaluronan-CD44 interaction stimulates Rac1 signaling and PKNγ kinase activation leading to cytoskeleton function and cell migration in astrocytes. In *J. Neurochem.*, pp. 1002-17: Blackwell Publishing Ltd

Branda CS, Dymecki SM. 2004. Talking about a revolution: The impact of site-specific recombinases on genetic analyses in mice. In *Developmental Cell*, pp. 7-28

Brinkmann BG, Agarwal A, Sereda MW, Garratt AN, Müller T, et al. 2008. Neuregulin-1/ErbB signaling serves distinct functions in myelination of the peripheral and central nervous system. In *Neuron*, pp. 581-95

Brown DA, London E. 2000. Structure and Function of Sphingolipid- and Cholesterol-rich Membrane Rafts. In *Journal of Biological Chemistry*, pp. 17221-24

Brown DA, Rose JK. 1992. Sorting of GPI-anchored proteins to glycolipid-enriched membrane subdomains during transport to the apical cell surface. In *Cell*, pp. 533-44

Camargo N, Goudriaan A, van Deijk A-LF, Otte WM, Brouwers JF, et al. 2017. Oligodendroglial myelination requires astrocyte-derived lipids. In *PLoS Biol.*, pp. e1002605

Cantuti-Castelvetri L, Fitzner D, Bosch-Queralt M, Weil M-T, Su M, et al. 2018. Defective cholesterol clearance limits remyelination in the aged central nervous system. In *Science*

Chamberlain LH. 2004. Detergents as tools for the purification and classification of lipid rafts. In *FEBS Lett.*, pp. 1-5

Chernoff GF. 1981. Shiverer: an autosomal recessive mutant mouse with myelin deficiency. In *J. Hered.*, pp. 128

Chrast R, Saher G, Nave K-A, Verheijen MHG. 2011. Lipid metabolism in myelinating glial cells: lessons from human inherited disorders and mouse models. In *J. Lipid Res.*, pp. 419-34

Chu B-B, Liao Y-C, Qi W, Xie C, Du X, et al. 2015. Cholesterol transport through lysosome-peroxisome membrane contacts. In *Cell*, pp. 291-306: Elsevier Inc.

Chuang T-Y, Guo Y, Seki SM, Rosen AM, Johanson DM, et al. 2016. LRP1 expression in microglia is protective during CNS autoimmunity. In *Acta Neuropathol Commun*, pp. 1-12

Chung W-S, Clarke LE, Wang GX, Stafford BK, Sher A, et al. 2013. Astrocytes mediate synapse elimination through MEGF10 and MERTK pathways. In *Nature*, pp. 394-400

Cohen GB, Rangan VS, Chen BK, Smith S, Baltimore D. 2000. The human thioesterase II protein binds to a site on HIV-1 Nef critical for CD4 down-regulation. In *J. Biol. Chem.*, pp. 23097-105

Colello RJ, Pott U, Schwab ME. 1994. The role of oligodendrocytes and myelin on axon maturation in the developing rat retinofugal pathway. In *J. Neurosci.*, pp. 2594-605

Comin CH, Santos JR, Corradini D, Morrison W, Curme C, et al. 2014. Statistical physics approach to quantifying differences in myelinated nerve fibers. In *Sci Rep*, pp. 4511

Courtney R, Landreth GE. 2016. LXR Regulation of Brain Cholesterol: From Development to Disease. In *Trends Endocrinol. Metab.*, pp. 404-14

Desvergne B, Wahli W. 1999. Peroxisome proliferator-activated receptors: nuclear control of metabolism. In *Endocr. Rev.*, pp. 649-88

Dixit E, Boulant S, Zhang Y, Lee ASY, Odendall C, et al. 2010. Peroxisomes are signaling platforms for antiviral innate immunity. In *Cell*, pp. 668-81

Dousset V, Brochet B, Vital A, Gross C, Benazzouz A, et al. 1995. Lysolecithin-induced demyelination in primates: preliminary in vivo study with MR and magnetization transfer. In *Am. J. Neuroradiol.*, pp. 225

Eggli PS, Lucocq J, Ott P, Graber W, van der Zypen E. 1992. Ultrastructural localization of hyaluronan in myelin sheaths of the rat central and rat and human peripheral nervous systems using hyaluronan-binding protein-gold and link protein-gold. In *Neuroscience*, pp. 737-44

Faust PL, Kovacs WJ. 2014. Cholesterol biosynthesis and ER stress in peroxisome deficiency. In *Biochimie*, pp. 75-85: Elsevier Masson SAS

Fok-Seang J, Mathews GA, ffrench-Constant C, Trotter J, Fawcett JW. 1995. Migration of Oligodendrocyte Precursors on Astrocytes and Meningeal Cells. In *Dev. Biol.*, pp. 1-15

Foster LJ, De Hoog CL, Mann M. 2003. Unbiased quantitative proteomics of lipid rafts reveals high specificity for signaling factors. In *Proc. Natl. Acad. Sci. U.S.A.*, pp. 5813-18

Fransen M, Lismont C, Walton P. 2017. The Peroxisome-Mitochondria Connection: How and Why? In *IJMS*, pp. 1126

Gaultier A, Arandjelovic S, Li X, Janes J, Dragojlovic N, et al. 2008. A shed form of LDL receptor-related protein-1 regulates peripheral nerve injury and neuropathic pain in rodents. In *J. Clin. Invest.*, pp. 161-72

Gielen E, Baron W, vandeVen M, Steels P, Hoekstra D, Ameloot M. 2006. Rafts in oligodendrocytes: Evidence and structure–function relationship. In *Glia*, pp. 499-512

Girgrah N, Letarte M, Becker LE, Cruz TF, Theriault E, Moscarello MA. 1991. Localization of the CD44 Glycoprotein to Fibrous Astrocytes in Normal White Matter and to Reactive Astrocytes in Active Lesions in Multiple Sclerosis. In *J. Neuropathol. Exp. Neurol.*, pp. 779-92

Groves AK, Entwistle A, Jat PS, Noble M. 1993. The Characterization of Astrocyte Cell Lines That Display Properties of Glial Scar Tissue. In *Dev. Biol.*, pp. 87-104

Gumy LF, Tan CL, Fawcett JW. 2010. The role of local protein synthesis and degradation in axon regeneration. In *Exp Neurol*, pp. 28-37

Guttman M, Betts GN, Barnes H, Ghassemian M, van der Geer P, Komives EA. 2009. Interactions of the NPXY microdomains of the low density lipoprotein receptor-related protein 1. In *Proteomics*, pp. 5016-28

Haimovich G, Cohen-Zontag O, Gerst JE. 2016. A role for mRNA trafficking and localized translation in peroxisome biogenesis and function? In *Biochim. Biophys. Acta*, pp. 911-21

Hegan PS, Ostertag E, Geurts AM, Mooseker MS. 2015. Myosin Id is required for planar cell polarity in ciliated tracheal and ependymal epithelial cells. In *Cytoskeleton (Hoboken)*, pp. 503-16

Hendrickx DAE, Koning N, Schuurman KG, van Strien ME, van Eden CG, et al. 2013. Selective upregulation of scavenger receptors in and around demyelinating areas in multiple sclerosis. In *J. Neuropathol. Exp. Neurol.*, pp. 106-18

Herz J, Clouthier DE, Hammer RE. 1992. LDL receptor-related protein internalizes and degrades uPA-PAI-1 complexes and is essential for embryo implantation. In *Cell*, pp. 411-21

Hildebrand C, Remahl S, Persson H, Bjartmar C. 1993. Myelinated nerve fibres in the CNS. In *Prog. Neurobiol.*, pp. 319-84

Hoepfner D, van den Berg M, Philippsen P, Tabak HF, Hettema EH. 2001. A role for Vps1p, actin, and the Myo2p motor in peroxisome abundance and inheritance in Saccharomyces cerevisiae. In *The Journal of Cell Biology*, pp. 979-90

Holtzman E, Teichberg S, Abrahams SJ, Citkowitz E, Crain SM, et al. 1973. Notes on synaptic vesicles and related structures, endoplasmic reticulum, lysosomes and peroxisomes in nervous tissue and the adrenal medulla. In *J. Histochem. Cytochem.*, pp. 349-85

Hsieh ST, Kidd GJ, Crawford TO, Xu Z, Lin WM, et al. 1994. Regional modulation of neurofilament organization by myelination in normal axons. In *J. Neurosci.*, pp. 6392-401

Irvine KA, Blakemore WF. 2006. Age increases axon loss associated with primary demyelination in cuprizone-induced demyelination in C57BL/6 mice. In *J Neuroimmunol*, pp. 69-76

Jones LL, Liu Z, Shen J, Werner A, Kreutzberg GW, Raivich G. 2000. Regulation of the cell adhesion molecule CD44 after nerve transection and direct trauma to the mouse brain. In *J Comp Neurol*, pp. 468-92: John Wiley & Sons, Inc.

Kassmann CM. 2014. Myelin peroxisomes - essential organelles for the maintenance of white matter in the nervous system. In *Biochimie*, pp. 111-18

Kassmann CM, Quintes S, Rietdorf J, Mobius W, Sereda MW, et al. 2011. A role for myelin-associated peroxisomes in maintaining paranodal loops and axonal integrity. In *FEBS Lett.*, pp. 2205-11

Kramer-Albers EM, Gehrig-Burger K, Thiele C, Trotter J, Nave KA. 2006. Perturbed Interactions of Mutant Proteolipid Protein/DM20 with Cholesterol and Lipid Rafts in Oligodendroglia: Implications for Dysmyelination in Spastic Paraplegia. In *J. Neurosci.*, pp. 11743-52

Lin H, Xiao Y, Chen G, Fu D, Ye Y, et al. 2011. HMG-CoA reductase inhibitor simvastatin suppresses Toll-like receptor 2 ligand-induced activation of nuclear factor kappa B by preventing RhoA activation in monocytes from rheumatoid arthritis patients. In *Rheumatol. Int.*, pp. 1451-58

Liu X, Bates R, Yin D-M, Shen C, Wang F, et al. 2011. Specific regulation of NRG1 isoform expression by neuronal activity. In *J. Neurosci.*, pp. 8491-501

Makinodan M, Rosen KM, Ito S, Corfas G. 2012. A critical period for social experience-dependent oligodendrocyte maturation and myelination. In *Science*, pp. 1357-60

May P, Bock HH, Nofer J-R. 2013. Low density receptor-related protein 1 (LRP1) promotes anti-inflammatory phenotype in murine macrophages. In *Cell Tissue Res.*, pp. 887-89

McKenna O, Arnold G, Holtzman E. 1976. Microperoxisome distribution in the central nervous system of the rat. In *Brain Res*, pp. 181-94

Meier H, MacPike AD. 1970. A neurological mutation (msd) of the mouse causing a deficiency of myelin synthesis. In *Exp Brain Res*, pp. 512-25

Miron VE, Boyd A, Zhao J-W, Yuen TJ, Ruckh JM, et al. 2013. M2 microglia and macrophages drive oligodendrocyte differentiation during CNS remyelination. In *Nat. Neurosci.*, pp. 1211-18

Moffitt JR, Hao J, Wang G, Chen KH, Babcock HP, Zhuang X. 2016. High-throughput single-cell gene-expression profiling with multiplexed error-robust fluorescence in situ hybridization. In *Proc. Natl. Acad. Sci. U.S.A.*, pp. 11046-51

Nair A, Frederick TJ, Miller SD. 2008. Astrocytes in multiple sclerosis: a product of their environment. In *Cell. Mol. Life Sci.*, pp. 2702-20

Nixon RA, Paskevich PA, Sihag RK, Thayer CY. 1994. Phosphorylation on carboxyl terminus domains of neurofilament proteins in retinal ganglion cell neurons in vivo: influences on regional neurofilament accumulation,

interneurofilament spacing, and axon caliber. In *The Journal of Cell Biology*, pp. 1031-46
Orth M, Bellosta S. 2012. Cholesterol: Its Regulation and Role in Central Nervous System Disorders. In *Cholesterol*, pp. 1-19
Paintlia AS, Paintlia MK, Khan M, Vollmer T, Singh AK, Singh I. 2005. HMG-CoA reductase inhibitor augments survival and differentiation of oligodendrocyte progenitors in animal model of multiple sclerosis. In *FASEB J.*, pp. 1407-21
Paintlia AS, Paintlia MK, Singh AK, Singh I. 2008. Inhibition of rho family functions by lovastatin promotes myelin repair in ameliorating experimental autoimmune encephalomyelitis. In *Mol Pharmacol*, pp. 1381-93
Pasquini LA, Calatayud CA, Bertone Uña AL, Millet V, Pasquini JM, Soto EF. 2007. The neurotoxic effect of cuprizone on oligodendrocytes depends on the presence of pro-inflammatory cytokines secreted by microglia. In *Neurochem Res*, pp. 279-92
Perrot G, Langlois B, Devy J, Jeanne A, Verzeaux L, et al. 2012. LRP-1-CD44, a New Cell Surface Complex Regulating Tumor Cell Adhesion. In *Mol. Cell. Biol.*, pp. 3293-307
Quackenbush EJ, Cruz TF, Moscarello MA, Letarte M. 1985. Identification of three antigens in human brain associated with similar antigens on human leukaemic cells. In *Biochem. J.*, pp. 291-99
Roth AD, Ivanova A, Colman DR. 2006. New observations on the compact myelin proteome. In *Neuron Glia Biol.*, pp. 15-21
Saher G, Brugger B, Lappe-Siefke C, Mobius W, Tozawa R-i, et al. 2005. High cholesterol level is essential for myelin membrane growth. In *Nat. Neurosci.*, pp. 468-75
Saher G, Stumpf SK. 2015. Cholesterol in myelin biogenesis and hypomyelinating disorders. In *BBA - Molecular and Cell Biology of Lipids*, pp. 1083-94: Elsevier B.V.
Sánchez I, Hassinger L, Paskevich PA, Shine HD, Nixon RA. 1996. Oligodendroglia regulate the regional expansion of axon caliber and local accumulation of neurofilaments during development independently of myelin formation. In *J. Neurosci.*, pp. 5095-105
Sanchez RM, Dunkelberger GR, Quigley HA. 1986. The number and diameter distribution of axons in the monkey optic nerve. In *Invest. Ophthalmol. Vis. Sci.*, pp. 1342-50
Schuck S, Honsho M, Ekroos K, Shevchenko A, Simons K. 2003. Resistance of cell membranes to different detergents. In *Proc. Natl. Acad. Sci. U.S.A.*, pp. 5795-800
Shai N, Schuldiner M, Zalckvar E. 2016. No peroxisome is an island - Peroxisome contact sites. In *Biochim. Biophys. Acta*, pp. 1061-69
Sidman RL, Dickie MM, Appel SH. 1964. Mutant mice (quaking and jimpy) with deficient myelination in the central nervous system. In *Science*, pp. 309-11
Simons K, Ikonen E. 1997. Functional rafts in cell membranes. In *Nature*, pp. 569-72
Skripuletz T, Hackstette D, Bauer K, Gudi V, Pul R, et al. 2012. Astrocytes regulate myelin clearance through recruitment of microglia during cuprizone-induced demyelination. In *Brain*

Smolders I, Smets I, Maier O, vandeVen M, Steels P, Ameloot M. 2010. Simvastatin interferes with process outgrowth and branching of oligodendrocytes. In *J. Neurosci. Res.*, pp. 3361-75

Stanislaus R, Gilg AG, Singh AK, Singh I. 2002. Immunomodulation of experimental autoimmune encephalomyelitis in the Lewis rats by Lovastatin. In *Neurosci Lett*, pp. 167-70

Sugiura A, Mattie S, Prudent J, McBride HM. 2017. Newly born peroxisomes are a hybrid of mitochondrial and ER-derived pre-peroxisomes. In *Nature Publishing Group*, pp. 251-54

Talbott JF, Loy DN, Liu Y, Qiu MS, Bunge MB, et al. 2005. Endogenous Nkx2.2+/Olig2+ oligodendrocyte precursor cells fail to remyelinate the demyelinated adult rat spinal cord in the absence of astrocytes. In *Exp Neurol*, pp. 11-24

Tall AR, Yvan-Charvet L. 2015. Cholesterol, inflammation and innate immunity. In *Nat Rev Immunol*, pp. 104-16: Nature Publishing Group

Taveggia C, Zanazzi G, Petrylak A, Yano H, Rosenbluth J, et al. 2005. Neuregulin-1 Type III Determines the Ensheathment Fate of Axons. In *Neuron*, pp. 681-94

Thoms S. 2015. Import of proteins into peroxisomes: piggybacking to a new home away from home. In *Open Biol*

Titorenko VI, Rachubinski RA. 2004. The peroxisome: orchestrating important developmental decisions from inside the cell. In *The Journal of Cell Biology*, pp. 641-45

Vitali C, Wellington CL, Calabresi L. 2014. HDL and cholesterol handling in the brain. In *Cardiovascular Research*, pp. 405-13

Waxman SG, Kocsis JD, Nitta KC. 1979. Lysophosphatidyl choline-induced focal demyelination in the rabbit corpus callosum: Light-microscopic observations. In *J. Neurol. Sci.*, pp. 45-53

Waxman SG, Swadlow HA. 1976. Ultrastructure of visual callosal axons in the rabbit. In *Exp Neurol*, pp. 115-27

Werner HB, Kuhlmann K, Shen S, Uecker M, Schardt A, et al. 2007. Proteolipid Protein Is Required for Transport of Sirtuin 2 into CNS Myelin. In *Journal of Neuroscience*, pp. 7717-30

White R, Krämer-Albers E-M. 2014. Axon-glia interaction and membrane traffic in myelin formation. In *Front. Cell. Neurosci.*, pp. 284

Yamazaki R, Baba H, Yamaguchi Y. 2018. Unconventional Myosin ID is Involved in Remyelination After Cuprizone-Induced Demyelination. In *Neurochem Res*, pp. 195-204

Yamazaki R, Ishibashi T, Baba H, Yamaguchi Y. 2014. Unconventional myosin ID is expressed in myelinating oligodendrocytes. In *J. Neurosci. Res.*, pp. 1286-94

Yamazaki R, Ishibashi T, Baba H, Yamaguchi Y. 2016. Knockdown of Unconventional Myosin ID Expression Induced Morphological Change in Oligodendrocytes. In *ASN NEURO*

Yamazaki R, Ishibashi T, Baba H, Yamaguchi Y. 2017. Expression of Unconventional Myosin VI in Oligodendrocytes. In *Neurochem Res*, pp. 3372-81

Yin X, Crawford TO, Griffin JW, Tu Ph, Lee VM, et al. 1998. Myelin-associated glycoprotein is a myelin signal that modulates the caliber of myelinated axons. In *J. Neurosci.*, pp. 1953-62

Youssef S, Stüve O, Patarroyo JC, Ruiz PJ, Radosevich JL, et al. 2002. The HMG-CoA reductase inhibitor, atorvastatin, promotes a Th2 bias and reverses paralysis in central nervous system autoimmune disease. In *Nature*, pp. 78-84